
**The calcium signature decoding
CCaMK/CYCLOPS complex activates the
transcription of symbiosis associated genes**

Sylvia Singh

**Dissertation
der Fakultät für Biologie der
Ludwig-Maximilians-Universität München**

vorgelegt von
Sylvia Singh
München, im September 2013

Dissertation eingereicht am: 05. September 2013

Tag der mündlichen Prüfung: 29. April 2014

1. Gutachter: Prof. Dr. Martin Parniske
2. Gutachter: PD. Dr. Arthur Schübler

Eidesstattliche Versicherung

Ich versichere hiermit an Eides statt, dass die vorliegende Dissertation von mir selbständig und ohne unerlaubte Hilfe angefertigt ist.

München, den 5. September 2013

Sylvia Singh

Erklärung

Hiermit erkläre ich, dass die Dissertation nicht ganz oder in wesentlichen Teilen einer anderen Prüfungskommission vorgelegt worden ist. Ich habe nicht versucht, anderweitig eine Dissertation einzureichen oder mich einer Doktorprüfung zu unterziehen.

München, den 5. September 2013

Sylvia Singh

Für Upsi

TABLE OF CONTENTS

I List of Abbreviations	9
II List of Publications	10
III Declaration of Contribution as Co-Author	11
III Erklärung über die erbrachte Leistung als Ko-Autor	11
IV Summary	15
IV Zusammenfassung	17
V Introduction	19
1 Root endosymbioses	19
2 Establishment of arbuscular mycorrhiza	20
3 Signaling in root symbiosis	21
3.1 The early phase: Symbiont recognition	22
3.2 Signaling components required for the generation of calcium spiking	23
3.3 Symbiosis induced calcium spiking	26
3.4 Decoding and transduction of symbiotic calcium spiking	27
4 Transcriptional regulation during symbiosis development	31
5 Aims of the study	33
VI Results	35
Chapter 1: Functional characterization of CCaMK and the role of its regulatory domains in symbiosis	35
1 Summary	35
2 Introduction	35
3 Results	38
3.1 The CCaMK domain structure and <i>CCaMK</i> mutant constructs used in this study	38
3.2 Restoration of RNS in the <i>L. japonicus ccamk-13</i> mutant by <i>CCaMK</i> mutant versions	40
3.3 Restoration of AM in the <i>L. japonicus ccamk-13</i> mutant by <i>CCaMK</i> mutant versions	42
3.4 Formation of spontaneous nodules in the <i>L. japonicus ccamk-13</i> mutant by <i>CCaMK</i> mutant versions	47
3.5 <i>In vitro</i> kinase activity of CCaMK mutant proteins.....	51
3.6 Subcellular localization of CCaMK mutant proteins.....	53
4 Discussion	54
4.1 Differential requirements of CCaMK domains for AM fungal and rhizobial infection	54
4.2 The phospho-mimetic and phospho-ablative form of CCaMK reveal differences in regulation	56
4.3 AM fungi exert a negative effect on spontaneous nodule formation	57
4.4 Correlation between kinase activity and <i>in vivo</i> activity of CCaMK mutant proteins.....	58
5 Material and Methods	59
5.1 Plant material, growth conditions, transformation and inoculation procedures	59

5.2 Symbiosis phenotyping	60
5.3 Protein blot analysis	60
5.4 Protein expression, purification and <i>in vitro</i> kinase assay	60
5.5 Protoplast preparation from <i>Lotus japonicus</i> cell culture	61
5.6 Transfection of protoplasts	62
5.7 Plasmid construction	62
5.7.1 Entry clones	62
5.7.2 Plasmids for <i>L. japonicus</i> hairy root transformation	63
5.7.3 Plasmids for protein expression	63
5.7.4 Plasmids for subcellular localization in <i>L. japonicus</i> protoplasts	64
5.8 Primers	64
Chapter 2: Negative regulation of CCaMK is essential for symbiotic infection	66
1 Summary	66
2 Introduction	67
3 Results.....	69
3.1 The <i>L. japonicus</i> suppressor 11 (<i>sup11</i>) mutant.....	69
3.2 Map-based cloning and next-generation sequencing identify two linked mutations	72
3.3 <i>ccamk-14</i> is responsible for the symbiosis-defective phenotypes	73
3.4 <i>ccamk-14</i> recapitulates the symbiotic defects of <i>sup11</i>	77
3.5 Substitutions at S337 modify binding of Ca ²⁺ /CaM.....	80
3.6 CCaMK ^{S337N} and CCaMK ^{S337D} are not impaired in the interaction with CYCLOPS	84
3.7 Substitution of the S337 autophosphorylation site alters the regulation of substrate phosphorylation.....	84
4 Discussion	88
4.1 <i>ccamk-14</i> enhances epidermal infection by bacteria	88
4.2 The <i>ccamk-14</i> phenotype suggests cell type-specific regulation of bacterial infection	89
4.3 Is CCaMK activity substrate-dependent?	89
4.4 The <i>ccamk-14</i> mutation removes negative regulation of CCaMK	90
4.5 Significance of negative regulation of CCaMK during symbiotic infection	91
5 Materials and Methods	92
5.1 Plant material and growth conditions.....	92
5.2 Genetic mapping of <i>sup11</i>	92
5.3 Next-generation sequencing and bioinformatic analyses.....	92
5.4 Genotyping.....	92
5.5 Site-directed mutagenesis	93
5.6 Complementation experiments	93
5.7 Protein expression, purification and <i>in vitro</i> kinase assay	94
5.8 Calmodulin binding assay.....	95
5.9 Yeast two-hybrid analysis	95
5.10 In-gel digestion of autophosphorylated CCaMK	96

5.11 LC-MS/MS of in gel-digested proteins	96
5.12 Database search	96
6 Acknowledgements	97
Chapter 3: CYCLOPS, a DNA-binding transcriptional activator, orchestrates symbiotic root nodule development	98
1 Summary	98
2 Introduction	99
3 Results.....	101
3.1 CYCLOPS is a phosphorylation substrate of CCaMK.....	101
3.2 The CYCLOPS phosphorylation sites S50 and S154 are essential for symbiotic development	103
3.3 The phosphorylation status of CYCLOPS does not affect complex formation with CCaMK.....	106
3.4 The <i>NIN</i> promoter is activated <i>in trans</i> by CYCLOPS in a phosphorylation dependent manner.....	107
3.5 Identification of a CYCLOPS responsive <i>cis</i> element (<i>CYC-RE</i>) within the <i>NIN</i> promoter.....	108
3.6 CYCLOPS-DD binds DNA in a sequence-specific and phosphorylation-dependent manner	109
3.7 CYCLOPS is a modular DNA-binding transcriptional activator	112
3.8 The CYCLOPS DNA binding domain binds the <i>CYC-RE in vitro</i>	114
3.9 CYCLOPS-DD transactivates the <i>NIN</i> promoter via the <i>CYC-RE</i> in <i>L. japonicus</i> independently of NSP1, NSP2 and NIN	116
3.10 The <i>2xCYC-RE:GUS</i> reporter is activated in <i>L. japonicus</i> roots after inoculation with <i>M. loti</i>	119
3.11 CYCLOPS-DD induced spontaneous nodules in <i>L. japonicus</i> roots independently of CCaMK.....	120
4 Discussion	124
4.1 CCaMK/CYCLOPS activates <i>NIN</i> transcription upon perception of calcium signals	124
4.2 CYCLOPS carries a non-canonical DNA binding domain.....	126
4.3 The CYCLOPS AD contains a peptide stretch with predicted intrinsic disorder	126
4.4 The N-terminal half of CYCLOPS functions as a negative regulatory domain	126
4.5 The consequences of CYCLOPS phosphorylation	126
4.6 Decoding of symbiotic calcium oscillations by the CCaMK/CYCLOPS complex provides a new paradigm in nuclear calcium-based signal transduction.....	127
5 Materials and Methods	128
5.1 Plant lines and plant transformation	128
5.2 Plant growth and inoculation conditions	1298
5.3 Symbiosis phenotyping	129
5.4 Nodule sectioning	129
5.5 Histochemical GUS staining	130
5.6 Fluorimetric GUS assay	130
5.7 FLIM-FRET analysis.....	130
5.8 Bimolecular fluorescence complementation (BiFC) and subcellular localization analysis.....	130
5.9 CYCLOPS domain analysis in <i>N. benthamiana</i>	130
5.10 CYCLOPS domain analysis in yeast.....	131

5.11 Protein expression and purification	131
5.12 <i>In vitro</i> phosphorylation and dephosphorylation	131
5.13 Mass spectrometric analysis	132
5.14 Electrophoretic mobility shift assay	132
5.15 Microscale thermophoresis	132
5.16 Protein blot analysis	132
5.17 Gene expression analysis	133
5.18 CYCLOPS amino acid sequence alignment	133
5.19 Computational analysis	134
5.20 Oligonucleotides used for primers and EMSA probes	134
5.21 Plasmid construction	139
6 Acknowledgements	144
7 Appendix: Biochemical characterisation of the CCaMK/CYCLOPS complex	144
7.1 Results and Discussion	144
7.1.1 Size-exclusion chromatography of purified CCaMK	144
7.1.2 Biochemical characterization of the CCaMK/CYCLOPS complex	145
7.2 Materials and Methods	149
7.2.1 Protein expression and purification	149
7.2.2 Size-exclusion chromatography	149
7.2.3 <i>In vitro</i> kinase assay	150
7.2.4 Protein blot analysis	150
7.2.5 Plasmids for protein expression	150
7.2.6 Oligonucleotides	151
VII General Discussion	152
1 CCaMK and the role of its calcium regulatory domains in symbiosis formation	152
2 Positive and negative regulation of CCaMK by autophosphorylation	155
3 The role of CCaMK and CYCLOPS in nodule organogenesis	157
4 Conclusions and outlook	158
VIII References	160
IX List of Figures	175
X List of Tables	177
XI Acknowledgements	178

I List of Abbreviations

aa	amino acid
AID	autoinhibition domain
AOM	autoregulation of mycorrhization
AON	autoregulation of nodulation
AM	arbuscular mycorrhiza
bp	base pair
CaM	calmodulin
CaM-BD	calmodulin binding domain
CaMK	calmodulin-dependent kinase
CBB	coomassie brilliant blue
CCaMK	calcium- and calmodulin-dependent kinase
CO	chitin oligomer
Da	Dalton
DMI	does not make infections
EMSA	electrophoretic mobility shift assay
ER	endoplasmic reticulum
ERF	ethylene response factor
ERN	ethylene response factor required for nodulation
GA	gibberellic acid
GFP	green fluorescent protein
GlcNAc	n-acetylglucosamine
IMAC	immobilized metal ion affinity chromatography
IT	infection thread
LCO	lipochito-oligosaccharides
LHKI	lotus histidine kinase I
LNP	lectin nucleotide phosphohydrolase
LRR	leucine-rich repeat
MW	molecular weight
NEC	N-terminal extracellular
NF	nuclear factor
NFP	nod factor perception
NIN	nodule inception
Nod	nodulation
NP	nodule primordium
NPL	nodulation pectate lyase
NSP	nodulation signaling pathway
NUP	nucleoporin
PAM	periarbuscular membrane
PPA	prepenetration apparatus
PT	phosphate transporter
RLK	receptor-like kinase
RLS	root legume symbiosis
RNS	root nodule symbiosis
SL	strigolactone
VLD	visinin-like domain
WT	wild-type

II List of Publications

Yano, K., Yoshida, S., Müller, J., **Singh, S.**, Banba, M., Vickers, K., Markmann, K., White, C., Schuller, B., Sato, S., et al. (2008). CYCLOPS, a mediator of symbiotic intracellular accommodation. *Proc. Natl. Acad. Sci. USA* *105*, 20540-20545.

Liao, J., **Singh, S.**, Hossain, M.S., Andersen, S.U., Ross, L., Bonetta, D., Zhou, Y., Sato, S., Tabata, S., Stougaard, J., et al. (2012). Negative regulation of CCaMK is essential for symbiotic infection. *Plant J.* *72*, 572-584.

Singh, S., and Parniske, M. (2012). Activation of calcium- and calmodulin-dependent protein kinase (CCaMK), the central regulator of plant root endosymbiosis. *Curr. Opin. Plant Biol.* *15*, 444-453.

Strauß, T., van Poecke, R.M., Strauß, A., Römer, P., Minsavage, G.V., **Singh, S.**, Wolf, C., Kim, S., Lee, H.A., Yeom, S.I., et al. (2012). RNA-seq pinpoints a *Xanthomonas* TAL-effector activated resistance gene in a large-crop genome. *Proc. Natl. Acad. Sci. USA* *109*, 19480-19485.

Singh, S., Katzer, K., Lambert, J., Cerri, M. and Parniske, M. (2014). CYCLOPS, a DNA-binding transcriptional activator, orchestrates symbiotic root nodule development. *Cell Host Microbe* *15*, 139-152.

III Declaration of Contribution as Co-Author

III Erklärung über die erbrachte Leistung als Ko-Autor

Sylvia Singh the author of this thesis contributed to the following manuscripts as follows:

Sylvia Singh die Autorin der vorliegenden Dissertation hat folgende Leistungen zu den im Folgenden aufgeführten Manuskripten beigetragen:

Manuscript 1: Negative regulation of CCaMK is essential for symbiotic infection

Reference:

Liao, J.*, **Singh, S.***, Hossain, M.S*., Andersen, S.U., Ross, L., Bonetta, D., Zhou, Y., Sato, S., Tabata, S., Stougaard, J., et al. (2012). Negative regulation of CCaMK is essential for symbiotic infection. *Plant J.* 72, 572-584.

* These authors contributed equally to the work.

Sylvia Singh

- designed, performed and analysed the entire biochemical experiments, comprising
 - the protein preparation for the CCaMK phosphorylation site analysis by mass spectrometry
 - all *in vitro* kinase and calmodulin binding assays.
- *hat alle biochemischen Experimente, einschliesslich*
 - *der Protein Präparation für die massenspektrometrische CCaMK Phosphorylierungsstellen Analyse,*
 - *aller in vitro Kinase- und Calmodulin-Binde-Assays geplant, durchgeführt und ausgewertet.*
- designed, performed and analysed the yeast two-hybrid interaction analysis between CCaMK, CCaMK mutant variants and CYCLOPS
- *hat die Hefe Zwei-Hybrid Interaktions Analysen zwischen CCaMK, CCaMK Mutanten Versionen und CYCLOPS geplant, durchgeführt und ausgewertet.*
- designed, performed and analyzed the AM complementation experiments of the *L. japonicus ccamk-13* mutant with cDNA-CCaMK, cDNACCaMK-S337D and cDNACCaMK-S337N under control of the *L. japonicus* ubiquitin promoter.
- *hat die AM Komplementations Experimente der L. japonicus ccamk-13 Mutante mit CCaMK (cDNA), CCaMK-S337D (cDNA) und CCaMK-S337N (cDNA) Konstrukten, die mit dem L. japonicus ubiquitin Promotor ausgestattet sind, geplant, durchgeführt und ausgewertet.*
- generated all data related to Figures 23, 24, 25g, 25h, 26, 27, 28 and 29 of this thesis.
- *hat alle Daten beigetragen die sich auf die Abbildungen 23, 24, 25g, 25h, 26, 27, 28 und 29*

der Dissertation beziehen.

- wrote the respective text sections of the results part, the materials and methods part and the figure legends (of the manuscript draft) which were partly modified by Krzysztof Szczyglowski, the main author of the manuscript.
- *hat die zugehörigen Textpassagen des Ergebnis- und des Material und Methoden Teils und die Abbildungslegenden (des Manuskript Entwurfs) verfasst, die zum Teil vom Hauptautor des Manuskripts, Krzysztof Szczyglowski, modifiziert wurden.*

Manuscript 2: CYCLOPS, a DNA-binding transcriptional activator, orchestrates symbiotic root nodule development

Reference:

Singh, S.*, Katzer, K.*, Lambert, J., Cerri, M. and Parniske M. (2014). CYCLOPS, a DNA-binding transcriptional activator, orchestrates symbiotic root nodule development. *Cell Host Microbe* 15, 139-152.

* These authors contributed equally to the work.

Sylvia Singh

- established CYCLOPS protein expression and purification conditions to obtain soluble CYCLOPS protein suitable to conduct *in vitro* kinase assays with CCaMK.
- *hat die CYCLOPS Protein Expressions- und Aufreinigungsbedingungen etabliert um lösliches CYCLOPS Protein für in vitro Kinase Assays mit CCaMK zu erhalten.*
- designed and performed *in vitro* kinase assays and obtained CCaMK phosphorylated CYCLOPS protein used for mass spectrometric analysis of CYCLOPS.
- *hat in vitro Kinase Assays geplant und durchgeführt und dadurch von CCaMK phosphoryliertes CYCLOPS Protein für die massenspektrometrische Analyse erhalten.*
- evaluated mass spectrometric data of phosphorylated CYCLOPS.
- *wertete die massenspektrometrischen Daten der phosphorylierten CYCLOPS Protein Probe aus.*
- designed, performed and analysed all AM and RNS complementation experiments of the *L. japonicus* Gifu wild-type and *L. japonicus* mutants with various CYCLOPS wild-type and CYCLOPS mutant constructs and generated the corresponding constructs.
- *hat alle AM und Wurzelknöllchensymbiose (RNS) Komplementations Experimente von L. japonicus Gifu Wildtyp Pflanzen und von den entsprechenden L. japonicus Mutanten Pflanzen mit CYCLOPS Wildtyp und verschiedenen CYCLOPS Mutanten Konstrukten geplant, durchgeführt und ausgewertet und hat die entsprechenden Konstrukte hergestellt.*

- generated the constructs for FLIM-FRET analysis.
- *hat die Konstrukte für die FLIM-FRET Analyse hergestellt.*
- designed, performed and analysed *NIN* promoter activation by CYCLOPS, CYCLOPS phospho-site mutant versions expressed with or without CCaMK-T265D in *N. benthamiana* and generated the corresponding constructs.
- *hat das Experiment der NIN Promotor Aktivierung in N. benthamiana durch CYCLOPS und CYCLOPS Phosphorylierungsstellen Mutanten, in Abwesenheit und Gegenwart (Ko-Expression) von CCaMK-T265D geplant, durchgeführt und ausgewertet und die entsprechenden Konstrukte hergestellt.*
- designed, performed and analysed transactivation experiments identifying and confirming the CYCLOPS-DD responsive *cis* element in the *NIN* promoter.
- *hat die Transaktivierungsexperimente, die zur Identifizierung und Bestätigung des CYCLOPS-DD responsiven cis-Elements im NIN Promoter führten, geplant, durchgeführt und ausgewertet und die entsprechenden Konstrukte erstellt.*
- Designed and performed electrophoretic mobility shift assays (EMSAs) of the co-expressed CCaMK/CYCLOPS protein complex in the absence and presence of lambda-phosphatase.
- *hat die electrophoretic mobility shift assays (EMSAs) mit dem ko-exprimierten CCaMK/CYCLOPS Protein Komplex in Abwesenheit und Anwesenheit von lambda-Phosphatase geplant und durchgeführt.*
- designed and generated the following constructs used for CYCLOPS domain analysis in *N. benthamiana* and yeast: p35S:BD_{Gal4}-3xHA-GW, the control vector p35S:3xHA-BD_{Gal4}-AD_{VP16} and the yeast constructs pBDGAL4:CYCLOPS, pBDGAL4:CYCLOPS-50A-154A and pBDGAL4:CYCLOPS-50D-154D.
- *hat die folgenden Konstrukte für die CYCLOPS Domänenanalyse in N. benthamiana und Hefe entworfen und hergestellt: p35S:BD_{Gal4}-3xHA-GW, den Kontroll Vektor p35S:3xHA-BD_{Gal4}-AD_{VP16} und die Hefe Konstrukte: pBDGAL4:CYCLOPS, pBDGAL4:CYCLOPS-50A-154A und pBDGAL4:CYCLOPS-50D-154D.*
- designed, performed and analysed transactivation experiments of the 2xCYC-RE:GUS reporter in *L. japonicus* Gifu wild-type and mutant plants.
- *hat die Transaktivierungsexperimente des 2xCYC-RE:GUS Reporters in L. japonicus Gifu Wildtyp und in L. japonicus Mutanten Pflanzen geplant, durchgeführt und ausgewertet.*
- designed, performed and analysed experiments to test spontaneous nodule formation by CYCLOPS-DD in the Gifu wild-type and *symrk-3*, *ccamk-3*, *ccamk-13* and *cyclops-3* mutants.

- *hat das Experiment zur spontanen Knöllchen Bildung durch CYCLOPS-DD im L. japonicus Gifu Wildtyp und in den Mutanten symrk-3, ccamk-3, ccamk-13 und cyclops-3 geplant, durchgeführt und ausgewertet.*
- designed, and performed the quantitative real-time RT-PCR experiment and analysed the data.
- *hat das quantitative real-time RT-PCR Experiment geplant, durchgeführt und ausgewertet.*
- performed data base searches and *in silico* analysis to analyse the deduced CYCLOPS transcriptional activation- and DNA-binding domains.
- *hat die Datenbanksuche und in silico Analyse zur Analyse der abgeleiteten CYCLOPS Transkriptionsaktivierungs- und DNA-Bindedomänen durchgeführt.*
- performed all protein blot analyses.
- *hat alle Proteinblot Analysen durchgeführt.*
- conducted subcellular localization studies of CYCLOPS and CYCLOPS phospho-site mutants in *N. benthamiana*.
- *hat die subzelluläre Lokalisations-Studie von CYCLOPS und den CYCLOPS Phosphorylierungsstellen Mutanten in N. benthamiana durchgeführt.*
- designed, performed and analysed homodimerization analysis of CYCLOPS and CYCLOPS phospho-site mutants by BiFC.
- *hat die Homodimerisierungs-Analyse von CYCLOPS und den CYCLOPS Phosphorylierungsstellen Mutanten mittels der Bimolekularen Fluoreszenz Komplementationsanalyse (BiFC) geplant und durchgeführt.*
- generated all data and pictures related to figures 30A, 31, 32, 34, 35B right panel, 38, 39, 40A-D, 40J-L, 40Q and 41 of the thesis.
- *hat alle Daten und Abbildungen beigetragen, die sich auf die Abbildungen 30A, 31, 32, 34, 35B rechtes Panel, 38, 39, 40A-D, 40J-L, 40Q und 41 der Dissertation beziehen.*
- wrote the draft of the manuscript; the materials and methods section describing:
 - CYCLOPS domain analysis in *N. benthamiana* and yeast, EMSA technique and MST was written by Katja Katzer
 - FLIM-FRET analysis was written by Jayne Lambert.
- *hat den Entwurf des Manuskripts verfasst; der Material und Methoden Teil worin:*
 - *Die CYCLOPS Domänen Analyse in N. benthamiana und Hefe, die EMSA Technik und die Microscale Thermophorese (MST) beschrieben werden, wurde von Katja Katzer verfasst*
 - *Die FLIM-FRET Analyse beschrieben wird, wurde von Jayne Lambert verfasst.*

IV Summary

Under nutrient limiting conditions legumes can form arbuscular mycorrhiza (AM) with phosphate acquiring AM fungi, and root nodule symbiosis (RNS) with nitrogen-fixing rhizobia. Common to both root endosymbioses is a conserved set of genes which act together in a signaling pathway required for the initiation and perception of perinuclear calcium oscillations provoked upon symbiont perception. Downstream of calcium spiking the nuclear calcium- and calmodulin-dependent kinase CCaMK is essential for the perception and transduction of the signal. The presence of a calmodulin binding domain (CaM-BD) and calcium chelating EF-hands indicates that CCaMK is subjected to complex regulation. Various amino acid substitutions of threonine 265, a presumed autophosphorylation site of *Lotus japonicus* CCaMK, or the kinase domain alone, confer calcium independent activity which gives rise to spontaneous nodulation. However, it remained unknown whether the calcium regulatory domains are differentially required for symbiotic processes. In this study mutational analysis of *CCaMK* was carried out to elucidate the requirement of the individual domains and autophosphorylation sites for the three symbiotic processes: Nodule organogenesis, rhizobial infection and AM. Rhizobial infection processes were strictly dependent on the presence of the CaM-BD, which otherwise was dispensable for AM, and nodule organogenesis with autoactivated constructs. AM fungi exerted a previously undescribed negative effect on spontaneous nodule organogenesis by autoactive CCaMK. Whether this effect is directly acting at the level of CCaMK or downstream is unclear, but T265 seems not to be involved. Phospho-mimetic and -ablative substitutions of T265 equally triggered spontaneous nodules, an observation that calls for further study on the activation mechanism of legume CCaMKs.

In addition, positional cloning of the *ccamk-14* mutant combined with calcium-induced autophosphorylation site identification in CCaMK pinpointed S337 in the CaM-BD as important regulatory site, as the expression of the phospho-mimetic version CCaMK-S337D in a *ccamk* mutant completely disabled symbiosis due to the proposed impairment of calmodulin binding.

The mechanism of calcium signal propagation downstream of CCaMK leading to symbiosis gene expression was previously unknown. This study identified the functionally uncharacterized CCaMK interacting protein and phosphorylation substrate CYCLOPS as CCaMK regulated transcription factor. Simultaneous phosphorylation at S50 and S154 in the N-terminal domain releases the C-terminal DNA-binding and transcriptional activation domains, turning CYCLOPS into an active transcription factor, which targets the promoter of the *NODULE INCEPTION (NIN)* gene. Accordingly, the phospho-mimetic version of CYCLOPS was solo-sufficient to trigger nodule organogenesis in the absence of rhizobia and CCaMK. Taken together, the identification of CYCLOPS as CCaMK activated transcription factor provides the missing link to the previously

unsolved question how calcium oscillations are decoded by CCaMK and translated into a symbiosis specific gene expression pattern.

IV Zusammenfassung

Leguminosen können unter Nährstoffmangel Bedingungen arbuskuläre Mykorrhiza (AM) mit Phosphat liefernden AM Pilzen und Wurzelknöllchen Symbiose mit Stickstoff fixierenden Rhizobien Bakterien ausbilden. Beide Symbiosen nutzen ein konserviertes Genset, das in einem gemeinsamen Signaltransduktionsweg zusammenwirkt, welcher für die Initiierung und Wahrnehmung der perinukleären Calcium Oszillationen erforderlich ist, die nach Perzeption von Symbionten hervorgerufen werden. Die unterhalb des Calcium Spiking platzierte nukleäre Calcium- und Calmodulin-abhängige Kinase CCaMK ist essentiell für die Perzeption und Weiterleitung des Signals. Das Vorhandensein einer Calmodulin Bindedomäne (CaM-BD) und von Calcium chelatisierenden EF-Händen deutet darauf hin, dass CCaMK einer umfangreichen Regulation unterliegt. Verschiedene Aminosäure Substitutionen an der mutmaßlichen Autophosphorylierungsstelle T265 von *Lotus japonicus* CCaMK oder die Expression der Kinase Domäne verleihen Calcium unabhängige Aktivität welche die Bildung spontaner Knöllchen hervorruft. Ob die Calcium regulierten Domänen für unterschiedliche symbiotische Prozesse benötigt werden, war bislang unbekannt. Um herauszufinden welche der Domänen und Autophosphorylierungsstellen an den symbiotischen Prozessen Knöllchen Organogenese, Rhizobien Infektion und AM Bildung beteiligt sind, wurde in dieser Studie eine CCaMK Mutationsanalyse durchgeführt. Diese Analyse ergab, dass die intakte CaM-BD unter autoaktiven Bedingungen für den rhizobiellen Infektionsprozess essentiell ist, jedoch nicht für die AM Bildung oder die Knöllchen Organogenese. Zudem führte diese Analyse zu dem Ergebnis, dass AM Pilze einen starken negativen Effekt auf die durch autoaktives CCaMK hervorgerufene spontane Knöllchenbildung ausüben. Ob dieser Effekt direkt auf der Ebene von CCaMK oder weiter unterhalb wirkt ist unklar, die Autophosphorylierungsstelle T265 scheint jedoch nicht involviert zu sein. Die Beobachtung, dass sowohl phospho-mimetische als auch phospho-ablative Aminosäure Substitutionen an T265 spontane Knöllchen Organogenese bewirken, legt nahe, dass der Calcium-abhängige Aktivierungsmechanismus von Leguminosen CCaMKs weiterer Aufklärung bedarf.

Die positionelle Klonierung des *L. japonicus ccamk-14* Mutanten Allels und die gleichzeitige Bestimmung von Calcium-induzierten CCaMK Autophosphorylierungsstellen führten zur Identifizierung der wichtigen regulatorische Autophosphorylierungsstelle S337 in der CaM-BD. Die Expression der phospho-mimetischen Version CCaMK-S337D in einer *ccamk* Mutante komplementierte nicht die Symbiosebildung, was vermutlich auf die Beeinträchtigung der Calmodulin Bindung zurückzuführen ist.

Wie das Calcium Signal von CCaMK weitergeleitet und schliesslich zur Expression von Symbiose spezifischen Genen führt war bislang unbekannt. In der vorliegenden Studie wurde das funktionell

uncharakterisierte, mit CCaMK interagierende CYCLOPS Protein als CCaMK regulierter Transkriptionsfaktor identifiziert. Die gleichzeitige Phosphorylierung von S50 und S154 in der N-terminalen Domäne führt zur Freisetzung der C-terminalen DNA-Binde- und Transkriptionsaktivierungsdomäne. Dadurch wird CYCLOPS zu einem aktivierten Transkriptionsfaktor, der die Expression des *NODULE INCEPTION (NIN)* Gens induziert. Demzufolge induzierte die entsprechende phospho-mimetische CYCLOPS Version Knöllchen Organogenese in Abwesenheit von Rhizobien und CCaMK. Mit der Identifizierung von CYCLOPS als CCaMK aktivierten Transkriptionsfaktor konnte somit die bisher ungeklärte Frage beantwortet werden, wie Calcium Oszillationen von CCaMK dekodiert, und unmittelbar in ein Symbiose spezifisches Transkriptionsmuster umgesetzt werden.

V Introduction

1 Root endosymbioses

The majority of land plants can engage in root endosymbiosis with beneficial microbes. Two major types of mutualistic root endosymbioses are distinguished: The ancient arbuscular mycorrhiza (AM) formed between fungi of the phylum *Glomeromycota* (Schüßler et al., 2001) and 70-90% of the existing land plants and the nitrogen-fixing root nodule symbiosis (RNS). Fossil records indicate that AM evolved at least 400 million years ago concomitant with the emergence of land plants and suggests that the beneficial association supported plants in terrestrial colonization (Remy et al., 1994). AM is probably the most widespread symbiosis and occurred early in the plant lineage (Parniske, 2008; Wang et al., 2010a). It connects plant roots to the AM fungal hyphal network in the soil thus greatly improving mineral nutrient (mainly phosphorus and nitrogen) uptake and water supply. Further, other beneficial effects of the AM have been described including improved tolerance to abiotic and biotic stress and involving also increased resistance to pathogens, toxic soil components, salinity and drought (Gianinazzi et al., 2010). In return, the fungus receives carbohydrates from the plant. RNS evolved approximately 60 million years ago coincident with the origin of the *Leguminosae* and, compared to AM, is a relatively young symbiosis (Doyle, 2011; Sprent, 2007). Phylogenetic analysis confined the ability to nodulate to a clade within the Eurosid I comprising the *Fabales*, *Fagales*, *Cucurbitales* and *Rosales* (termed the ‘FaFaCuRo’ clade) (Kistner and Parniske, 2002). Due to differences in the interacting bacterial and plant partner, two major types of RNS are distinguished: Root legume symbiosis (RLS) and actinorhiza (Markmann and Parniske, 2009). RLS is formed between a phylogenetically dispersed group of bacteria called rhizobia and leguminous plants, belonging to the *Fabales*, whereas in actinorhiza actinobacteria of the genus *Frankia* interact with members of the three Eurosid I orders *Fagales*, *Cucurbitales* and *Rosales*. The relatively close phylogenetic clustering of the nodulator clades led to the hypothesis that the common ancestor acquired a genetic predisposition for nodulation (Soltis et al., 1995). However it is still an open question why RNS is not a consistent feature within the nodulator clades and why the non-legume *Parasponia* (*Ulmacea*) is nodulated by rhizobia (Op den Camp et al., 2012; Trinick, 1973). These observations may indicate that RNS has evolved independently several times, or has been lost in several species.

Extensive research on mutants of the two model legumes *Lotus japonicus* and *Medicago truncatula* during the last decade identified a functional overlap between AM and RNS (Catoira et al., 2000; Kistner et al., 2005). Both symbioses use a common set of genes for early symbiosis signaling and symbiont accommodation (termed the ‘common sym genes’) indicating that plants which form RNS have co-opted the genetic framework used for AM formation to evolve RNS.

2 Establishment of arbuscular mycorrhiza

Under phosphate limiting conditions plant roots produce the phytohormone strigolactone (SL) (Akiyama et al., 2005; Umehara et al., 2008) which in petunia is released by the ABC transporter PDR1 (Kretschmar et al., 2012). SLs, also known as ‘branching factors’, stimulate fungal spore germination and hyphal outgrowth and induce a hyphal branching response which is accompanied by an increased fungal energy metabolism (Akiyama et al., 2005; Besserer et al., 2006; Buee et al., 2000). Analysis of germinated spore exudates revealed that in response to plant derived SLs, AM fungi secrete a mixture of signaling molecules, which trigger various symbiosis related host responses including transcriptional activation (Kuhn et al., 2010; Ortu et al., 2012), induction of nuclear calcium spiking (Chabaud et al., 2011; Sieberer et al., 2012), lateral root formation (Oláh et al., 2005) and starch accumulation (Gutjahr et al., 2009). Isolation and characterisation of distinct biologically active compounds has been achieved with different bioassays. Using lateral root formation, root hair branching and activation of the symbiosis reporter *ENOD11:GUS* as read-out, which are all responses also induced by rhizobial nodulation (Nod) factors, Maillet et al. identified a mixture of sulphated and non-sulphated short chain lipochito-oligosaccharides (LCOs) chemically highly reminiscent of rhizobial Nod factors (Maillet et al., 2011). In contrast, Genre et al. employed a Nod factor independent bioassay by conducting calcium spiking analysis in legume and non-legume root organ cultures which led to the identification of tetra- and pentameric chitin oligomers (COs) as the most potent AM fungal signaling molecules (Genre et al., 2013). Chitin-derived signaling molecules (COs and LCOs) are recognized by LysM domain containing receptors suggesting that a LysM domain receptor-like kinase (RLK) is involved in Myc factor perception (Antolin-Llovera et al., 2012; Gust et al., 2012; Tirichine et al., 2007). In the non-legume *Parasponia andersonii* establishment of AM and RNS was found to be dependent on the single common receptor ‘PaNFP’ which is orthologous to *M. truncatula* NFP (Op den Camp et al., 2011). This finding suggests that PaNFP can equally recognize Nod factor and Myc factor, and that in legume plants the duplication of the *Lys* gene family led to the functional diversification of the original Myc factor receptor, and the subsequent evolution of Myc factor and Nod factor specific receptors (Lohmann et al., 2010; Young et al., 2011).

Upon contact with a host root, fungal hyphae form a hyphopodium, an attachment structure which marks the invasion point of the fungus. Successful root colonization and hyphopodium formation requires monomeric cutin signaling molecules, which are produced by the glycerol-3-phosphate acyltransferase RAM2 (Wang et al., 2012). *RAM2* expression is regulated by the AM-specific GRAS type transcription factor *RAM1*, whose induction is dependent on the common sym genes *Does not Make Infections 1 (DMI1)*, *DMI2* and *DMI3* (described in more detail in 3.2) (Gobbato et

al., 2012). Subsequently, the mechanistically stimulated plant cell actively prepares the uptake of the fungus by assembly of the so-called prepenetration apparatus (PPA), a dense cytoplasmic bridge composed of cytoskeletal filaments and components of the endoplasmic reticulum (ER) (Genre et al., 2005). Formation of the PPA is blocked in *symrk* and *ccamk* mutants and it has been recently shown that a gain-of function version of the calcium- and calmodulin-dependent kinase CCaMK, lacking the calcium regulatory domains (CCaMK-1-314) spontaneously induced the formation of cytoplasmic structures resembling PPAs (Takeda et al., 2012). Hyphal penetration of the epidermal cell and thus access into the PPA and later into the inner cortical cell file, is dependent on vapyrin, a novel protein with a role in cellular rearrangements, comprising an N-terminal VAMP-associated protein (VAP)/major sperm protein (MSP) domain and a C-terminal ankyrin-repeat domain (Feddermann et al., 2010; Murray et al., 2011; Pumplin et al., 2010). Guided through the PPA, the fungus traverses the epidermal and outer cortical cells till it reaches the inner cortical cell layer. There, the fungal hyphae spread longitudinally in the apoplast and penetrate cells of the inner cortical cell layer, where finally the symbiotic exchange organs, the arbuscules, are formed. Arbuscules are highly branched tree-like fungal structures, which serve nutrient, mainly phosphate, delivery into and carbon uptake from the periarbuscular space and are separated from the plant cell cytosol by the plant-derived periarbuscular membrane (PAM) (Parniske, 2008). Although continuous with the plasma membrane, the PAM has a distinct protein composition with domain-specific enrichment of transporter proteins such as the AM specific phosphate transporter PT4 and of the two half-size ATP binding cassette transporters STR1 and STR2 with unknown function (Gutjahr et al., 2012; Harrison et al., 2002; Pumplin and Harrison, 2009; Zhang et al., 2010). The phosphate transporter PT4 of *M. truncatula* is located in PAM domains which surround the arbuscule branches but is neither present in membranes surrounding the arbuscule trunk or in the plasma membrane (Harrison, 2012; Pumplin and Harrison, 2009). This polar and site-specific localization is achieved by the timely defined expression of *MtPT4* during arbuscule development, which is accompanied by a phase of transient reorientation of secretion (Pumplin et al., 2012). How the photosynthates are transferred in the form of carbon compounds to the fungus is still unclear but the AM fungal glucose transporter MST2 seems to be involved (Helber et al., 2011).

3 Signaling in root symbiosis

Basically, nodulation is initiated by attachment of rhizobia bacteria to the root hair tip which curls and entraps the bacterial microcolony. The bacteria are then taken up into the root hair cell via plant-derived inwardly growing infection threads (ITs), which are formed by tubular invaginations of the plasma membrane at the site where the cell wall has been locally degraded (Murray, 2011). ITs containing the proliferating bacteria extend from the root hair through the outer cortical cells

into inner cortical cells, whereby the route is dictated by pre-infection threads, cytoplasmic bridges (analogous to PPAs in AM) formed by the plant cell in advance to direct the path of infection (van Brussel et al., 1992; Yokota et al., 2009). Concomitantly, at sites below infection foci, cell divisions are initiated in inner cortical root cells, which redifferentiate in order to form nodule primordia (NP) (Oldroyd and Downie, 2008). Finally, the NP cells are invaded by the ITs and bacteria are released intracellularly where they differentiate into nitrogen-fixing symbiosomes (Kereszt et al., 2011).

3.1 The early phase: Symbiont recognition

Signaling in RLS is initiated by the plant under nitrogen limiting conditions, which leads to the secretion of flavonoids into the soil (Abdel-Lateif et al., 2012). Flavonoids are recognized by rhizobia and induce the synthesis and secretion of strain specific Nod factors. Chemically, Nod factors are lipochito-oligosaccharidic compounds composed of four to five β -1-4 linked n-acetylglucosamine (GlcNAc) units. Depending on the bacterial strain this GlcNAc backbone carries specific decorations: N-acyl groups which vary in length and degree of saturation at the non-reducing end, and further chemical substitutions (e.g. sulphuryl, methyl or fucosyl groups) attached to the reducing end (Gough and Cullimore, 2011). These decorations confer specificity between symbiont and plant host.

Nod factors are perceived by the LysM domain containing Nod factor receptors NFR1 and NFR5 which in *L. japonicus* are both required for early responses to Nod factors as well as for nodulation and infection related processes at later stages (Madsen et al., 2003; Radutoiu et al., 2003). In *M. truncatula* the *Lotus* NFR1 ortholog LYK3 plays a predominant role in IT initiation and the infection process, thus functioning as entry-receptor, while the *Lotus* NFR5 ortholog NFP has a less stringent requirement for the appropriate Nod factors structure and is considered as signaling receptor, since it is required for early Nod factor induced signaling responses (Arrighi et al., 2006; Limpens et al., 2003; Smit et al., 2007). NFRs localize to the plasma membrane (Haney et al., 2011; Lefebvre et al., 2012; Madsen et al., 2011), and NFR1 and 5 have been shown to assemble as heteromeric complex (Madsen et al., 2011). Both receptors directly bind Nod factor with high affinity *in vitro* (Broghammer et al., 2012). Domain swap and mutational analyses suggest that recognition specificity is mediated via a Nod factor binding groove within the LysM2 domain of NFR5/NFP (Bek et al., 2010; Bensmihen et al., 2011; Radutoiu et al., 2007).

The NFRs and the symbiosis RLK SYMRK interact with the symbiotic remorin protein SYMREM1, a scaffolding protein localized in plasma membrane microdomains and involved in rhizobial infection (Lefebvre et al., 2010; Tóth et al., 2012). Similar to remorins, flotillins (FLOT) are also associated with plasma membrane microdomains and required for the rhizobial infection process together with the symbiosis receptor kinases (Haney and Long, 2010; Haney et al., 2011;

Lefebvre et al., 2010). Upon rhizobia treatment the initially dynamic LYK3 plasma membrane localization becomes stabilized, resulting in the colocalization with FLOT4 in microdomains at the root hair tip (Haney et al., 2011). Altogether, these observations indicate that receptors and microdomain specific scaffold proteins are enriched within microdomains to form signaling platforms, which are proposed to serve the increase of signaling efficiency and specificity (Bapaume and Reinhardt, 2012; Jarsch and Ott, 2011). LYK3 interacts at the plasma membrane with the E3 ubiquitin ligase PUB1 (plant U-box protein 1), which negatively regulates bacterial infection and nodulation presumably via LYK3 stability (Mbengue et al., 2010).

3.2 Signaling components required for the generation of calcium spiking

After Nod factor (and by inference also Myc factor) perception, the signal is presumed to be transduced via the leucine-rich repeat (LRR) RLK SYMRK (termed DMI2 in *M. truncatula*), which is essential for the establishment of both root endosymbioses (Endre et al., 2002; Stracke et al., 2002). Consistent with the idea of symbiosis signaling specific plasma membrane microdomains, SYMRK has been shown to interact with the NFRs and SYMREM1 at the plasma membrane (Lefebvre et al., 2010; Tóth et al., 2012). The activating mechanism and putative ligand(s) are unknown. At least three different SYMRK versions exist in angiosperms varying in the length of their extracellular domain, which has been shown to be essential for the extent of symbiotic capability (Markmann et al., 2008). Only the longest version, which contains three LRRs and is predominantly present in legumes supports RNS and AM, whereas shorter versions comprising only two LRRs, or lacking the entire N-terminal extracellular (NEC) domain (but retain two of the LRRs) only confer functional AM (Markmann et al., 2008). This finding indicates that AM fungal and rhizobial signals are perceived and discriminated via the extracellular LRR domain(s). Presumably, the signal is transduced by substrate phosphorylation via the intracellular kinase domain (Yoshida and Parniske, 2005). Several putative SYMRK downstream targets have been identified by interaction analysis. One promising candidate with a putative direct role in signaling is 3-hydroxy-3-methylglutaryl-CoA reductase (HMGR) which catalyses the production of mevalonate, a compound which directly triggers calcium oscillations in *Medicago* root hairs (Kevei et al., 2007; Oldroyd, 2013). In addition, SYMRK interacts with the E3 ubiquitin ligase SEVEN IN ABSENTIA 4 (SINA4) in distinct microdomains at the plasma membrane (Den Herder et al., 2012) and similar to the LYK3/PUB1 complex is involved in the negative regulation of nodulation and rhizobial infection via the control of SYMRK abundance (Den Herder et al., 2012).

The following genes have been conceptually placed into a the common symbiosis gene network (Figure 1): *Lectin Nucleotide Phosphohydrolase (LNP)*, encoding a Nod factor binding apyrase with unknown function, placed upstream of *SYMRK* (Roberts et al., 2013). *SYMRK* (*M. truncatula*

DMI2) (Endre et al., 2002; Stracke et al., 2002), the ion channel encoding genes *CASTOR* & *POLLUX* (*M. truncatula DMI1*) (Ané et al., 2004; Charpentier et al., 2008; Imaizumi-Anraku et al., 2005), the SERCA-type calcium-ATPase encoding *MCA8* gene (Capoen et al., 2011), the three nucleoporine genes *NUP85*, *NUP133* and *NENA* (Groth et al., 2010; Kanamori et al., 2006; Saito et al., 2007), *CCaMK* (*M. truncatula DMI3*) (Lévy et al., 2004; Mitra et al., 2004; Tirichine et al., 2006), *CYCLOPS* (*M. truncatula IPD3*) encoding a coiled-coil protein (Messinese et al., 2007; Yano et al., 2008), the two GRAS protein encoding genes *Nodulation Signaling Pathway1* (*NSP1*) and *NSP2* (Kalo et al., 2005; Smit et al., 2005) and *Vapyrin* (Feddermann et al., 2010; Murray et al., 2011; Pumplin et al., 2010). Calcium spiking analysis in symbiosis mutants is used as a tool to categorize the common sym genes into those placed upstream of and thus required for the generation of calcium spiking and those placed downstream and involved in calcium signal perception, transduction or other common symbiotic responses (Miwa et al., 2006b).

LNP, *SYMRK*, *CASTOR*, *POLLUX*, *MCA8*, *NUP85*, *NUP133* and *NENA* act upstream of calcium spiking. Signal perception via the symbiont-specific receptors and activation of *SYMRK* at the plasma membrane lead within minutes to sustained perinuclear calcium oscillations, possibly triggered via the second messenger mevalonate, which may directly activate calcium channels (Ehrhardt et al., 1996; Oldroyd, 2013; Sieberer et al., 2009). The activated, presumably nuclear membrane localized calcium channels still await identification, while the main components constituting the minimal calcium spike generation machinery have been identified. *CASTOR* and *POLLUX* are two highly similar non-selective ion channels (with a preference for potassium over anions) located in the nuclear envelope (Charpentier et al., 2008). Both may either act as counter ion channels to compensate for the loss of positive charge upon calcium release, or may regulate voltage-gated calcium channels by changing the membrane potential upon opening (Charpentier et al., 2008). In *Medicago* *DMI1*, the ortholog of *Lotus* *POLLUX* can compensate for the function of both, *CASTOR* and *POLLUX*, and is solo-sufficient for symbiosis, which was recently attributed to an amino acid exchange in the selectivity filter causing an increase in channel opening time (Venkateshwaran et al., 2012). The nuclear envelope targeted SERCA-type calcium ATPase pump *MCA8* has been identified as candidate pump removing the released calcium back into the ER store (Capoen et al., 2011).

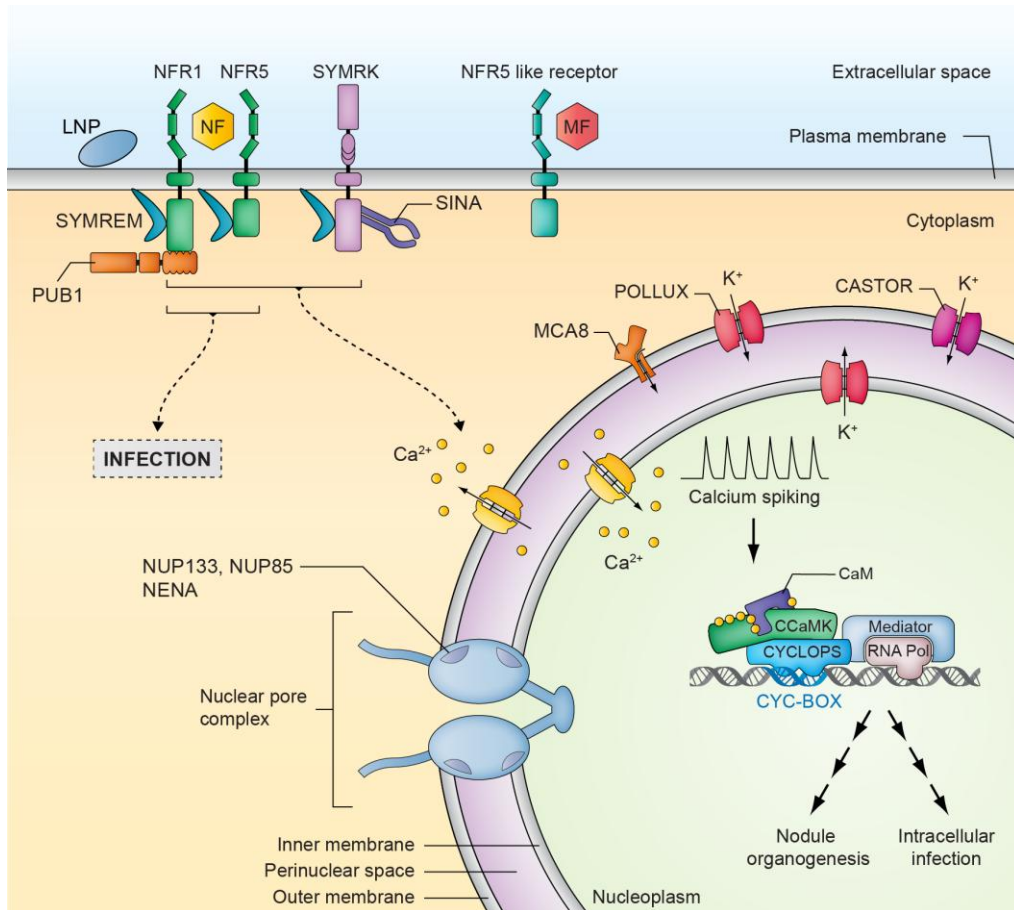


Figure 1. Symbiotic signal transduction in plant root cells.

Perception of rhizobial Nod factors (NFs), presumably at the plasma membrane (PM) (Haney et al., 2010), is mediated by LysM-receptor-like kinases (LYKs) including *L. japonicus* Nod factor receptor 1 (NFR1) and NFR5 (corresponding to LYK3 and NFP in *M. truncatula*) (Amor et al., 2003, Arrighi et al., 2006, Limpens et al., 2003, Madsen et al., 2003, Radutoiu et al., 2003). An NFR5/NFP-like receptor may mediate perception of an AM fungus-derived ‘Myc factor’ (MF) (Maillet et al., 2011, Op den Camp et al., 2011). LNP: Lectin Nucleotide Phosphohydrolase is a NF binding peripheral membrane protein required for AM and RNS, and has been positioned between the LYKs and SYMRK (Roberts et al., 2013). The plant U-box protein 1 (PUB1) of *M. truncatula*, is an E3 ubiquitin ligase which interacts with the kinase domain of LYK3, and was found to exert a negative regulatory effect on nodulation signaling (Mbengue et al., 2010). The SEVEN IN ABSENTIA homolog SINA4 interacts with the kinase domain of SYMRK and mediates its relocation and degradation, thereby negatively impacting on rhizobial nodulation and infection processes (Den Herder et al., 2012). The symbiotic receptors NFR1/LYK3, NFR5/NFP and SYMRK/DMI2 interact at the PM with SYMREM1, a remorin protein specifically upregulated during nodulation and required for IT formation (Lefebvre et al., 2010, Tóth et al., 2012). Within minutes, LCO perception at the PM leads to a sustained perinuclear calcium spiking response (Ehrhardt et al., 1996), the generation, decoding and transduction of which is mediated by components common to both types of symbioses (Kistner and Parniske, 2002). These are genetically positioned upstream (*LNP*, *SYMREK/DMI2*, *CASTOR* & *POLLUX/DMI1*, *NUP85*, *NUP133*, *NENA*, *MCA8*) or downstream (*CCaMK/DMI3*, *CYCLOPS/IPD3*) of the calcium spiking response. CYCLOPS has been identified as transcription factor which upon phosphorylation by CCaMK binds to the *CYC-Box* in the *NIN* (*Nodule Inception*) promoter inducing *NIN* expression (Singh et al., 2014). *NIN* is a nodulation specific transcription factor involved in nodule organogenesis and rhizobial infection (Marsh et al., 2007, Schausser et al., 1999). In addition, several other transcriptional regulators including NSP1/2 (Kalo et al., 2005, Smit et al., 2005), ERN1/2 (Andriankaja et al., 2007, Middleton et al., 2007), NF-YA1/-YB1 (Comber et al., 2006, Soyano et al., 2013) and others have been implicated in symbiosis-related gene expression. The observation that autoactive CCaMK does not restore epidermal IT formation in *nfr* mutants suggests the existence of a common sym gene independent pathway (Hayashi et al., 2010, Madsen et al., 2010). Figure modified from Singh et al., 2012.

The precise role of the nucleoporins NUP85, NUP133 and NENA in calcium spike generation is still elusive. They may either regulate calcium fluxes, or might be involved in the transport of calcium spike machinery components or transmission of secondary signals from the cytosol to the nucleus, or from the outer to the inner nuclear membrane (Binder and Parniske, 2013), where DMII and a fraction of MCA8 have been immunolocalized (Capoen et al., 2011; Charpentier et al., 2008).

3.3 Symbiosis induced calcium spiking

Although both symbioses share the same calcium based signaling pathway, the symbiotic responses in AM and RNS are remarkably different, and it is still a major open question how this specificity is achieved. One hypothesis is that specificity is encoded in the calcium spiking pattern which accordingly should be different during AM and RNS signaling. Initially, calcium spiking analysis has been carried out with microinjection of calcium sensitive dyes into root hair cells. This analysis established that oscillations are initiated in the perinuclear region within 10 min after application of low Nod factor concentration (in the pico- to nanomolar range) (Ehrhardt et al., 1996; Shaw and Long, 2003). The use of genetically encoded cameleon calcium sensors enabled non-invasive, simultaneous calcium imaging in multiple nuclei and in different cell types such as the epidermal and cortical cell layer. Analysis of calcium spiking using cytoplasmic and nucleus-targeted cameleon sensors revealed that outside and within the nucleus calcium spiking originates at the nuclear periphery, is a cell autonomous event and non-synchronous between spiking cells (Sieberer et al., 2009). A minimum number of 36 spikes has been determined to be required for the induction of the early symbiosis marker *ENOD11:GUS* in *Medicago* roots upon Nod factor application (Miwa et al., 2006a). Also AM fungi have been shown to elicit a calcium spiking response in legume and AM forming plant roots which is *DMII* and *DMI2* dependent (Chabaud et al., 2011; Kosuta et al., 2008). High frequency oscillations were recorded in atrichoblast cells, which were directly contacted by fungal hyphopodia and where the nucleus has moved beneath the contact site. This observation indicates that high frequency spiking is a prerequisite for the cellular remodeling required for fungal accommodation (Chabaud et al., 2011; Sieberer et al., 2012). Further, similar to Nod factor induced calcium spiking in RNS, calcium oscillations are also induced by AM fungal exudates and initiate within 10 min after treatment, whereby the spike duration equals that of a Nod factor induced spike (Chabaud et al., 2011). *Medicago* root organ cultures are not responsive to Nod factor treatment consistent with the observation that root organs lose the ability for RNS, which is strictly dependent on signal transduction processes from the shoot (Akashi et al., 2003).

By monitoring the spiking profiles of cortical cells subjected to either rhizobial or AM fungal infection, Sieberer and associates recorded distinct calcium oscillatory profiles characterizing the pre-infection and infection stage (Sieberer et al., 2012). Remarkably, the spiking pattern induced by

AM fungi or rhizobia was highly similar for each stage. Cells in immediate proximity to rhizobia infected root hairs or AM infected atrichoblasts invariably displayed low frequency calcium spiking and intracellular rearrangements which were interpreted as ‘pre-infection priming’. These changes included nuclear repositioning to the site of anticipated microbial entry and cytoplasmic remodeling as observed for pre-infection thread and PPA assembly (Genre et al., 2005; van Brussel et al., 1992). A distinct switch in calcium signature from low to high frequency spiking was exclusively detected in infected cells and only during the initial phase of IT penetration and elongation. This high frequency phase was proposed to mark cellular commitment to infection (Sieberer et al., 2012). The high frequency spiking is of limited duration (40–55 min, corresponding to 35–45 spikes), with a progressive reduction in the amplitude and frequency of calcium spikes during IT progression and cell transversion which completely disappear once infection is completed (after four to five hours). This switch from low to high frequency spiking in infected cells was also observed during AM infection with a spiking pattern and periodicity similar to that induced by rhizobia. However, as the duration and thus approximate number of high frequency spikes could not be determined due to technical limitations, it remains unclear whether rhizobia and AM induced calcium oscillations differ in spike number (Sieberer et al., 2012).

3.4 Decoding and transduction of symbiotic calcium spiking

The nuclear calcium- and calmodulin-dependent kinase CCaMK is widely considered as *the* central regulator of plant root endosymbioses (Singh and Parniske, 2012). Due to several features this molecule is considered as the prime decoder of symbiotic calcium oscillations. The serine/threonine protein kinase possesses two calcium sensing domains which is a unique feature among calcium regulated kinases (Hrabak et al., 2003; Patil et al., 1995). Further, CCaMK is only present in symbiotic plants, thus not occurring in the asymbiotic model plant *Arabidopsis* (Hrabak et al., 2003). CCaMK contains a CaM-BD/autoinhibition domain (AID) adjacent to the kinase domain and a C-terminal visinin-like domain (VLD) comprising three EF-hand motifs (Gleason et al., 2006; Tirichine et al., 2006). CCaMK was initially cloned from lily (*Lilium longiflorum*) (Patil et al., 1995) and biochemical characterization has established a model of CCaMK activation, which has also been applied to legume CCaMK regulation (Sathyanarayanan et al., 2000). In this model binding of free calcium ions to the EF-hand motifs induces autophosphorylation of the conserved threonine residue LIT267, which allows binding of CaM to the CaM-BD. CaM binding fully releases the kinase from autoinhibition and promotes substrate phosphorylation (Figure 2) (Sathyanarayanan et al., 2000; Sathyanarayanan et al., 2001). The N-terminal domain of CCaMK (CCaMK-1-340) shares sequence homology with calmodulin-dependent kinase II (CaMKII), a calcium spike decoding metazoan kinase involved in neuronal signal transduction (De Koninck and

Schulman, 1998; Hudmon and Schulman, 2002b; Rellos et al., 2010). Similar to CCaMK, CaMKII is activated by autophosphorylation at a conserved threonine residue T286 (α CaMKII) which imparts autoactivity to the kinase (Hudmon and Schulman, 2002b). Strikingly, the AID/CaM-BD of CCaMK is 79% homologous to the corresponding CaMKII domain (Patil et al., 1995). CaMKII activity is also regulated by autophosphorylation of two conserved sites (T305 and T306 in α CaMKII) in the CaM-BD, which leads to CaM repulsion (Hudmon and Schulman, 2002b). Two conserved phosphorylation sites are present at an equivalent position in CCaMK (LjS337 and LjS338). The identification and characterization of the *ccamk-14* mutant (described in chapter 2 of this thesis) confirmed the existence of a similar autoregulatory mechanism in CCaMK (Figure 2) (Liao et al., 2012). *ccamk* mutants are absolutely symbiosis defective, although they initiate calcium spiking upon Nod factor perception (Lévy et al., 2004; Mitra et al., 2004; Miwa et al., 2006b), suggesting a position of CCaMK downstream of the calcium oscillations. Consistent with the identification of the activating autophosphorylation site T267 in lily CCaMK (and also in CaMKII), a point mutation in the orthologous site T265 in *L. japonicus* CCaMK (T265D or T265I) confers a gain-of-function phenotype *in planta* leading to spontaneous nodule formation in the absence of rhizobia (Hayashi et al., 2010; Tirichine et al., 2006). The same effect is also observed when the CCaMK kinase domain alone (CCaMK-1-314 or DMI3-1-311) is expressed *in planta* (Gleason et al., 2006; Shimoda et al., 2012; Takeda et al., 2012). Yet, both versions display differential patterns of symbiosis complementation. Whereas the autoactive full-length version CCaMK-T265D restores RNS and AM in *ccamk* mutants, the kinase domain variant can complement AM but is impaired in rhizobial infection (Hayashi et al., 2010; Shimoda et al., 2012). This finding indicates that the CaM-BD and the EF-hands are required for RNS, but the necessity of these domains is less stringent for AM establishment. Takeda and associates employed symbiosis gene expression profiling to pinpoint marker genes upregulated by the two different autoactive CCaMK versions and to also detect potential AM related gain-of function responses mediated by deregulated CCaMK (Takeda et al., 2012). This approach discovered that the AM specific subtilase *SbtM1* (Takeda et al., 2009) is specifically upregulated by CCaMK-1-314, but not by full-length CCaMK-T265D (Takeda et al., 2012). In addition, CCaMK-1-314 spontaneously induced PPA-like structures in cortical cells in a distinct pattern resembling the pattern described for PPA formation during AM establishment (Genre et al., 2005; Takeda et al., 2012). This finding revealed differential requirements for the CCaMK domains in both symbioses, with higher stringency for both domains for RNS formation.

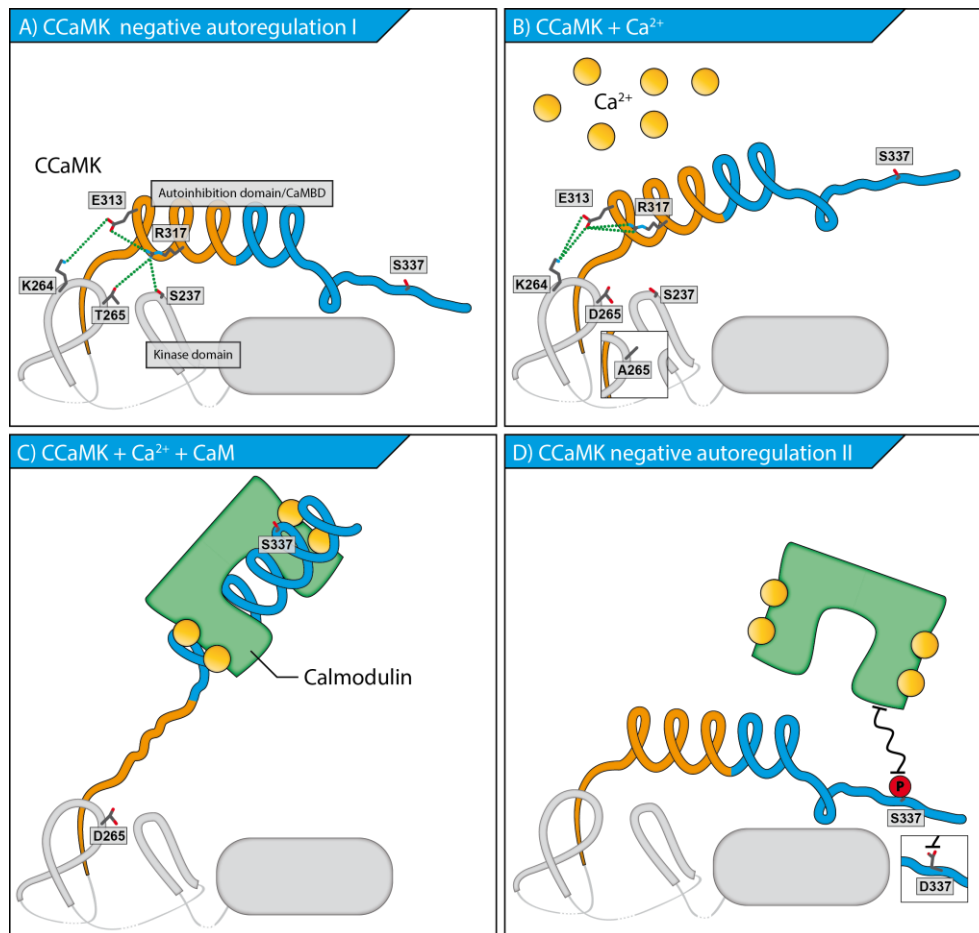


Figure 2. CCaMK regulation.

(A) CCaMK negative autoregulation I. Partial representation of CCaMK comprising the autoinhibition domain (AID, orange) and the calmodulin binding domain (CaMBD, blue) based on homology modeling onto the CaMKII crystal structure (Shimoda et al., 2012). The position of the active center of the kinase is schematized in gray. In the absence of calcium, CCaMK is autoinhibited. The AID assumes a helical structure and acts as a molecular brake impairing kinase activity. Shimoda et al., (2012) postulate that in the absence of calcium, the conserved autophosphorylation site T265 of *L. japonicus* CCaMK engages in a hydrogen-bond network (involving residues S237, K264, E313 and R317), stabilizing the inhibitory helical structure of the AID.

(B) CCaMK activation by calcium.

In the presence of calcium ions (Ca²⁺), which are bound by the C-terminal EF-hand motifs (not shown), CCaMK is released from autoinhibition (Sathyanarayanan et al., 2001) presumably due to the disruption of a hydrogen bond network (Shimoda et al., 2012). This disruption is also predicted to occur in case T265 is replaced by acidic (e.g. T265D), or by non-polar, uncharged amino acids (e.g. T265A, T265I) (Shimoda et al., 2012). Likewise the R317H substitution was predicted to disrupt the hydrogen bond network. Consistently, the corresponding mutants lost autoinhibition, as indicated by the formation of spontaneous nodules in the absence of rhizobia (Tirichine et al., 2006, Shimoda et al., 2012).

(C) CCaMK activation in the presence of Ca²⁺/calmodulin (CaM).

The calcium induced release of CCaMK autoinhibition increases its Ca²⁺/CaM binding affinity. Analogous to CaMKII, Ca²⁺/CaM binding is predicted to confer a structural reorganization of the AID/CaMBD, whereby the inhibitory segment adopts an extended conformation and the unstructured CaMBD becomes helical (Rellos et al., 2010). This conformational change improves accessibility to the catalytic cleft resulting in high substrate phosphorylation activity of CCaMK. S337 is a newly identified regulatory autophosphorylation site in the CaMBD and allows CaM binding only in the unphosphorylated state (Liao et al., 2012).

(D) CCaMK negative autoregulation II.

Autophosphorylation at S337 impairs Ca²⁺/CaM binding and prevents the structural reorganization of the AID/CaMBD domain thus stabilizing the autoinhibited state (Liao et al., 2012). Consequently, the phospho-mimetic version CCaMK-S337D is impaired in Ca²⁺/CaM stimulated substrate phosphorylation and does not restore symbiosis when expressed in a *ccamk* mutant. In contrast, the *ccamk-14* mutant (CCaMK-S337N) forms nodules but cortical infection is aberrant, indicating that this negative autoregulatory circuit is essential for intracellular infection. Figure modified from Singh et al., 2012.

Strikingly, expression of the autoactive CCaMK mutant versions CCaMK-T265I, (carrying the *L. japonicus snf1-1* mutation) or CCaMK-T265D in various *Lotus* mutants affected in genes required for calcium spiking generation, led to the restoration of rhizobia infected nodules and AM (Hayashi et al., 2010; Madsen et al., 2010). This landmark discovery unequivocally revealed that the main purpose of these genes is calcium spike generation and thus activation of CCaMK. Homology modeling of the CCaMK N-terminal part onto the CaMKII structure and proof-of-concept mutational analysis provided insights into the mechanism underlying spontaneous CCaMK activity (Figure 2) (Shimoda et al., 2012). In the modeled structure, T265 is located between the kinase and the CaM binding domain and engages in a hydrogen bond network, stabilizing the autoinhibitory helix, thus rendering CCaMK inactive (Figure 2A). Certain amino acid substitutions of T265 (T265A/D/I) (and by inference phosphorylation), disrupt this network and release the molecular brake resulting in ectopic activity and spontaneous nodule organogenesis (Figure 2B) (Shimoda et al., 2012).

CCaMK is proposed to form a preassembled nuclear complex with CYCLOPS (or the *Medicago* ortholog IPD3), a coiled-coil protein of previously unknown function (Yano et al., 2008). CYCLOPS is required for AM and RNS and is placed downstream of calcium spiking (Horvath et al., 2011; Ovchinnikova et al., 2011; Yano et al., 2008). Compared to other common sym gene mutants its phenotype is extraordinary, as *cyclops* mutants initiate nodule primordia upon rhizobial infection, but nodule formation is blocked at this stage (Yano et al., 2008). Further, they respond towards rhizobia with the formation of tight root hair curls, but ITs are not formed and AM is not restored (Chen et al., 2008; Larkan et al., 2013; Yano et al., 2008). In *Medicago*, the severity of the *ipd3* phenotype depends on the genetic background which could be explained by genetic redundant components, partly compensating CYCLOPS' function (Horvath et al., 2011; Ovchinnikova et al., 2011). *M. truncatula* R108 *ipd3* mutants display the same severe phenotype as *cyclops* mutants, whereas *M. truncatula* Jemalong *ipd3* mutants occasionally form more developed nodules and misshaped ITs, but bacterial release into nodule cells was not observed. This finding points to an additional later role of CYCLOPS/IPD3 in symbiosome formation (Ovchinnikova et al., 2011). Interestingly, the postulated genetic redundant component could not support spontaneous nodulation mediated by DMI3-1-311 when expressed in the Jemalong *ipd3* mutant (Ovchinnikova et al., 2011).

CYCLOPS is phosphorylated by CCaMK, suggesting that CCaMK transduces the calcium signal via CYCLOPS (Madsen et al., 2010; Yano et al., 2008). Although it has been shown that overexpression of autoactive CCaMK triggers nodules in a *cyclops* mutant the nodule frequency was markedly reduced and infection was blocked, corroborating a role of CYCLOPS in both

processes with some level of genetic redundancy in terms of nodule organogenesis (Madsen et al., 2010; Yano et al., 2008).

The signal propagation downstream of CCaMK and CYCLOPS ultimately leading to the activation of nodulation- and AM-specific genes is unclear. Apart from a Scythe-N domain (ubiquitin-like domain) containing protein, CIP73 which was found to interact with CCaMK (Kang et al., 2011), no further interactors of CCaMK or CYCLOPS have been identified. Besides, the precise function of CYCLOPS in symbiosis signaling remained elusive not least, due to its unknown function and uncharacterized protein domain structure.

4 Transcriptional regulation during symbiosis development

A number of symbiosis related transcriptional regulators belonging to the GRAS domain, ethylene response factor (ERF) or CAAT-box (Nuclear Factor Y) family, or unrelated factors such as NODULE INCEPTION (NIN), has been identified (Andriankaja et al., 2007; Combier et al., 2006; Gobbato et al., 2012; Kalo et al., 2005; Marsh et al., 2007; Middleton et al., 2007; Schaarschmidt et al., 2013; Schauser et al., 1999; Smit et al., 2005; Soyano et al., 2013; Vernié et al., 2008). GRAS proteins, ERFs and Nuclear Factors act in both symbioses, while NIN is considered nodulation specific.

The GRAS domain proteins NSP1 and NSP2 were initially placed on the nodulation specific pathway, but refined analysis also implicates a role in AM and, under asymbiotic conditions, in the SL biosynthesis pathway (Delaux et al., 2013; Kalo et al., 2005; Laressergues et al., 2012; Liu et al., 2011; Maillet et al., 2011; Smit et al., 2005). *nsp1* and *nsp2* mutants are RNS deficient and required for root nodule formation and rhizobial infection downstream of CCaMK. Both form a heteromeric complex which has been shown to bind via NSP1 to the *ENOD11*, *ERN1* (*Ethylene Response Factor Required for Nodulation 1*), and *NIN* promoters (Hirsch et al., 2009). Analysis and characterization of Myc LCOs has revised the exclusive function of NSP1 and NSP2 in nodulation (Maillet et al., 2011). Myc LCOs stimulate a root branching response, which was found to be dependent on *DMI1*, *DMI2*, *DMI3* and *NSP2*. The requirement of *NSP1* appears to be dependent on the Myc-LCO structure. The lateral root response to sulfated LCO is at least at low concentrations dependent on *NSP1*, whereas the response to non-sulfated Myc-LCO is not. Further, *nsp1* and *nsp2* mutants show reduced AM fungal colonization compared to wild-type plants (Delaux et al., 2013; Maillet et al., 2011). As in addition to their symbiotic role NSP1 and NSP2 are involved in the activation of SL biosynthesis genes and SLs are signaling molecules in AM, the deficient or reduced SL content in *nsp1* and *nsp2* mutants in host roots may explain the delayed AM colonization phenotype (Liu et al., 2011). Myc-LCOs also stimulate the expression of microRNA miR171h, which negatively regulates *NSP2* expression in the root elongation zone during AM

colonization (Lauressergues et al., 2012). This regulatory mechanism was proposed to prevent root over-colonization by AM fungi.

A mycorrhiza specific GRAS protein involved in the early steps of AM establishment is RAM1, which regulates the expression of *RAM2*, a glycerol-3-phosphate acyltransferase involved in cutin biosynthesis, which is a signaling molecule required for hyphopodia formation during the pre-infection stage (Gobbato et al., 2012; Wang et al., 2012).

NSP1 and 2 bind to and activate the *ERN1* promoter and ERN1 in turn activates the transcription of the early nodulin gene *ENOD11* (Cerri et al., 2012; Hirsch et al., 2009). ERN1 has a nodulation specific function and is predominantly associated with infection initiation and progression. The closely related ERN2 also plays a role during rhizobial infection and can replace ERN1 when expressed from the *ERN1* promoter (Cerri et al., 2012). Interestingly, *ERN2* expression is upregulated in AM infected cells corroborating the concept of a common accommodation program for symbiotic microbes, characterized by the functional diversification of a common ancestor which later evolved a RNS specific function in legumes (Cerri et al., 2012; Hogekamp et al., 2011; Kistner and Parniske, 2002; Young et al., 2011).

NIN is a nodulation specific RWP-RK domain containing transcription factor required for nodule formation and rhizobial infection (Marsh et al., 2007; Schauser et al., 1999). The *NIN* gene is rapidly (within a few hours) upregulated in response to Nod factor and its expression is severely hampered in *cyclops* mutants (Horvath et al., 2011; Yano et al., 2008). NIN has been shown to bind to the promoter of *Nodulation Pectate Lyase (NPL)* *in vitro* and the induction of a *NPL_{pro}:GUS* reporter was markedly reduced in a *L. japonicus nin* mutant compared to wild-type plants (Xie et al., 2012). NPL activity is required for the localized degradation of plant cell wall pectin during IT formation in root hair cells. Curiously, the *npl* mutant phenotype resembles that of *cyclops*, with the exception that in rare cases aberrantly infected nodules are formed. In addition, NIN has been also shown to directly target the promoters of *LjNF-YA1* and *LjNF-YB1*, which are two subunits of the heterotrimeric CAAT-box binding NF-Y complex (Soyano et al., 2013). Ectopic overexpression of *NIN* or the *NF-Y* subunits induced aberrant root cortical cell divisions, which led to the formation of primordia-like structures. Thus, this finding provides a mechanistic explanation how root nodule organogenesis is initiated. *LjNF-YA1* is the ortholog of *MtHAP2-1*, involved in the regulation of nodule development, which shows a distinct expression pattern in the meristematic zone of indeterminate nodules (Combiere et al., 2006). NF-Ys are also emerging as positive regulators of AM formation whose expression is negatively controlled by a mechanism termed autoregulation of mycorrhization (AOM) (Schaarschmidt et al., 2013). This mechanism is analogous to autoregulation of nodulation (AON) in RNS and, in a shoot-dependent manner, controls the extent

of AM colonization or nodulation, respectively (Mortier et al., 2012; Schaarschmidt et al., 2013).

5 Aims of the study

This study was conducted in order to better understand how symbiosis induced calcium spiking is decoded and transduced in the nucleus. CCaMK is generally considered as the prime candidate involved in the decoding and transduction of symbiotic calcium oscillations. Although both symbionts, AM fungi and rhizobia, elicit sustained calcium oscillations which presumably lead to the activation of CCaMK, the symbiotic responses are different. During RNS, CCaMK activation leads to the formation of root nodules, which are not formed during AM, although CCaMK in its autoactivated form is able to trigger the nodule organogenesis program. One hypothesis for the differential readout is that AM fungi and rhizobia elicit distinct calcium signatures which lead to the differential activation of CCaMK possibly via different requirements of the CCaMK calcium regulatory domains. Another possibility is that signaling specificity is mediated by additional components, which might be activated in a common sym gene independent manner. Evidence for such alternative, common sym gene independent pathways has been obtained recently for both symbioses (Gutjahr et al., 2008; Madsen et al., 2010). These pathways might confer signaling specificity via the Nod factor and Myc factor receptors.

In order to dissect whether the regulatory domains of CCaMK are differentially required for AM and RNS establishment, or involved in different processes during symbiosis establishment, a *CCaMK* mutant analysis was conducted. To this end, *CCaMK* mutant constructs were generated and introduced into a *L. japonicus ccamk* null mutant to analyse AM and RNS restoration and spontaneous nodule organogenesis *in vivo*. Furthermore, the *in vitro* kinase activity of the mutant proteins and their subcellular localization was determined and correlated to the *in vivo* activity. The results of this analysis are presented in chapter 1.

A suppressor screen conducted with the hypernodulating *L. japonicus har1-1* mutant line (Murray et al., 2006) identified the *ccamk-14* mutant, which is specifically impaired in cortical cell infection by AM fungi and rhizobia. Characterisation of this mutant concomitant with mass spectrometric autophosphorylation site analysis of calcium stimulated CCaMK discovered a novel autoregulatory mechanism. This mechanism involves autophosphorylation of the conserved residue S337 located in the CaM binding domain, which leads to CaM repulsion. This negative autoregulation is proposed to serve the deactivation of CCaMK once calcium oscillations cease and intracellular infection is completed. The results of the detailed *ccamk-14* mutant analysis are shown in chapter 2.

CCaMK's strong nuclear interaction with the protein of unknown function CYCLOPS, suggested that the calcium signal perceived by CCaMK is propagated via CYCLOPS to mediate the

appropriate symbiotic responses. The calcium/calmodulin dependent phosphorylation of CYCLOPS suggested that CYCLOPS' activity might be regulated by phosphorylation and that the phosphorylated CYCLOPS is the functionally active signaling molecule. To test this hypothesis, phosphorylation site analysis of CCaMK phosphorylated CYCLOPS was performed which pinpointed two regulatory sites whose functional characterization led to the identification of CYCLOPS as transcriptional regulator. The results of this study are summarized in chapter 3.

VI Results

Chapter 1: Functional characterization of CCaMK and the role of its regulatory domains in symbiosis

1 Summary

The two plant root endosymbioses, arbuscular mycorrhiza (AM) and root nodule symbiosis (RNS) use a common genetic program for symbiosis establishment. A hallmark of symbiosis signaling are perinuclear calcium oscillations initiating within minutes after symbiont recognition which are required for the transcriptional reprogramming accompanying symbiosis establishment. The nuclear calcium and calmodulin-dependent kinase (CCaMK) is the presumed decoder and transducer of the calcium spiking response. The molecule combines two calcium regulatory domains, a CaM binding domain (CaM-BD) and a visinin-like domain (VLD) comprising three calcium binding EF-hands. The presence of both domains in AM forming non-legume plants indicates that CCaMK executes a conserved function in both symbioses. However, the finding that a gain-of-function mutation in the autophosphorylation site of CCaMK triggers spontaneous nodule development in the absence of rhizobia suggested that CCaMK has acquired a novel function in RNS, associated with nodule organ development. As legume CCaMKs are proposed to be involved in the decoding of calcium spiking during both, AM and RNS signaling, it is still an open question why nodule organogenesis is not triggered during AM formation. In this study a CCaMK construct series with mutations in various calcium regulatory domains and in the autophosphorylation site was characterised *in vitro* and *in vivo*. This analysis revealed a less stringent requirement of the CaM-BD for the AM infection process with autoactivated constructs, but a strict requirement for rhizobial infection. Furthermore, ectopic activity of autoactivated constructs caused the extension of arbuscule development beyond inner cortical cell files, indicating a function of CCaMK in arbuscule differentiation. Excitingly, this analysis also revealed that AM fungi exert a negative effect on spontaneous nodulation, which presumably acts downstream of CCaMK.

2 Introduction

Entering root symbiosis with nutrient delivering microbes is an ancient strategy of plants to overcome nutrient shortage. Most (>80%) of the extant plant species can establish AM with the widespread fungi of the phylum *Glomeromycota* (Schüßler et al., 2001; Smith and Read, 2008). AM connects the plant root to the huge extraradical hyphal network in the soil, expanding the area exploited for nutrient uptake. In addition to AM, legume plants acquired the ability to form the evolutionary younger RNS with nitrogen-fixing rhizobia bacteria (Doyle, 2011; Sprent, 2007). Mutant analysis using the model legumes *Lotus japonicus* and *Medicago truncatula* revealed that

both symbioses utilize the same genetic components required for initial symbiotic signal transduction suggesting that the evolution of RNS was facilitated by the recruitment of AM symbiosis genes combined with an advantageous genetic predisposition for nodulation (Kistner and Parniske, 2002; Markmann and Parniske, 2009, Soltis et al., 1995). A hallmark of symbiosis signaling is the initiation of sustained perinuclear calcium oscillations which are detected within minutes after perception of symbiont-specific mycorrhization (Myc) or nodulation (Nod) factors by the corresponding LysM-domain receptor-like kinases (Bek et al., 2010; Ehrhardt et al., 1996; Genre et al., 2013; Lerouge et al., 1990; Madsen et al., 2003; Maillet et al., 2011; Op den Camp et al., 2011; Radutoiu et al., 2003). This calcium spiking response is presumed to activate symbiosis specific gene expression required for the synthesis of components mediating cellular rearrangements to accommodate the symbionts within root cells (Genre et al., 2005; Miwa et al., 2006a; van Brussel et al., 1992; Yokota et al., 2009). Subsequently, symbiont accommodation also leads to the development of the symbiotic exchange organs, phosphate-delivering arbuscules in AM and nitrogen-fixing root nodules in RNS, respectively. The establishment of both symbioses is dependent on a common set of genes (termed ‘common sym genes’) which encode the leucine-rich-repeat receptor-like kinase SYMRK, the ion channels CASTOR and POLLUX, the calcium ATPase pump MCA8, the NUCLEOPORINs (subunits of the nuclear pore complex) NUP85, NUP133 and NENA, a nuclear calcium- and calmodulin-dependent kinase (CCaMK) and CYCLOPS, a nuclear coiled-coil protein of unknown function (Ané et al., 2004; Charpentier et al., 2008; Endre et al., 2002; Gleason et al., 2006; Capoen et al., 2011; Groth et al., 2010; Horvath et al., 2011; Kanamori et al., 2006; Lévy et al., 2004; Mitra et al., 2004; Ovchinnikova et al., 2011; Saito et al., 2007; Stracke et al., 2002; Tirichine et al., 2006; Yano et al., 2008). Based on calcium spiking analysis in the corresponding mutants, SYMRK, CASTOR & POLLUX, MCA8 and the NUPs are conceptually placed upstream of calcium spiking and are implicated in the generation of the repetitive calcium signal, whereas CCaMK and CYCLOPS are positioned downstream as presumed decoders and transducers of the signal (Miwa et al., 2006b). Due to several characteristics it is common belief that CCaMK is the main target of the spikes. CCaMK is a calcium responsive kinase, composed of an N-terminal Ser/Thr kinase domain which is linked to two calcium sensing domains: A CaM-BD which overlaps with an autoinhibitory domain and a VLD comprising three EF-hand motifs (Patil et al., 1995; Tirichine et al., 2006). Biochemical characterization of lily (*Lilium longiflorum*) CCaMK has established a working model of CCaMK activation (Sathyanarayanan et al., 2000). The binding of calcium ions to the VLD induces autophosphorylation of the conserved residue LIT267 (LjT265/MtT271), which induces the exposure of the CaM-BD. Subsequent CaM binding leads to the full release of the kinase from

autoinhibition and promotes substrate phosphorylation. The importance of CCaMK in symbiosis signaling is also supported by its mutant phenotype, as *ccamk* mutants are absolutely symbiosis defective and show no phenotypic responses upon symbiotic stimulation (Lévy et al., 2004; Mitra et al., 2004; Perry et al., 2009). CCaMK interacts with and phosphorylates CYCLOPS suggesting, that the signal is transduced by CCaMK via CYCLOPS phosphorylation (Yano et al., 2008). However it is still unresolved how signaling specificity is achieved downstream of the nuclear CCaMK/CYCLOPS complex to activate AM and RNS specific readouts.

CCaMK and *CYCLOPS* orthologs are present in all major plant lineages including bryophytes, the common ancestor of land plants, and a conserved interaction between various bryophyte CCaMKs/DMI3s with the *Medicago* CYCLOPS ortholog IPD3 has been demonstrated (Wang et al., 2010a; Yano et al., 2008; Zhu et al., 2006). Further, the CCaMK ortholog of the AM forming monocot rice (*Oryza sativa*), OsCCaMK, was able to fully restore RNS in a *L. japonicus ccamk* mutant demonstrating a high degree of functional conservation (Banba et al., 2008). These observations indicate that both calcium regulatory domains of CCaMK play a role in AM and RNS establishment, but it is not clear whether there are differential requirements for these domains at different stages, or for different processes during symbiosis formation. The *L. japonicus snf1-1* mutant carrying a point mutation in the CCaMK autophosphorylation site (T265I) triggers the spontaneous formation of nodules in the absence of rhizobia (Tirichine et al., 2006). According to the working model of CCaMK activation, elevated calcium concentration, and thus presumably calcium spiking *in vivo*, induce autophosphorylation of CCaMK which *per se* can trigger nodule development. This exciting finding raises the question whether CCaMK activation via calcium oscillations elicited by AM fungi is different from the activation elicited by rhizobia, as nodules are not formed in AM symbiosis. Alternatively, AM fungi may exert an inhibitory effect, which suppresses the nodule organogenesis program in legume roots.

In order to examine in more detail the mechanism of CCaMK activation and the role of the distinct CCaMK regulatory domains in symbiosis formation, a CCaMK mutant series was constructed and analysed *in vivo* and *in vitro*. This analysis revealed differential requirements of the calcium regulatory domains for the two symbiotic processes nodule organogenesis and rhizobial infection and found a less stringent requirement for the calcium responsive domains to enable AM infection. However, an unusual AM phenotype was observed with two autoactivated constructs lacking both (CCaMK-1-314) or only one of the calcium regulatory domains (CCaMK-FNDD), where arbuscule formation extended into the outer cortical cell layer, indicating a certain degree of aberrant signaling. The phospho-ablative (CCaMK-T265A) and phospho-mimetic (CCaMK-T265D) autophosphorylation site mutants displayed differences in the proportion of infected versus

uninfected nodules, which might be due to different kinase activity levels. Interestingly, this analysis also revealed a significant (~50%) reduction of spontaneous nodules in the presence of AM fungi compared to asymbiotic cultivation conditions. This reduction was less severe (~20%), but still observed with the *snf2* mutant, encoding an autoactive cytokinin receptor (Lhk1-L266F) positioned downstream of CCaMK which triggers spontaneous nodulation (Tirichine et al., 2007). This important finding indicates that nodule organogenesis is attenuated in the presence of AM fungi and several possibilities concerning the cause of this inhibitory effect are discussed.

3 Results

3.1 The CCaMK domain structure and CCaMK mutant constructs used in this study

CCaMK (57.5 kDa) is composed of three distinct domains, an N-terminal Ser/Thr kinase domain, an autoinhibition domain overlapping with a CaM-BD and the C-terminal VLD comprising three EF-hand motifs (Figure 3A). Located within the kinase domain is a conserved autophosphorylation site T265, whose substitution by various amino acids (T265A, T265D, T265I), leads to the deregulation of the kinase conferring autoactivity (Gleason et al., 2006; Hayashi et al., 2010; Shimoda et al., 2012; Tirichine et al., 2006). In order to dissect domains and amino acid residues differentially required for RNS and AM, various CCaMK mutant constructs (Figure 3B) were expressed under the control of the *L. japonicus* ubiquitin promoter in the *L. japonicus ccamk-13* mutant and restoration of RNS and AM and the formation of spontaneous nodules was analysed. The *ccamk-13* mutant harbours a 7 bp insertion after G462 leading to a premature stop codon (Perry et al., 2009). The mutation leads to a predicted truncated protein with a putative molecular weight of 17.3 kDa, comprising amino acids 1-154 of the CCaMK protein plus seven additional amino acids (PPRGSQG). Protein blot analysis using three different polyclonal anti-LjCCaMK antibodies did not detect the truncated CCaMK protein suggesting that *ccamk-13* is a null mutant (Figure 4).

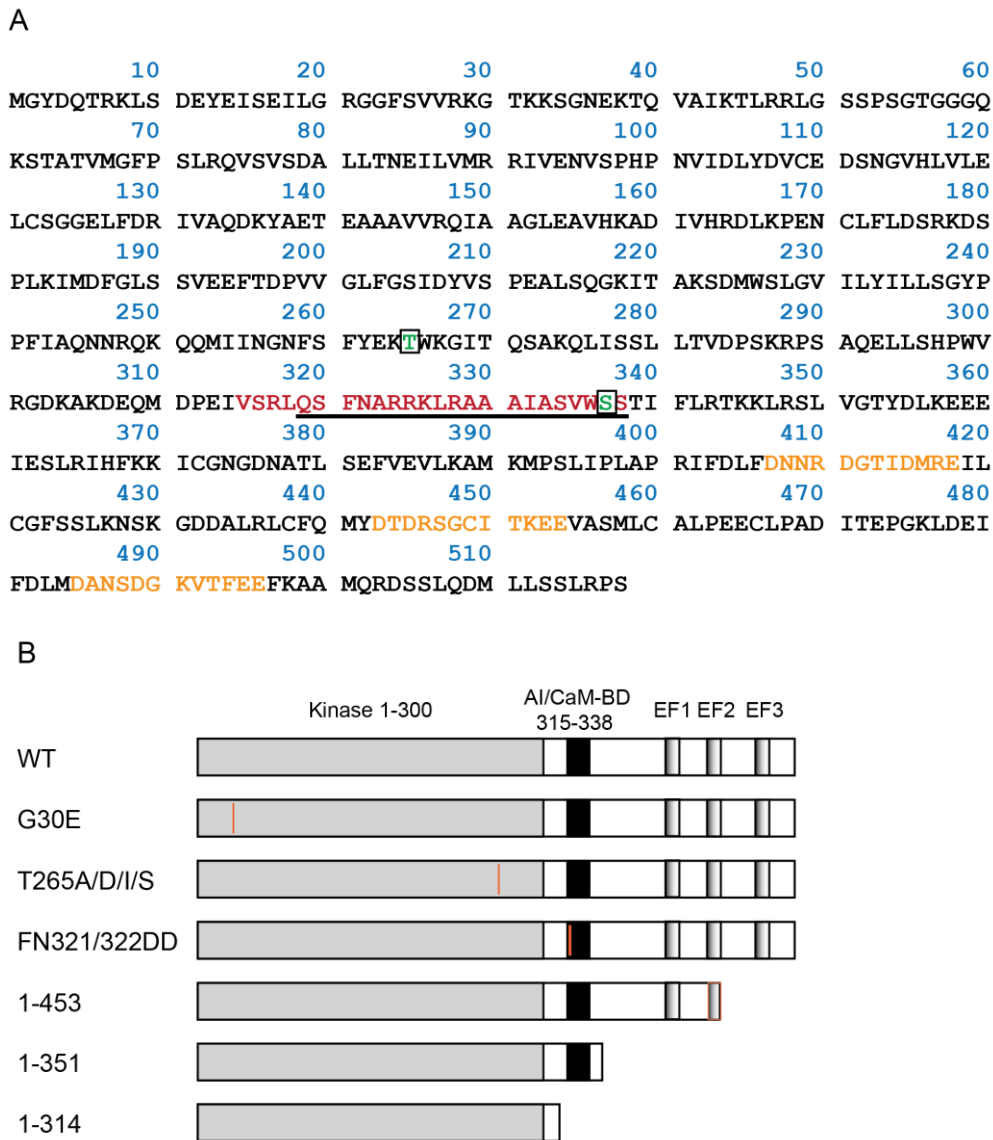


Figure 3. Overview of *L. japonicus* CCaMK domain structure and mutant derivatives.

(A) The wild-type *L. japonicus* CCaMK protein is composed of an N-terminal Ser/Thr kinase domain (aa 1-300), an overlapping autoinhibition and calmodulin binding domain (AI/CaM-BD, aa 315-338/319-338, depicted in red, CaM-BD underlined) and a visinin-like domain comprising three calcium ion binding EF-hand motifs (EF1: aa 407-418, EF2: aa 443-454, EF3: aa 485-496, depicted in orange). T265 and S337 are regulatory autophosphorylation sites located in the kinase domain and AI/CaM-BD, respectively (depicted in green and boxed).

(B) Schematic representation of CCaMK mutant derivatives. CCaMK-G30E is a kinase-dead mutant which corresponds to the *ccamk-3* mutant allele and is impaired in RNS and AM (Perry et al., 2009). CCaMK-T265A, CCaMK-T265D, CCaMK-T265I (corresponding to the deregulated *snf1-1* allele) and CCaMK-T265S are autophosphorylation site mutants. Replacement of the threonine residue by aspartic acid (D, phospho-mimetic version) or isoleucine (I) lead to a deregulated autoactive kinase conferring spontaneous nodulation (Hayashi et al., 2010; Tirichine et al., 2006). CCaMK-T265A represents the phospho-ablative version. CCaMK-T265S substitutes threonine by a serine phosphorylation site. CCaMK-FN321/322DD (CCaMK-FNDD) is a mutant affected in the CaM-BD which was generated analogous to the CaMKII FN-ED mutant, (Yang and Schulman, 1999). CCaMK-1-453, is a truncated mutant where EF-hand 1 is retained, EF-hand 2 lacks the invariant chelating glutamate residue at position 12 and EF-hand 3 is missing. CCaMK-1-351, is a truncated version lacking EF-hands 1-3. CCaMK-1-314 consists only of the kinase domain.

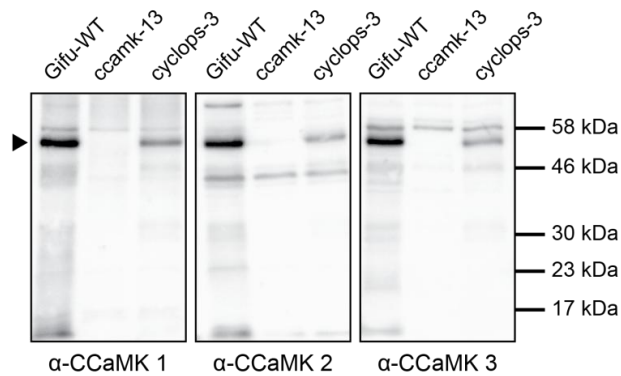


Figure 4. Immunodetection of CCaMK in root extract of the *ccamk-13* mutant.

Immunodetection of CCaMK in protein extracts prepared from equal amounts of root material (20 roots from 8 days old seedlings) obtained from the *L. japonicus* Gifu wild-type, *ccamk-13* and *cyclops-3* mutants. SDS-PAGE (10%) resolved protein extracts were blotted onto a PVDF membrane and probed with three different polyclonal CCaMK antibodies (α -CCaMK-1, -2, or -3). The full-length CCaMK protein (57.5 kDa, indicated by an arrowhead) is detected in the Gifu wild-type and the *cyclops-3* mutant. The predicted peptide encoded by the *ccamk-13* mutant (CCaMK-1-154 + PPRGSQG, 17.3 kDa) is not detected.

3.2 Restoration of RNS in the *L. japonicus ccamk-13* mutant by CCaMK mutant versions

The results of RNS complementation by the CCaMK mutant derivatives are illustrated in Figure 5 and Table 1. The *L. japonicus* Gifu wild-type was used as positive control and all plants developed an average number of 15 *M. loti* DsRed infected nodules. Compared to Gifu wild-type plants, overexpression of wild-type CCaMK in *ccamk-13* mutant roots led to a significant (66%) increase in nodule number (25 nodules per transformed root system) (Figure 5C, Table 1). Exclusively infected nodules were also formed with CCaMK-T265S and the truncated versions CCaMK-1-351 and CCaMK-1-453, albeit a certain degree of impairment was observed with CCaMK-1-453, where only 57% of the transformed root systems formed infected root nodules, while the rest formed none (Figure 5A, B and Table 1). This result may indicate insufficient penetrance of the mutant protein. Mixed (*M. loti*-DsRed infected and uninfected) nodules were formed with CCaMK-T265A and CCaMK-T265D. Strikingly, >50% of the nodules formed on roots expressing CCaMK-T265D were uninfected whereas the majority (89%) of the nodules on roots transformed with CCaMK-T265A was infected (Figure 5A, C and Table 1). This finding suggests that the phospho-ablative and phospho-mimetic form of T265 behave different and that autophosphorylation may negatively impact on the infection process. Plants expressing CCaMK-FNDD and CCaMK-1-314 developed 3-4 spontaneous, uninfected nodules with lower frequency (25-30%), which compared to either infected wild-type nodules or spontaneous nodules formed by CCaMK-T265A or CCaMK-T265D appeared to be smaller (Figure 5 A-C, Table 1). Taken together, CCaMK-T265S and CCaMK-1-351 restored RNS wild-type-like. CCaMK-1-453 also restored RNS wild-type-like, but the complementation efficiency was significantly reduced. CCaMK-T265A and CCaMK-T265D partly lacked synchronisation between nodule organogenesis and infection, which was more pronounced with CCaMK-T265D. CCaMK-FNDD and CCaMK-1-314 with low efficiency formed empty uninfected nodules.

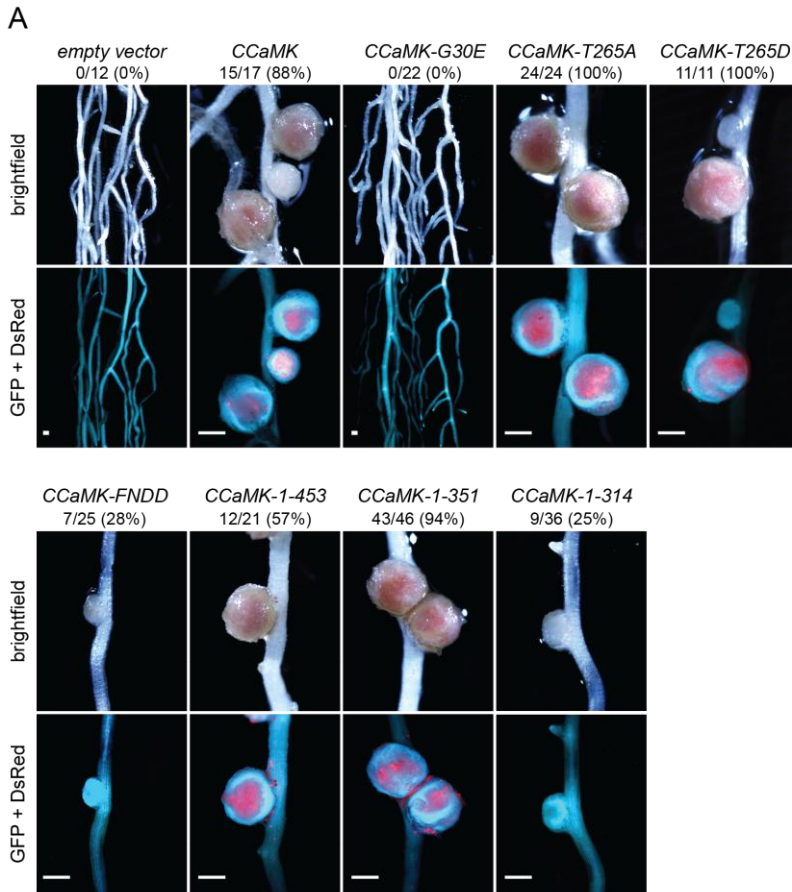


Figure 5. Restoration of RNS in the *L. japonicus ccamk-13* mutant by various CCaMK versions.

Transgenic roots expressing various CCaMK versions (as indicated) under the control of the *L. japonicus* ubiquitin promoter were co-cultivated with *M. loti*-DsRed for 4 weeks and restoration of RNS was evaluated. RNS was restored, if *M. loti*-DsRed infected root nodules were observed (visualized with a DsRed fluorescence filter). Transformed root systems were selected based on the GFP transformation marker (visualised with a GFP filter). Scale bars: 0.5 mm.

(A) The empty vector control and CCaMK-G30E did not restore RNS. Infected root nodules were formed on plants expressing CCaMK-WT, CCaMK-T265A, CCaMK-T265D, CCaMK-1-453 and CCaMK-1-351, whereby part of the nodules formed by CCaMK-T265A and CCaMK-T265D were uninfected (see quantification in C). Expression of CCaMK-FNDD and CCaMK-1-314 induced the formation of small uninfected nodules. Upper pictures show brightfield images, lower pictures show overlay of micrographs recorded with GFP and DsRed filters.

Numbers below construct names indicate number of root systems with root nodules per number of total transformed root systems analysed. (B) Graph showing the percentage of transformed root systems which developed infected root nodules upon expression of the indicated constructs. CCaMK-FNDD and CCaMK-1-314 did not restore the formation of infected root nodules, only uninfected nodules were formed (shown in C). Formation of infected root nodules was impaired in 43% of the root systems transformed with CCaMK-1-453, indicating a certain degree of impairment in the penetrance of this mutant protein.

(C) Graph showing the average number of infected (grey bars) and uninfected (white bars) root nodules per transformed, nodulated root system. Note that >50% of the nodules formed with CCaMK-T265D were uninfected, while CCaMK-T265A produced only 11% uninfected nodules. Error bars represent SE. Shown are data obtained from one experimental set-up, n=8-46.

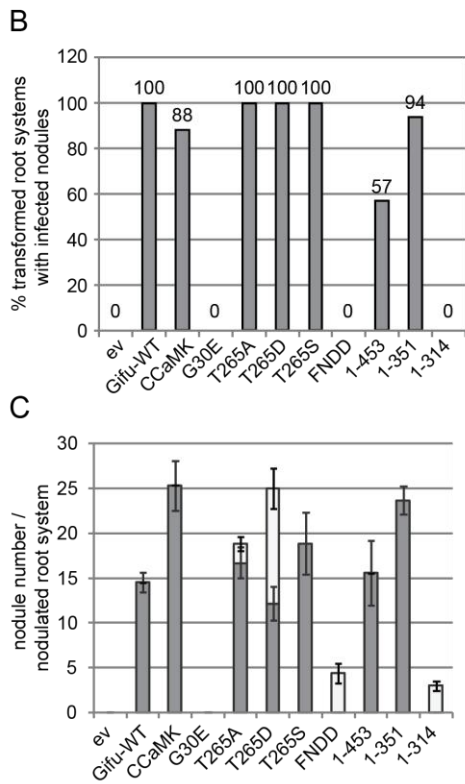


Table 1. Restoration of RNS in the *L. japonicus ccamk-13* mutant by various *CCaMK* versions.

Plant genotype	Transgene	Nod+ (%) ^a	# Nod/ Nod+Plant ^b	#infected Nod ^c	#uninfected Nod ^d
Gifu WT	no	13/13 (100%)	15 (± 1.1)	15 (± 1.1)	0
<i>ccamk-13</i>	<i>pUB:empty vector</i>	0/12 (0%)	0	0	0
<i>ccamk-13</i>	<i>pUB:CCaMK</i>	15/17 (88%)	25 (± 2.7)	25 (± 2.7)	0
<i>ccamk-13</i>	<i>pUB:CCaMK-G30E</i>	0/22 (0%)	0	0	0
<i>ccamk-13</i>	<i>pUB:CCaMK-T265A</i>	24/24 (100%)	19	17 (± 1.7)	2 (± 0.8)
<i>ccamk-13</i>	<i>pUB:CCaMK-T265D</i>	11/11 (100%)	25	12 (± 1.9)	13 (± 2.2)
<i>ccamk-13</i>	<i>pUB:CCaMK-T265S</i>	8/8 (100%)	19 (± 3.5)	19 (± 3.5)	0
<i>ccamk-13</i>	<i>pUB:CCaMK-FNDD</i>	7/25 (28%)	4 (± 1.1)	0	4 (± 1.1)
<i>ccamk-13</i>	<i>pUB:CCaMK-1-453</i>	12/21 (57%)	16 (± 3.6)	16 (± 3.6)	0
<i>ccamk-13</i>	<i>pUB:CCaMK-1-351</i>	43/46 (94%)	24 (± 1.6)	24 (± 1.6)	0
<i>ccamk-13</i>	<i>pUB:CCaMK-1-314</i>	9/36 (25%)	3 (± 0.5)	0	3 (± 0.5)

^aNumber of root systems with root nodules per number of total transformed root systems analysed. Transformed roots were analysed 4 weeks post *M. loti*-DsRed inoculation.

^bAverage number of nodules per nodulated root system \pm SE.

^cAverage number of infected nodules per nodulated root system \pm SE.

^dAverage number of uninfected nodules per nodulated root system \pm SE.

3.3 Restoration of AM in the *L. japonicus ccamk-13* mutant by *CCaMK* mutant versions

The results of the AM complementation analysis are illustrated in Figures 6 and 7 and Tables 2 and 3. All symbiotic structures characterizing successful AM establishment, including arbuscules, vesicles and intraradical hyphae, were observed in *L. japonicus ccamk-13* roots expressing wild-type *CCaMK* (Figure 6).

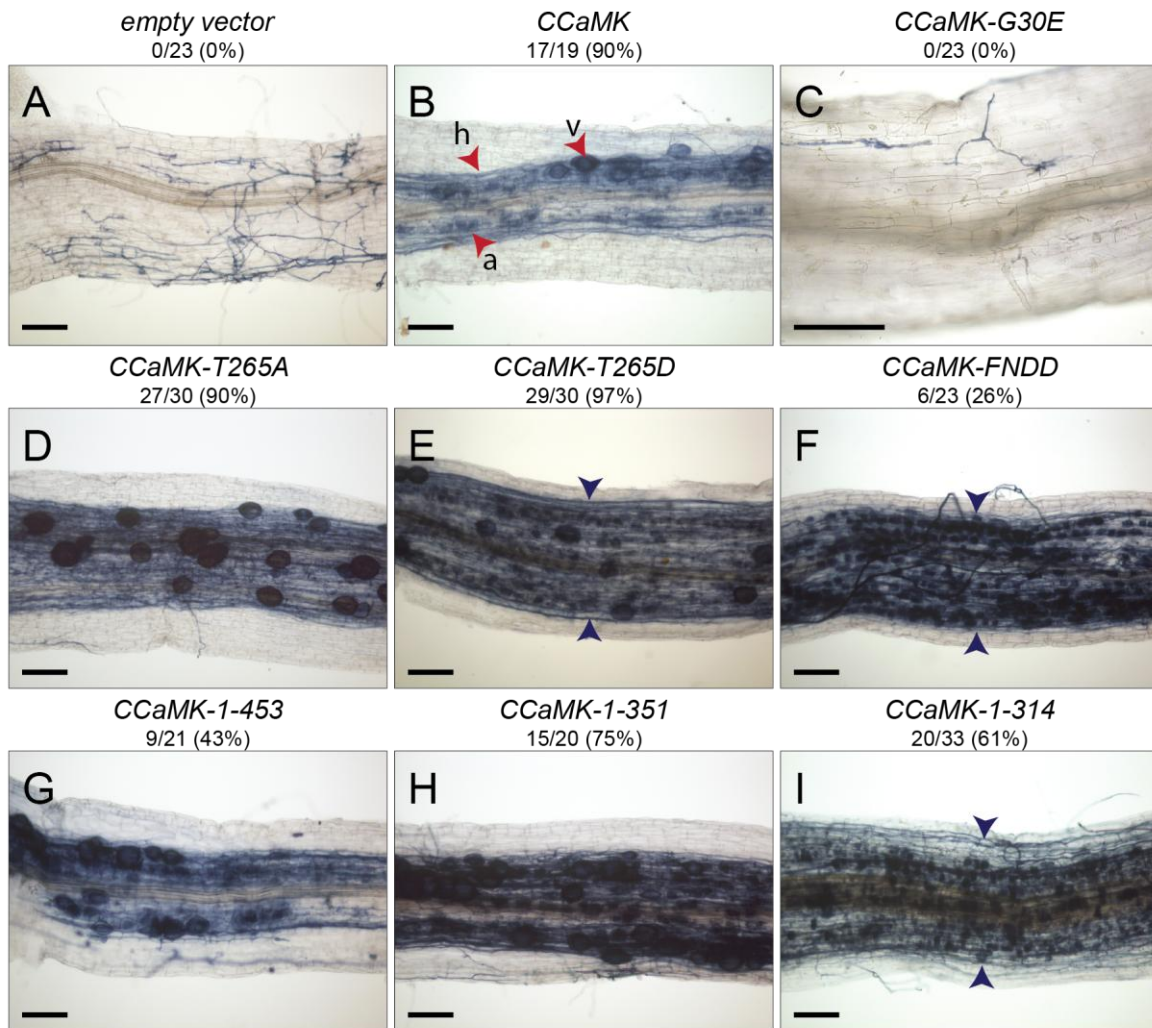


Figure 6. Restoration of AM in the *L. japonicus* *ccamk-13* mutant by various *CCaMK* versions.

Transgenic roots expressing various *CCaMK* versions (as indicated) under the control of the *L. japonicus* ubiquitin promoter were cocultivated with the AM fungus *R. irregularis* for 4 weeks and restoration of AM was evaluated by brightfield microscopy of ink stained root systems. Numbers below construct names indicate number of transformed root systems showing restoration of AM per total number of transformed root systems analysed and are also given as percent values. Scale bars: 100 μ m. Red arrowheads in (B) indicate the following AM fungal structures: a= arbuscule, h= hypha, v= vesicle.

(A,C) AM was not restored in roots transformed with the empty vector control and *CCaMK*-G30E, as only superficial hyphal colonization, but no arbuscule formation was observed.

(B,D-I) Expression of *CCaMK*-WT, *CCaMK*-T265A, *CCaMK*-T265D, *CCaMK*-FNDD, *CCaMK*-1-453, *CCaMK*-1-351 and *CCaMK*-1-314 restored AM formation. In all cases dense intraradical hyphal colonization and the formation of arbuscules was observed. Note the striking extension of the arbuscule containing cell layers into the outer cortical cell files (marked by blue arrowheads) in roots expressing *CCaMK*-T265D, *CCaMK*-FNDD and *CCaMK*-1-314.

All mutant constructs except CCaMK-G30E, where only extraradical hyphae were observed, restored AM formation in *ccamk-13* mutant roots, but differences in the extent and efficiency of AM colonization were observed (Figure 6 and 7A, B and Table 2). AM was only restored in 26% (CCaMK-FNDD), 43% (CCaMK-1-453), 61% (CCaMK-1-314) and 75% (CCaMK-1-351) of the corresponding transformed roots which was significantly reduced when compared to CCaMK-WT (90%), CCaMK-T265A (90%) and CCaMK-T265D (97%). In addition, the proportion of the symbiotic structures, per AM fungal colonized root length was markedly reduced in roots expressing CCaMK-FNDD, or the three truncated versions (25% - 43% arbuscule and/or vesicle formation) compared to those expressing CCaMK-WT, CCaMK-T265A or -T265D (78% - 87% arbuscule and/or vesicle formation) (Figure 7B, Table 2). Microscopic analysis of AM colonized root segments indicated that the expression of some of the auto-activated constructs permitted an over-colonization of the root with extension of arbusculated cell files into the outer cortical cell layers (Figure 6 E, F, I). In order to test whether this finding was significant, the number of arbusculated cell layers (counted from one side of the vascular bundle) was quantified for each construct (see materials and methods) (Figure 7C and Table 3). Expression of wild-type CCaMK led to the formation of maximal three cortical cell layers (15%), but mainly two cell layers (60%) were formed. Strikingly, expression of CCaMK-FNDD resulted in a significant extension of the cell layers beyond the inner cortical cells, with 58% of the colonized root segments developing 4-5 cell files. Further, a weak tendency towards cell layer extension was also observed with the auto-activated versions CCaMK-1-314, CCaMK-T265D and CCaMK-T265A where 19%, 12% and 7% of the colonized root segments developed 4-5 cell files.

Table 2. AM fungal root length colonization of *L. japonicus ccamk-13* roots expressing various *CCaMK* versions.

Transgene ^a	% no col.	% hyphae	% vesicles	% arbuscules	% arbuscules & vesicles
<i>pUB:empty vector</i>	42 (±6.5)	58 (±6.5)	0	0	0
<i>pUB:CCaMK-G30E</i>	62 (±4.9)	38 (±4.9)	0	0	0
<i>pUB:CCaMK</i>	2 (±1.0)	9 (±0.9)	3 (±1.2)	50 (±5.5)	36 (±4.9)
<i>pUB:CCaMK-T265A</i>	3 (±1.8)	15 (±4.3)	4 (±1.7)	48 (±2.0)	30 (±5.9)
<i>pUB:CCaMK-T265D</i>	6 (±3.7)	6 (±1.2)	1 (±0.6)	49 (±5.7)	38 (±3.8)
<i>pUB:CCaMK-FNDD</i>	43.5 (±1.9)	31 (±3.6)	1 (±0.7)	18 (±4.4)	6.5 (±0.3)
<i>pUB:CCaMK-1-453</i>	37 (±3.6)	25 (±3.2)	1 (±0.3)	19 (±3.3)	18 (±0.9)
<i>pUB:CCaMK-1-351</i>	18 (±7.9)	32 (±3.1)	11 (±1.5)	14 (±2.4)	26 (±6.0)
<i>pUB:CCaMK-1-314</i>	24 (±1.7)	32 (±10.1)	1 (±0.9)	35 (±6.1)	8 (±2.8)

^aThree root systems per construct were analysed. Given are average values in percent for each category ± SE.
col.: colonization.

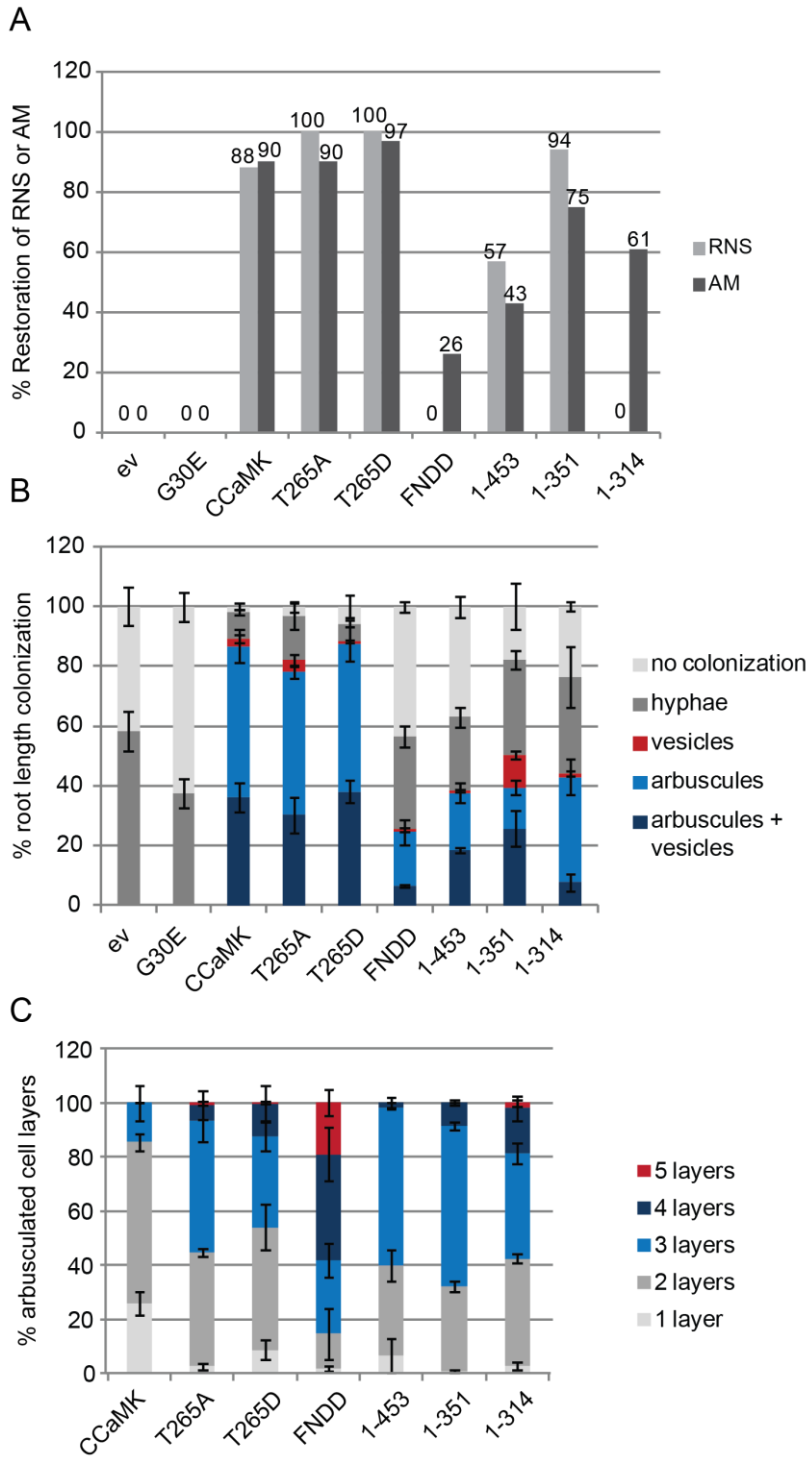


Figure 7. Quantitative analysis of AM restoration in *L. japonicus ccamk-13* mutant roots expressing various CcCaMK versions.

Transgenic roots expressing various CcCaMK versions (as indicated) under the control of the *L. japonicus* ubiquitin promoter were co-cultivated with the AM fungus *R. irregularis* for 4 weeks and restoration of AM was quantified by brightfield microscopy of ink stained root systems.

(A) Graph showing the percentage of transformed root systems evaluated as AM positive due to the formation of arbuscule containing cells (dark grey bars). For comparison, the percentage of transformed root systems showing successful RNS restoration due to the formation of infected nodules 4 weeks post *M. loti*-DsRed inoculation is depicted side-by-side (light grey bars, duplicated values of Figure 5B).

(B) Quantitative AM analysis using the line intersect method. The presence of the following categories was scored per intersect (in a total of 100 intersects): No AM fungal colonization, hyphae, vesicles, arbuscules, arbuscules + vesicles. The proportion (%) of the individual categories is given for each construct (depicted as percent root length colonization). The mean values obtained from the analysis of three root systems are given for the indicated categories. Error bars represent SE.

(C) Quantitative analysis of the number of arbusculated cell files. The number of arbusculated cell files (ranging from 1-5 and calculated from one side of the vascular system) was scored per arbusculated intersect (in a total of 100 arbusculated intersects). Mean values of arbusculated cell files for each construct were obtained from the analysis of three root systems. Error bars represent SE.

Table 3. Quantification of arbusculated cell files in *L. japonicus ccamk-13* roots expressing various CCaMK versions.

Transgene	% ^a 1 layer	% ^a 2 layers	% ^a 3 layers	% ^a 4 layers	% ^a 5 layers
<i>pUB:CCaMK</i>	25 (±4.4)	60 (±3.2)	15 (±6.6)	0.0	0.0
<i>pUB:CCaMK-T265A</i>	2 (±1.4)	42 (±1.4)	49 (±7.5)	6 (±5.2)	1 (±0.8)
<i>pUB:CCaMK-T265D</i>	8.6 (±3.7)	45 (±8.5)	34 (±5.6)	12 (±6.8)	0.4 (±0.4)
<i>pUB:CCaMK-FNDD</i>	2 (±0.9)	13 (±9.4)	27 (±6.3)	39 (±9.9)	19 (±4.8)
<i>pUB:CCaMK-1-453</i>	6 (±6.5)	33 (±5.8)	58 (±0.2)	2 (±2.0)	0.0
<i>pUB:CCaMK-1-351</i>	1 (±0.6)	31 (±1.8)	59 (±1.5)	8 (±1.0)	0.0
<i>pUB:CCaMK-1-314</i>	3 (±1.3)	40 (±1.9)	39 (± 4.1)	17 (±4.6)	2 (±1.1)

^a100 arbusculated intersects were scored per transformed root system and the number of arbusculated cell layers was determined (counted from one side of the vascular bundle) per intersect. Three root systems per construct (transgene) were analysed. Given are average values in percent for each category ± SE.

3.4 Formation of spontaneous nodules in the *L. japonicus ccamk-13* mutant by CCaMK mutant versions

The results of spontaneous nodule formation under asymbiotic conditions and in the presence of the AM fungus *R. irregularis* are illustrated in Figure 8 and in Tables 4 and 5. As has been reported previously, expression of CCaMK autophosphorylation site mutants, or of the kinase domain alone (*L. japonicus* CCaMK-1-314, or *M. truncatula* DMI3-1-311) leads to spontaneous nodule development in the absence of rhizobia (Gleason et al., 2006; Tirichine et al., 2006). In order to reproduce these results and find out whether other CCaMK mutant versions are also able to spontaneously trigger the nodulation program, all constructs were transformed into the *ccamk-13* mutant, incubated in the absence of rhizobia and spontaneous nodule formation was analysed 7 weeks post transformation (or 5 weeks post transplantation into sterile soil, respectively). In addition, in order to evaluate whether the mycorrhizal interaction influences spontaneous nodule development, the same construct series was also tested for spontaneous nodule formation in the presence of *R. irregularis*. Expression of wild-type CCaMK and the empty vector was used as negative control, *snf1-1* and *snf2* plants were used as positive controls.

Under both cultivation conditions spontaneous nodules were not observed on roots expressing wild-type CCaMK, or the empty vector control (Figure 8, Tables 4 and 5). On plants transformed with CCaMK-T265A, CCaMK-T265D, CCaMK-T265S, CCaMK-FNDD, CCaMK-1-314 and on control plants (*snf1-1* and *snf2*) spontaneous nodules were formed under asymbiotic conditions and also during cocultivation with AM fungi (Figure 8, Tables 4 and 5). Spontaneous nodule numbers induced by CCaMK-T265A and CCaMK-T265D under asymbiotic conditions did not significantly differ from the average nodule number formed on

snf1-1 mutant roots ($p>0.01$) (Figure 8B, Table 4). However, the average nodule number formed on *snf2* roots significantly differed from the number formed on *snf1-1* roots ($p<0.01$). Furthermore, the spontaneous nodulation frequencies and nodule numbers induced by CCaMK-FNDD and CCaMK-1-314 were markedly lower compared to those induced by the autophosphorylation site mutants (CCaMK-T265A and CCaMK-T265D). Curiously, also the expression of *CCaMK-T265S* induced spontaneous nodules with low frequency (Figure 8, Tables 4 and 5), indicating that negative regulation of CCaMK is strictly dependent on the endogenous autophosphorylation site and that even similar substitutions impact on the negative autoregulatory mechanism of CCaMK.

Spontaneous nodules were also formed upon expression of the same mutant proteins during cocultivation with AM fungi, but strikingly, in all cases a decrease in nodule number was observed (Figures 8B, C and Tables 4 and 5). A statistically significant reduction during AM fungal cocultivation was found with the autophosphorylation site mutants *snf1-1* (52% reduction, from 31 to 15 nodules), CCaMK-T265A (46% reduction, from 28 to 15 nodules) and CCaMK-T265D (57% reduction, from 23 to 10 nodules). Furthermore, a significant reduction (22% reduction, from 9 to 7 nodules) was observed with *snf2* plants, which was less pronounced compared to the reduction observed with the CCaMK autophosphorylation site mutants. Taken together this unexpected finding suggests that AM fungal cocultivation exerts a negative effect on spontaneous nodulation.

To find out whether this negative regulatory effect is directly affecting CCaMK protein abundance, immunoblot analysis on protein extracts prepared from *snf1-1* roots (and also from *snf2* roots), cultivated in the absence and presence of AM fungi was performed. This analysis showed no difference in the CCaMK protein levels of *snf1-1* roots cultivated in either condition, whereas in *snf2* roots even slightly more CCaMK protein was detected in samples cultivated with AM fungi (Figure 8C). This result suggested that the reduction of spontaneous nodule number in the presence of AM fungi is not caused by a decrease of the CCaMK protein level.

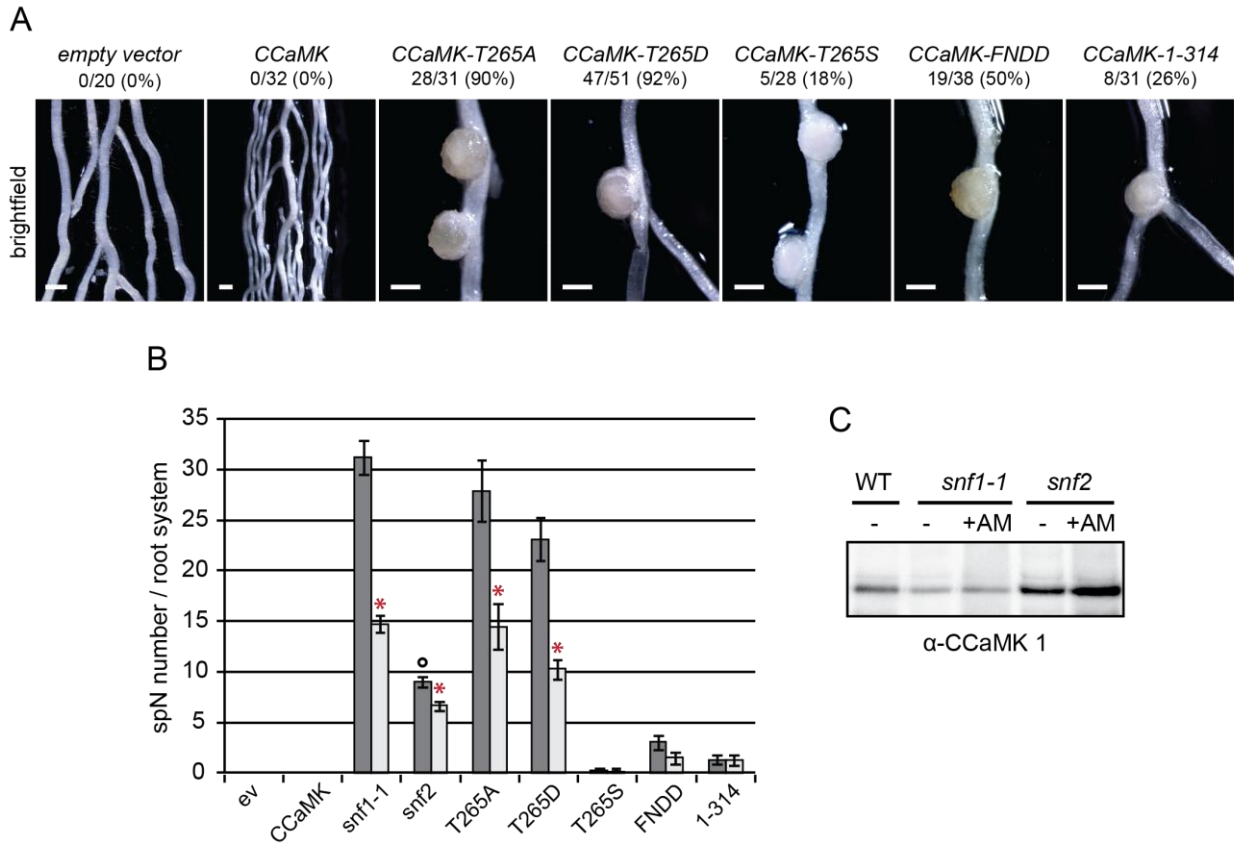


Figure 8. Induction of spontaneous nodules in the *L. japonicus ccamk-13* mutant by CCaMK mutant versions.

Transgenic *L. japonicus ccamk-13* roots expressing various CCaMK versions (as indicated) under the control of the *L. japonicus* ubiquitin promoter were cultivated under asymbiotic conditions, or cocultivated with the AM fungus *R. irregularis* for 5 weeks. The formation of spontaneous nodules was analysed 7 weeks post hairy root transformation. *snf1-1* and *snf2* plants were used as controls and analysed 7 weeks post germination, or 5 weeks post cultivation under asymbiotic conditions or with AM fungi, respectively. spN: spontaneous nodule.

(A) Spontaneous nodules were induced on *ccamk-13* roots upon expression of CCaMK-T265A, CCaMK-T265D, CCaMK-T265S, CCaMK-FNDD and CCaMK-1-314. No spontaneous nodules were formed upon expression of the empty vector control, or wild-type CCaMK. Numbers below construct names indicate number of root systems with spontaneous nodules per number of transformed root systems analysed and are also given as percent values. Scale bars: 0.5 mm.

(B) Spontaneous nodule number induced by the individual constructs (as indicated) or in *snf1-1* and *snf2* mutant roots is reduced upon cocultivation with the AM fungus *R. irregularis*. Dark grey bars depict spontaneous nodule numbers induced under asymbiotic cultivation, light grey bars depict spontaneous nodule numbers formed after cocultivation with the AM fungus *R. irregularis*. Bars represent average value of spontaneous nodule number per transformed root system and SE. Red asterisks and black circle indicate significance levels determined by Student's t-test ($p < 0.01$), whereby red asterisks represent significance levels between asymbiotic cultivation condition and cultivation in the presence of the AM fungus and black circle indicates significance level of spontaneous nodule numbers related to *snf1-1*.

(C) Immunodetection of CCaMK protein levels in *L. japonicus* Gifu wild-type (WT), *snf1-1* and *snf2* root extracts after cultivation under asymbiotic conditions (-), or cocultivation with *R. irregularis* (+AM) for five weeks. Protein blot analysis was performed on protein extracts prepared from equal amounts of spontaneously nodulated root material (three root systems per sample). SDS-PAGE (10%) resolved and blotted protein extracts were probed with a polyclonal CCaMK antibody (α -CCaMK 1).

Table 4. Spontaneous nodule formation under asymbiotic conditions.

Plant Genotype	Transgene	SpN+ (%) ^a	#SpN/SpN+ root ^b	#SpN/total roots ^c
<i>ccamk-13</i>	<i>pUB:empty vector</i>	0/20 (0%)	0	0
<i>ccamk-13</i>	<i>pUB:CCaMK</i>	0/32 (0%)	0	0
<i>ccamk-13</i>	<i>pUB:CCaMK-G30E</i>	0/24 (0%)	0	0
<i>ccamk-13</i>	<i>pUB:CCaMK-T265A</i>	28/31 (90%)	31 (± 2.8)	28 (± 3.0)
<i>ccamk-13</i>	<i>pUB:CCaMK-T265D</i>	47/51 (92%)	25 (± 2.1)	23 (± 2.1)
<i>ccamk-13</i>	<i>pUB:CCaMK-T265S</i>	5/28 (18%)	1 (± 0.2)	0.2 (± 0.1)
<i>ccamk-13</i>	<i>pUB:CCaMK-FNDD</i>	19/38 (50%)	6 (± 0.9)	3 (± 0.7)
<i>ccamk-13</i>	<i>pUB:CCaMK-1-453</i>	0/30 (0%)	0	0
<i>ccamk-13</i>	<i>pUB:CCaMK-1-351</i>	0/19 (0%)	0	0
<i>ccamk-13</i>	<i>pUB:CCaMK-1-314</i>	8/31 (26%)	5 (± 1.1)	1.3 (± 0.5)
<i>snf1-1</i>	no	65/65 (100%)	31 (± 1.7)	31 (± 1.7)
<i>snf2</i>	no	81/81 (100%)	9 (± 0.5)	9 (± 0.5)

^aSpN+: Number of root systems with spontaneous nodules per number of transformed root systems analysed. Spontaneous nodules were scored 7 weeks post transformation.

^bAverage number of spontaneous nodules per spontaneously nodulated root system \pm SE.

^cAverage number of spontaneous nodules per total number of root systems analysed \pm SE.

Table 5. Spontaneous nodule formation in the presence of the AM fungus *R. irregularis*.

Plant Genotype	Transgene	SpN+ (%) ^a	#SpN/SpN+ root ^b	#SpN/total roots ^c
<i>ccamk-13</i>	<i>pUB:empty vector</i>	0/15 (0%)	0	0
<i>ccamk-13</i>	<i>pUB:CCaMK</i>	0/17 (0%)	0	0
<i>ccamk-13</i>	<i>pUB:CCaMK-G30E</i>	0/23 (0%)	0	0
<i>ccamk-13</i>	<i>pUB:CCaMK-T265A</i>	19/22 (86%)	17 (± 2.2)	15 (± 2.3)
<i>ccamk-13</i>	<i>pUB:CCaMK-T265D</i>	42/44 (96%)	11 (± 0.9)	10 (± 1.0)
<i>ccamk-13</i>	<i>pUB:CCaMK-T265S</i>	1/23 (4%)	2 (n.d)	0.1 (± 0.1)
<i>ccamk-13</i>	<i>pUB:CCaMK-FNDD</i>	9/24 (38%)	4 (± 1.2)	1.5 (± 0.6)
<i>ccamk-13</i>	<i>pUB:CCaMK-1-453</i>	0/37 (0%)	0	0
<i>ccamk-13</i>	<i>pUB:CCaMK-1-351</i>	0/21 (0%)	0	0
<i>ccamk-13</i>	<i>pUB:CCaMK-1-314</i>	7/29 (24%)	5 (± 1.2)	1.2 (± 0.5)
<i>snf1-1</i>	no	66/66 (100%)	15 (± 0.8)	15 (± 0.8)
<i>snf2-2</i>	no	42/42 (100%)	7 (± 0.4)	7 (± 0.4)

^aSpN+: Number of root systems with spontaneous nodules per number of transformed root systems analysed. Spontaneous nodules were scored 7 weeks post transformation and 5 weeks post cocultivation with the AM fungus.

^bAverage number of spontaneous nodules per spontaneously nodulated root system \pm SE.

^cAverage number of spontaneous nodules per total number of root systems analysed \pm SE.

(n.d.): not determined due to insufficient spontaneous nodulation events (n=1).

3.5 *In vitro* kinase activity of CCaMK mutant proteins

The results of the *in vitro* kinase assays are shown in Figure 9. To correlate the *in vivo* activity of the individual CCaMK derivatives with their kinase activity, *in vitro* kinase assays with recombinant N-terminal maltose-binding-protein tagged CCaMK proteins and myelin basic protein (MBP) (Figure 9A), or CYCLOPS-81-366 (Figure 9B) as substrate were carried out. Wild-type CCaMK showed low autophosphorylation activity in the presence of calcium and $\text{Ca}^{2+}/\text{CaM}$. Phosphorylation of MBP and CYCLOPS-81-366 was observed in the presence of calcium and increased strongly upon addition of $\text{Ca}^{2+}/\text{CaM}$, as has been observed previously (Tirichine et al., 2006; Yano et al., 2008). Considering the autophosphorylation site mutants, only CCaMK-T265I showed no autophosphorylation activity, while CCaMK-T265A showed faint autophosphorylation with calcium and $\text{Ca}^{2+}/\text{CaM}$. Further, CCaMK-T265D showed high autophosphorylation levels with calcium and a further increase with $\text{Ca}^{2+}/\text{CaM}$. This finding indicated that apart from T265 additional CCaMK autophosphorylation sites with a putative autoregulatory function exist. Furthermore, the strong autophosphorylation activity of the phospho-mimetic form CCaMK-T265D suggests, that autophosphorylation at T265 may trigger autophosphorylation of further regulatory CCaMK sites.

With regard to substrate phosphorylation activity, the autophosphorylation site mutants showed remarkable variation. CCaMK-T265A showed slightly weaker MBP phosphorylation compared to the CCaMK wild-type protein, while CCaMK-T265I activity towards MBP was only faintly detected. On the other hand, substrate phosphorylation by CCaMK-T265D by far exceeded wild-type activity. The truncated mutants CCaMK-1-351 and CCaMK-1-453 performed equally low in their autophosphorylation and MBP substrate phosphorylation activity. Autophosphorylation activity was undetectable with the kinase mutant CCaMK-1-314 and MBP phosphorylation appeared weaker compared to CCaMK-1-351, or CCaMK-1-453, respectively. No kinase activity was detected when CCaMK-FNDD was tested with MBP as substrate.

When kinase assays were performed with CYCLOPS-81-366 as substrate, a clearer picture of kinase activity was obtained for the truncated CCaMK versions and CCaMK-FNDD. CCaMK-1-314 showed the same constitutive activity in all conditions tested, whereas CCaMK-1-351 and CCaMK-1-453 showed highest CYCLOPS-81-366 phosphorylation activity in the presence of $\text{Ca}^{2+}/\text{CaM}$, indicating that both proteins are activated by $\text{Ca}^{2+}/\text{CaM}$. Interestingly, also CCaMK-FNDD, for which a loss of the CaM binding site is predicted was inactive towards MBP, but showed clear, albeit weak, $\text{Ca}^{2+}/\text{CaM}$ stimulated activity towards CYCLOPS-81-366.

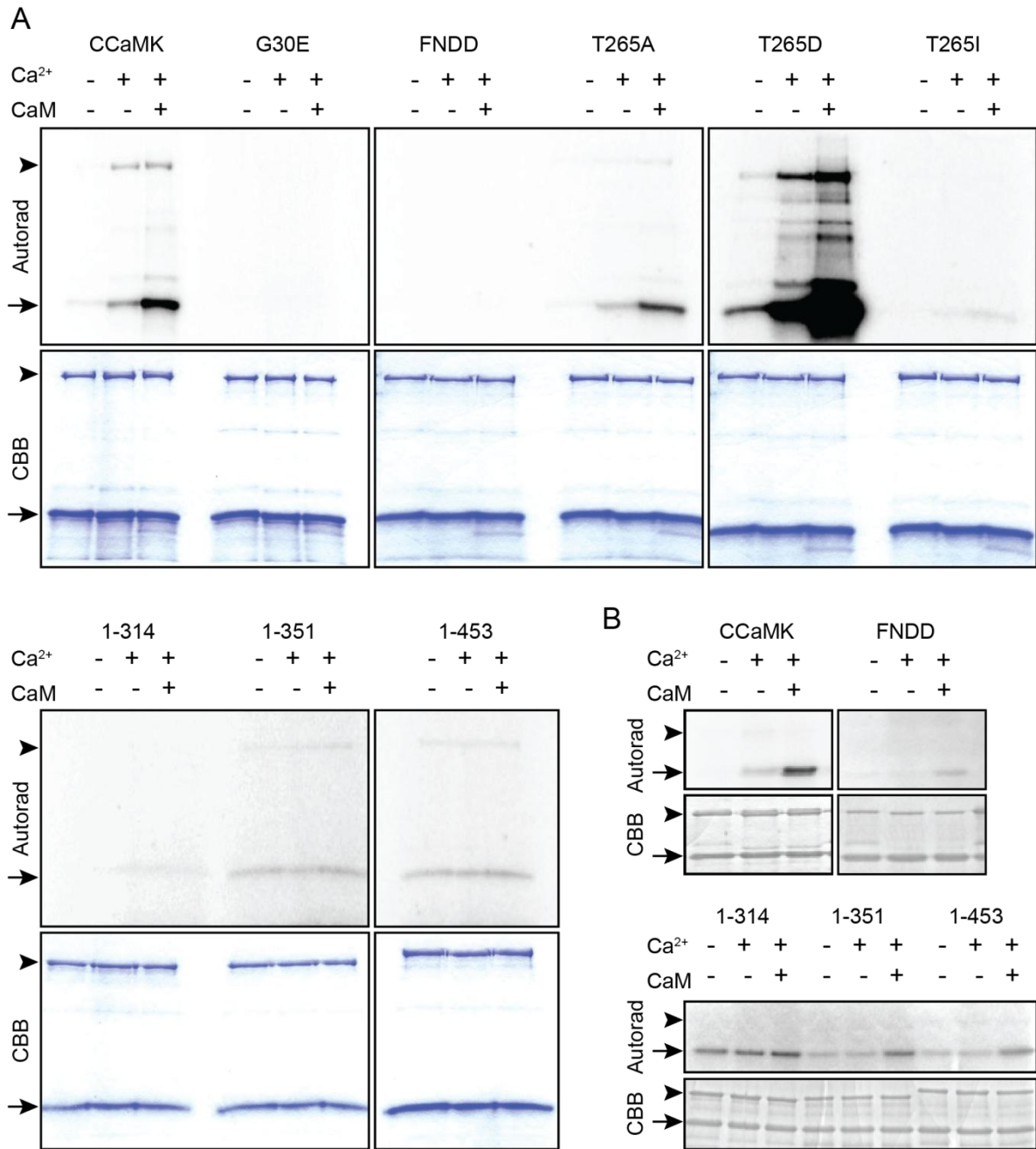


Figure 9. *In vitro* kinase activity of recombinant CCaMK mutant proteins.

In vitro kinase activity of maltose-binding-protein tagged CCaMK and CCaMK mutant proteins was tested in the presence of either 4 mM EGTA (-), 0.1 mM CaCl₂ (Ca²⁺), or 0.1 mM CaCl₂ and 1 μM calmodulin (CaM). Each reaction was performed with 1 μg CCaMK wild-type, or mutant protein (indicated by arrowheads) and (A) 10 μg of myelin basic protein (MBP) or (B) 1 μg CYCLOPS-81-366 as substrate (indicated by arrows). Samples were resolved on 12% SDS-PAGE gels. Incorporation of radioactive phosphate was visualised using a Typhoon phosphorimager. Upper panels show autoradiographs (autorad), which illustrate autophosphorylation of CCaMK, or CCaMK mutant proteins (marked by arrowheads) and (A) MBP or (B) CYCLOPS-81-366 phosphorylation (marked by arrows); lower panels show Coomassie stained protein bands (CBB).

3.6 Subcellular localization of CCaMK mutant proteins

GFP tagged CCaMK localizes exclusively to the nucleus in *L. japonicus* root cells (Yano et al., 2008), indicating that CCaMK fulfills its signaling function in the nucleus. Intriguingly, no canonical nuclear localization signal (NLS) is predicted in the CCaMK protein sequence, therefore it is still unclear, whether a latent NLS is present, or CCaMK is transported via an yet unknown mechanism to the nucleus. To investigate whether the CCaMK mutant variants are equally located in the nucleus, subcellular localization of GFP tagged CCaMK wild-type and mutant versions was carried out in *L. japonicus* protoplast cells. This analysis revealed that only wild-type CCaMK is exclusively localized to the nucleus (Figure 10), while the mutant variants were also partly localized to the cytosol. Further, in several protoplast cells, the CCaMK-FNDD mutant protein was found to form aggregates which were visible as larger and smaller fluorescent dots.

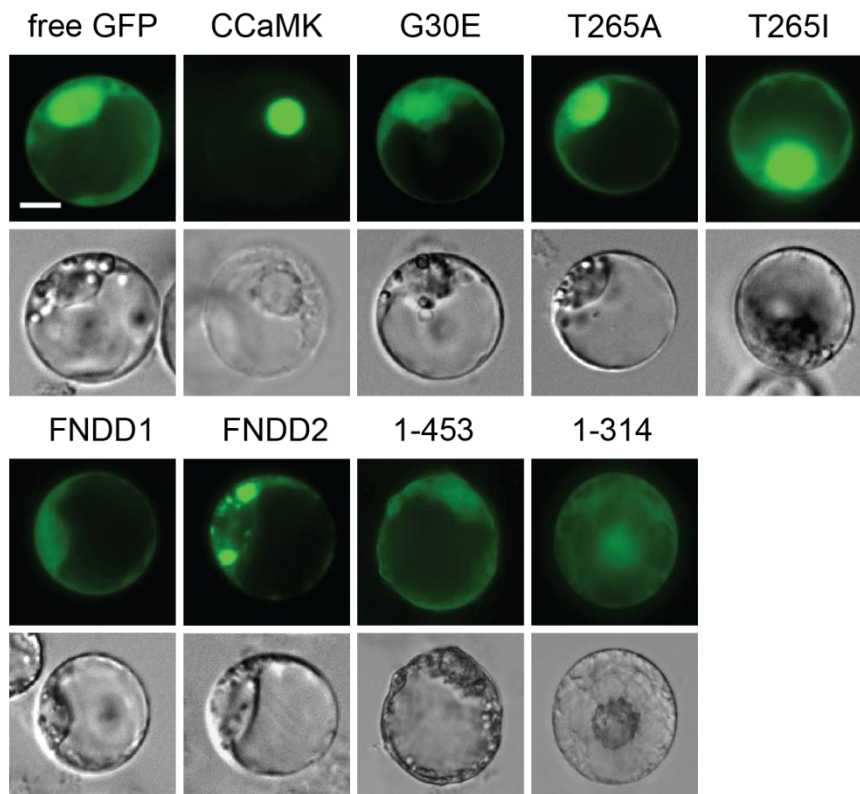


Figure 10. Subcellular localization of CCaMK and CCaMK mutant proteins in *L. japonicus* protoplasts.

Plasmid DNA encoding *p35S:GFP*, *p35S-GFP-CCaMK*, *p35S-GFP-G30E*, *p35S-GFP-T265A*, *p35S-GFP-T265I*, *p35S-GFP-FNDD*, *p35S-GFP-1-314*, or *p35S-GFP-1-453* was transformed into *L. japonicus* Gifu wild-type protoplasts by PEG mediated transformation. The expression and localization of GFP-fusion proteins was analysed 16 h post transformation. Micrographs were recorded with a GFP filter (upper panels) and with brightfield illumination (lower panels). Scale bar: 10 μ m. Note that GFP-CCaMK-FNDD tends to form aggregates (FNDD2).

4 Discussion

CCaMK is the presumed target of the calcium oscillations which immediately initiate after perception of symbiont specific signals. Due to the ancient origin of the AM symbiosis, CCaMK presumably evolved as the decoder and transducer of AM fungal calcium signals and was later co-opted by legume plants as signaling molecule for the establishment of RNS. The finding that autoactive CCaMK is sufficient to trigger the nodule organogenesis program revealed that in legumes and other RNS forming plants CCaMK acquired a novel function required for the initiation of nodule organ development (Gleason et al., 2006; Svistoonoff et al., 2013; Tirichine et al., 2006). Central to this function is the autophosphorylation site T265 which, if substituted by other amino acids, triggers spontaneous nodule formation. As no nodules are formed during AM, it is possible that regulation of this site by phosphorylation is different during AM signaling. Likewise, nodule organogenesis could also be prevented by other mechanisms, or a combination of both. Our finding obtained with autophosphorylation site mutants indicates that a preventive mechanism is involved. Further, the herein presented analysis of CCaMK domain specificity in symbiosis signaling confirms the previous finding that RNS formation is absolutely dependent on the presence of both, the kinase and the CaM binding domains, while AM is more permissive and can be restored with the expression of the kinase domain alone.

4.1 Differential requirements of CCaMK domains for AM fungal and rhizobial infection

The complementation analysis revealed that AM fungal, but not rhizobial infection, is possible with the autoactive mutant proteins CCaMK-1-314 and CCaMK-FNDD, which indicated a requirement of the C-terminal CCaMK region (comprising the CaM-BD and VLD) for rhizobial infection. The truncated mutant CCaMK-1-351 which is not autoactive and lacks the VLD was able to restore rhizobial infection, indicating that the VLD is dispensable and pinpoints the CaM-BD as the key domain required for rhizobial infection processes. A discrepancy was observed in the efficiency of RNS and AM complementation between CCaMK-1-351 and CCaMK-1-453, with the longer version performing in both cases >30% less efficient compared to the shorter CCaMK-1-351 (Figure 7A). This difference could be due to various reasons: Either, the CCaMK-1-453 protein is more tightly autoinhibited and therefore less accessible for CaM than CCaMK-1-351, or the protein expression levels or protein stability *in vivo* are different. *In vitro* kinase assays revealed no difference in kinase activity between both proteins under standard kinase assay conditions with excess amounts of calcium and CaM (Figure 9). To test whether compared to CCaMK-1-351, CCaMK-1-453 is more stringently autoinhibited, titration of kinase activity with

increasing concentrations of $\text{Ca}^{2+}/\text{CaM}$ need to be performed. In addition, if the impairment observed with CCaMK-1-453 was due to lower expression levels *in vivo*, less protein level would be expected in immunoblot analysis performed with equal root material. The difference in root length colonization and formation of AM fungal infection structures was less severe between CCaMK-1-351 and CCaMK-1-453 (Figure 6 and 7B) pointing towards an impairment in the early steps of fungal infection, e.g at the stage of epidermal opening and/or PPA formation, processes which are both dependent on CCaMK (Demchenko et al., 2004; Genre et al., 2005). An impaired rhizobial infection process at the initial stage of root hair infection could also account for the lower number of infected nodules observed with CCaMK-1-453 compared to CCaMK-1-351 (Figure 5C and Table 1).

CCaMK-1-314 and the autoactive CCaMK-FNDD were also able to restore AM, albeit a tendency towards extension of arbusculated cell files from the inner to the outer cortical cell layers was observed (Figure 6 and 7, Table 3). Simultaneously, compared to wild-type CCaMK, root length colonization was severely impaired (Figure 7B and Table 2), implying that expression of these mutant proteins impedes horizontal spread of the fungus which is then forced to expand vertically. This phenotype resembles the phenotype of *Medicago CDPK1* knockdown roots, characterized by impaired progression of rhizobial and mycorrhizal infection through cortical cells (Ivashuta et al., 2005). Likewise, longitudinal AM fungal colonization was blocked, which was explained by the concomitant increase of cell wall and defense related genes resulting also in reduced root cell elongation. Aberrant or diminished CCaMK signaling may induce similar changes in cell wall structure and defense responses as observed under *CDPK1* suppression. Indeed, transcriptional profiling of PPA forming *Medicago* root cells found an expansin-like gene to be up-regulated and *ACRE264*, a basal defense-related gene to be down-regulated in a *CCaMK/DMI3* dependent fashion (Siciliano et al., 2007). Expansins are proteins with an essential role in cell wall loosening, while *ARE264* is a protein kinase required for resistance against *C. fulvum* strains expressing the *Avr9* gene (Rowland et al., 2005; Siciliano et al., 2007). The CCaMK kinase activity or the extent of signaling may not suffice to regulate both genes appropriately.

Additionally, the autoactive CCaMK mutant proteins may lead to perturbation in hormonal signaling. Expression of both proteins, triggers, albeit with low frequency, the formation of spontaneous nodules. Nodule organogenesis relies on the production of the hormone cytokinin, which in *Lotus* roots is perceived by the cytokinin receptor LHK1 leading to the reinitiation of cell divisions and nodule organogenesis (Murray et al., 2007; Tirichine et al., 2007). The observation that CCaMK-1-314 and CCaMK-FNDD trigger nodule organogenesis

indicates the induction of cytokinin production by these mutant proteins, which could influence AM establishment. Yet, whether cytokinin impacts on AM establishment is unknown (Foo et al., 2013). There is emerging evidence that gibberellic acid (GA) inhibits arbuscule development. The GA biosynthesis mutant *na-1* of pea shows significantly enhanced arbuscule formation, even in the outer cortical cell layers (Foo et al., 2013). In contrast, mutations in either of the two *DELLA* genes of pea, in the *M. truncatula* *della1/della2* double mutant, or application of GA lead to a drastic reduction or impairment of arbuscule development (Floss et al., 2013, Foo et al., 2013). DELLA proteins are GRAS domain proteins acting as repressors of GA signaling. The presence of GA leads to their degradation and activation of GA responsive genes. It has recently been shown that the expression of a dominant (GA insensitive) DELLA mutant promotes arbuscule formation in *M. truncatula* roots even upon GA treatment, revealing a pivotal role of DELLA proteins in arbuscule development (Floss et al., 2013). *DELLA* expression is confined to the vasculature and endodermis, in this way restricting arbuscule formation to the adjacent inner cortical cell layers. Surprisingly, expression of the dominant DELLA mutant restored arbuscule formation in a *cyclops* mutant. This finding indicates that GA signaling is suppressed during symbiosis signaling perhaps via CCaMK or CYCLOPS, which may activate the expression of DELLAs during symbiosis signaling. Thus, the extension of arbuscule cell files observed with the expression of autoactive CCaMK proteins may be a consequence of ectopic signaling, leading to ectopic *DELLA* expression (or inhibition of GA signaling), inducing arbuscule formation. This interesting hypothesis remains to be tested in future experiments.

4.2 The phospho-mimetic and phospho-ablative form of CCaMK reveal differences in regulation

Unexpectedly, both the phospho-ablative CCaMK-T265A and the phospho-mimetic CCaMK-T265D induced the formation of spontaneous nodules. Normally, opposite phenotypes would have been expected, one form (presumably CCaMK-T265D) triggering spontaneous nodules and the other form (CCaMK-T265A) being impaired in this process. Similar results were obtained by Shimoda and associates, who provided a convincing explanation found by homology modeling of CCaMK-1-340 onto the CaMKII crystal structure (Shimoda et al., 2012). According to this model, the unphosphorylated hydroxyl group of the threonine residue is part of a hydrogen bond network autoinhibiting the kinase. Phosphorylation or substitution by the residues alanine, aspartate or isoleucine in all cases was predicted to disrupt the network leading to the release of autoinhibition. Although CCaMK-T265A and CCaMK-T265D were autoactive a striking difference in kinase activity was observed between

both forms (Figure 9). CCaMK-T265D displayed constitutive autoactivity in the absence of calcium and a further activity increase was observed upon addition of calcium and Ca^{2+} /CaM. The high autoactivity level might explain the high proportion of uninfected nodules (~50%) observed with roots expressing CCaMK-T265D compared to those expressing CCaMK-T265A (~10%) (Figure 5C, Table 1). As spontaneous nodules are formed ectopically in the absence of rhizobia, in rhizobia inoculated roots spontaneous nodule organogenesis and rhizobial infection are largely uncoupled events. It is possible that the high kinase activity of CCaMK-T265D leads to the aberrant phosphorylation of a CCaMK downstream target, such as CYCLOPS. Aberrant phosphorylation may lead to impaired activation or aberrant activity of the phosphorylated CCaMK substrate, resulting in uninfected nodules.

4.3 AM fungi exert a negative effect on spontaneous nodule formation

Another interesting finding of this study was the discovery that the spontaneous nodule number produced by CCaMK autophosphorylation site mutants was reduced by 50% upon cocultivation with AM fungi compared to asymbiotic cultivation conditions. The cause of this suppressive effect is elusive, but there are different possibilities, which could be tested in future experiments. The results of these investigations may provide an answer to the longstanding question why nodules are not formed during AM signaling upon activation of CCaMK. One possibility was that the negative regulatory effect could be directly acting on the CCaMK protein. This would imply that (autoactive) CCaMK protein levels diminish during cocultivation with AM fungi compared to protein expression levels in roots cultivated under asymbiotic conditions. According to immunoblot analysis performed in this study (Figure 8C), no difference in CCaMK-T265I protein level was detected between *snf1-1* roots cultivated under asymbiotic conditions and those cultivated in the presence of AM fungi, largely excluding this possibility. Hormonal changes associated with AM fungal colonization could be another reason. It has been recently shown that treatment of transgenic roots expressing CCaMK-T265D with GA, reduced spontaneous nodule number by >60% (Maekawa et al., 2009). As AM fungal colonization is accompanied with a significant GA increase (Shaul-Keinan et al., 2002), elevated GA levels in mycorrhizal roots could be the cause of spontaneous nodule reduction. In order to test this hypothesis, comparative expression analysis of GA marker genes in transgenic roots could be carried out and an increase in roots cocultivated with AM fungi would lend support for this hypothesis. In addition, *snf1-1* roots could be transformed with a dominant *DELLA* construct, which would lead to the repression of GA signaling and alleviate the suppression of spontaneous nodule number by AM fungi. No suppression of spontaneous nodule number would also be expected

in roots supplemented with a GA biosynthesis inhibitor during cocultivation with AM fungi. Furthermore, endogenous SLs were identified as positive regulators of nodulation in pea, as the SL mutant *rms* produced 40% fewer nodules compared to wild-type plants (Foo and Davies, 2011). Mycorrhizal colonization has been shown to downregulate SL levels in tomato roots (Lopez-Raez et al., 2011). Thus, the negative effect of mycorrhiza on nodulation could also be caused by the decrease in SL level during fungal colonization.

Finally, establishment of AM or RNS is accompanied with the onset of a systemic autoregulatory mechanism termed autoregulation of nodulation (AON) or autoregulation of mycorrhization (AOM) controlling the extent of nodule formation or AM fungal colonization, which also involves signaling via the shoot (Catford et al., 2003; Reid et al., 2011). Interestingly, this effect is also exerted reciprocally, with AM fungal colonization controlling nodule number and RNS formation controlling the extent of AM colonization (Catford et al., 2003). Using the split-root system it has been shown that AM fungal colonization of one root half significantly reduced nodule numbers upon rhizobial inoculation of the second half compared to plants not pretreated with AM (Catford et al., 2003). Whether the effect observed with the CCaMK autophosphorylation site mutants is produced by AOM could be equally analysed with *snf1-1* plants in a split root system set-up, where one half is co-cultivated with AM fungi, while the second half stays untreated. An adequate control set-up would be the cultivation in a split root system leaving both halves untreated.

In summary, several possibilities how AM fungal colonization could lead to the reduction of spontaneous nodule number in CCaMK autophosphorylation site mutants exist. Conceivably, several mechanisms act together in a synergistic manner. The observation that the inhibitory effect was less pronounced in the *snf2* mutant suggests that the regulatory effect acts predominantly between *CCaMK* and *LHK1*.

4.4 Correlation between kinase activity and *in vivo* activity of CCaMK mutant proteins

Considering the kinase activity of the autophosphorylation site mutants, CCaMK-T265A and CCaMK-T265D clearly behaved different, with CCaMK-T265A displaying wild-type-like activity while CCaMK-T265D by far exceeded wild-type activity and as a phenotypic consequence produced more uninfected nodules than CCaMK-T265A (as discussed above). CCaMK-1-314 showed the same constitutive activity in the absence and presence of calcium or $\text{Ca}^{2+}/\text{CaM}$, while intriguingly CCaMK-FNDD, whose mutations predict a loss of the CaM-BD (Rellos et al., 2010) was only substantially active in the presence of $\text{Ca}^{2+}/\text{CaM}$. However, both proteins displayed the same symbiotic phenotype when expressed *in vivo*: Spontaneous nodule formation, lack of rhizobial infection and decreased, aberrant AM fungal infection.

The spontaneous nodulation phenotype of CCaMK-FNDD suggests that the protein is autoactive, which is also supported by the *in vitro* kinase assay showing faint activity in the absence of calcium if CYCLOPS is used as phosphorylation substrate (Figure 9B). CaM binding assays carried out with CCaMK-FNDD need to be performed to clarify whether this mutant can still bind CaM. Otherwise, the absence of the CaM-BD in both, CCaMK-1-314 and CCaMK-FNDD may be the cause for impaired rhizobial infection. The precise role of the CaM binding domain in rhizobial infection remains to be identified. Possibly, rhizobial infection requires higher kinase activity levels (achieved by Ca²⁺/CaM stimulation) while spontaneous nodule formation is triggered with lower levels (achieved via calcium induced kinase activation). Further, Ca²⁺/CaM stimulation may simultaneously confer substrate phosphorylation specificity. Besides, it is equally conceivable that the presence of the CaM-BD confers an essential protein conformation during RNS signaling, required for infection related signal propagation.

5 Material and Methods

5.1 Plant material, growth conditions, transformation and inoculation procedures

The following *L. japonicus* plant lines were used in this study: Gifu B-129 wild-type, *ccamk-13* (Perry et al., 2009), *snf1-1* (Tirichine et al., 2006), *snf2* (Tirichine et al., 2007). Transgenic hairy roots were induced by *A. rhizogenes* strain AR1193 (Offringa et al., 1986) as described (Diaz et al., 2005). Selection of transformed plant roots was carried out with the GFP transformation marker encoded on the T-DNA. Two weeks post transformation plants with transformed hairy roots were transplanted into autoclaved pots containing a 1:1 mixture of sterilized sand/vermiculite (300 ml) supplemented with 100 ml sterile half-strength Hoagland solution (Hoagland and Arnon, 1950). Plants were watered regularly and supplied with 100 ml sterile half-strength Hoagland solution once per week. Plant growth conditions were 24 °C constant at 16-h-light/8-h-dark cycles in growth chambers.

Spontaneous nodule formation in the absence of rhizobia was evaluated seven weeks post hairy root transformation, or five weeks post cultivation in sterile soil, respectively. To evaluate restoration of RNS, plants were inoculated with *M. loti* MAFF303099 carrying DsRed as fluorescent marker (Maekawa et al., 2008) set to a final OD₆₀₀ of 0.05 and incubated for four weeks. AM establishment was tested with the AM fungus *Rhizophagus irregularis*, which was propagated in a chive (*Allium schoenoprasum*) nurse pot system (Demchenko et al., 2004). Prior to cocultivation, an appropriate number of nurse pots was used to produce a homogeneous fungal inoculum in the following way: The chive shoot was cut off, the mycorrhized chive root system was removed from the soil (sterilized

sand/vermiculite mixture), cut into small (~1cm) pieces and then homogeneously mixed with the soil. The homogeneous mixture was used as cocultivation substrate for each set-up. Plants were cocultivated with the fungal inoculum substrate for five weeks.

5.2 Symbiosis phenotyping

Formation of *M. loti*-DsRed infected root nodules was evaluated by microscopic observation of red fluorescent root nodules indicating the presence of DsRed-tagged *M. loti* inside the nodules. Microscopy was performed with a stereomicroscope (Leica MZt6 FA). AM fungal colonization was visualized after ink vinegar staining of the root system (Vierheilig et al., 1998) using brightfield microscopy (inverted microscope Leica DMI6000).

Quantification of the AM fungal structures was carried out essentially as described (McGonigle et al., 1990). Samples were prepared and evaluated in the following way: The stained root system was cut into 1 cm pieces which were randomly chosen and mounted on a glass slide. Using 200x magnification, 100 line intersects per root system were scored for the presence of the following categories: 1= no fungal colonization, 2= presence of hyphae only, 3= presence of arbuscules, 4= presence of vesicles and 5= simultaneous presence of arbuscules and vesicles. The percentage (%) of each category was calculated; the sum of categories 2-5 corresponds to total percent of AM fungal root length colonization.

To quantify the arbusculated cell layers, samples were prepared as described for the determination of AM fungal colonization. 100 intersects with arbuscules were scored (200x magnification) and the number of arbusculated cell files (determined from one side of the central vasculature) was counted for each intersect. If the number of arbusculated cell files was different for both sides, the higher cell file number was scored and used for calculation.

5.3 Protein blot analysis

Root systems were weighed, frozen in liquid nitrogen and root material was ground to fine powder with a tissue lyser (Qiagen). Proteins were extracted as described (Waadt et al., 2008). Extracts were clarified by centrifugation (10.000xg, 15 min, 4 °C), equal volumes of clarified extracts were separated on 10% SDS gels and proteins were transferred to a PVDF membrane (GE-Healthcare). The immunodetection of CCaMK proteins was performed with polyclonal rabbit anti-CCaMK primary antibodies (<http://www.pineda-abservice.de>) and anti-rabbit-HRP (Amersham) secondary antibody.

5.4 Protein expression, purification and *in vitro* kinase assay

Expression of Maltose-Binding-Protein (MalBP) tagged CCaMK, and mutant derivatives thereof, was induced from *E. coli* Rosetta pLqI (Novagen) by addition of 0.5 mM IPTG for 4

h at 28 °C. MalBP tagged proteins were purified *via* amylose resin (New England Biolabs) according to the manufacturer's protocol. Proteins were desalted via PD10 desalting columns (GE Healthcare) and eluted in buffer containing 25 mM Tris, 10 mM β-mercaptoethanol (pH 7.6). Expression and purification of 6xHis-CYCLOPS-81-366 was performed as described (Yano et al., 2008). *In vitro* kinase assays were carried out for 30 min at 25 °C in buffer containing 25 mM Tris (pH 7.6), 10 mM MgCl₂, 0.5 mM DTT, 200 μM ATP and 5 μCi [γ -³²P] ATP (Hartmann Analytic). 1 μg MalBP-CCaMK (and CCaMK mutant proteins) was tested in each reaction, in the presence of either 10 μg myelin basic protein (Sigma), or 1 μg 6xHis-CYCLOPS-81-366 as phosphorylation substrate. Kinase activity was assayed in the presence of either 4 mM EGTA, or 0.1 mM CaCl₂, in the absence or presence of 1 μM bovine calmodulin (Sigma). Kinase reactions were stopped by addition of SDS-PAGE sample buffer and boiled (95 °C, 5 min). Samples were separated on 12% SDS-PAGE gels and stained with Coomassie brilliant blue. Stained radioactive gels were dried, exposed to phosphorimage screens and visualized by scanning with Typhoon Trio scanner (GE Healthcare).

5.5 Protoplast preparation from *Lotus japonicus* cell culture

Protoplasts were generated from a 6 days old dedifferentiated *Lotus japonicus* Gifu wild-type cell culture. Protoplast preparation, harvesting and transfection was performed essentially as described (Sprenger-Haussels and Weisshaar, 2000). 50 ml *Lotus japonicus* root cell culture were centrifuged (860xg, 3 min, RT) the pellet was resuspended in 25 ml CaCl₂ (240 mM) and centrifuged (860xg, 3 min, RT). The cell pellet was resuspended in 20 ml CaCl₂ (240 mM). 10 ml of the cell suspension were mixed with 30 ml enzyme solution (3.5 % cellulose R10 from Onozuka, 0.6 % macerozyme R10 from Serva in 240 mM CaCl₂ and incubated in large petri dishes on a horizontal shaker at 60 rpm for 14 h at 25 °C. The protoplast solution was filtered through a 40 μm pore nylon mesh into 50 ml Falcon tubes and centrifuged (860xg, 3 min, RT). Pelleted protoplasts were resuspended in 25 ml 240 mM CaCl₂, centrifuged (860xg, 3 min, RT) and resuspended in 25 ml P5 medium (1x Gamborg B5 medium, 283 mM sucrose, 4.5 μM 2,4 dichlorophenoxyacetic acid, pH 5.7 with NaOH). 2x 12.5 ml of protoplast solution were centrifuged (300xg, 5 min, RT). The floating protoplasts (supernatant) were harvested and the suspension was analysed for the presence of protoplasts by light microscopy. The cell suspension (100 μl) was stained with 1 μl FDA (fluor diacetate stain) and cell quantification was carried out by determining the number of viable protoplasts per ml in a Neubauer counting chamber via fluorescence microscopy. Prior to transfection the protoplast suspension was adjusted to 10⁶ protoplast cells/ml.

5.6 Transfection of protoplasts

The constructs transformed into *L. japonicus* protoplasts are listed in 5.7.4. Prior to transfection plasmid DNA was isolated by Midiprep (Macherey & Nagel).

For protoplast transfection single stranded salmon sperm carrier DNA (10 mg/ml), 10-30 µg plasmid DNA, 200 µl protoplast solution (10^6 cells/ml) and 200 µl polyethylene glycol solution (25% PEG 6000, 100 mM $\text{Ca}(\text{NO}_3)_2$, 450 mM mannitol, pH 9.0) were carefully mixed and incubated for 15 min at RT. After addition of 3 ml $\text{Ca}(\text{NO}_3)_2$ (275 mM), the transfection mixture was centrifuged (860xg 30 sec, RT), and 0.5 ml P5 medium were added to the pellet. Transfection reactions were incubated for 18 h at 25 °C in the dark. Expression and subcellular localization of GFP tagged CCaMK proteins in transfected protoplasts was visualized with a Leica DMI6000 inverted microscope using a GFP filter.

5.7 Plasmid construction

5.7.1 Entry clones

Name	Construction
pENTR:CCaMK	Yano et al., 2008
pENTR:CCaMK-G30E	Site directed mutagenesis Phusion PCR with primers CCaMK-G30E_fwd/rev on pENTR:CCaMK
pENTR:CCaMK-T265A	Site directed mutagenesis Phusion PCR with primers CCaMK-T265A_fwd/rev on pENTR:CCaMK
pENTR:CCaMK-T265D	Yano et al., 2008
pENTR:CCaMK-T265I	Tirichine et al., 2006
pENTR:CCaMK-T265S	Site directed mutagenesis Phusion PCR with primers CCaMK-T265S_fwd/rev on pENTR:CCaMK
pENTR:CCaMK-FNDD	Site directed mutagenesis Phusion PCR with primers CCaMK-FNDD_fwd/rev on pENTR:CCaMK
pENTR:CCaMK-1-453	Site directed mutagenesis Phusion PCR with primers CCaMK-1-453_fwd/rev on pENTR:CCaMK
pENTR:CCaMK-351stop	Site directed mutagenesis Phusion PCR with primers CCaMK-1-351_fwd/rev on pENTR:CCaMK
pENTR:CCaMK-314stop	Site directed mutagenesis Phusion PCR with primers CCaMK-1-314_fwd/rev on pENTR:CCaMK

5.7.2 Plasmids for *L. japonicus* hairy root transformation

Name	Construction
pUB:empty vector	Restriction digest of pUB:GW-GFP (Maekawa et al., 2008) with <i>PvuI</i> to remove Gateway cassette and self ligation.
pUB:CCaMK	LR reaction (Invitrogen) of pENTR:CCaMK and pUB:GW-GFP (Maekawa et al., 2008)
pUB:CCaMK-G30E	LR reaction (Invitrogen) of pENTR:CCaMK-G30E and pUB:GW-GFP (Maekawa et al., 2008)
pUB:CCaMK-T265A	LR reaction (Invitrogen) of pENTR:CCaMK-T265A and pUB:GW-GFP (Maekawa et al., 2008)
pUB:CCaMK-T265D	LR reaction (Invitrogen) of pENTR:CCaMK-T265D and pUB:GW-GFP (Maekawa et al., 2008)
pUB:CCaMK-T265I	LR reaction (Invitrogen) of pENTR:CCaMK-T265I and pUB:GW-GFP (Maekawa et al., 2008)
pUB:CCaMK-T265S	LR reaction (Invitrogen) of pENTR:CCaMK-T265S and pUB:GW-GFP (Maekawa et al., 2008)
pUB:CCaMK-FNDD	LR reaction (Invitrogen) of pENTR:CCaMK-FNDD and pUB:GW-GFP (Maekawa et al., 2008)
pUB:CCaMK-1-453	LR reaction (Invitrogen) of pENTR:CCaMK-1-453 and pUB:GW-GFP (Maekawa et al., 2008)
pUB:CCaMK-1-351	LR reaction (Invitrogen) of pENTR:CCaMK-1-351 and pUB:GW-GFP (Maekawa et al., 2008)
pUB:CCaMK-1-314	LR reaction (Invitrogen) of pENTR:CCaMK-1-314 and pUB:GW-GFP (Maekawa et al., 2008)

5.7.3 Plasmids for protein expression

Name	Construction
pKM:CCaMK	LR reaction (Invitrogen) of pENTR:CCaMK and pKM596 (Fox et al., 2003)
pKM:CCaMK-G30E	LR reaction (Invitrogen) of pENTR:CCaMK-G30E and pKM596 (Fox et al., 2003)
pKM:CCaMK-T265A	LR reaction (Invitrogen) of pENTR:CCaMK-T265A and pKM596 (Fox et al., 2003)
pKM:CCaMK-T265D	LR reaction (Invitrogen) of pENTR:CCaMK-T265D and pKM596 (Fox et al., 2003)
pKM:CCaMK-T265I	LR reaction (Invitrogen) of pENTR:CCaMK-T265I and pKM596 (Fox et al., 2003)
pKM:CCaMK-FNDD	LR reaction (Invitrogen) of pENTR:CCaMK-FNDD and pKM596 (Fox et al., 2003)
pKM:CCaMK-1-453	LR reaction (Invitrogen) of pENTR:CCaMK-1-453 and pKM596 (Fox et al., 2003)
pKM:CCaMK-1-351	LR reaction (Invitrogen) of pENTR:CCaMK-1-351 and pKM596 (Fox et al., 2003)
pKM:CCaMK-1-314	LR reaction (Invitrogen) of pENTR:CCaMK-1-314 and pKM596 (Fox et al., 2003)

5.7.4 Plasmids for subcellular localization in *L. japonicus* protoplasts

Name	Construction
pAMPATp35S:GFP	pAMPAT-MCS derivative with <i>GFP</i> insert (GenBank accession AY436765)
pAMPATp35S:GFP-CCaMK	LR reaction (Invitrogen) of pENTR:CCaMK with pAMPATp35S:GFP-GW (Gateway-compatible pAMPAT-MCS derivative (GenBank accession AY436765))
pAMPATp35S:GFP-CCaMK-G30E	LR reaction (Invitrogen) of pENTR:CCaMK-G30E with pAMPATp35S:GFP-GW (Gateway-compatible pAMPAT-MCS derivative (GenBank accession AY436765))
pAMPATp35S:GFP-CCaMK-T265A	LR reaction (Invitrogen) of pENTR:CCaMK-T265A with pAMPATp35S:GFP-GW (Gateway-compatible pAMPAT-MCS derivative (GenBank accession AY436765))
pAMPATp35S:GFP-CCaMK-T265I	LR reaction (Invitrogen) of pENTR:CCaMK-T265I with pAMPATp35S:GFP-GW (Gateway-compatible pAMPAT-MCS derivative (GenBank accession AY436765))
pAMPATp35S:GFP-CCaMK-FNDD	LR reaction (Invitrogen) of pENTR:CCaMK-FNDD with pAMPATp35S:GFP-GW (Gateway-compatible pAMPAT-MCS derivative (GenBank accession AY436765))
pAMPATp35S:GFP-CCaMK-1-453	LR reaction (Invitrogen) of pENTR:CCaMK-1-453 with pAMPATp35S:GFP-GW (Gateway-compatible pAMPAT-MCS derivative (GenBank accession AY436765))
pAMPATp35S:GFP-CCaMK-1-314	LR reaction (Invitrogen) of pENTR:CCaMK-1-314 with pAMPATp35S:GFP-GW (Gateway-compatible pAMPAT-MCS derivative (GenBank accession AY436765))

5.8 Primers

f = forward

r = reverse

CCaMK-G30E (SY119, SY120)

gtcagaaaagaaaccaaatacagg_f

cctgatttttggtttctttctgac_r

CCaMK-T265A (SY172, SY173)

ctatgagaaggcctggaaggcat_f

atgccctccaggccttctcatag_r

CCaMK-T265S (SY100, SY101)

ctatgagaagagttggaaggc_f

gccctccaactcttctcatag_r

CCaMK-FNDD (SY176, SY177)

ggctgcagagcgatgatcaagacg_f

cgtcttcatcatcgctctgcagcc_r

CCaMK-1-453 (SY97, SY116)

caccatgggatgatcaaaccag_f

ttacttggtgatgcacctg_r

CCaMK-1-351 (SY97)
caccatgggatatgatcaaaccag_f
ttataccaaggatctcagcttttgg

CCaMK-1-314 (SY97, SY121)
caccatgggatatgatcaaaccag_f
ttactcagggtccattgctc_r

Chapter 2: Negative regulation of CCaMK is essential for symbiotic infection

This chapter is based on the following publication:

Negative regulation of CCaMK is essential for symbiotic infection

Liao, J.*, **Singh, S.***, Hossain, M.S*., Andersen, S.U., Ross, L., Bonetta, D., Zhou, Y., Sato, S., Tabata, S., Stougaard, J., Szczyglowski, K. and Parniske M. (2012). Negative regulation of CCaMK is essential for symbiotic infection. *Plant J.* 72, 572-584.

* These authors contributed equally to the work.

This work was performed in collaboration with other researchers (mentioned above). The manuscript was mainly written by Krzysztof Szczyglowski. Contributions of the author of this thesis to this manuscript are listed in detail under ‘III Declaration of Contribution as Co-Author’ on pages 11-12 of this thesis. Unless otherwise stated, experiments related to the figures of this chapter were performed by the author of this thesis.

1 Summary

One of the earliest responses of legumes to symbiotic signaling is oscillation of calcium concentration in the nucleoplasm of root epidermal cells. The integration and decoding of the calcium-spiking signal involves a calcium- and calmodulin-dependent protein kinase (CCaMK) and its phosphorylation substrates, such as CYCLOPS. Here we describe the *Lotus japonicus ccamk-14* mutant that originated from a *har1-1* suppressor screen. The *ccamk-14* mutation causes a serine to asparagine substitution at position 337 located within the calmodulin binding site, which we determined as an *in vitro* phosphorylation site in CCaMK. We show that *ccamk-14* exerts cell-specific effects on symbiosis. It is characterized by increased frequency of epidermal infections and significantly compromised cortical infections by *Mesorhizobium loti* and also the AM fungus *Rhizophagus irregularis*. The S³³⁷ residue is conserved across angiosperm CCaMK and testing discrete substitutions at this site showed that it participates in a negative regulation of CCaMK activity, which is required for the cell-type-specific integration of symbiotic signaling.

2 Introduction

In plants, changes in cytosolic Ca^{2+} concentration have been linked to a variety of developmental and physiological processes (Berridge et al., 2000; Lecourieux et al., 2006; Rudd and Franklin-Tong, 2001), including responses to biotic stimuli associated with the presence of pathogens and symbionts. In contrast to pathogenic interactions, in which rapid increases in intracellular Ca^{2+} concentration contribute to plant defence signaling (Jeworutzki et al., 2010; Lecourieux et al., 2006), the calcium spiking in and around the nucleus represents an early symbiotic response that is required for intracellular colonization of plant roots by arbuscular mycorrhiza (AM) fungi and rhizobial symbionts (Capoen et al., 2011; Ehrhardt et al., 1996; Kosuta et al., 2008; Sieberer et al., 2009). During AM formation, fungal hyphae penetrate the *Lotus japonicus* root between epidermal cells, and subsequently invade the inner cortex, where they form intracellular arbuscules, highly branched hyphal structures that are thought to be sites of nutrient exchange between the two symbiotic partners (Bonfante and Genre, 2010; Parniske, 2008). The evolutionarily younger root nodule symbiosis (RNS) exhibited by legumes and nitrogen-fixing rhizobia (Sprent and James, 2007) is characterized by intracellular accommodation of bacteria by the host plant. In many legumes, including *L. japonicus*, rhizobia invade root hairs and subsequently the root cortex by plant plasma membrane-derived conduits, called infection threads (ITs) (Brewin, 2004; Fournier et al., 2008; Held et al., 2010). This is accompanied by the formation of subtending regions of cortical cell divisions for nodule primordia (NP) initiation. Growing ITs ramify within these regions, and bacteria are released inside the NP cells. Final differentiation of both symbiotic partners culminates in the development of fully functional nitrogen-fixing root nodules (Madsen et al., 2010; Oldroyd and Downie, 2008). In both AM and RNS, oscillation of nuclear Ca^{2+} concentrations in the root epidermis and cortex, termed Ca^{2+} spiking, constitutes one of the earliest cellular responses of the host plant cells to infection (Sieberer et al., 2012; Wais et al., 2000; Walker and Downie, 2000). Although it has been reported that fungal and bacterial microsymbionts induce Ca^{2+} oscillation responses with unique signatures at the pre-infection stage (Kosuta et al., 2008; Oldroyd et al., 2009), conserved Ca^{2+} spiking profiles were found to be associated with their intracellular entry into host roots (Sieberer et al., 2012). During both symbioses, Ca^{2+} spiking is thought to be decoded by the same Ca^{2+} and calmodulin-dependent protein kinase (CCaMK). This protein is characterized by the kinase domain, a CaM-binding domain and the EF-hand motif-containing neural visinin-like Ca^{2+} -binding domain, and its activity is subject to dual regulation by Ca^{2+} and Ca^{2+} /CaM (Gleason et al., 2006; Tirichine et al., 2006). Deleterious mutations in CCaMK prevent root infections

by both AM fungi and rhizobial microsymbionts, and also abolish NP formation in the root cortex during RNS, indicating that CCaMK performs an essential signaling role in these processes (Lévy et al., 2004; Mitra et al., 2004). Genetic analyses in *L. japonicus* and *Medicago truncatula* positioned the CCaMK function downstream of symbiont specific perception, within an ancient signal transduction pathway termed the common symbiosis pathway (Duc et al., 1998; Kistner and Parniske, 2002). This pathway is fundamental for successful establishment of AM and RNS, and its activity is stimulated by corresponding fungal Myc factor (Maillet et al., 2011) and bacterial Nod factor signaling molecules (Bek et al., 2010; Lerouge et al., 1990; Lopez-Lara et al., 1995). At least eight genes comprise the common symbiosis pathway in *L. japonicus* (Groth et al., 2010; Kistner et al., 2005). Six of these genes, namely *Symbiotic Receptor Kinase (SYMRK)* (Kosuta et al., 2011; Stracke et al., 2002), two ion channel-encoding genes *CASTOR* and *POLLUX* (Ané et al., 2004) and three nucleoporin genes *NUP85*, *NUP133* and *NENA* (Groth et al., 2010; Kanamori et al., 2006; Saito et al., 2007), are required to generate Ca²⁺ spiking responses (Kosuta et al., 2008; Miwa et al., 2006b; Oldroyd and Downie, 2006). CCaMK, the seventh element of the pathway, is considered to be the main decoder of these responses (Gleason et al., 2006; Lévy et al., 2004; Mitra et al., 2004; Tirichine et al., 2006), leading to activation of symbiont-specific effectors (Hogslund et al., 2009; Kistner et al., 2005). The eighth signaling element CYCLOPS/IPD3, forms a complex with CCaMK that is required for infection but appears non-essential for CCaMK-dependent signaling for NP initiation (Messinese et al., 2007; Yano et al., 2008). In the presence of the gain-of-function CCaMK-T265I or CCaMK-T265D, six common symbiosis genes upstream of calcium spiking are dispensable for AM and RNS (Hayashi et al., 2010; Madsen et al., 2010; Tirichine et al., 2006). Substitution of T265 also leads to spontaneous nodule formation in the absence of rhizobia (Hayashi et al., 2010; Tirichine et al., 2006), probably due to disruption of a network of hydrogen bonds in the vicinity of this site that is required for auto-inhibition of CCaMK activity. This disruption and loss of auto-inhibition also occurs when this site is phosphorylated (Shimoda et al., 2012). The spontaneous nodulation phenotype was also observed for a truncated *M. truncatula* CCaMK (DMI3) that lacked both CaM-binding/auto-inhibition and the EF-hand motif-containing visinin-like domains (e.g. DMI3 1–311, containing the kinase domain only) (Gleason et al., 2006). However, DMI3 1–311 fails to support bacterial colonization (Gleason et al., 2006). Taken together, these data indicate that negative regulation of CCaMK is essential to inhibit the induction of inappropriate gene expression and ectopic organogenesis. The CaM-binding/auto-inhibition and visinin-like domains mediate a complex regulatory behaviour of

CCaMK (Patil et al., 1995; Sathyanarayanan and Poovaiah, 2002; Sathyanarayanan et al., 2001; Takezawa et al., 1996) that appears to be required for coordination of infection and organogenesis during RNS (Takeda et al., 2012).

Here we have analysed the symbiosis-defective *L. japonicus ccamk-14* allele, and show that this mutation comprises replacement of serine at position 337 (S337), which we identified as an *in vitro* auto-phosphorylation site within the CaM binding region. Root infection by AM fungus and *Mesorhizobium loti* was impaired in *ccamk-14*, but no effect on NP formation was detected. Importantly, during RNS, *ccamk-14* specifically compromised cortical infection but enhanced epidermal infection. This result indicates that requirements for CCaMK activity, as orchestrated by its Ca²⁺ and Ca²⁺/CaM-dependent behaviour, are different in these two cell types.

3 Results

3.1 The *L. japonicus suppressor 11 (sup11)* mutant

The *sup11* mutant emerged from a genetic screen for suppressors of the *L. japonicus har1-1* hypernodulation phenotype (Murray et al., 2006). Compared to the *har1-1* parental line, an unusual mixture of pink and pale-pink nodules was observed in *sup11* mutants 21 days after inoculation (dai) with *M. loti* (Figure 11A). This change was accompanied by a slightly improved shoot growth and more elongated roots (Figure 11C). However, the presumed secondary mutation in *sup11* did not suppress, the *har1-1* hypernodulation phenotype (Figure 11A) and the kinetics of nodulation was not significantly altered in *sup11* compared to *har1-1* (Figure 12). Nevertheless, numerous NP that formed on *sup11* roots at 7 dai with *M. loti* were not invaded by the bacteria. Later, at 14 and 21 dai, partially colonized nodules comprised the majority of events in *sup11*, which differed significantly from *har1-1*, where only fully colonized nodules and a few NP were formed (Figure 12). A closer inspection of roots showed that unlike *har1-1* (Figure 13a), progression of many ITs was halted in *sup11* within the outer cortex, above the subtending NP (Figure 13b and c). Furthermore, the number of microcolonies and epidermal ITs was significantly increased in the *sup11* mutant (Figure 13d). The apparent defect in bacterial colonization of the root cortex prompted the analysis of the *sup11* arbuscular mycorrhiza (AM) phenotype. *sup11* roots showed a significantly reduced symbiotic interaction with the AM fungus, *R. irregularis* (Krüger et al., 2012) suggesting that the underlying mutation affected a common symbiosis function in *L. japonicus* (Figure 13e and 13f).

In order to select a corresponding single mutant, *sup11* was backcrossed to the *L. japonicus* wild-type (Gifu) and an F2 segregating population was obtained. A mapping population,

derived from the cross between *sup11* (ecotype Gifu) and the polymorphic *L. japonicus* MG20 carrying an introgressed *har1-1* Gifu allele (Murray et al., 2006), was established in parallel to identify the location of the causative lesion (see Materials and Methods).

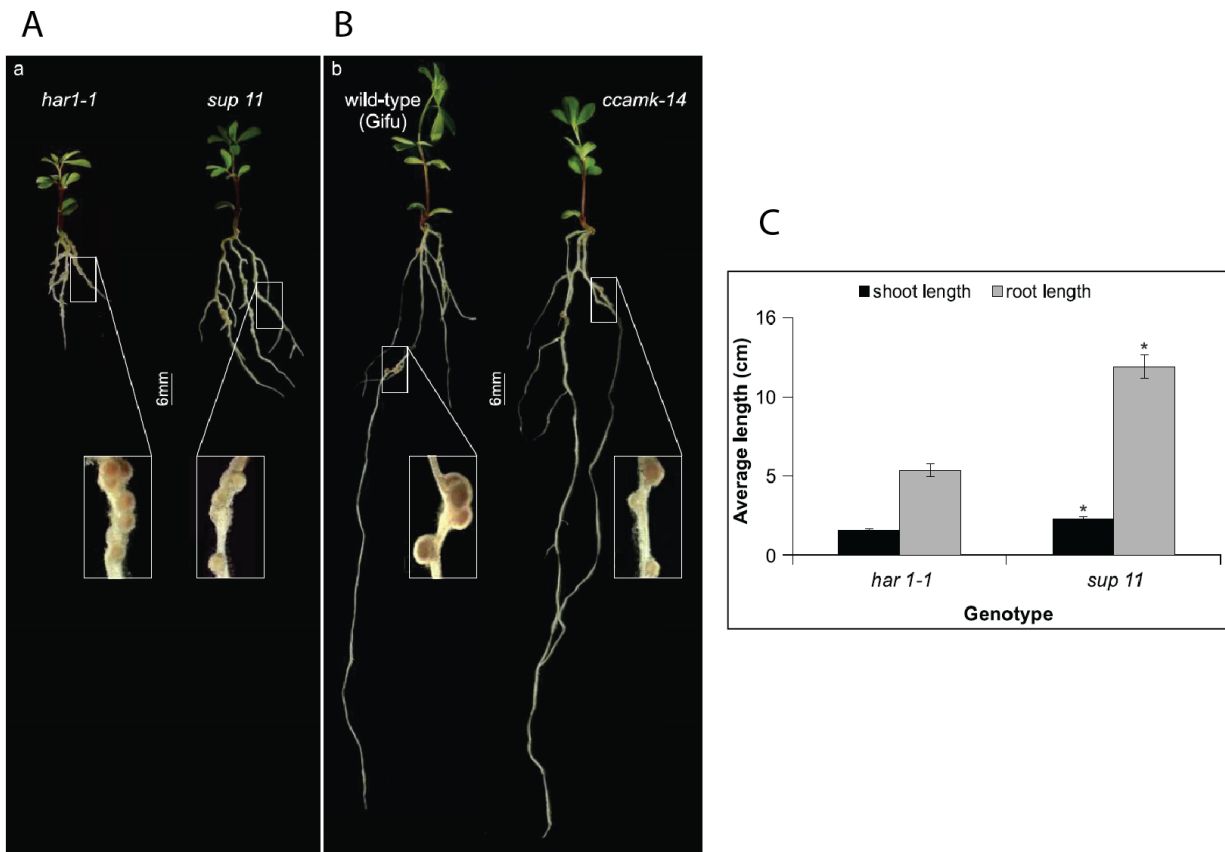


Figure 11. Plant phenotypes.

(A) *har1-1* parental line and the *sup11* mutant at 21 days after inoculation. (B) Wild-type *Lotus japonicus* Gifu and the *ccamk-14* single mutant at 14 days after inoculation. Note that *har1-1* and the wild-type plant form pink nodules (see insets), and *sup11* and the *ccamk-14* develop a mixture of pink and white nodules. *Mesorhizobium loti* strain NZP2235 was used for plant inoculation. (C) Measurements of shoot and root length in *har1-1* and *sup11*. Data represent mean values \pm SE for $n = 10$. Asterisks (*) denote statistically significant differences between genotypes within corresponding categories as determined using a Student's *t*-test ($P < 0.05$). The measurements were performed 21 dai on plants grown in soil.

Data related to this figure were generated in the lab of Krzysztof Szczyglowski. Figure and legend adopted from Liao et al., 2012.

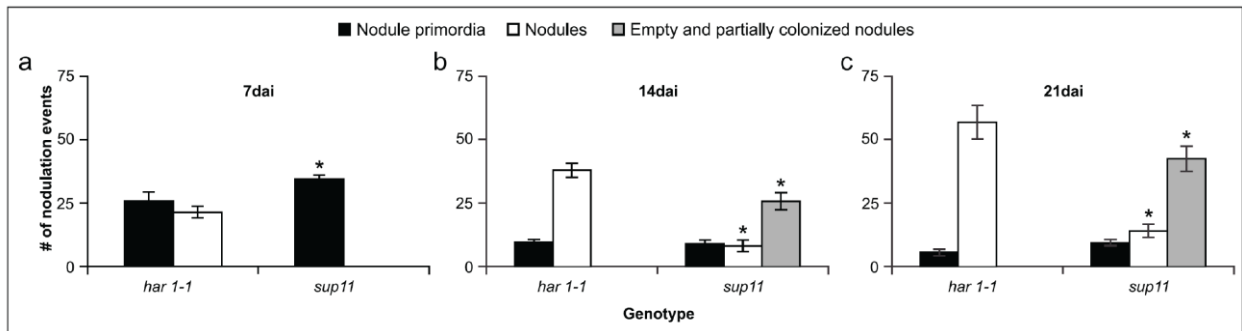


Figure 12. Kinetics of nodule development in *har1-1* parental line and *sup11*.

M. loti strain NZP2235 tagged with constitutive *hema::LacZ* reporter gene fusion was used for inoculation and roots were stained for β -galactosidase activity (blue) prior to nodule counting. Note that all nodule-associated cortical cell division events that have not yet emerged from the epidermis were categorized as nodule primordia. Un-colonized and partially colonized nodules were categorized following examples shown in Figure 19. Data represent mean values \pm SE for $n = 10$. Asterisks (*) denote statistically significant differences between genotypes within corresponding nodulation categories, as determined using a Student's t-test ($P < 0.05$). Data related to this figure were generated in the lab of Krzysztof Szczyglowski. Figure and legend adopted from Liao et al., 2012.

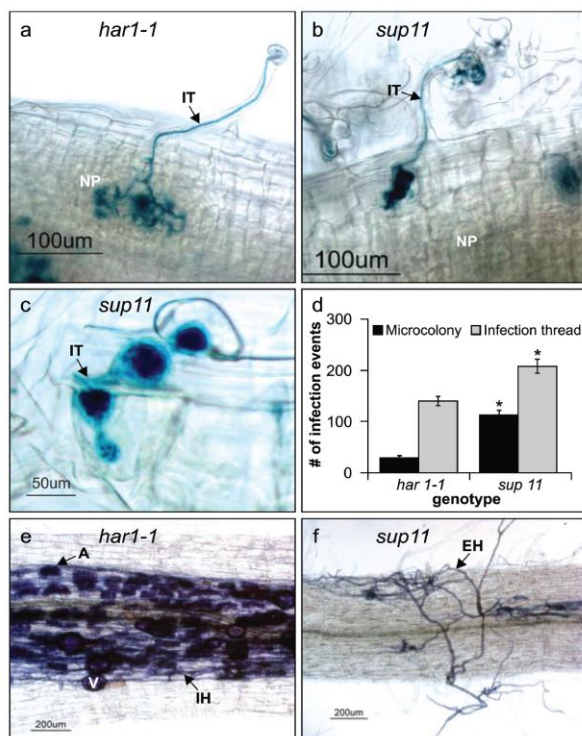


Figure 13. *sup11* aborts normal root colonization by *M. loti* and AM fungus.

Plants were inoculated with *M. loti* strain NZP2235 tagged with a constitutive *hema::LacZ* reporter gene fusion (a-d). Roots were stained (see Materials and Methods) and the symbiotic phenotypes were evaluated 7 dai. (a) The parental *har1-1* line; note that *M. loti* (blue) migrated through a root hair infection thread (IT), which then ramified within the underlying nodule primordium (NP). (b) Unsuccessful root colonization by *M. loti* in *sup11*; note that block of infection has occurred, which led to the accumulation of bacteria within swollen IT in the subepidermal cortical cell. (c) Enlarged microcolonies of *M. loti* formed at the *sup11* root epidermis; notice that IT was initiated from one of the microcolonies but its normal progression was halted, such that it became swollen upon entry into the subtending cortical cell. (d) Scores of infection events in *har1-1* and *sup11* mutant. Data represent mean values \pm SE for $n = 10$. Asterisks (*) denote statistically significant differences between the *har1-1* and *sup11* genotypes for a given category as determined using a Student's t-test ($P < 0.05$). (e and f) Representative fragments of *L. japonicus har1-1* and *sup11* roots 8 weeks after inoculation (wai) with *Rhizophagus irregularis*; note that unlike in *har1-1* (e), the fungus failed to penetrate *sup11* roots (f). IH: intraradical hypha; A: arbuscule; EH: extraradical hypha; V: vesicle.

Data related to this figure were generated in the lab of Krzysztof Szczyglowski. Figure and legend adopted from Liao et al., 2012.

3.2 Map-based cloning and next-generation sequencing identify two linked mutations

In the initial mapping population, 33 of 165 F2 individuals showed the *sup11* AM phenotype, consistent with a recessive monogenic trait ($P > 0.05$). Using linkage analysis, the mutated locus was positioned on chromosome 3 within an approximately 17 cM genetic interval, as delimited by the TM0155 and TM1468 molecular markers (Figure 14a, b). The contiguity of this interval was interrupted by three markers that showed no recombination events. Nevertheless, the *CCaMK* locus was encompassed by this interval, and sequence analysis of this common symbiosis gene revealed the presence of a single nucleotide polymorphism (G3922A) in *sup11* (Figure 14c). The mutation led to substitution of S337 by N (asparagine) in the CaM-binding domain of CCaMK (Figure 14d). The identified mutant *CCaMK* allele is referred to hereafter as *ccamk-14*, and the predicted mutant protein is referred to as CCaMK^{S337N}. We presumed that the apparent lack of recombinants at TM0226, TM0246 and TM0213 was the result of suppressed recombination in this region. In order to verify this assumption, the whole genome sequence of *sup11* was obtained by next-generation sequencing (see Materials and Methods). Bioinformatic analysis confirmed the presence of the *ccamk-14* allele, but also revealed an additional polymorphism (C272T) within the CM0226 contig in the *LjNPH3* locus (Figure 14e). This locus was predicted to encode a *L. japonicus* homolog of *Arabidopsis* NPH3 (Figure 14e), the NPH1 photoreceptor-interacting protein that is essential for phototropism (Motchoulski and Liscum, 1999). The identified *L. japonicus* mutant allele of *NPH3* is referred to hereafter as *nph3-1*. In summary, these results showed that *sup11* carries at least three mutant loci, namely *har1-1*, *ccamk-14* and *nph3-1*.

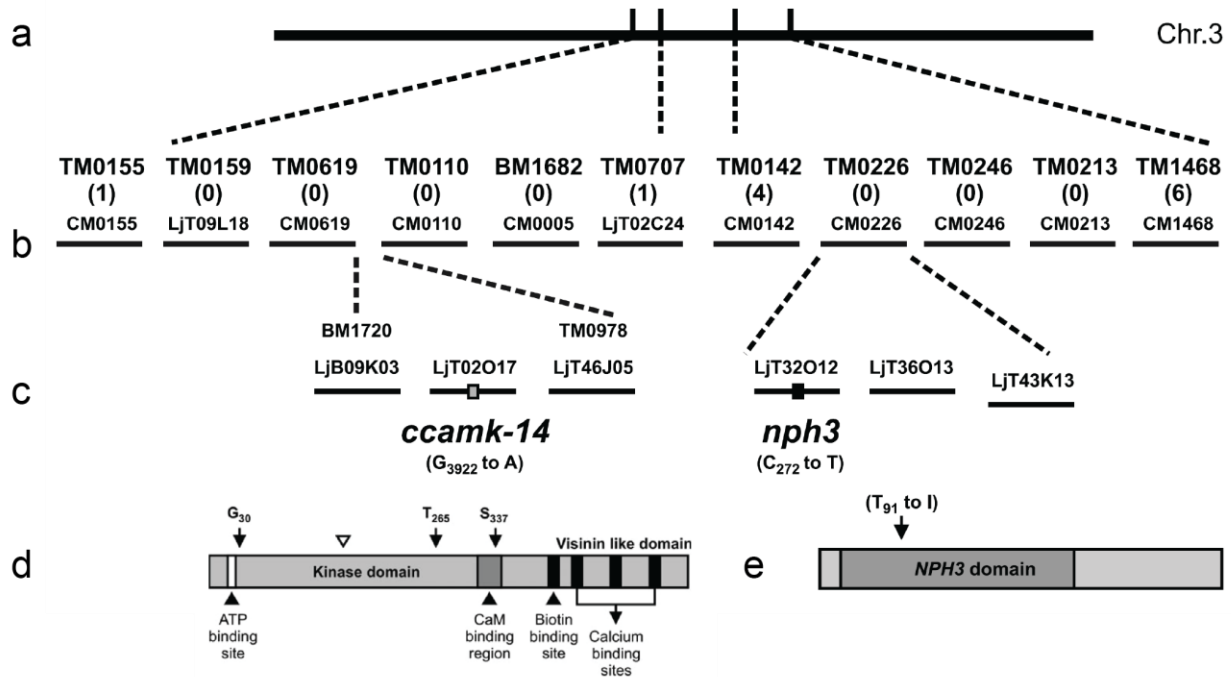


Figure 14. Map-based cloning and next generation sequencing identify two linked mutations.

(a) A schematic representation of the *L. japonicus* chromosome 3. (b) A portion of the chromosome 3, as represented by large insert clones (TM or BM) and the corresponding sequence contigs (CM) or sequenced genomic clones (LjT). Frequency of recombination events at the given position is provided in parentheses. (c) A mutant *ccamk-14* allele (gray box), containing G3922 to A nucleotide substitution, as identified by map-based cloning and sequencing. Next generation sequencing has confirmed the presence of the *ccamk-14* mutation and also revealed an additional mutant allele (black box), called *npH3-1* (C272 to T). (d) Schematic representation of the *L. japonicus* CCaMK protein with main domains indicated. Arrows indicate the approximate position of the predicted amino acid substitution in *ccamk-14* (S337N), and the locations of mutations in *ccamk-3* (G30E) and *snf1-1* (T265I). The white triangle indicates the approximate position of the 7 bp insertion that leads to a frame shift in *ccamk-13* (Perry et al., 2009). (e) A schematic representation of the predicted *L. japonicus* NPH3 protein with main domains indicated. Arrow indicates an approximate position of the predicted amino-acid substitutions in *npH3-1* (T91 to I).

Data related to this figure were generated in the lab of Krzysztof Szczyglowski. Figure and legend adopted from Liao et al., 2012.

3.3 *ccamk-14* is responsible for the symbiosis-defective phenotypes

Using gene-specific molecular markers and F2/F3 segregants derived from the genetic cross between *sup11* and wild-type *L. japonicus* Gifu (see Materials and Methods), individuals carrying the corresponding single homozygous mutant loci were selected (Figure 15). Subsequent analyses showed that *npH3-1* had no discernible negative impact on nodulation and AM development, although shoot growth of the mutant plant was somewhat diminished in comparison with wild-type Gifu (Figure 16). Consistent with these observations, the wild-type *L. japonicus* CCaMK gene was able to restore normal AM formation in transgenic hairy roots induced on *sup11* shoots (Figure 17). The defective nodule infection and AM root colonization phenotypes of the *ccamk-14* single mutant (see below) were also restored by the CCaMK gene (Figure 18). Thus, *ccamk-14* was defined as the causative mutation, which was further confirmed through detailed analyses of the *ccamk-14* single mutant.

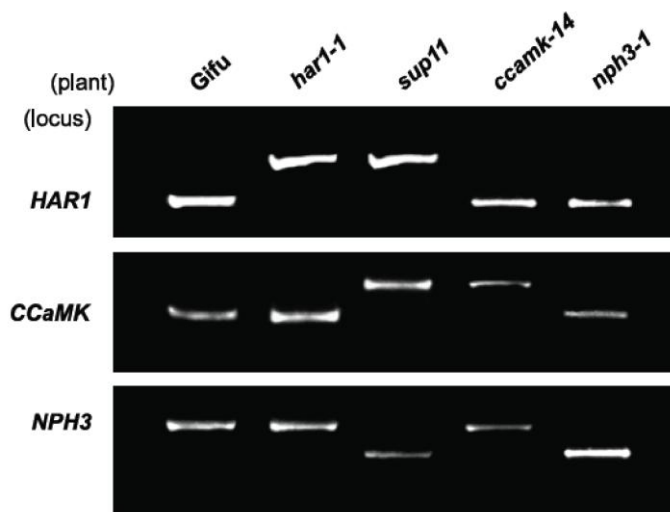


Figure 15. The genotypes.

The *HAR1* locus specific *Mva*I-CAPS marker and *Bsr*BI- and *Bsr*DI-dCAPS markers for the *CCaMK* and *nph3-1* loci, respectively, were used (see Materials and Methods). The following size (bp) of PCR fragments for wild-type and mutant alleles were obtained, as predicted by the position of gene-specific primers and digestion products: (1) *HAR1*: 369, *har1-1*: 463; (2) *CCaMK*: 125, *ccamk-14*: 150; (3) *NPH3*: 244; *nph3-1*: 216. Note that “*sup11*” reflects the original mutant line carrying *har1-1*, *ccamk-14* and *nph3-1* mutant alleles.

Data related to this figure were generated in the lab of Krzysztof Szczyglowski. Figure and legend adopted from Liao et al., 2012.

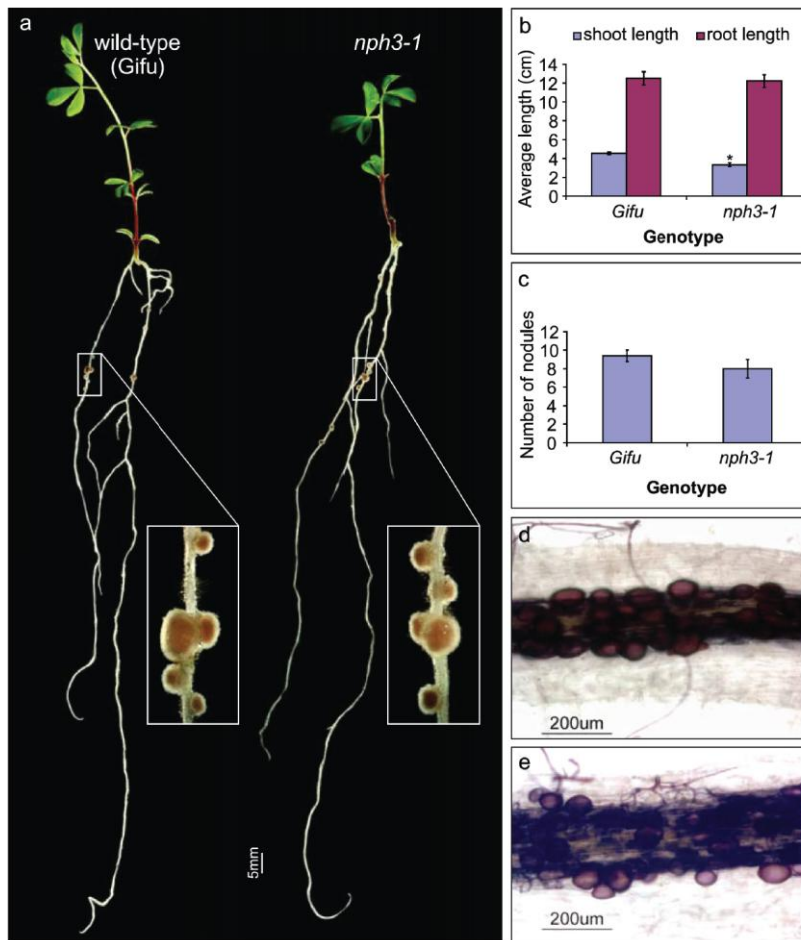


Figure 16. *nph3-1* single mutant phenotypes.

M. loti strain NZP2235 was used for plant inoculation. (a) Wild-type *L. japonicus* Gifu and the *nph3-1* single mutant, 14 dai. Note that the wild-type Gifu and the *nph3-1* develop only pink nodules (see inserts). (b) Measurements of shoot and root length in wild-type and *nph3-1* 14 dai on plants grown in soil. (c) Counts of nodules at 14 dai. Data shown in b and c represent mean values \pm SE for $n = 10$. Asterisk (*) denotes statistically significant difference between genotypes within the corresponding category as determined using a Student's t-test ($P < 0.05$). (d-e) Representative fragments of *L. japonicus* wild-type (d) and *nph3-1* mutant roots (e) showing successful colonization by *R. irregularis*. Data related to this figure were generated in the lab of Krzysztof Szczyglowski. Figure and legend adopted from Liao et al., 2012.

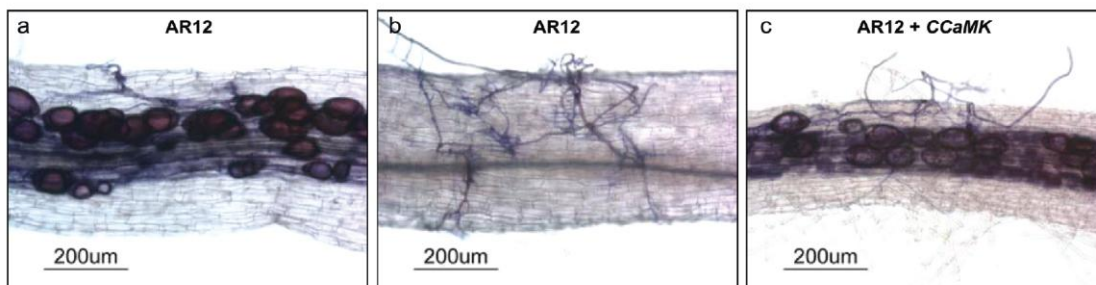


Figure 17. The *L. japonicus* CCaMK gene restores AM development in *sup11*.

A genomic fragment containing the entire *CCaMK* locus was introduced by *A. rhizogenes* (AR12)-mediated transformation (see Materials and Methods) to generate transgenic hairy roots on non-transgenic shoots. The resulting hairy roots were stained with 5% ink in 5% acetic acid eight weeks after inoculation to reveal the location of *R. irregularis*. (a) *har1-1* transformed with the AR12 strain; (b) *sup11* transformed with the AR12 strain; (c) *sup11* transformed with the AR12 strain containing the *CCaMK* gene.

Data related to this figure were generated in the lab of Krzysztof Szczyglowski. Figure and legend adopted from Liao et al., 2012.

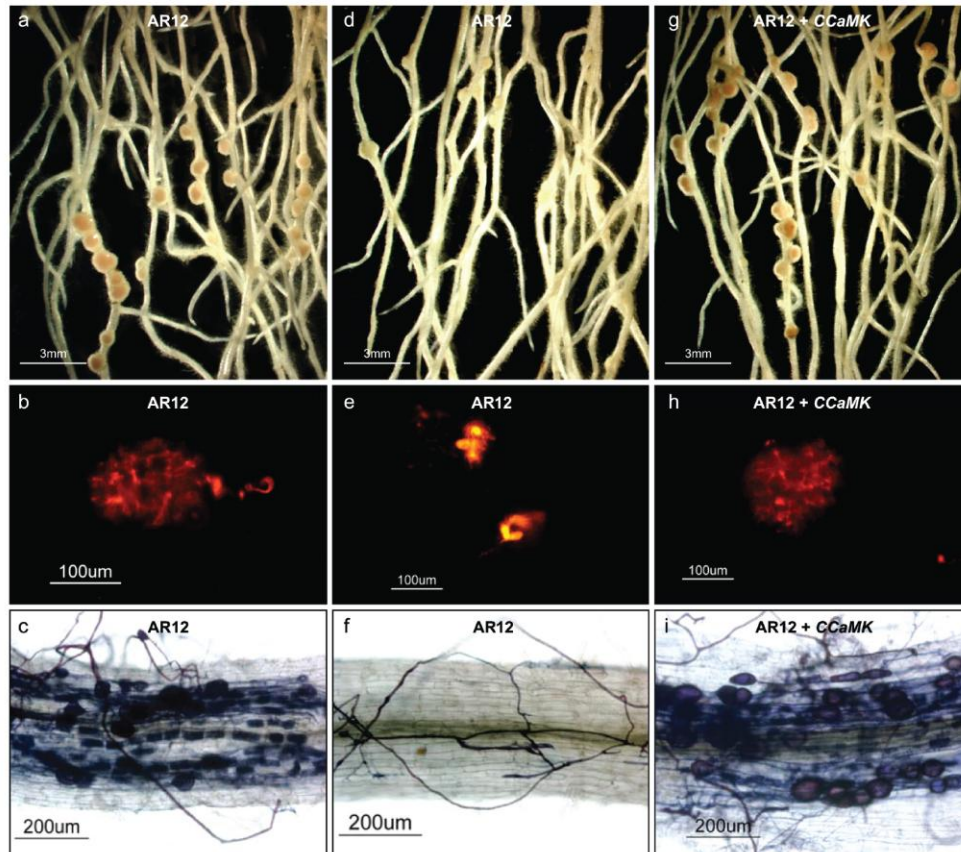


Figure 18. The *L. japonicus* *CCaMK* gene restores wild-type nodulation and AM development in *ccamk-14*.

A genomic fragment containing the entire *CCaMK* locus was introduced by *A. rhizogenes* (AR12)-mediated transformation to generate transgenic hairy roots on non-transgenic shoots. The resulting plants were inoculated with the DsRed-containing *M. loti* or *R. irregularis* and their nodulation (a, b, d, e, g, h) and mycorrhiza (c, f, i) phenotypes were evaluated 11 dai or 8 wai, respectively. (a-c) wild-type *L. japonicus* transformed with the AR12 strain; notice the formation of pink nodules (a), presence of DsRed fluorescence inside a small nodule primordium (b) and the wild-type AM symbiotic phenotype (c). (d-f) *ccamk-14* transformed with the AR12 strain; notice that white or pale-pink nodules are present (d) and clumps of fluorescence are visible at the surface of a small nodule primordium (e). Fungal hyphae failed to penetrate the *ccamk-14* roots (f). (g-i) *ccamk-14* transformed with the AR12 strain containing the *CCaMK* genomic DNA. The wild type nodulation (g and h) and AM symbiotic phenotype are restored.

Data related to this figure were generated in the lab of Krzysztof Szczyglowski. Figure and legend adopted from Liao et al., 2012.

3.4 *ccamk-14* recapitulates the symbiotic defects of *sup11*

When grown in the absence of *M. loti*, *ccamk-14* did not form spontaneous nodules or affect shoots or root growth (data not shown). In the presence of *M. loti*, *ccamk-14* developed a mixture of un-colonized, partially colonized and wild-type-like nodules (Figures 11b and 19). The partially colonized nodules represented the majority of events at 14 and 21 days after inoculation (Figure 20). The progression and subsequent ramification of ITs within the NP interior were restricted in *ccamk-14* (Figure 21a, b). Microcolonies were readily formed, but often appeared enlarged (Figure 21c, j). Like the microcolonies, epidermal root hair ITs were significantly more frequent than in wild-type Gifu (Figure 21d, j). They were intact, although spillage of bacteria from a presumably destabilized epidermal IT into the interior of the epidermal cell was detected in at least one case (Figure 21d). The major block in the infection process was observed to occur during passage of ITs inside the sub-epidermal cortex. ITs became grossly swollen inside the outer cortex (Figure 21d–f). Their further progression into deeper regions of NP was associated with frequent looping and secondary swellings, leading to the partially colonized nodule phenotype (Figure 21e–g). In at least a few instances, the infection process in *ccamk-14* more closely resembled wild-type events (Figure 21h, i). These events probably contributed to the formation of fully colonized nodules in *ccamk-14* (Figure 19e, f). AM infection of *ccamk-14* was generally blocked (Figure 22), such that only very sporadic intra-radical colonization events were observed. The fungus formed balloonshaped hyphal swellings on or within *ccamk-14* root outer cell layers (Figure 22b, c), reminiscent of the block observed in ‘common symbiosis’ mutants (Kistner et al., 2005). In *ccamk-14*, the extent of intra-radical root colonization was only 5% of the wild-type (Figure 22d). However, once the fungus managed to penetrate the mutant root, wild-type structures, including vesicles and arbuscules, were formed.

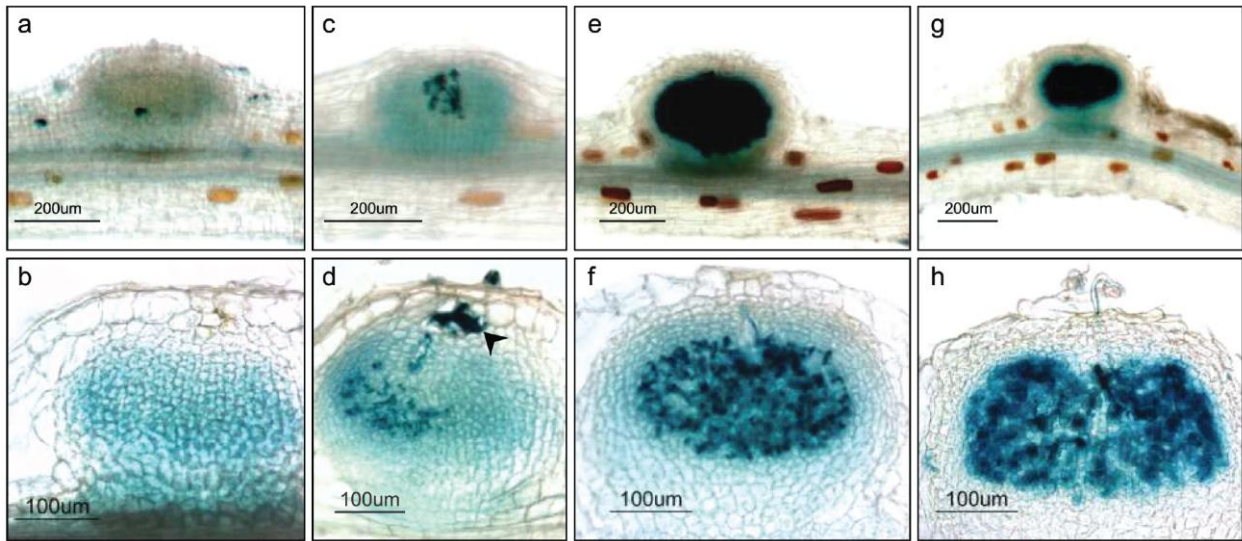


Figure 19. *ccamk-14* forms a mixture of un-colonized, partially colonized and wild-type-like nodules.

M. loti strain NZP2235 tagged with a constitutive *hema::LacZ* reporter gene fusion was used, and roots were stained for β -galactosidase activity at 14 days after inoculation to reveal the location of bacteria (dark blue colour). (a, b) Example of an empty nodule in *ccamk-14* (a) and the corresponding nodule section (b). (c, d) A partially colonized nodule in *ccamk-14* (c) and the corresponding nodule section (d), showing the presence of an extensive sub-epidermal infection region (arrow) and limited colonization of the nodule interior. (e, f) Wild-type-like nodule in *ccamk-14* that is fully colonized by *M. loti* (e), and the corresponding nodule section (f). (g, h) Representative wild-type (Gifu) nodule colonized by *M. loti* (g), and the corresponding nodule section (h). Images shown in (b), (d), (f) and (h) represent approximately 35 μ m thick sections. Note that a light blue color, for example in (b), reflects background staining.

Data related to this figure were generated in the lab of Krzysztof Szczyglowski. Figure and legend adopted from Liao et al., 2012.

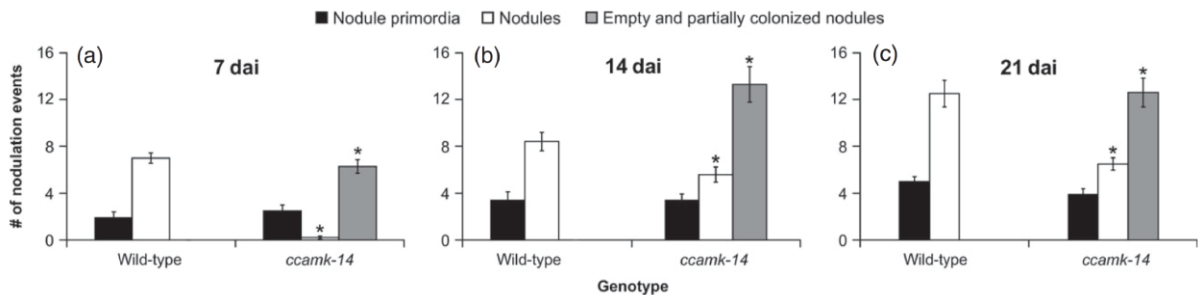


Figure 20. Kinetics of nodule formation in wild-type Gifu and *ccamk-14*.

Mesorhizobium loti strain NZP2235 tagged with a constitutive *hema::LacZ* reporter gene fusion was used for inoculation, and roots were stained for β -galactosidase activity (blue) prior to nodule counting. Note that all nodules that have not yet emerged from the epidermis were categorized as nodule primordia. Un-colonized and partially colonized nodules were categorized based on the examples shown in Figure 19. Values are means \pm SE (n = 10). Asterisks indicate statistically significant differences between genotypes within corresponding nodulation categories, as determined using Student's t-test (*P < 0.05).

Data related to this figure were generated in the lab of Krzysztof Szczyglowski. Figure and legend adopted from Liao et al., 2012.

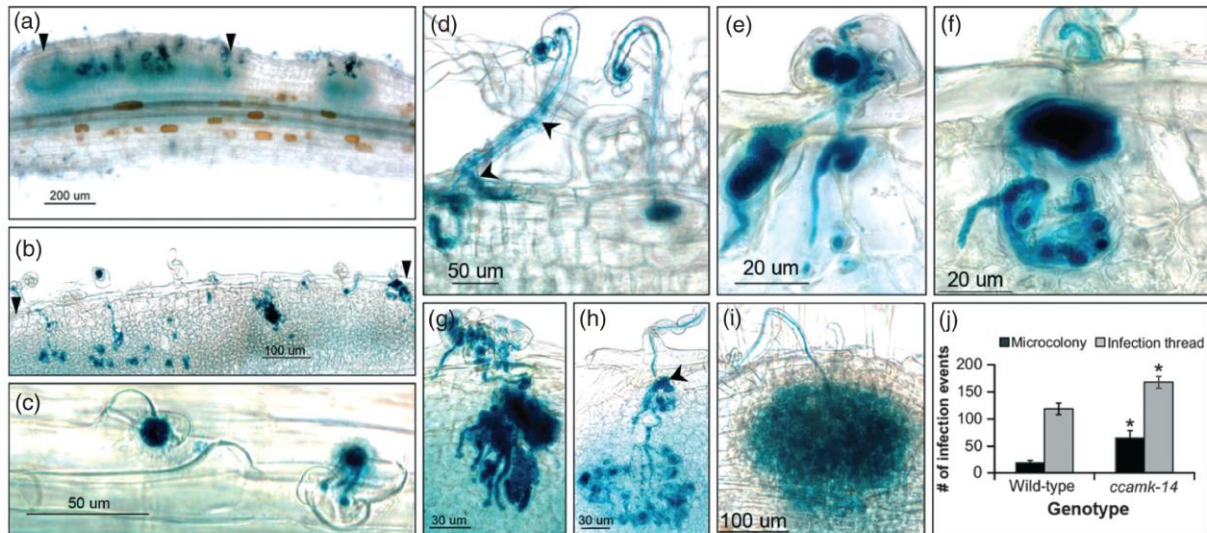


Figure 21. The *ccamk-14* mutation impairs cortical infections.

Mesorhizobium loti strain NZP2235 tagged with a constitutive *hemaA::LacZ* reporter gene fusion was used for inoculation and roots were stained for β -galactosidase activity at 7 and 14 days after inoculation to reveal the location of bacteria (dark blue colour). (a, b) Fragment of *ccamk-14* root showing partial colonization of subtending nodule primordia (a), and the corresponding section (b); arrowheads in (a) indicate the approximate position of the sectioned portion shown in (b). (c) Grossly enlarged colonies of *M. loti* formed within short coiled root hairs in *ccamk-14*. (d) Example of two epidermal infection threads in *ccamk-14* root hairs. Note that one of the ITs (left) migrated into the sub-epidermal cortex where it has begun looping. A limited discharge of bacteria from the IT into the epidermal cell is noticeable (arrows). The second IT (right) remained intact; however, its progression was halted within the subtending cortical cell, as reflected by the IT swelling. (e–g) Multiple secondary infection events originating from swollen ITs. Note the progressive migration of disfigured ITs into deeper regions of the nodule cortex (e–g), which was usually associated with looping and twisting (f). (h) Successful ramification of ITs within the nodule interior in *ccamk-14*. Note the presence of a swollen IT (arrow) at or near the epidermis/cortex interface. (i) Small nodule that was fully colonized by *M. loti* in wild-type *L. japonicus* Gifu. Images shown in (b) and (d–h) represent approximately 30 μ m thick sections. (j) Number of infection events at 7 dai in wild-type Gifu and *ccamk-14*. Values are means \pm SE (n = 10). Asterisks indicate statistically significant differences between genotypes within the corresponding infection event categories as determined using Student's t-test ($P < 0.05$). Data related to this figure were generated in the lab of Krzysztof Szczyglowski. Figure and legend adopted from Liao et al., 2012.

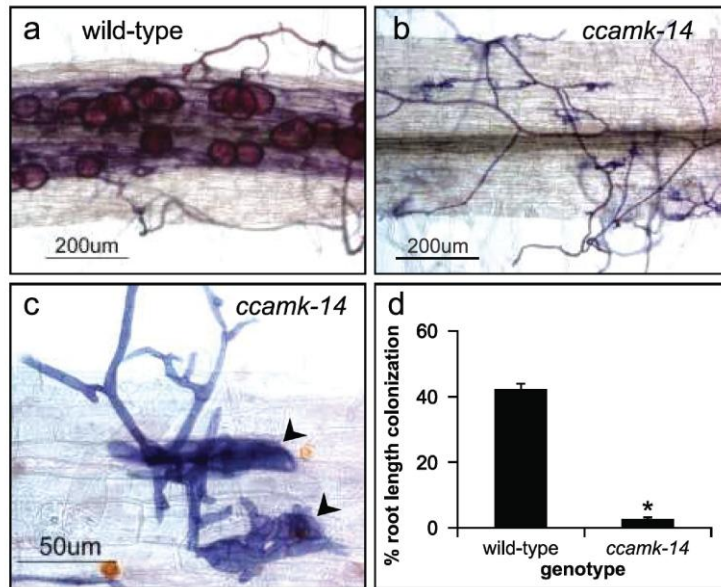


Figure 22. *ccamk-14* is defective in AM symbiosis.

(a) Representative fragment of *L. japonicus* wild-type roots that was successfully colonized by *R. irregularis*. (b) Segment of *ccamk-14* root showing multiple unsuccessful colonization attempts. (c) Close-up of the *ccamk-14* root surface showing swollen hyphae at places of attempted fungus entry (arrows).

(d) Quantification of root colonization by *R. irregularis* in wild-type and *ccamk-14*. Values are means \pm SE (n = 6). The asterisk indicates a statistically significant difference between the two genotypes as determined using Student's t test ($P < 0.05$).

Data related to this figure were generated in the lab of Krzysztof Szczyglowski. Figure and legend adopted from Liao et al., 2012.

3.5 Substitutions at S337 modify binding of Ca^{2+} /CaM

We have identified the S337 residue as a potential additional auto-phosphorylation site on recombinant *L. japonicus* CCaMK subjected to *in vitro* auto-phosphorylation (Figure 23). As S337 is located within the CaM-binding domain (Figures 14d and 24a), we tested whether addition of the phosphate group interferes with CaM binding. In addition to CCaMK^{S337N} (corresponding to the *ccamk-14* mutation), a phospho-mimetic mutant CCaMK^{S337D} was constructed (see Materials and Methods) and used in CaM binding and CCaMK kinase activity assays. In the presence of Ca^{2+} , wild-type CCaMK and CCaMK^{S337N} were both retained on CaM beads and were released by EGTA (Figure 24b), indicating a specific and calcium-dependent interaction. However, approximately twice as much CCaMK^{S337N} was retained in comparison with CCaMK (Figure 24b, c). In contrast, significantly lower amounts of CCaMK^{S337D} were bound by CaM (Figure 24b, c), indicating interference by the phospho-mimetic replacement. The biological relevance of the S337 to D (aspartic acid) substitution was subsequently tested by expressing CCaMK^{S337D} from the *L. japonicus* CCaMK promoter or the strong *L. japonicus* polyubiquitin promoter (Maekawa et al., 2008) in transgenic hairy roots induced on non-transgenic *ccamk-13* mutant shoots (Madsen et al., 2010). Unlike wildtype CCaMK, which restored normal nodulation and arbuscular mycorrhiza to the *ccamk-*

13 null mutant background when expressed from the endogenous or the polyubiquitin promoter, no complementation was observed with CCaMK^{S337D}, indicating impaired functionality of this mutant protein (Figure 25). Like CCaMK^{S337N}, CCaMK^{S337D} did not confer spontaneous nodule formation in transgenic hairy roots grown in the absence of *M. loti* (Figure 25).

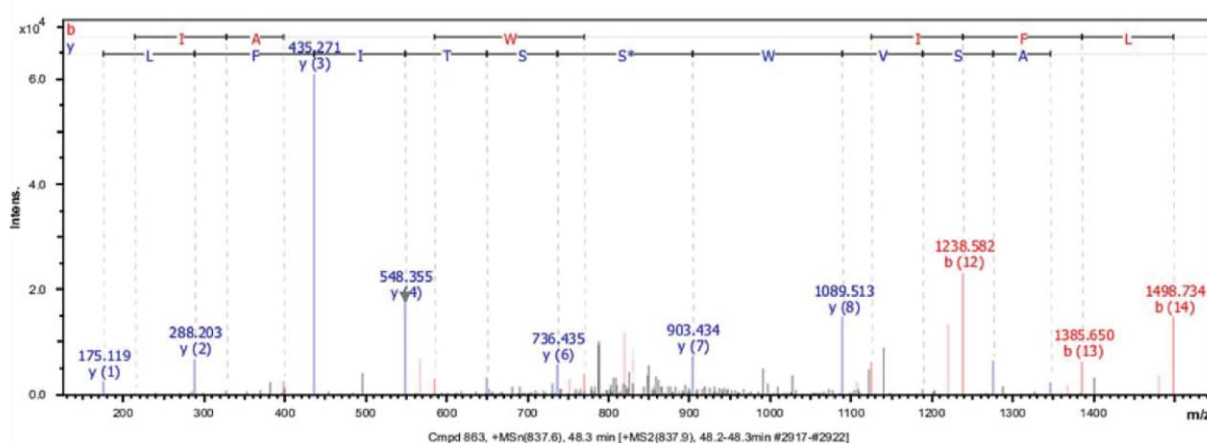


Figure 23. MS/MS spectrum of CCaMK phosphopeptide 329-AAAIASVWpSSTIFLR-343 containing pS337.

The mass difference of 167 Da between fragment ions y6 (mass: 736.435 Da) and y7 (mass: 903.434 Da) indicates specific phosphorylation of serine 337 (S*) resulting in a mass increment of serine (87 Da) of 80 Da by the attached phosphate group (pS = 167 Da).

(a) 320-SFNARRKLRAAAIASVW**SS**-338

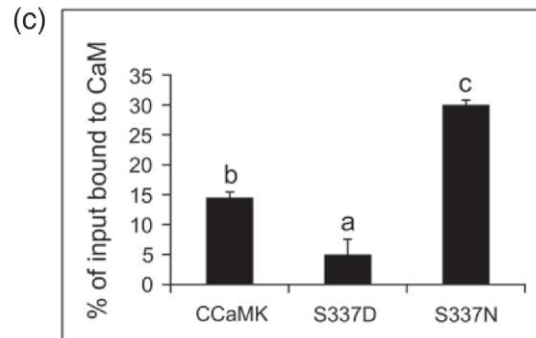
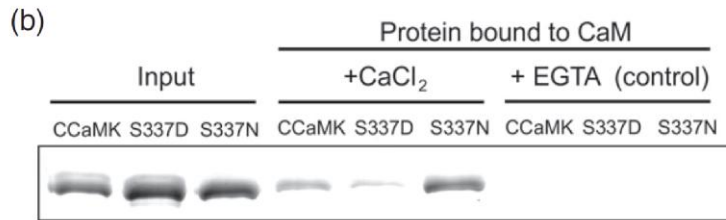


Figure 24. Calmodulin binding capability of CCaMK and calmodulin binding site mutants CCaMK^{S337N} and CCaMK^{S337D}.

Equal amounts (25 µg) of purified protein (MBP-CCaMK, MBP-CCaMK^{S337D}, or MBP-CCaMK^{S337N}) were incubated with CaM-Sepharose beads in the presence or absence of CaCl₂. Calmodulin-bound protein was eluted using buffer containing 2 mM EGTA and visualized by SDS-PAGE and Coomassie staining.

(a) Amino acid sequence of the CCaMK calmodulin binding domain. Serine 337 (S) (substituted by asparagine (N) in *ccamk-14*) is boxed.

(b, c) The wild-type protein binds with moderate strength. Markedly reduced CaM binding affinity was observed with the presumed auto-phosphorylation mimic CCaMK^{S337D}, while CCaMK^{S337N} retains high-affinity binding. Values are means ±SD from two independent experimental set-ups. Different letters indicate significant differences between activity values, as determined using Tukey multiple comparisons of means with a 95% family-wise confidence level.

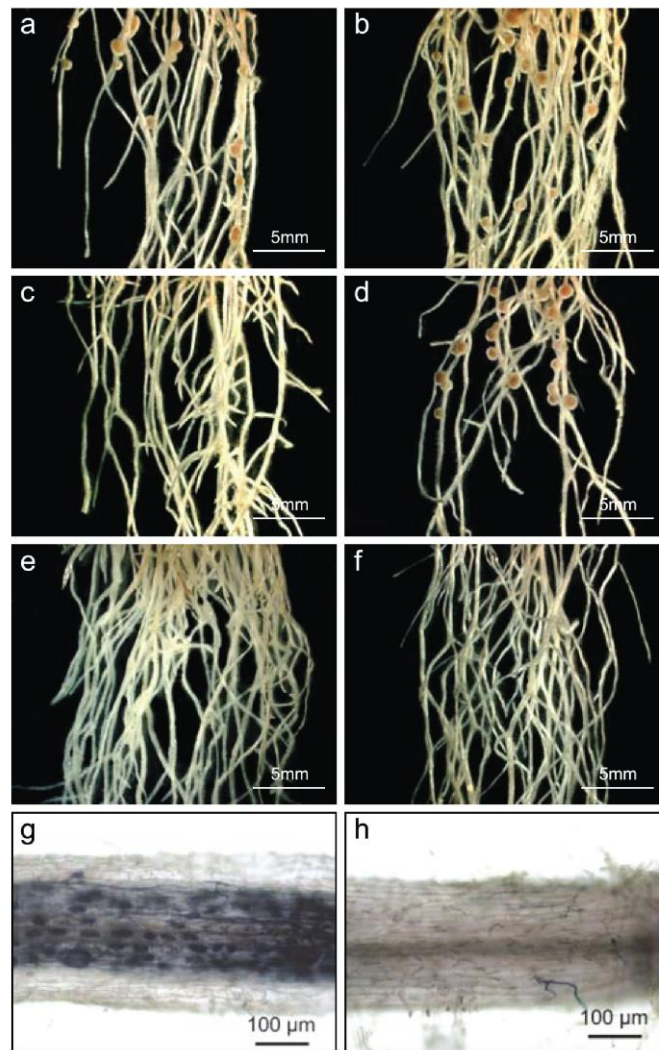


Figure 25. Expression of CCaMK^{S337D} does not rescue the *ccamk-13* null symbiotic phenotype.

The wild-type CCaMK cDNA (cDNACCaMK) and a cDNA encoding the CCaMK^{S337D} variant (cDNACCaMK^{S337D}) under the control of the cognate CCaMK promoter (b, d, e and f) or polyubiquitin promoter (g and h) were introduced by *A. rhizogenes* AR1193 mediated transformation to either wild-type *L. japonicus* Gifu (b) or *ccamk-13* mutant (c-h) to generate transgenic hairy roots on non-transgenic shoots. The resulting chimeric plants along with those carrying control transgenic hairy roots (a and c) were inoculated with *M. loti* or *R. irregularis* and their nodulation (a-e) and mycorrhiza (g and h) phenotypes were evaluated 11 dai and 8 wai, respectively. (a) wild-type Gifu transformed with the control AR1193 strain; (b) wild-type Gifu transformed with AR1193 containing cDNACCaMK^{S337D}; (c) *ccamk-13* transformed with the control AR1193 strain; (d and g) *ccamk-13* transformed with AR1193 containing cDNACCaMK (note the complementation of nodulation and mycorrhization) (e and h) *ccamk-13* transformed with AR1193 containing cDNACCaMK^{S337D} (f) *ccamk-13* transformed with AR1193 containing cDNACCaMK^{S337D} and grown in the absence of either *M. loti* or *R. irregularis* for 6 weeks (note lack of spontaneous nodules). Although the mycorrhiza phenotypes in g and h are shown for *ccamk-13* plants transformed with constructs driven by the polyubiquitin promoter, the same results were obtained with *ccamk-13* plants expressing the corresponding constructs from the endogenous promoter. Data related to figures 25a-f were generated in the lab of Krzysztof Szczyglowski. Figure and legend adopted from Liao et al., 2012.

3.6 CCaMK^{S337N} and CCaMK^{S337D} are not impaired in the interaction with CYCLOPS

Given the influence of S337 modification on CaM binding, we also tested whether CCaMK, CCaMK^{S337N} and CCaMK^{S337D} exhibit an alteration in the interaction with CYCLOPS, a known interactor and an *in vitro* phosphorylation substrate of CCaMK (Yano et al., 2008). Quantitative yeast two-hybrid analysis revealed that a kinase-dead CCaMK^{G30E} version, encoded by the *ccamk-3* allele (Shimoda et al., 2012; Tirichine et al., 2006), was strongly impaired in its interaction with CYCLOPS, but the interaction of both CCaMK^{S337N} and CCaMK^{S337D} with CYCLOPS was at a similar level as wild-type CCaMK (Figure 26).

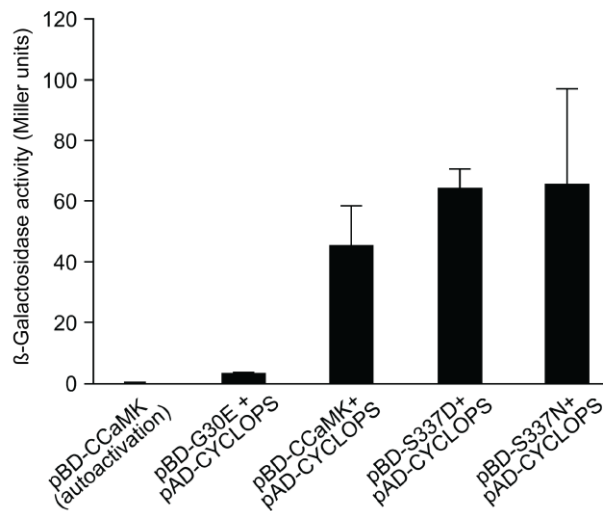


Figure 26. Quantitative yeast two-hybrid interaction analysis of CCaMK, kinase dead CCaMK^{G30E}, CCaMK^{S337N} and CCaMK^{S337D} with CYCLOPS.

The interaction was assayed by the quantitative analysis of β-galactosidase activity obtained from *Saccharomyces cerevisiae* HF7c cells transformed with the indicated constructs. Compared to the kinase inactive mutant CCaMK^{G30E} which is impaired in the interaction with CYCLOPS, CCaMK^{S337} mutant variants (S337D, S337N) show wild-type-like interaction. Presented are mean values and standard deviations obtained from three biological replicates. One Miller unit of β-galactosidase is defined as the amount which hydrolyzes 1 μmol of ONPG to o-nitrophenol and D-galactose per min per cell. BD: fusion to the Gal4 DNA binding domain, AD: fusion to the Gal4 activation domain.

3.7 Substitution of the S337 autophosphorylation site alters the regulation of substrate phosphorylation

We subsequently tested the relevance of the S337 autophosphorylation site for CCaMK kinase activity *in vitro*. In the absence of Ca²⁺, CCaMK and CCaMK^{S337N} showed low autophosphorylation activities, although the basal CCaMK^{S337N} activity was approximately twofold lower compared to CCaMK (Figure 27a and Figure 28a). Autophosphorylation activity of CCaMK doubled in the presence of calcium alone and returned to non-stimulated levels in the presence of calcium and calmodulin (Figure 27a). This reduction is consistent with previous reports (Kang et al., 2011; Yano et al., 2008), and was observed in the presence

of CYCLOPS (Figure 27a) but not with myelin basic protein (Figure 28a) or in the absence of any substrate (Figure 29). This behaviour may reflect protection of auto-phosphorylation sites in wild-type CCaMK specifically in the presence of calmodulin and CYCLOPS. This negative regulation of the *in vitro* auto-phosphorylation activity by $\text{Ca}^{2+}/\text{CaM}$ in the presence of CYCLOPS was absent in CCaMK^{S337N} (Figure 27a), while CCaMK^{S337D} was almost totally unresponsive to addition of Ca^{2+} or $\text{Ca}^{2+}/\text{CaM}$, regardless of the presence or absence of a substrate (Figure 27a, 28a and 29). CYCLOPS phosphorylation by wild-type CCaMK was very strongly increased only in the presence of $\text{Ca}^{2+}/\text{CaM}$ (Figure 27b), which clearly demonstrates the essential role of CaM in phosphorylation of CYCLOPS. Consistent with the observed interference of the S337 phospho-mimetic replacement with calmodulin binding, CYCLOPS phosphorylation activity by CCaMK^{S337D} was not stimulated or was only marginally stimulated by addition of Ca^{2+} or $\text{Ca}^{2+}/\text{CaM}$, respectively (Figure 27b). In contrast, CYCLOPS phosphorylation by CCaMK^{S337N}, which carries a phospho-ablative substitution, reached a threefold higher level relative to wildtype in the presence of $\text{Ca}^{2+}/\text{CaM}$ (Figure 27b). The pattern observed with the commonly used artificial phosphorylation substrate myelin basic protein was overall similar to that with CYCLOPS, but revealed some differences, which may indicate a substrate-dependent behavior of CCaMK. Phosphorylation of myelin basic protein by CCaMK^{S337N} was stimulated approximately 15-fold by $\text{Ca}^{2+}/\text{CaM}$ in comparison with its basal activity, exceeding the corresponding 10-fold activation shown by the wild-type (Figure 28); however, the relative level was less than the phosphorylation observed for CYCLOPS (Figure 27b).

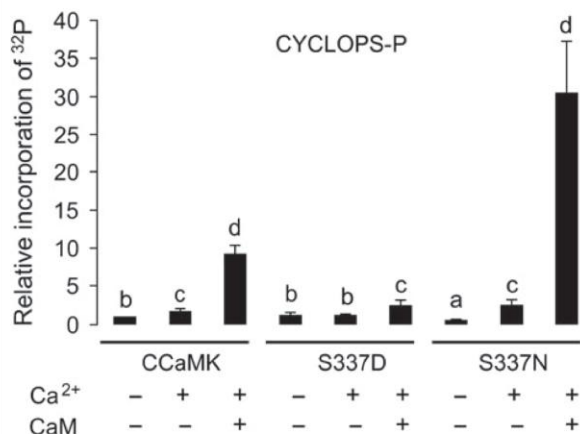
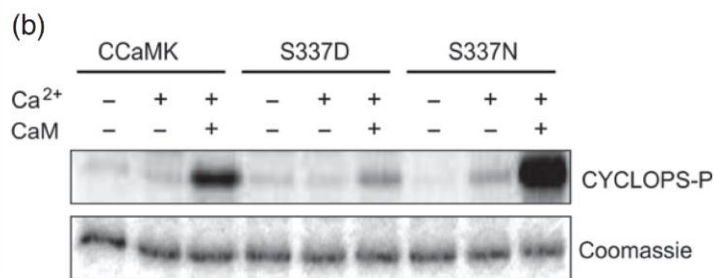
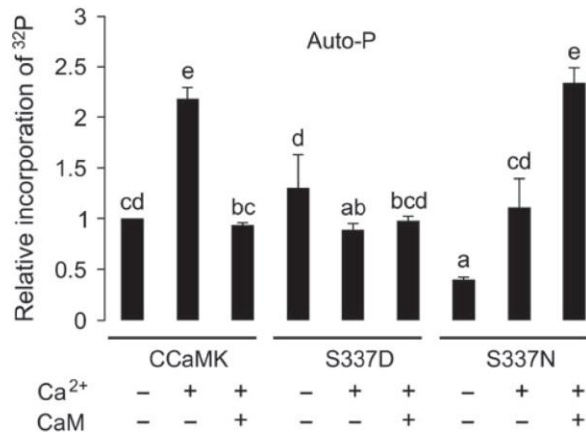
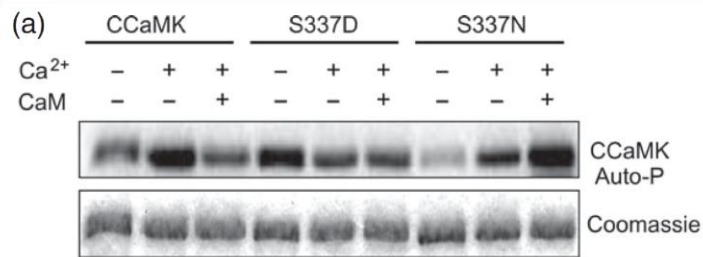


Figure 27. *In vitro* kinase activity of CCaMK, CCaMK^{S337N} and CCaMK^{S337D} in the presence of CYCLOPS.

MBP-tagged CCaMK and the mutant variants CCaMK^{S337D} and CCaMK^{S337N} were tested for *in vitro* kinase activity in the presence of either 4 mM EGTA (-), 0.1 mM CaCl₂ (Ca²⁺) or 0.1 mM CaCl₂ and 1 μM calmodulin (CaM). Each reaction contained 2 μg CCaMK protein and 2 μg CYCLOPS as substrate.

(a) Auto-phosphorylation of CCaMK, CCaMK^{S337D} or CCaMK^{S337N}.

(b) Phosphorylation of the CCaMK phosphorylation substrate CYCLOPS.

(a, b) Quantification of auto-phosphorylation and CYCLOPS phosphorylation. Incorporation of radioactive phosphate was quantified using a Typhoon phosphor imager, and band intensities were normalized to values determined for CCaMK wild-type in the presence of EGTA, which were set to 1. Values are means ±SD of kinase activity from two independent experimental set-ups. The same letter denotes a lack of significant differences between activity values, as determined using the Kruskal–Wallis multiple comparison with Bonferroni correction; α= 0.05.

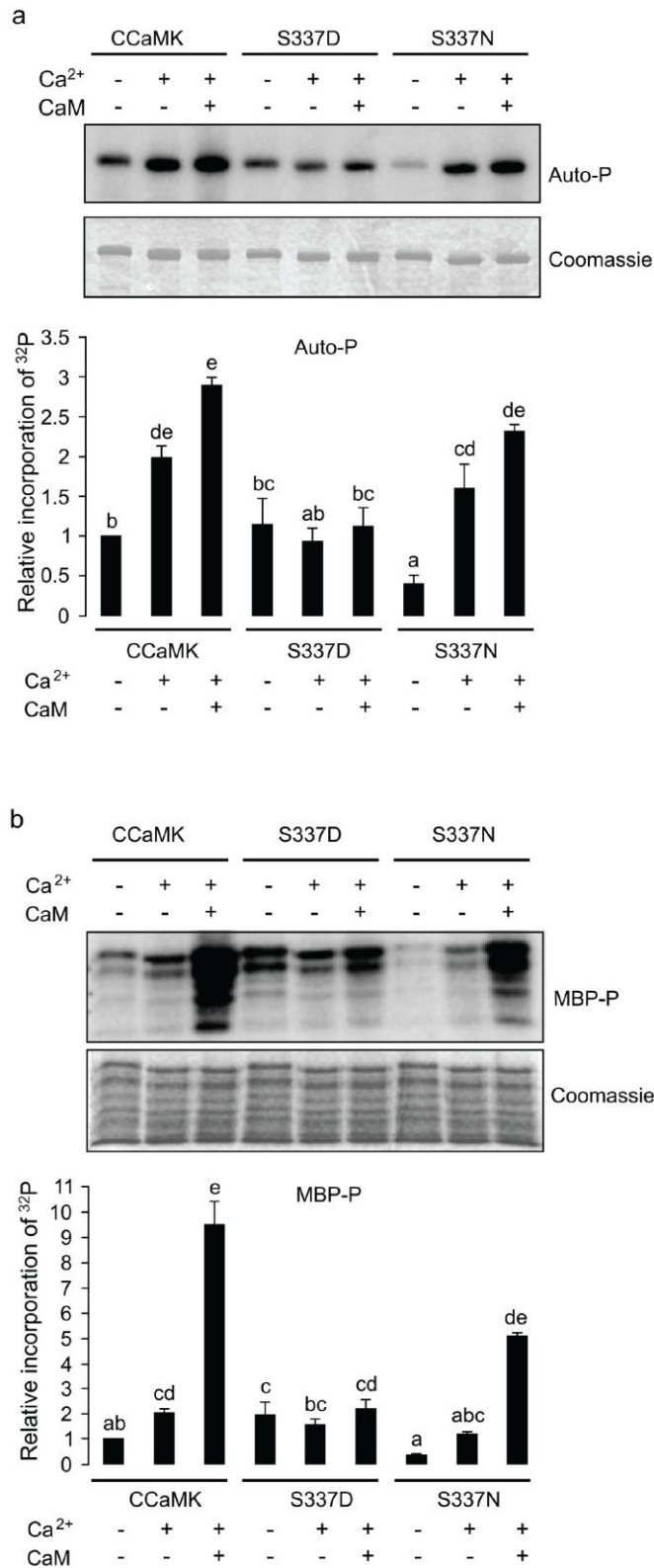


Figure 28. *In vitro* kinase activity of CCaMK, CCaMK^{S337N} and CCaMK^{S337D} in the presence of MBP.

Maltose-binding-protein tagged CCaMK and the mutant variants CCaMK^{S337D} and CCaMK^{S337N} were tested for *in vitro* kinase activity in the presence of either 4 mM EGTA (-), 0.1 mM CaCl₂ (Ca²⁺), or 0.1 mM CaCl₂ and 1 μM calmodulin (CaM). Each reaction contained 2 μg of CCaMK protein and 10 μg of myelin basic protein (MBP) as substrate. Incorporation of radioactive phosphate was visualised using a Typhoon phosphorimager.

(a) Auto-P: Autophosphorylation of CCaMK, CCaMK^{S337D}, or CCaMK^{S337N}. (b) MBP-P: Phosphorylation of the artificial phosphorylation substrate, MBP.

(a, b) Quantitation of autophosphorylation (Auto-P) and MBP phosphorylation (MBP-P). Incorporation of radioactive phosphate was quantified using a Typhoon phosphorimager and band intensities (auto-, or MBP phosphorylation) were normalized to values determined for CCaMK wild type in the presence of EGTA (1-fold incorporation). Graph represents mean values ± standard deviation of kinase activity from two independent experimental set-ups. The same letter denotes lack of significant differences between activity values, as determined using the Kruskal-Wallis multiple comparison with the Bonferroni correction; α=0.05.

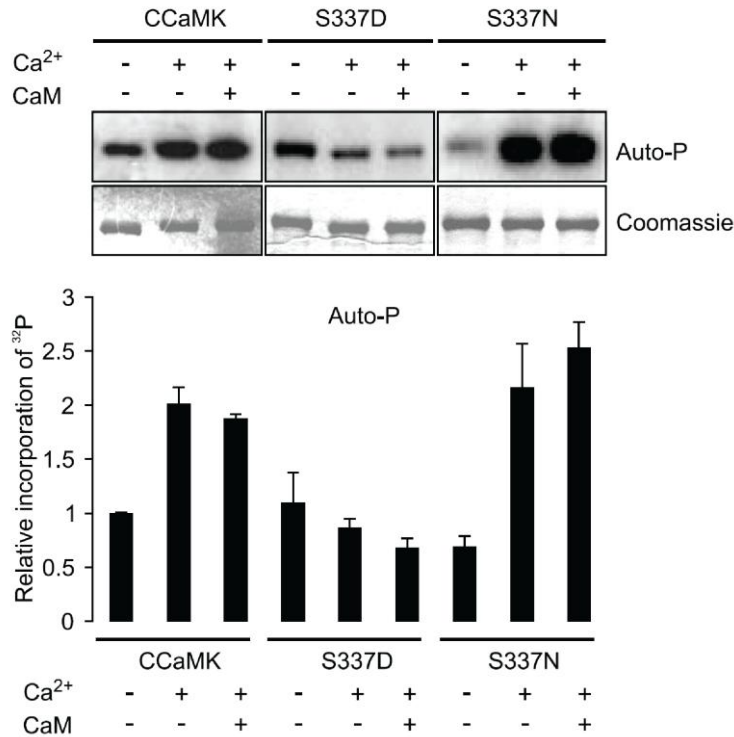


Figure 29. *In vitro* autophosphorylation activity of CCaMK, CCaMK^{S337N} and CCaMK^{S337D} in the absence of substrate.

Maltose-binding-protein tagged CCaMK, CCaMK^{S337D} and CCaMK^{S337N} were tested for *in vitro* autophosphorylation in the presence (+) of either 4 mM EGTA, 0.1 mM CaCl₂ (Ca²⁺), or 0.1 mM CaCl₂ and 1 μM calmodulin (CaM). Each reaction contained 2 μg of CCaMK protein. Auto-P: Autophosphorylation of CCaMK, CCaMK^{S337D}, or CCaMK^{S337N}. Incorporation of radioactive phosphate was quantified using a Typhoon phosphorimager and band intensities were normalized to values determined for CCaMK wild-type in the presence of EGTA (1-fold incorporation). Graph represents mean values ± standard deviation from two technical replicates of one experimental set-up.

4 Discussion

Here we show that the *ccamk-14* mutation, which leads to substitution of S337 by asparagine within the Ca²⁺/CaM binding domain of the *L. japonicus* CCaMK aborts normal infection of *L. japonicus* roots by AM fungi and rhizobia. The S337 residue is conserved in CCaMK across the angiosperm lineage (Tirichine et al., 2006), and our data demonstrate that it participates in the negative regulation of CCaMK activity.

4.1 *ccamk-14* enhances epidermal infection by bacteria

Like NP formation, initiation of the infection process within root hairs is carefully regulated by the host plant (Jones et al., 2007). The significantly increased number of microcolonies and root hair ITs in *ccamk-14* compared to wild-type Gifu plants possibly reflects the onset of a compensatory mechanism. This mechanism is known to operate in legumes to modulate root susceptibility to rhizobial infections, depending on the outcome of prior infection events

(Ferguson et al., 2010). Indeed, plant mutants that are hyper-infected by rhizobia have been described, such as the *Medicago truncatula sickle* mutant (Penmetsa and Cook, 1997) and the *L. japonicus lhk1-1* mutant (Murray et al., 2007), supporting the existence of a feedback regulatory mechanism(s) that limits the extent of root colonization by bacteria. Importantly, it has been postulated that the Nod factor signal transduction pathway is subjected to negative feedback regulation that originates at or downstream of DMI3, the *M. truncatula* ortholog of *L. japonicus* CCaMK (Oldroyd et al., 2001). We therefore postulate that the enhanced frequency of the epidermal infection events in *ccamk-14* is a reflection of the de-regulated nature of CCaMK^{S337N}. Such a notion is consistent with the observed lack of regulation of *in vitro* CCaMK^{S337N} auto-phosphorylation activity by Ca²⁺/CaM and hyper-phosphorylation of CYCLOPS. These effects may also account for the presence of larger microcolonies in *ccamk-14*.

4.2 The *ccamk-14* phenotype suggests cell type-specific regulation of bacterial infection

In contrast to its apparent gain-of-function effect on epidermal infection by bacteria, the *ccamk-14* mutation impaired normal progression of the cortical infection process during both RNS and AM. As NP formation was unaffected, we have interpreted the presence of empty to fully infected nodules in *ccamk-14* to be the result of slowly advancing aberrant cortical infections. Such an interpretation is consistent with the delay of approximately 7 days in appearance of the first fully colonized nodules in *ccamk-14* compared to wild-type Gifu (Figure 20). Previous data have shown that epidermal and cortical infections by *M. loti* are differentially regulated and may be uncoupled in specific *L. japonicus* mutants, such as *symrk-14* (Kosuta et al., 2011), *nenal* (Groth et al., 2010) and the *nfr1 nfr5 symrk-3 snfl* quadruple mutant (Madsen et al., 2010). The *ccamk-14* phenotype supports these observations, and further suggests that CCaMK participates in this cell type dependent regulation.

4.3 Is CCaMK activity substrate-dependent?

In comparison to wild-type CCaMK, the three apparent differences in *in vitro* CCaMK^{S337N} regulation were a reduced basal activity in the absence of calcium, lack of negative regulation of auto-phosphorylation in the presence of CYCLOPS, and an altered substrate phosphorylation capacity. As argued below, the absence of negative regulation of auto-phosphorylation in CCaMK^{S337N} is probably sufficient to explain the mutant *ccamk-14* infection phenotype. Although it is possible that the diminished basal activity of CCaMK^{S337N} was detrimental to symbiosis and may account for the observed cell-specific properties of the

ccamk-14 mutation, we consider this unlikely as the symbiosis-specific stimulation of CCaMK is believed to be mediated by Ca^{2+} spiking and the relevant defects should occur in the presence of Ca^{2+} and/or $\text{Ca}^{2+}/\text{CaM}$. It has been shown that $\text{Ca}^{2+}/\text{CaM}$ -dependent suppression of the *in vitro* auto-phosphorylation activity of lily (*Lilium longiflorum*) CCaMK occurs in the presence of some but not all phosphorylation targets (Takezawa et al., 1996). Our *in vitro* results on auto-phosphorylation of CCaMK in the presence of myelin basic protein or CYCLOPS are consistent with these observations. They also show that, in comparison to wild-type CCaMK, myelin basic protein and CYCLOPS were hypo- and hyper-phosphorylated *in vitro* by CCaMK^{S337N}, respectively, suggesting that the effect of the *ccamk-14* mutation may be substrate-dependent. However, like other commonly used *in vitro* phosphorylation targets, such as histone IIAS or GS peptide, myelin basic protein is an artificial substrate; therefore caution is required when considering this possibility. Interpretation of the data is further confounded by the fact that biological activities of CCaMK do not always correlate with its apparent kinase activity *in vitro* (Shimoda et al., 2012).

4.4 The *ccamk-14* mutation removes negative regulation of CCaMK

Using three alternative CCaMK variants, which differed in the amino acid (S/N/D) at position 337 within the CaM binding domain, we show that S337 is essential for the regulation of CCaMK and symbiosis. Our *in vitro* results suggest at least one possible mechanism, whereby the S337 residue participates, directly or indirectly, in regulation of $\text{Ca}^{2+}/\text{CaM}$ binding. Although it remains to be further confirmed whether the underlying mechanism involves auto-phosphorylation of the S337 residue, as suggested by the HPLC-MS/MS data, we consider this likely as phospho-mimetic CCaMK^{S337D} almost entirely lost its $\text{Ca}^{2+}/\text{CaM}$ binding capacity *in vitro*, and became unresponsive or only marginally responsive to $\text{Ca}^{2+}/\text{CaM}$ treatment. This presumed mechanism of phosphorylation-dependent repulsion of $\text{Ca}^{2+}/\text{CaM}$ in CCaMK is analogous to the phenomenon of ‘CaM capping’ described for mammalian CaMKII (Hudmon and Schulman, 2002b). Importantly, however, in addition to attenuated $\text{Ca}^{2+}/\text{CaM}$ binding, CCaMK^{S337D} also lost its responsiveness to Ca^{2+} , indicating that this phospho-mimetic substitution had a more global regulatory impact, possibly impairing the function of the CCaMK visinin domain. The fact that CCaMK^{S337D} was not auto-activated probably explains why it remained biologically inert. CCaMK^{S337N}, in contrast to CCaMK^{S337D}, maintained responsiveness to Ca^{2+} , and, unlike wild-type CCaMK, its *in vitro* auto-phosphorylation activity in the presence of CYCLOPS was further enhanced by addition of $\text{Ca}^{2+}/\text{CaM}$. This was associated with increased $\text{Ca}^{2+}/\text{CaM}$ binding and enhanced

CYCLOPS phosphorylation *in vitro*, indicating that CCaMK^{S337N} is hyperactive. Taken together, these data suggest that CCaMK activity is subjected to a negative regulation that requires the S337 residue. As inferred from the results for CCaMK^{S337D}, phosphorylation of S337 probably limits further activation of CCaMK by preventing its responsiveness to Ca²⁺ and restricting Ca²⁺/CaM binding, the regulatory capacity that has been lost in CCaMK^{S337N}. Future experiments are required to establish whether phosphorylation of T265 within the CCaMK kinase domain triggers a phosphorylative burst that targets S337 within the CaM binding domain.

4.5 Significance of negative regulation of CCaMK during symbiotic infection

It has recently been proposed that Ca²⁺ stimulation of CCaMK is sufficient for nodule organogenesis and AM infection, while Ca²⁺/CaM is involved only during rhizobial colonization (Shimoda et al., 2012). This model is primarily based on the analysis of auto-activated, gain-of-function CCaMK molecules. We show that neither CCaMK^{S337D} nor CCaMK^{S337N} lead to an auto-activated gain-of-function phenotype, and our data indicate that the inherent capacity of CCaMK to negatively regulate its own responsiveness to Ca²⁺ and competence for Ca²⁺/CaM binding is important. This is apparently dispensable for nodule formation but is required to maintain symbiotic homeostasis at the root epidermis and during colonization of the root cortex by *M. loti* and AM fungus. The need for negative regulation of Ca²⁺ signaling during cortical infection is suggested by the observation that, although high-frequency Ca²⁺ spiking is associated with the initial apoplastic cell entry by both microsymbionts, this is progressively attenuated and is totally absent during IT growth along a cytoplasmic bridge (Sieberer et al., 2012). Whether similar attenuation occurs during transcellular growth of fungal hyphae is currently unknown, but Ca²⁺ spiking was shown to be absent in cells that have been fully traversed by AM hyphae (Sieberer et al., 2012). These observations indicate that Ca²⁺ signaling is carefully regulated depending on the particular stage of infection, and, as suggested by the *ccamk-14* phenotype, the capacity to negatively control CCaMK activity may be essential in this context. In contrast to the root cortex, rapid attenuation of Ca²⁺ spiking soon after initiation of root hair infection by bacteria has not yet been observed in *M. truncatula*, possibly reflecting different requirements for Ca²⁺ signaling in the root epidermis (B. Sieberer and D. Barker, Laboratoire des Interactions Plantes Micro-Organismes, UMR CNRS-INRA, Castanet-Tolosan, France, personal communication). If confirmed, and assuming that a similar mechanism operates in *L. japonicus*, this may explain the cell-specific effects of the *ccamk-14* mutation and may also imply a remarkably fine control of microbe–host signaling during intracellular accommodation.

5 Materials and Methods

5.1 Plant material and growth conditions

sup11 was back-crossed to wild-type *L. japonicus* Gifu in order to identify the corresponding single mutant individuals. Genotyping of the resulting 504 F2 and a few F3 progenies led to the selection of single *har1-1*, *ccamk-14* and *nph3-1* mutant lines. Plants were germinated and grown, and their root and symbiotic phenotypes evaluated as described previously (Kosuta et al., 2011).

Root and nodule sections were generated and processed as described by (Karas et al., 2005). For evaluation of mycorrhiza phenotypes, plants were inoculated with *R. irregularis* and processed 8 weeks later as previously described (Kosuta et al., 2005).

5.2 Genetic mapping of *sup11*

sup11 was crossed to a polymorphic mapping partner, *L. japonicus* ecotype MG20, carrying the *har1-1* Gifu allele (Murray et al., 2006). As the *sup11* nodulation phenotype was not readily recognizable, the *sup11* AM mutant phenotype was used in the initial selection scheme. The F2 segregants were scored 8 weeks after inoculation with *R. irregularis*, and selected mutant individuals were subjected to linkage analysis using simple sequence repeat (SSR) polymorphic markers, as previously described (Murray et al., 2006).

5.3 Next-generation sequencing and bioinformatic analyses

Next-generation sequencing of the *sup11* nuclear DNA was performed at the Centre for Analysis of Genome & Evolutionary Function (CAGEF) of the University of Toronto using an Illumina Genome Analyzer Iix sequencer (Illumina, www.illumina.com/). A total of 126 million 38 bp reads from a 200 bp paired-end Illumina library were aligned to the *L. japonicus* MG20 release 2.5 reference genome (www.kazusa.or.jp/lotus/index.html) using Bowtie version 0.12.3 (Langmead et al., 2009). The candidate region on chromosome 3 was subsequently annotated for single-nucleotide polymorphisms using SHOREmap (Schneeberger et al., 2009).

5.4 Genotyping

The presence of the *har1-1* allele was confirmed as previously described (Karas et al., 2005). For genotyping the *CCaMK* and *NPH3* loci, derived cleaved amplified polymorphic sequence (dCAPS) markers were developed. Briefly, for *CCaMK*, a pair of primers (*CCaMK* forward: 5'-AGTCATCCATGGGTCAGAGGTG-3'; *CCaMK* reverse: 5'-TTTGGTTCTCAGGAAGATTGTGCCG-3') was used to amplify a 150 bp fragment

containing the engineered *Bsr*BI restriction site. This site was maintained in the fragment derived from the wild-type allele, thus generating two restriction fragments of 125 and 25 bp in length upon digestion. It was absent in the mutant fragment due to the *ccamk-14* substitution. For the *NPH3* locus, the primer pair *NPH3* forward (5'-CCAATTCCCCTCTGAATGCT-3') and *NPH3* reverse (5'-GAAGAACCTCTTCTTCATCCATGCA-3') was used to amplify a 244 bp fragment. The substitution of C272 by T in the *nph3-1* mutant allele, together with the engineered sequence of the reverse primer, led to creation of a *Bsr*DI restriction site, with resulting fragments of 216 and 28 bp in length. This site was absent in the fragment derived from the wild-type *NPH3* allele.

5.5 Site-directed mutagenesis

The Gateway vector pENTR/D-TOPO (Invitrogen, www.invitrogen.com), containing a full copy of the *CCaMK* cDNA, was subjected to site-directed mutagenesis using a QuikChange II XL kit (Stratagene, www.stratagene.com/), according to the manufacturer's instructions. To generate *CCaMK*^{S337N}, the following pair of primers was used: forward, 5'-CAATTGCTAGTGTTTGGAACAGCACAATCTTCCTGAG-3'; reverse, 5'-CTCAGGAAGATTGTGCTGTTCCAAACACTAGCAATTG-3'. For *CCaMK*^{S337D}, the primers were 5'-CTGCAATTGCTAGTGTTTGGGACAGCACAATCTTCCTGAGAA-3' (forward) and 5'-TTCAGGAAGATTGTGCTGTCCAAACACTAGCAATTGCAG-3' (reverse). The integrity of the final products was confirmed by sequencing.

5.6 Complementation experiments

The *sup11*, *ccamk-13* and *ccamk-14* complementation experiments were performed as described by (Murray et al., 2007). The *Agrobacterium rhizogenes* AR12 strain carrying the entire *L. japonicus* *CCaMK* locus, including a 3.1 kb promoter region and a 1.3 kb 3' UTR, integrated into a modified Ri plasmid (Radutoiu et al., 2005; Tirichine et al., 2006), was used to generate transgenic hairy roots on non-transgenic shoots. The same AR12 strain, carrying the Ri plasmid without the *CCaMK* locus, was used in these experiments as a negative control. For *ccamk-13* complementation, the AR1193 strain carrying a cDNA encoding the *CCaMK*^{S337D} protein (see above) or the *CCaMK* wild-type protein under the control of the endogenous *L. japonicus* *CCaMK* promoter or the polyubiquitin promoter was used. The *CCaMK* promoter (2063 bp fragment immediately upstream of the *CCaMK* start codon) was amplified from the Gifu wild-type genomic DNA using primers 5'TTAAAGTCGACAGTTGAAAAGTTGGAGCGCA-3' (forward) and 5'-

TCAAAGTCGACTCAGACTCAGAAAATGTTC-3' (reverse), and cloned into the binary expression vector pK7WG2D,1 (Karimi et al., 2002), from which the 35S promoter was removed by *SalI* digestion, generating the vector pK7CCpWG2D. The coding sequences for CCaMK or CCaMK^{S337D} were then recombined into vector pK7CCpWG2D to give pK7CCpWG2D-CCaMK and pK7CCpWG2DCCaMK^{S337D}, respectively. For complementation experiments with expression from the polyubiquitin promoter, the corresponding coding sequences were recombined into vector pUB-GW-GFP (Maekawa et al., 2008). The nodulation phenotypes were evaluated 11 and 21 days after inoculation using DsRED-containing *M. loti*, and the AM phenotype was scored 6–8 weeks after inoculation with *R. irregularis*.

5.7 Protein expression, purification and *in vitro* kinase assay

To generate N-terminal maltose-binding protein (MBP)-tagged CCaMK protein, the coding sequences of CCaMK, CCaMK^{S337N} or CCaMK^{S337D} were recombined from the pENTR/D-TOPO vector into vector pKM596 (Fox et al., 2003) by Gateway LR reaction (Invitrogen). Expression of MBP-CCaMK, MBP-CCaMKS337N and MBP-CCaMKS337D was induced from *Escherichia coli* Rosetta pLaqI (Novagen, www.novagen.com) by addition of 0.5 mM isopropyl thio-β-D-galactoside for 4 h at 28 °C. MBP-tagged proteins were purified via amylose resin (New England Biolabs, www.neb.uk.com) according to the manufacturer's protocol. Proteins were desalted by use of PD10 desalting columns (GE Healthcare, www.gehealthcare.com), and eluted in buffer containing 25 mM Tris, 10 mM β-mercaptoethanol (pH 7.6). Expression and purification of 6xHis-tagged CYCLOPS was performed as described by (Yano et al., 2008). *In vitro* kinase assays were performed for 30 min at 25 °C in buffer containing 25 mM Tris (pH 7.6), 10 mM MgCl₂, 0.5 mM dithiothreitol, 200 μM ATP and 5 μCi [γ-³²P]ATP (Hartmann Analytic, www.hartmann-analytic.de). MBP-CCaMK, MBP-CCaMK^{S337N} or MBP-CCaMK^{S337D} (2 μg) were tested in each reaction, without addition of substrate or in the presence of either 10 μg myelin basic protein (Sigma, www.sigmaldrich.com/), or 2 μg 6xHis-tagged CYCLOPS as phosphorylation substrate. Kinase activity was assayed in the presence of either 4 mM EGTA or 0.1 mM CaCl₂, in the absence or presence of 1 μM bovine calmodulin (Sigma), as indicated. Kinase reactions were stopped by addition of SDS-PAGE sample buffer and boiled for 5 min. Samples were separated by 12% SDS-PAGE, and subsequently stained with Coomassie brilliant blue. Radioactive gels were exposed to phosphorimaging screens, and visualized by scanning with a Typhoon Trio scanner (GE Healthcare). Radioactive bands (autophosphorylated MBP-CCaMK, MBP-CCaMK^{S337N}, MBP-CCaMK^{S337D} and phosphorylated myelin basic protein or

CYCLOPS) were quantified using Image Quant TL software (GE Healthcare). The quantitative kinase assay data shown in Figure 27 and Figure 28 were obtained from two independent experimental set-ups. The data were first normalized by defining the wild-type CCaMK protein activity in the absence of calcium (EGTA) as 1. As this resulted in a mean of one and a variance of zero for the CCaMK (EGTA) activity, non-parametric Kruskal-Wallis multiple comparison with the Bonferroni correction was performed to test for pairwise differences. The significance threshold was defined as $\alpha = 0.05$. As the kinase activity data shown in Figure 29 were obtained from only two technical replicates, statistical analysis was not performed.

5.8 Calmodulin binding assay

MBP-CCaMK, MBP-CCaMK^{S337D} and MBP-CCaMK^{S337N} (25 μ g) were diluted in either 1 ml CaM binding buffer (50 mM Tris, 150 mM NaCl, 1 mM CaCl₂, pH 7.6) or in 1 ml EGTA buffer (50 mM Tris, 150 mM NaCl, 2 mM EGTA, pH 7.6; control for non-specific binding). Diluted proteins were then added to 50 μ l CaM-Sepharose beads (GE Healthcare) equilibrated in either CaM binding buffer or EGTA buffer. The samples were incubated for 2 h at 4 °C under rotation to allow binding of the proteins to the CaM resin. Beads were washed six times (2 minutes per wash) with 1 ml of the corresponding buffer (see above). CaM-bound proteins were eluted twice using 50 μ l EGTA buffer. A 2 μ g aliquot of each protein was loaded as input, and 15 μ l of combined elution fractions of each protein were loaded as a representative elution fraction on 10% SDS-PAGE, separated and stained with Coomassie brilliant blue. Quantification of the Coomassie-stained protein bands was performed using ImageJ software. Quantitative CaM binding assay data were obtained from two independent experiments. Data were analysed using oneway ANOVA followed by Tukey's HSD (honest significant difference) post hoc test with 95% family-wise confidence level.

5.9 Yeast two-hybrid analysis

Coding sequences for CCaMK, CCaMK^{S337D}, CCaMK^{S337N}, CCaMK^{G30E} and CYCLOPS were recombined from the pENTR/D-TOPO vector into modified (Gateway-compatible) pBDGAL4 (Stratagene) and pGAD424 (Clontech, www.clontech.com/) vectors by LR reaction. The resulting constructs were co-transformed into yeast strain HF7c (Feilotter et al., 1994) by the lithium acetate transformation method (Gietz and Woods, 2002). Co-transformants were selected on synthetic drop-out medium lacking Trp and Leu, and expressed proteins were tested for interaction by the quantitative interaction assay (β -galactosidase assay) described in Clontech's yeast protocols handbook, with slight

modifications.

5.10 In-gel digestion of autophosphorylated CCaMK

Coomassie-stained protein bands were excised from the gel and chopped into small cubes. For triple enzyme digests, the gel cubes were divided into three aliquots and were washed three times with acetonitrile/water (1:1). The gel pieces were shrunk using acetonitrile, rehydrated in 50 mM NH_4HCO_3 , and dried in a speedvac. (Thermo Fisher Scientific, www.thermoscientific.com). Then 10 mM dithiothreitol in 50 mM NH_4HCO_3 was added to the dried gel pieces, and proteins were reduced for 45 min at 56 °C. To alkylate reduced cysteine residues, the remaining liquid was removed and an equal volume of 50 mM iodoacetamide in 50 mM NH_4HCO_3 was added, and the reaction was allowed to proceed for 30 min in the dark. Prior to in-gel digestion, the gel pieces were washed and dried as above. The gel pieces were rehydrated in an ice-cold solution of either 10 ng/ μl trypsin (sequencing grade, Promega, www.promega.com/) or 10 ng/ μl chymotrypsin in 10 mM NH_4HCO_3 , or 20 ng/ μl Gluc protease (sequencing grade, New England Biolabs, www.neb.com) in 50 mM Tris/HCl, 0.5 mM glutamic acid dipeptide (Glu-Glu), pH 8.0. After 45 min on ice, excess enzyme solution was replaced by 20 μl of buffer without enzyme, and proteins were digested at 37 °C overnight. The digests were stopped by addition of 20 μl of 10% formic acid, and peptides were extracted for 30 min at 37 °C. For each sample, extracts from multiple protease digests were combined prior to LC-MS analysis.

5.11 LC-MS/MS of in gel-digested proteins

CCaMK auto-phosphorylation was performed in the presence of 0.1 mM CaCl_2 using the same procedure as described for the *in vitro* kinase assay, but omitting radioactive [^{32}P]ATP. LC-MS data were acquired on a HCT ETD II iontrap mass spectrometer (Bruker Daltonics, www.bdal.com) equipped with a nano ESI source (Bruker Daltonics).

5.12 Database search

Peptides and phospho-peptides were identified by searching expected protein sequences in a custom database using a local installation of MASCOT 2.2 (Matrix Science Ltd, www.matrixscience.com/). Searches were submitted via Proteinscape 2.0 (Bruker Daltonics) using the following parameter settings: enzyme, 'none'; fixed modifications, 'carbamidomethyl'; optional modifications, 'Methionine oxidation' and 'Phosphorylation ST'; missed cleavages, '1'. The mass tolerance was set to 0.4 Da for peptide and fragment spectra.

6 Acknowledgements

We thank Alex Molnar for his expert help in preparation of figures and Axel Strauß (Biocenter University of Munich, Department of Genetics, Germany) for statistical analysis of the biochemical data. This work was supported by grants from the Agriculture and AgriFood Canada Crop Genomics Initiative and the National Science and Engineering Research Council of Canada (grant number 3277A01) to K.S. J.L. was partially supported by the Chinese Scholarship Council under the The Ministry of Education of The People's Republic of China (MOE) and The Department of Agriculture and Agri-Food Canada (AAFC) PhD Research Program. Work on CCaMK biochemistry was funded by a grant from the Deutsche Forschungsgemeinschaft to M.P. within Research Unit FOR 964 'Calcium signaling via protein phosphorylation in plant model cell types during environmental stress adaptation'.

Chapter 3: CYCLOPS, a DNA-binding transcriptional activator, orchestrates symbiotic root nodule development

This chapter is based on the following manuscript:

Singh, S.*, Katzer, K.*, Lambert, J., Cerri, M. and Parniske, M. (2014). CYCLOPS, a DNA-binding transcriptional activator, orchestrates symbiotic root nodule development. *Cell Host Microbe* 15, 139-152.

* These authors contributed equally to the work.

This work was performed in collaboration with other researchers (mentioned above). The manuscript draft was written by the author of this thesis. Contributions of the author of this thesis to this manuscript are listed in detail under ‘III Declaration of Contribution as Co-Author’ on pages 12-14 of this thesis. Unless otherwise stated, experiments related to the figures of this chapter were performed by the author of this thesis.

1 Summary

Nuclear calcium oscillations are a hallmark of symbiotically stimulated plant root cells. Activation of the central nuclear decoder, calcium- and calmodulin-dependent kinase (CCaMK), triggers the entire symbiotic program including root nodule organogenesis, but the mechanism of signal transduction by CCaMK was unknown. We show that CYCLOPS, a phosphorylation substrate of CCaMK, constitutes a novel class of DNA-binding transcriptional activator. Two phosphorylated residues within the N-terminal negative regulatory domain are necessary to release CYCLOPS from autoinhibition. A phospho-mimetic version was solusufficient for triggering root nodule organogenesis in the absence of rhizobia and CCaMK. Our data pinpoint the CCaMK/CYCLOPS complex as central regulatory node, which directly translates nuclear calcium oscillations into the activation of the *NODULE INCEPTION (NIN)* gene. CYCLOPS thus emerges as the master regulator of a cascade of transcriptional regulation, in which NIN and a heterotrimeric NF-Y complex act in hierarchical succession to initiate symbiotic root nodule development.

2 Introduction

A striking feature of symbiosis between legume plants and rhizobia is the development of a new plant organ, the root nodule. Plant root cells undergo a remarkable de-differentiation process upon symbiotic stimulation. A fully differentiated, resting root cell completely reprograms and either enters cell division to initiate nodule organogenesis or develops an intracellular structure for accommodation of the microsymbionts (Parniske, 2008). The establishment of root symbioses between phosphate-acquiring arbuscular mycorrhiza (AM) fungi and the majority of land plants or between nitrogen-fixing rhizobia and legumes is initiated by an ancient signal transduction system (Oldroyd, 2013). The perception of symbiont-specific AM fungal factors or rhizobia-derived nodulation factors ('nod factors') via cognate transmembrane receptors leads within minutes to the generation of sustained oscillations of calcium concentration ('calcium-spiking') in the nucleus, a hallmark of symbiotic signal transduction (Ehrhardt et al., 1996; Oldroyd, 2013). In mammals, stimulus-dependent elevations of nuclear calcium concentration have been linked to changes in transcription, resulting in cell proliferation and growth (Bootman et al., 2009). Similarly, during plant root symbiosis, nuclear calcium spiking is believed to trigger, in an hitherto unknown manner, the expression of symbiosis-associated genes (Miwa et al., 2006a). The nuclear calcium- and calmodulin-dependent kinase CCaMK is the central regulator of symbiotic development of the root (Singh and Parniske, 2012). A calmodulin (CaM) binding domain and three calcium binding EF-hands in CCaMK mediate regulation by calcium signatures (Swainsbury et al., 2012). *ccamk* mutants are completely symbiosis-deficient. Rhizobia do not induce nodule organogenesis or infection threads and arbuscules, highly branched fungal structures within plant cells that are the site of nutrient exchange between the symbionts, do not form upon inoculation with AM fungi (Lévy et al., 2004; Mitra et al., 2004). Importantly, deregulated autoactive CCaMK versions carrying various amino acid substitutions in the regulatory autophosphorylation site (T265D, or T265I) can compensate for the loss-of upstream genes involved in calcium-spike generation, consistent with the idea that the primary function of calcium spiking is the activation of CCaMK (Hayashi et al., 2010; Madsen et al., 2010). Deregulated CCaMK versions trigger the spontaneous development of root nodules in the absence of external symbiotic stimuli demonstrating that CCaMK acts as central regulator of this developmental program (Gleason et al., 2006; Tirichine et al., 2006).

Since its identification as essential gene for symbiosis development, the molecular function of *CYCLOPS*, encoding a nuclear coiled-coil protein remained enigmatic (Yano et al., 2008).

CYCLOPS interacts with and is phosphorylated by CCaMK *in vitro*, implicating CYCLOPS as direct CCaMK phosphorylation target. Although *Lotus japonicus cyclops* mutants are impaired in AM and root nodule symbiosis, they do not recapitulate the *ccamk* mutant phenotype. They respond to rhizobia with root hair curling, but infection is aborted at the root hair stage. Likewise, nodule primordia form, but nodule development is prematurely arrested (Yano et al., 2008). Root nodule organogenesis is initiated by cell divisions in the inner root cortex (Oldroyd, 2013) and depends on the GRAS proteins Nodulation Signaling Pathway 1 (NSP1) and NSP2 and the transcriptional regulator NODULE INCEPTION (NIN) (Kalo et al., 2005; Schauser et al., 1999; Smit et al., 2005). *NIN* expression is rapidly induced after nod factor perception, but severely reduced in *cyclops* mutants (Yano et al., 2008). A relatively high hierarchical position of *NIN* in the initiation of lateral root organs is indicated by the observation that *NIN* targets the promoters of two subunits of the heterotrimeric CCAAT-box binding Nuclear Factor Y (NF-Y) complex: NF-YA1 (orthologous to *M. truncatula* HAP2-1) and NF-YB1 (Combier et al., 2006; Soyano et al., 2013). Furthermore, ectopic overexpression of *NIN* or *NF-YA1* stimulated cell divisions resulting in the formation of aberrant lateral root organs that differed morphologically from both, roots and nodules (Soyano et al., 2013). Nuclear calcium elevations are implicated in the activation of transcription and root cells undergo substantial transcriptional reprogramming during symbiosis establishment. Given the fact that CCaMK is a likely receiver of calcium spikes, its phosphorylation targets should either directly or indirectly be implicated in the transcriptional reprogramming that leads to reinitiation of cell division. Here we show that CYCLOPS is a CCaMK regulated DNA-binding transcriptional activator which initiates gene expression leading to nodule organogenesis. Our data reveal a direct mechanism of nuclear calcium signal decoding by the CCaMK/CYCLOPS complex. Perception of calcium signals stimulates phosphorylation of CYCLOPS, which in turn activates gene expression sufficient for the initiation of cell division and symbiotic organ development.

3 Results

3.1 CYCLOPS is a phosphorylation substrate of CCaMK

We hypothesized that CCaMK-mediated CYCLOPS phosphorylation would be a consequence of nuclear calcium spiking and thus a potential intermediate transduction step in symbiosis signaling. CYCLOPS was strongly phosphorylated by CCaMK only in the presence of calcium/CaM (Figure 30A). We detected five phosphorylated serines by mass spectrometry, which were all preceded by an arginine at position -3, suggesting that the consensus sequence 'RXXS' was a preferred phosphorylation motif of CCaMK (Figure 30B).

Figure 30. CYCLOPS is phosphorylated by CCaMK *in vitro* and the identified phosphorylation sites S50 and S154 are conserved in symbiotic plants and the moss *Physcomitrella*.

A) *In vitro* phosphorylation of 6xHis-CYCLOPS by CCaMK. Phosphorylation of CYCLOPS (34.5 pmol) by equal amounts of CCaMK was tested in the presence of either 4 mM EGTA, 0.1 mM CaCl₂ (Ca²⁺), or 0.1 mM CaCl₂ and 1 μM calmodulin (Ca²⁺/CaM). Upper panel: Autoradiograph (³²P) of a 10% SDS-PAGE gel separating the reaction products. Lower panel: Coomassie staining of the same gel.

B) Alignment of CYCLOPS amino acid sequences from the legumes *Lotus japonicus*, *Medicago truncatula* and *Pisum sativum* (pea), the non-legume AM forming plants *Oryza sativa* (rice) and *Populus trichocarpa* (poplar) and the moss *Physcomitrella patens*.

The phosphorylation sites (S14, S50, S154, S251 and S412) identified by mass spectrometry are indicated. The four phosphorylation sites S14, S50, S154 and S412 are conserved between all plant species analysed, except for *P. patens* in which serine 14 is replaced by a threonine. The corresponding phospho-peptides are depicted in green, or magenta in cases where they overlap with potential DNA binding motif residues, depicted in blue as predicted by BindN+ (Wang et al., 2010). These are confined to three longer stretches (13-15 amino acids in length): S1= aa 377-391, S2 = aa 402-415, S3 = aa 424-436. Red bars indicate coiled-coils as predicted by the coils program (Lupas et al., 1991), with the percent probability indicated in red.

The experimentally delimited extensions of the activation domain (AD) and DNA-binding domain (BD) are indicated by a black bar and grey bar, respectively. A stretch of serines located in the deduced AD within an intrinsically unstructured region (as predicted by DIPHOS; Iakoucheva et al., 2004) is highlighted in orange.

Residues highlighted in white on black background are identical between the majority (>66.7%) of the aligned plant species, residues shaded in grey are identical between some (<66.7% and >33.3%) of the aligned plant species, residues on white background are not conserved. NLS: Nuclear localization signal.

Figure 30B was prepared by Katja Katzer.

3.2 The CYCLOPS phosphorylation sites S50 and S154 are essential for symbiotic development

To examine whether phosphorylation of the identified sites is essential for symbiotic development, we generated single- and multi-site phospho-ablative mutant versions of S14, S50, S154, S251 and S412, by amino acid (aa) exchange to Ala and analysed restoration of root symbiosis in transformed *cyclops-3* mutant roots (Table 6, Figure 31). The results of the transgenic complementation analysis demonstrated that the simultaneous presence of both phosphorylatable serine residues S50 and 154 is essential for symbiosis (Figure 31). If phosphorylation at these two residues was important, the corresponding phospho-mimetic Ser to Asp replacements may be tolerated. Indeed, individual replacements or the combination of S50D-S154D (*3xHA-gCYCLOPS-DD*) all restored symbiosis (Table 7). To address the relevance of the three remaining sites we transformed *cyclops-3* roots with *CYC_{pro}:3xHA-gCYCLOPS-A-DD-AA* (carrying replacements of Ser 14, 251 and 412 by Ala) and found that root symbiosis was restored (Table 7). In summary, phosphorylation of S14, S251 and S412 is dispensable, while phosphorylation of CYCLOPS at S50 and S154 appears to be a prerequisite for symbiotic development.

Figure 31. Serines 50 and 154 are redundantly required for root symbiosis.

(A-O) *L. japonicus cyclops-3* mutant roots were transformed with *3xHA-gCYCLOPS*, or mutant derivatives encoding the indicated phospho-ablative double mutants, or the empty vector control (all equipped with the endogenous promoter). Transformed roots were either inoculated with DsRed tagged *M. loti*, or the AM fungus *R. irregularis* and the nodulation (A-J) and AM phenotype (K-Q) was analysed.

Root nodule symbiosis and AM was restored by *3xHA-gCYCLOPS wild-type* (B, G), (AM: L, P), *3xHA-gCYCLOPS-S14A-S50A* (D, I), (AM: N) and *3xHA-gCYCLOPS-S14A-S154A* (E, J), (AM: O) as abundant formation of *M. loti*-DsRed infected root nodules and arbusculated cell files in the cortex, spanning the entire root length, were observed.

In roots transformed with the empty vector control (A, F) or with *3xHA-gCYCLOPS-S50A-S154A* (C, H), root nodule symbiosis was not restored since only uninfected nodule primordia with superficial rhizobial growth (visible as red dots), resembling the *cyclops-3* mutant phenotype, were observed. AM was not restored, since intracellular hyphae and arbuscules were not formed in roots transformed with the empty vector control (K). In three root systems out of ten transformed with *3xHA-gCYCLOPS-S50A-S154A* (M, Q) 1-3 small patches (0.5-1.5 mm in size) with arbuscules were formed (indicated by black arrowheads in Q) indicating that AM formation was largely impaired.

(A-E) Brightfield images. (F-J) Overlay of images recorded with GFP and DsRed filters. Green fluorescence indicates transformed plant roots, red fluorescence originated from *M. loti-DsRed*, present either in infected root nodules, or microcolonies growing on the root surface. (K-Q) Brightfield images of ink-stained roots visualizing AM fungal structures. Bars: (A-J) 1 mm, (K-O) 0.1 mm, (P, Q) 0.3 mm.

(R) Protein blot probed with anti-HA-HRP antibody demonstrating that *3xHA-CYCLOPS* wild-type and phospho-ablative mutant derivatives thereof (as indicated and AAASS = *CYCLOPS-S14A-S50A-S154A*, AAAAS = *CYCLOPS-S14A-S50A-S154A-S251A*) are expressed at similar levels in transformed roots of the *cyclops-3* mutant. Protein extracts were prepared from transgenic roots four weeks post inoculation with *M. loti-DsRed*. Molecular weight of *3xHA-CYCLOPS* is 65 kDa. No protein band equal in size to *3xHA-CYCLOPS* was detected in roots transformed with the empty vector control. Coomassie stained blot shows equal sample loading of the gel.

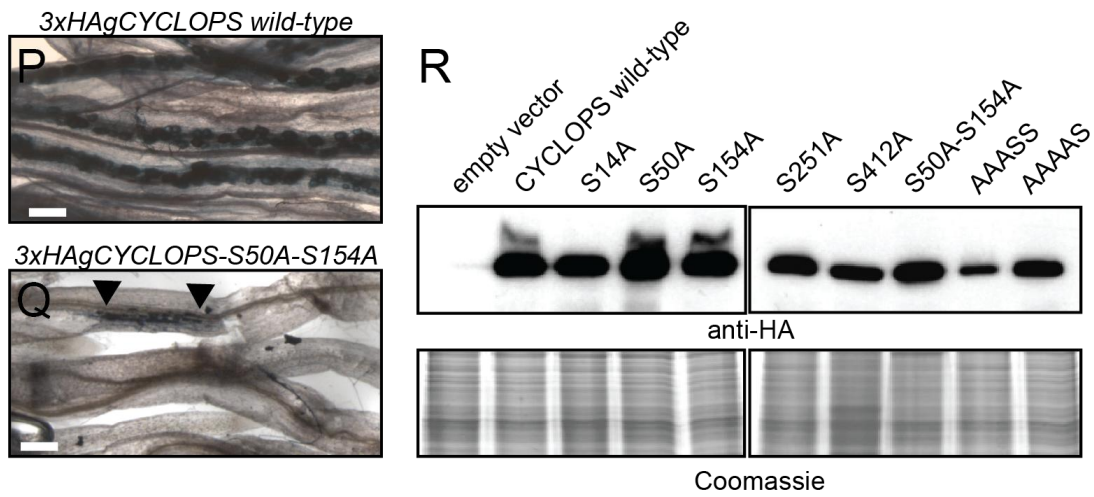
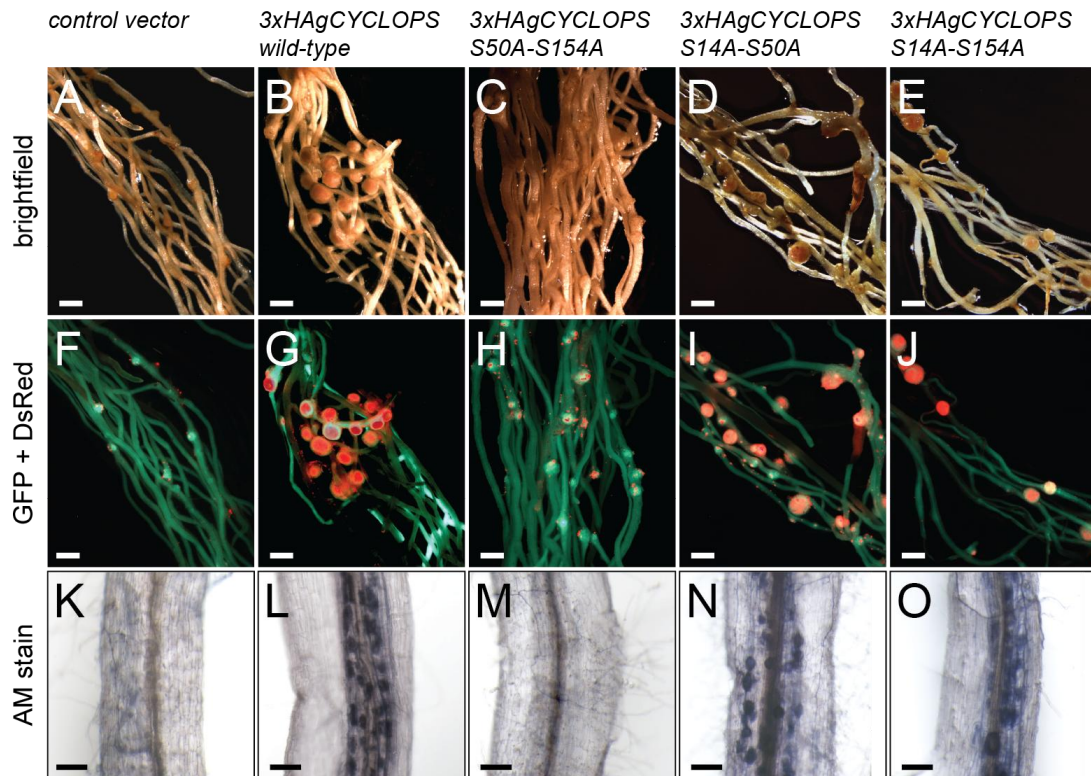


Table 6. Restoration of root symbiosis in *cyclops-3* by *CYCLOPS* phospho-ablative mutant versions.

Plant Genotype	Transgene ^a	Nod+ ^b	#Nod/ Nod+ Plant ^c	AM+ ^d
<i>cyclops-3</i>	empty vector	0/30 ^e	0 ^e	0/21
<i>cyclops-3</i>	3xHA-g <i>CYCLOPS</i>	20/20	18 ± 7	8/8
<i>cyclops-3</i>	3xHA-g <i>CYCLOPS-S14A</i>	19/19	14 ± 5	7/7
<i>cyclops-3</i>	3xHA-g <i>CYCLOPS-S50A</i>	13/13	15 ± 4	8/9
<i>cyclops-3</i>	3xHA-g <i>CYCLOPS-S154A</i>	24/24	24 ± 8	6/7
<i>cyclops-3</i>	3xHA-g <i>CYCLOPS-S251A</i>	38/38	16 ± 8	8/8
<i>cyclops-3</i>	3xHA-g <i>CYCLOPS-S412A</i>	19/19	15 ± 4	10/10
<i>cyclops-3</i>	3xHA-g <i>CYCLOPS-S14A-S50A</i>	11/14	8 ± 3	7/7
<i>cyclops-3</i>	3xHA-g <i>CYCLOPS-S14A-S154A</i>	18/18	13 ± 6	5/8
<i>cyclops-3</i>	3xHA-g <i>CYCLOPS-S50A-S154A</i>	0/38 ^e	0 ^e	3 ^f /10
<i>cyclops-3</i>	3xHA-g <i>CYCLOPS-S14A-S50A-S154A</i>	0/27 ^e	0 ^e	3 ^f /13
<i>cyclops-3</i>	3xHA-g <i>CYCLOPS-S14A-S50A-S154A-S251A</i>	0/25 ^e	0 ^e	3 ^f /16
<i>cyclops-3</i>	3xHA-g <i>CYCLOPS-S14A-S50A-S154A-S251A-S412A</i>	0/72 ^e	0 ^e	7 ^f /32

^aConstructs were equipped with the endogenous promoter.

^bNod+: Number of root systems with infected root nodules per number of total root systems analysed. Transformed roots were analysed 5 weeks post *M. loti*-DsRed inoculation.

^cAverage number of nodules per nodulated root system ± standard deviation.

^dAM+: Number of root systems showing restoration of AM per number of total root systems analysed. Transformed roots were analysed 6 weeks post co-cultivation with the AM fungus *R. irregularis*.

^eRoot systems showed *cyclops* mutant phenotype characterized by uninfected nodule primordia.

^fNumber of root systems forming few (1-3) small (0.5-1.5 mm) patches with arbuscules per total number of root systems analysed.

Table 7. Restoration of root symbiosis in *cyclops-3* by *CYCLOPS* phospho-mimetic mutant versions.

Plant Genotype	Transgene ^a	Nod+ ^b	#Nod/ Nod+ Plant ^c	AM+ ^d
<i>cyclops-3</i>	empty vector	0/18 ^e	0 ^e	0/8
<i>cyclops-3</i>	3xHA-gCYCLOPS	12/12	11 ± 3	9/9
<i>cyclops-3</i>	3xHA-gCYCLOPS-S14D	35/35	16 ± 6	7/7
<i>cyclops-3</i>	3xHA-gCYCLOPS-S50D	20/20	12 ± 6	14/14
<i>cyclops-3</i>	3xHA-gCYCLOPS-S154D	33/33	15 ± 6	9/9
<i>cyclops-3</i>	3xHA-gCYCLOPS-S251D	36/36	11 ± 5	8/8
<i>cyclops-3</i>	3xHA-gCYCLOPS-S412D	32/32	14 ± 5	5/6
<i>cyclops-3</i>	3xHA-gCYCLOPS-S50D-S154D	13 ^f /13	16 ^f ± 7	6/7
<i>cyclops-3</i>	3xHA-gCYCLOPS-S14AS50D-S154DS251AS412A	4 ^f /5	11 ^f ± 4	7/7
<i>ccamk-3</i>	empty vector	0/12	0	0/7
<i>ccamk-3</i>	3xHA-gCYCLOPS	0/12	0	0/5
<i>ccamk-3</i>	3xHA-gCYCLOPS-S14D	0/13	0	0/6
<i>ccamk-3</i>	3xHA-gCYCLOPS-S50D	0/12	0	0/8
<i>ccamk-3</i>	3xHA-gCYCLOPS-S154D	0/15	0	0/8
<i>ccamk-3</i>	3xHA-gCYCLOPS-S251D	0/17	0	0/11
<i>ccamk-3</i>	3xHA-gCYCLOPS-S412D	0/13	0	0/10
<i>ccamk-3</i>	3xHA-gCYCLOPS-S50D-S154D	16 ^g /40	4 ^g ± 3	0/8

^aConstructs were equipped with the endogenous promoter.

^bNod+: Number of root systems with infected root nodules per number of total root systems analysed. Transformed roots were analysed 5 weeks post *M. loti*-DsRed inoculation.

^cAverage number of nodules per nodulated root system ± standard deviation.

^dAM+: Number of root systems showing restoration of AM per number of total root systems analysed. Transformed roots were analysed 6 weeks post co-cultivation with the AM fungus *R. irregularis*.

^eRoot systems showed *cyclops* mutant phenotype characterized by uninfected nodule primordia.

^fFormation of partly infected (60-70%), partly uninfected (30-40%) nodules.

^gFormation of spontaneous, uninfected nodules.

3.3 The phosphorylation status of CYCLOPS does not affect complex formation with CCaMK

Ablation of phosphorylation at S50 and S154 of CYCLOPS impaired symbiosis. In order to unravel the mechanistic cause for the functional defect, we investigated the consequences for protein expression levels, subcellular localization and complex formation with CCaMK. All tested CYCLOPS versions were abundantly expressed (Figure 32A) and, similar to the WT protein, localized exclusively to the nucleus (Figure 32B). Also, complex formation with CCaMK was not compromised, as CYCLOPS and the phospho-site mutant variants still interacted with CCaMK in bimolecular fluorescence complementation (BiFC) analysis (Figure 38D-I). Furthermore, fluorescence lifetime imaging microscopy (FLIM)-FRET

measurements revealed no significant lifetime change when TSapphire-CYCLOPS or either of the phospho-mutant versions was expressed together with CCaMK-mOrange in *N. benthamiana* leaf cell nuclei (Figure 33D-F). Compared to the control measurements, in which CCaMK-mOrange was replaced by free mOrange quencher, all CYCLOPS versions showed a decrease in fluorescence lifetime in the presence of CCaMK-mOrange, clearly indicating interaction (Figure 33A-F).

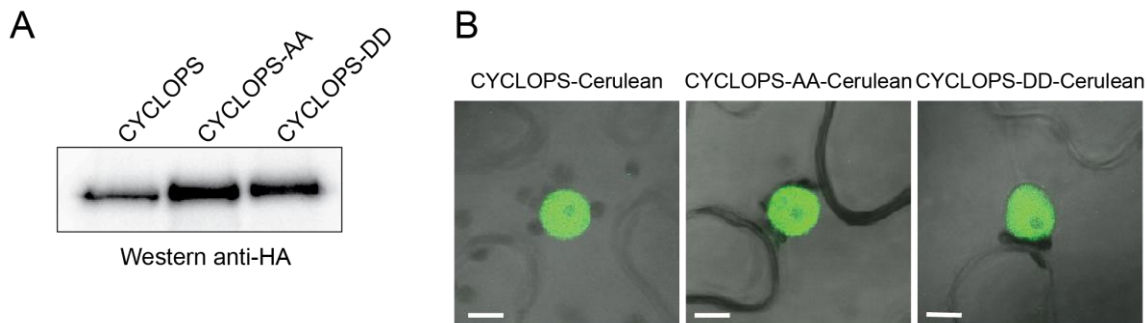


Figure 32. CYCLOPS and CYCLOPS phospho-site mutant proteins are expressed and localize to the nucleus in *N. benthamiana* leaf cells.

(A) 3xHA-CYCLOPS and phospho-site mutant derivatives were expressed in *N. benthamiana* leaf cells. Protein blot of protein extracts was prepared 60 hours post transformation (hpt) from equal amounts of leaf material and probed with anti-HA-HRP antibody.

(B) CYCLOPS-Cerulean and phospho-site mutant derivatives localize to the nucleus in *N. benthamiana* leaf cells. *N. benthamiana* leaf cells were transformed with T-DNAs encoding the indicated CYCLOPS-Cerulean fusion proteins and confocal laser scanning microscopy of fluorescent protein fusions was performed 60 hpt. Images show overlay of brightfield and fluorescence micrographs. Bars: 5 μm.

3.4 The *NIN* promoter is activated *in trans* by CYCLOPS in a phosphorylation dependent manner

Deregulated CCaMK is sufficient to induce symbiosis-related transcriptional reprogramming (Gleason et al., 2006; Tirichine et al., 2006). Since CYCLOPS is a phosphorylation target of CCaMK, the most parsimonious model implicated CYCLOPS directly in transcriptional regulation of target genes. To test this hypothesis, a *NIN* promoter (>2 kb) fusion to the *uidA* gene (*pNIN:GUS*) was mobilized together with 3xHA-CYCLOPS and with or without autoactive 3xHA-CCaMK-T265D into *N. benthamiana* leaf cells. CYCLOPS alone caused only a faint reporter expression while co-expression with CCaMK-T265D induced a significant increase (Figure 34A). CCaMK-T265D alone did not elicit *GUS* expression, indicating that the observed transactivation was not mediated by phosphorylation of endogenous proteins. This finding suggested that the increase in transactivation resulted from phosphorylation of CYCLOPS by CCaMK-T265D. To test whether phosphorylation of S50

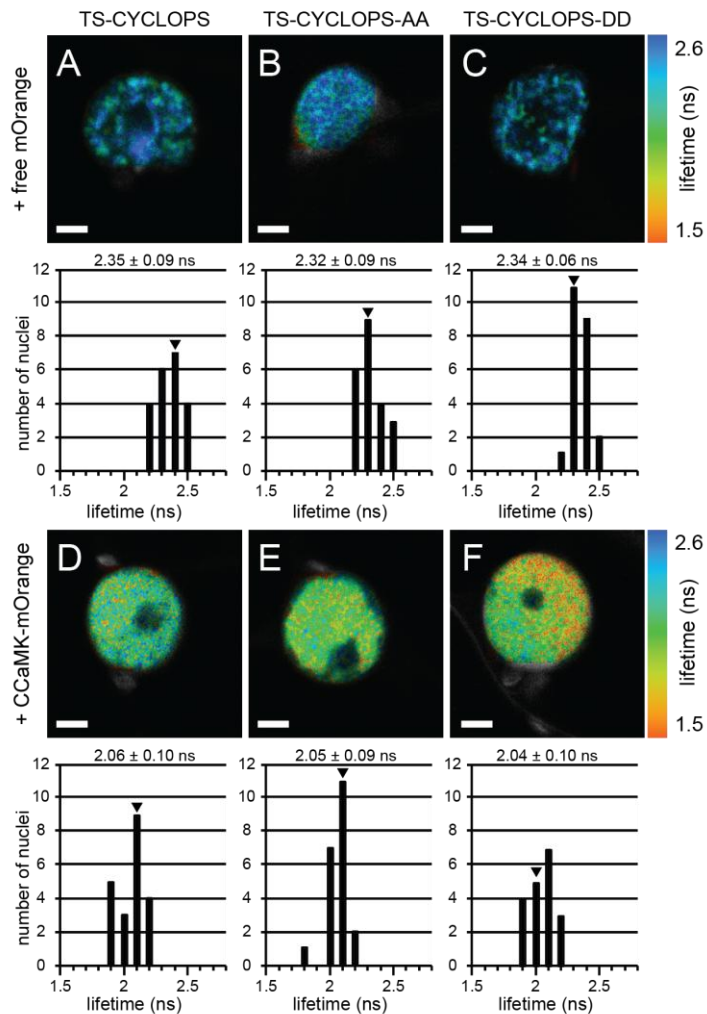


Figure 33. FLIM-FRET interaction analysis between CCaMK and CYCLOPS phospho-site variants.

FLIM-FRET analysis of TSapphire-CYCLOPS and phospho-site mutants in the presence of free mOrange (A-C) or CCaMK-mOrange (D-F). The lifetime of the TSapphire donor fluorophore is depicted in a color code ranging from blue (2.6 ns) to red (1.5 ns) for one representative nucleus per construct combination. Histograms below lifetime images represent lifetimes of all nuclei analysed per construct combination. The graphs show the number of nuclei observed with the indicated lifetime values. Insets above the histograms show mean values and standard deviations obtained per construct combination. Lifetime value for each depicted nucleus (A-F) is indicated in the histogram by arrowheads. Analysis was performed in nuclei of *N. benthamiana* leaf cells 60 hours post transformation. TS: TSapphire. Bars: 2 μ m.

Data related to this figure were generated by Jayne Lambert.

and S154 is involved, we examined whether this effect can be recapitulated or prevented by the phospho-mimetic and phospho-ablative versions, respectively. CYCLOPS-DD alone transactivated strongly, while CYCLOPS-AA alone or in combination with CCaMK-T265D did not (Figure 34A). In conclusion these observations suggested, that CYCLOPS has properties of a transcriptional activator. Since the co-expression of CYCLOPS with autoactive CCaMK transactivated the *NIN* promoter and this effect was not observed with the phospho-ablative version, but was fully recapitulated with the phospho-mimetic version alone, we concluded that phosphorylation at S50 and S154 was the likely mechanism of CYCLOPS activation.

3.5 Identification of a CYCLOPS responsive *cis* element (*CYC-RE*) within the *NIN* promoter

We performed a detailed deletion and substitution analysis of the *NIN* promoter to identify *cis* elements targeted by CYCLOPS-DD (Figure 34B-F). We delimited a CYCLOPS response element '*CYC-RE*' to a 30 bp fragment containing a palindromic sequence (Figure 34F).

Substitution analysis pinpointed the palindrome as essential *cis* element, or ‘*CYC-box*’ for CYCLOPS-DD mediated *CYC-RE* reporter induction (Figure 34F).

3.6 CYCLOPS-DD binds DNA in a sequence-specific and phosphorylation-dependent manner

In order to test direct binding of CYCLOPS-DD to DNA, electrophoretic mobility shift assays (EMSAs) were performed. CYCLOPS-DD caused a shift of IR-labeled *CYC-RE* probe, which was gradually lost when increasing amounts of unlabeled *CYC-RE* DNA were added (Figure 35A). Importantly, incubation with *mCYC-RE* competitor DNA did not outcompete binding to the WT sequence (Figure 35A). This analysis demonstrated that CYCLOPS-DD has sequence-specific DNA binding properties, pinpointing the ‘*CYC-box*’ as required for CYCLOPS binding.

Figure 34. CYCLOPS-DD transactivates the *NIN* promoter via a minimal responsive palindromic *cis* element.

(A) GUS reporter assay in *N. benthamiana* showing that co-expression of CYCLOPS with autoactive CCaMK-T265D leads to a strong transcriptional activation of the *NIN* promoter and that the same effect is produced by CYCLOPS-DD. *N. benthamiana* leaf cells were co-transformed with T-DNAs encoding the indicated 3xHA-CYCLOPS variants and the *pNIN:GUS* reporter, with or without 3xHA-CCaMK-T265D. GUS activity was determined histochemically and quantitatively in leaf discs. Mean value and standard deviation was determined from three biological replicates. Photographs of leaf discs represent two biological replicates.

(B-G) Identification of a CYCLOPS-DD responsive *cis* element (*CYC-RE*) within the *NIN* promoter. Various *NIN* promoter fusions to the *GUS* reporter gene were co-expressed with 3xHA-CYCLOPS-DD in *N. benthamiana* leaf cells and GUS expression was quantified. Mean value of GUS activity and standard deviation from three biological replicates is given for each promoter construct. The *NIN* promoter length is annotated from the transcriptional start site (Start).

(B) Rough mapping derived two CYCLOPS-DD response elements (RE). A strong RE (-870 to -299 bp) and a weaker RE (-298 to -99 bp). The 98 bp fragment resulted in background activity and was defined as *NIN*-minimal promoter (*pNINmin*). GUS expression is shown relative to the value obtained for the *pNIN(-7):GUS* reporter construct (set to 1).

(C-F) Fine mapping of the upstream RE (‘*CYC-RE*’, shaded in grey) via *NIN* promoter deletions fused to the 5’ end of *pNINmin:GUS*. GUS activity is shown relative to the value obtained for *pNINmin:GUS* (set to 1).

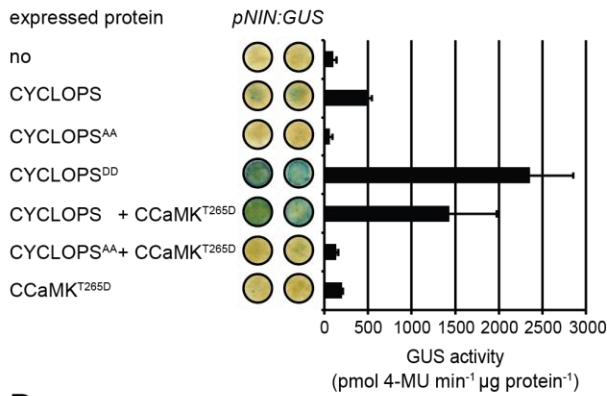
(C) A ~50 bp deletion series (*D1-D6*) delimited the position of the *CYC-RE* to the interval from -785 to -685 bp. Deletion constructs were tested in the background of a -298 to -99 bp deletion (dotted line). *D1* = -834 to -299 bp, *D2* = -785 to -299 bp, *D3* = -735 to -299 bp, *D4* = -685 to -299 bp, *D5* = -635 to -299 bp, *D6* = -579 to -299 bp.

(D) Analysis of overlapping promoter fragments (*B1-B4*) delimited the *CYC-RE* location to a 71 bp fragment (*B4*). *B1* = -735 to -615 bp, *B2* = -785 to -716 bp, *B3* = -785 to -615 bp, *B4* = -735 to -666 bp.

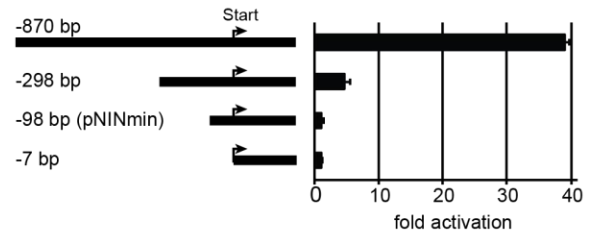
(E) Dissection of *B4* into three overlapping 36 bp fragments (*F1-F3*) identifies *F2* as a minimal element containing the *CYC-RE* depicted in (F). *F1* = -735 to -701 bp, *F2* = -717 to -683 bp and *F3* = -700 to -666 bp.

(F) *CYC-RE* contains a palindromic sequence (*CYC-box*) which is essential for CYCLOPS-DD mediated transactivation. *CYC-RE*, five mutant versions (*M1-M5*) and a mutant variant of the entire palindrome (*mCYC-RE*) were analysed as tandem repeat (‘2x’) fusions to *pNINmin:GUS*. Nucleotide sequences of *CYC-RE*, *mCYC-RE*, *M1-M5*, , *1PAL1*, *mPAL*, *CYC-box* (= palindrome ‘*PAL*’) are depicted; the palindrome sequence is depicted in blue letters, mutated nucleotides are depicted in red.

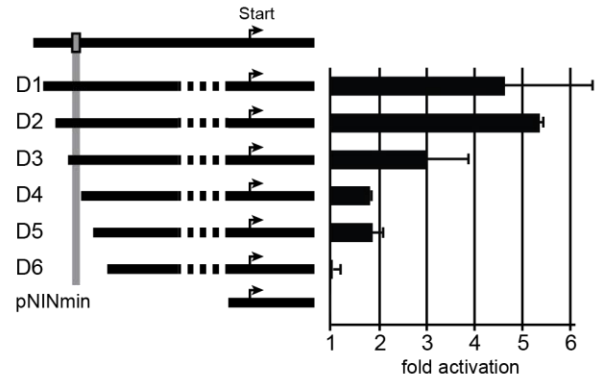
A



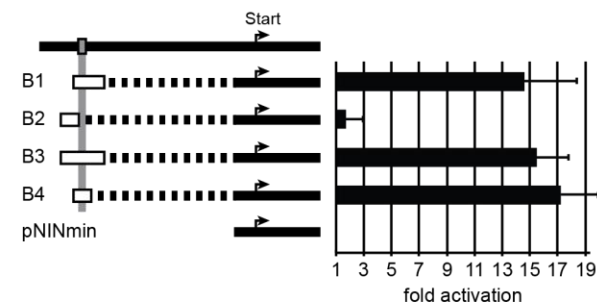
B



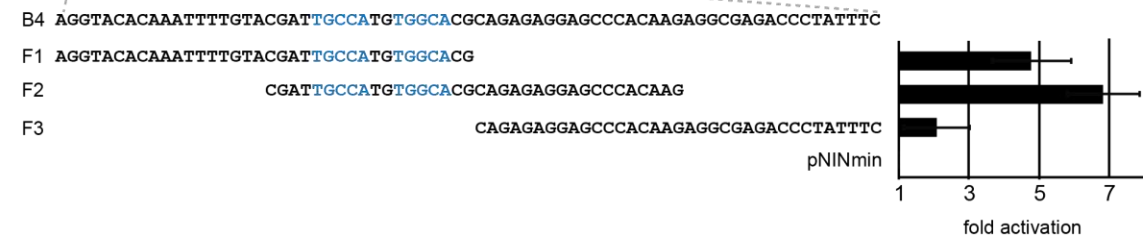
C



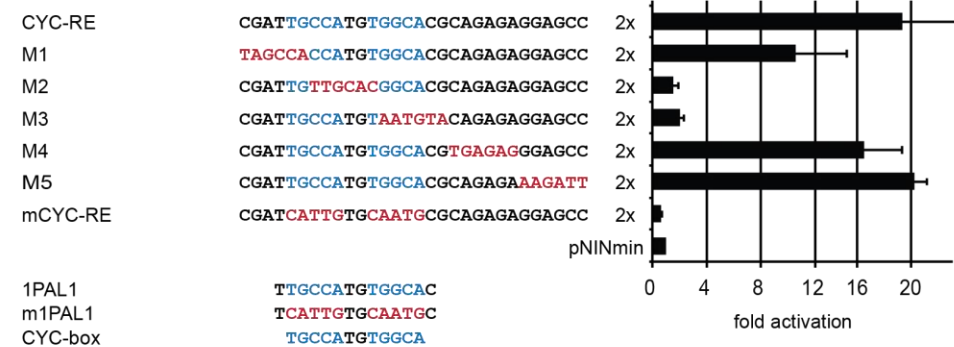
D



E



F



The sequence specificity was similar to that observed for the transcriptional activation by CYCLOPS-DD (Figure 34F), implicating direct DNA binding of CYCLOPS-DD as the most likely mechanism mediating sequence-specific transcriptional activation.

Co-expression of CYCLOPS with CCaMK in *E.coli* resulted in a strong phosphorylation of CYCLOPS, which was not observed when CYCLOPS was expressed alone (Figure 44A-C). To assess whether CYCLOPS binding to the *CYC-RE* depended on the phosphorylation state, CYCLOPS expressed without or with CCaMK was tested in EMSAs with *CYC-RE* as probe. Only CYCLOPS-DD and the CYCLOPS-WT protein obtained upon co-expression with CCaMK bound to *CYC-RE*, while binding was not detected with CYCLOPS-WT and CYCLOPS-AA expressed in the absence of CCaMK (Figure 35B, left panel). CCaMK alone caused no shift of the *CYC-RE* probe (data not shown). The shift obtained by CCaMK-pretreated CYCLOPS-WT protein was lost after phosphatase treatment (Figure 35B, right panel). This finding is consistent with the idea that phosphorylation confers CYCLOPS' DNA binding activity.

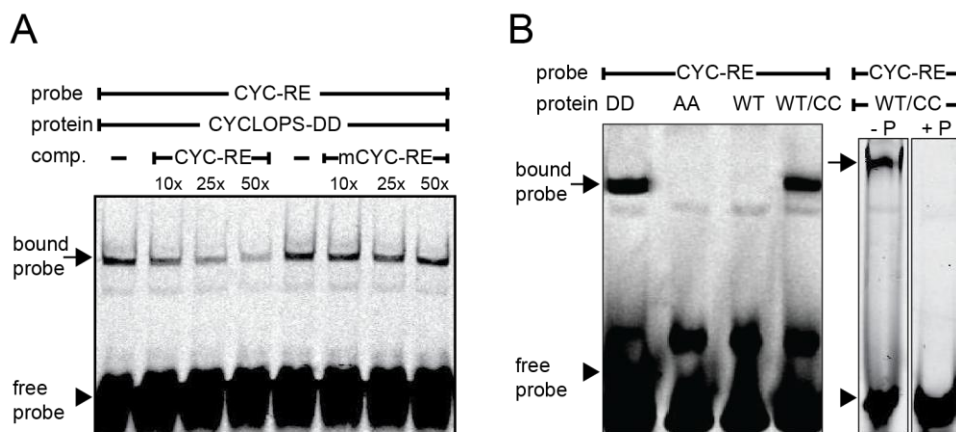


Figure 35. CYCLOPS binds the *NIN* promoter in a sequence-specific and phosphorylation dependent manner.

A) EMSA showing that CYCLOPS-DD has higher affinity to WT *CYC-RE* than to mutant *mCYC-RE* DNA. EMSA was performed with GST-CYCLOPS-DD (35 pmol), IR-labeled *CYC-RE* (0.1 pmol) as probe, and unlabeled competitor (comp.) DNA (*CYC-RE* or *mCYC-RE*) at 10-, 25- and 50-fold molar excess. Samples were resolved on a native 6% polyacrylamid gel.

B) CYCLOPS binds the *CYC-RE* in a phosphorylation-dependent manner.

Left panel: Equal concentrations (35 pmol) of GST-CYCLOPS-DD (DD), GST-CYCLOPS-AA (AA), and GST-CYCLOPS-WT (WT) protein and 40 pmol of Strep-CYCLOPS-WT protein purified after co-expression with CCaMK (WT/CC) were tested for binding to IR-labeled *CYC-RE* (0.1 pmol). Samples were resolved on a native 4% polyacrylamid gel. Right panel: Untreated (-P) and phosphatase treated (+P) Strep-CYCLOPS-WT protein (20 pmol) purified after co-expression with CCaMK (WT/CC) was tested with IR-labeled *CYC-RE* (0.1 pmol) as probe. Samples were resolved on a native 6% polyacrylamid gel. (A, B) The position of specifically bound and free probe is indicated by an arrow and an arrowhead, respectively.

Figure 35A and left panel of Figure 35B: Experiment was performed by Katja Katzer. Right panel of Figure 35B: Experiment was performed by the author of this thesis.

3.7 CYCLOPS is a modular DNA-binding transcriptional activator

As CYCLOPS exhibited DNA-binding and transcriptional activation properties, we aimed to assign these activities to distinct CYCLOPS domains. To detect and map the transcriptional activation domain of CYCLOPS (AD_{CYC}), DNA-BD_{Gal4} fusions to the N-terminus of CYCLOPS derivatives were tested in *N. benthamiana* for transactivation of the cognate reporter *p5xUAS:eGFP-GUS_{intron}* (providing five repeats of the Gal4 binding site) (Figure 36A). CYCLOPS or CYCLOPS-DD mediated strong transactivation, confirming the presence of an activation domain in CYCLOPS. CYCLOPS-AA did not confer transactivation, indicating that the phospho-ablative mutations compromised the functionality of AD_{CYC} (Figure 36A and 34A). The position of the AD_{CYC} could be narrowed down to aa 267-380, as this truncation triggered ~5-fold higher values compared to full-length CYCLOPS (Figure 36A), while the N-terminal half of CYCLOPS-DD (aa 1-265) and the C-terminal domain (aa 364-518) did not confer transactivation. In order to test whether plant specific proteins are required for the transactivation mediated by AD_{CYC} , the same constructs were tested in yeast. Importantly, a tandem repeat fusion of AD_{CYC} was able to trigger strong autoactivation when fused to the DNA-BD_{Gal4} (Figure 36D).

To identify the DNA-binding domain (DNA-BD_{CYC}), fusions of the AD_{VP16} to the N-terminus of CYCLOPS derivatives were analysed for their ability to activate a *NIN promoter:GUS* reporter in *N. benthamiana* (Figure 36B). Strong GUS expression was induced by CYCLOPS and CYCLOPS-DD, whereas with CYCLOPS-AA, GUS activity remained at the same level as the negative control (Figure 36B). An AD_{VP16} fusion to the C-terminal half of CYCLOPS (aa 255-518) and a fusion to the C-terminal coiled-coil (364-518) were both able to transactivate (Figure 36B) indicating that the DNA-BD_{CYC} is located at the C-terminal end. Consistent with this, the deletion of the C-terminal coiled-coil (aa 1-449) led to a severe reduction in transactivation strength (Figure 36B).

From these findings we concluded that the DNA-BD_{CYC} and AD_{CYC} were located in the C-terminal half of the protein and predicted a minimal CYCLOPS version ('CYCLOPS-min', comprising aa 255-518) as sufficient to mediate DNA binding and transcriptional activation (Figure 36A, B). This prediction was verified by the observation of transactivation of the *2xCYC-RE:GUS* reporter by CYCLOPS-min (Figure 36C).

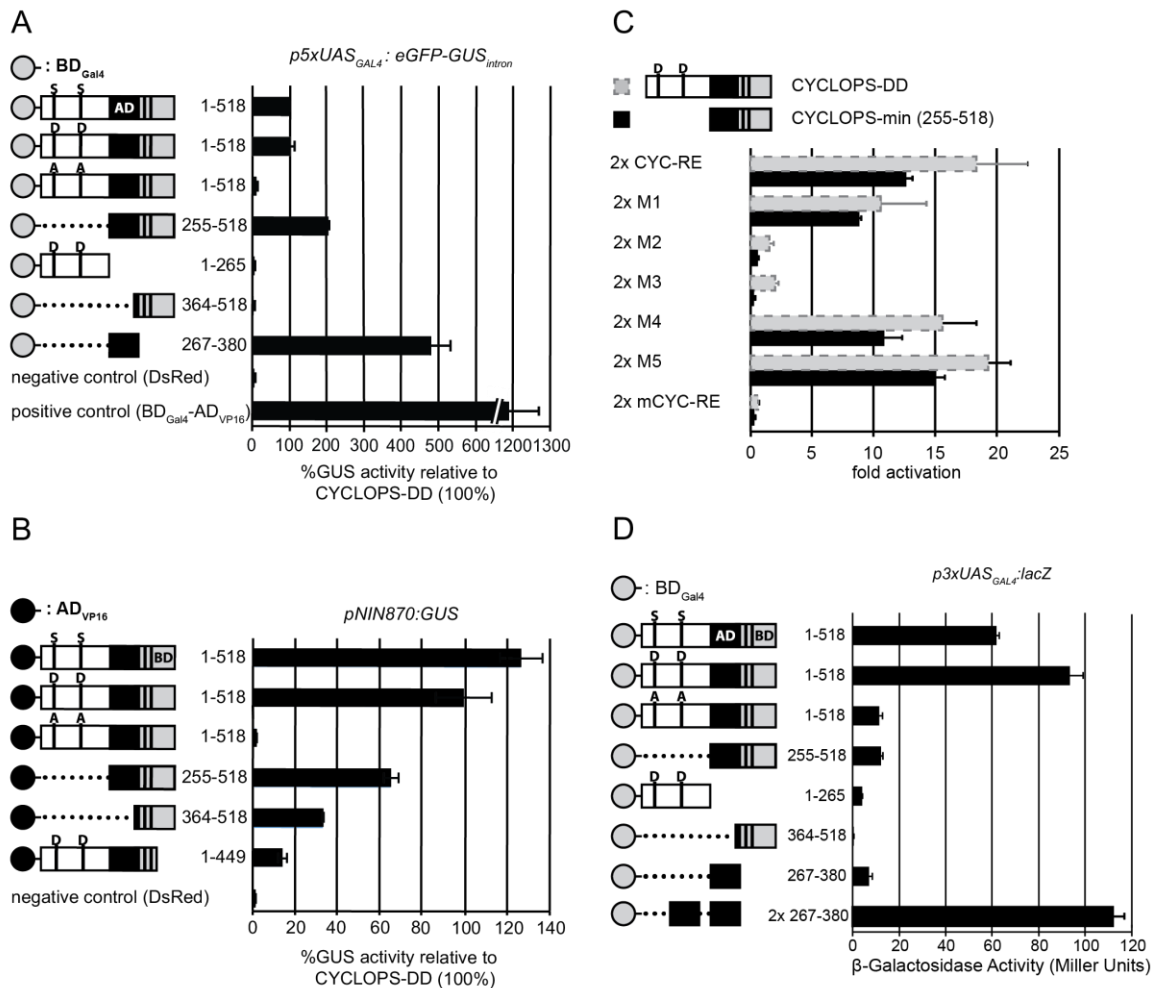


Figure 36. CYCLOPS is a modular DNA-binding transcriptional activator.

(A, B) Mapping of the CYCLOPS transcriptional activation domain (AD) (shown in A) and DNA binding domain (BD) (shown in B). *BD_{Gal4}-* or *AD_{VP16}-CYCLOPS-WT*, phospho-site mutants or truncated versions and the reporter *p5xUASGal4:eGFP-GUS_{intron}* (A) or *pNIN870:GUS* (B) were cotransformed into *N. benthamiana* leaves. A T-DNA encoding a *BD_{Gal4}-AD_{VP16}* fusion served as positive control in (A), a T-DNA encoding DsRed was used as negative control in (A) and (B). Mean values of reporter activation were calculated from three biological replicates and are presented relative to the mean value obtained with *BD_{Gal4}-CYCLOPS-DD* (A) or *AD_{VP16}-CYCLOPS-DD* (B) (each set to 100% GUS activity). The deduced region harbouring the CYCLOPS AD is depicted in black. *BD_{Gal4}* is depicted as grey circle in (A). The deduced region harbouring the CYCLOPS BD is depicted in grey. *AD_{VP16}* is depicted as black circle in (B).

(C) A minimal CYCLOPS version (CYCLOPS-min, aa 256-518) comprising the CYCLOPS AD and BD is sufficient to mediate transcriptional activation via the *CYC-RE* in *N. benthamiana*. *3xHA-CYCLOPS-min* and the WT reporter *2xCYC-RE:GUS*, or the indicated mutant versions were co-transformed into *N. benthamiana* leaf cells. GUS expression is shown relative to the value obtained with the *pNINmin:GUS* reporter construct (set to 1). Transactivation values obtained with *3xHA-CYCLOPS-min* (black bars) are shown in comparison to transactivation values obtained with *3xHA-CYCLOPS-DD* (grey bars; values are duplicates from Figure 34F). The graph shows mean values and standard deviations calculated from three biological replicates.

(D) The CYCLOPS transcriptional activation domain is functional in the heterologous system yeast. Wild-type CYCLOPS, phospho-site mutants and truncated versions fused to the yeast Gal4 DNA-binding domain (*BD_{Gal4}*, grey circle) were analyzed in the yeast reporter strain HF7c for transactivation of the *3xUASGal4:lacZ* reporter. LacZ (β -galactosidase) reporter activity was determined in Miller units. AD: Activation domain. BD: DNA-binding domain.

Data related to this figure were generated by Katja Katzer.

Importantly, the observed sequence-specific transactivation pattern of CYCLOPS-min matched that of CYCLOPS-DD (Figure 36C). This important finding is in line with the idea that the deleted N-terminus, which also contains the two critical phosphorylation sites, is a negative regulatory domain of CYCLOPS.

3.8 The CYCLOPS DNA binding domain binds the *CYC-RE* *in vitro*

The delimitation of the DNA-BD_{CYC} to aa 364-518 was substantiated by direct DNA binding assays. Binding of CYCLOPS-BD (aa 364-518) and CYCLOPS-DD-1-366 (CYCLOPS-DD- Δ BD), lacking the deduced DNA BD, to the *CYC-RE* was tested in an EMSA (Figure 37A). CYCLOPS-BD bound strongly and the binding was competitive with the WT palindromic sequence ('1PAL1'; sequence depicted in Figure 34F), but not efficiently with the mutated palindrome (1mPAL1; sequence depicted in Figure 34F), thus not only demonstrating sequence specificity but narrowing down the DNA fragment sufficient for CYCLOPS binding to the *CYC-box*. A palindromic target sequence is in agreement with the observation that CYCLOPS-DD formed dimers in plant cell nuclei (Figure 38). Importantly, CYCLOPS-DD- Δ BD caused no shift (Figure 37A). Sequence-specific DNA binding of CYCLOPS-BD and no binding of CYCLOPS-DD- Δ BD were also confirmed by microscale thermophoresis (Figure 37B and C). Taken together, these findings underscored that CYCLOPS-BD binds the *CYC-box* in a sequence-specific manner, matching the sequence specificity of CYCLOPS-DD.

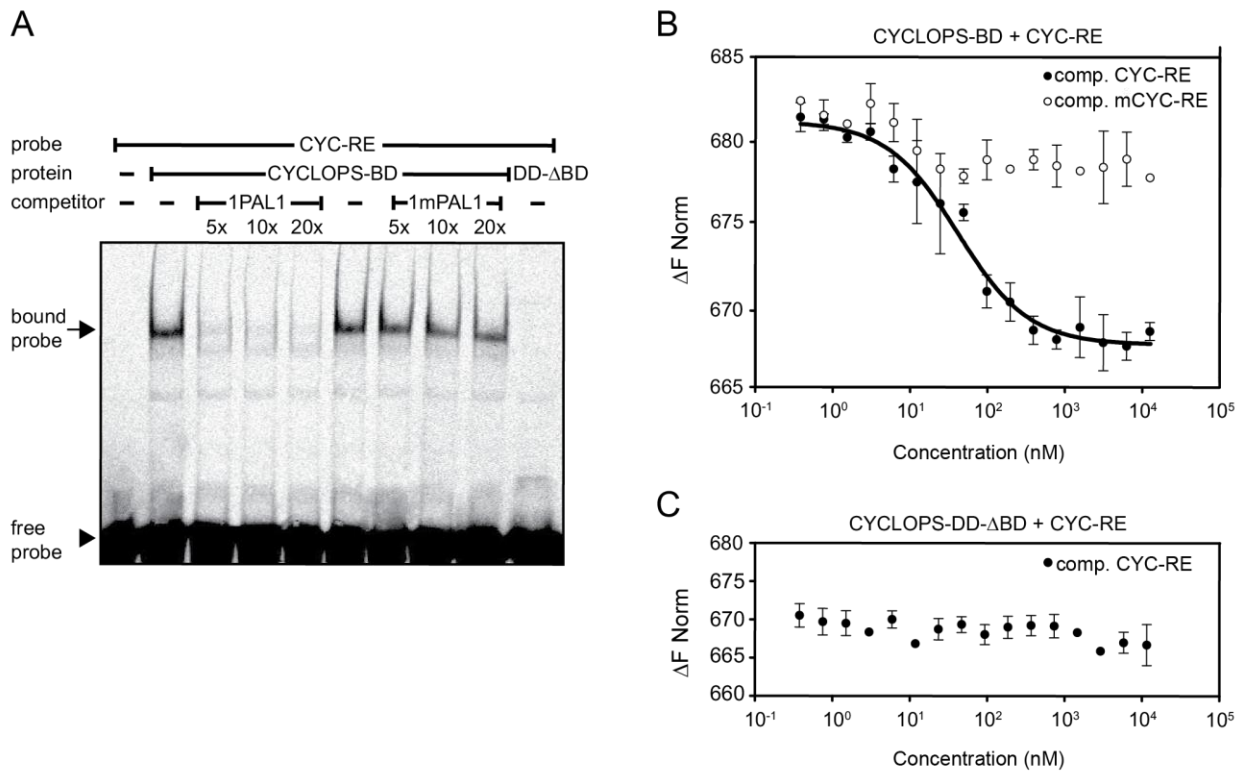


Figure 37. The delimited CYCLOPS DNA binding domain specifically binds the *CYC-box* *in vitro*.

(A) 75 pmol of recombinant GST-CYCLOPS-BD and of GST-CYCLOPS-DD-ΔBD (DD-ΔBD) lacking the DNA-BD were probed with IR-labeled *CYC-RE* (0.1 pmol) by EMSA. Unlabeled competitor DNA containing either the WT (1PAL1) or mutated palindrome (1mPAL1) (sequences depicted in Figure 34F), was used in 5-, 10- and 20-fold molar excess ratios. Arrow and arrowhead indicate position of specifically bound and free probe, respectively. Samples were resolved on a native 6% polyacrylamid gel.

(B) Microscale thermophoresis demonstrating that GST-CYCLOPS-BD specifically binds to the *CYC-RE* *in vitro*. Binding of recombinant GST-CYCLOPS-BD (1.3 μM) to labeled *CYC-RE* (25 nM) was competed by unlabeled WT *CYC-RE* (black circles) or mutated *mCYC-RE* (white circles) added in increasing concentrations (381 pM to 12.5 μM).

(C) Microscale thermophoresis showing that GST-CYCLOPS-DD-ΔBD does not bind to the *CYC-RE*. The reaction of GST-CYCLOPS-DD-ΔBD (1.3 μM) with labeled *CYC-RE* (25 nM) showed no change in thermophoresis values when unlabeled *CYC-RE* was added in increasing concentrations (381 pM to 12.5 μM), indicating an impairment in *CYC-RE* binding. (B, C) Average thermophoresis values and standard deviations of three experimental replicates are shown. Comp. = competitor.

Data related to this figure were generated by Katja Katzer.

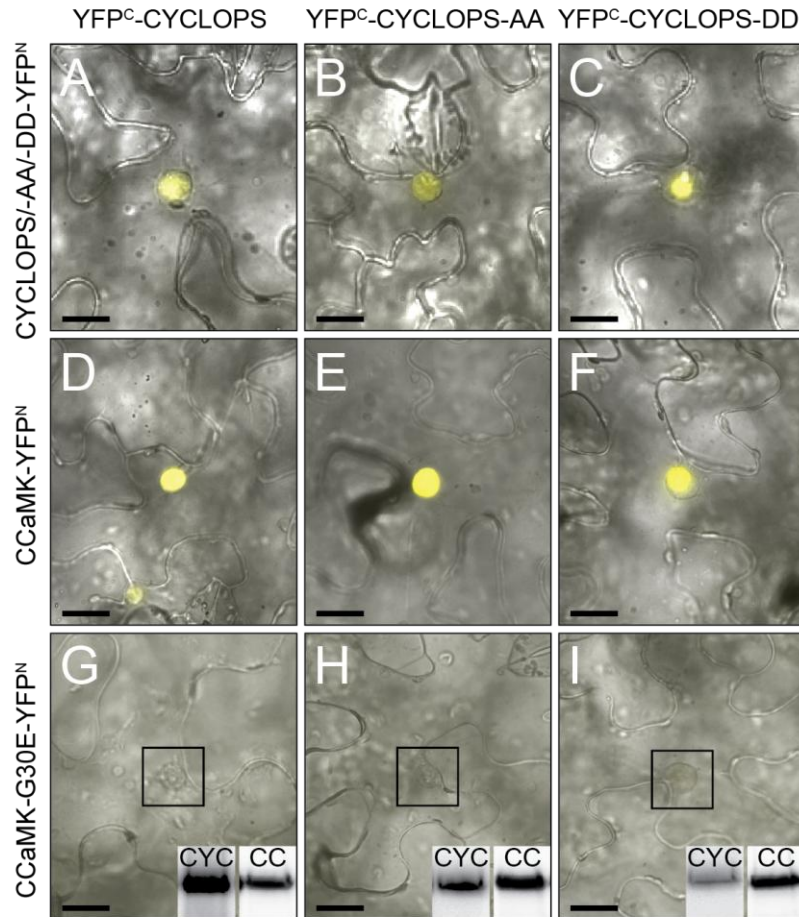


Figure 38. CYCLOPS and CYCLOPS phospho-site mutants form homodimers and interact with CCaMK.

Analysis of CYCLOPS, CYCLOPS-AA and CYCLOPS-DD self-interaction, interaction with CCaMK and the kinase-dead version CCaMK-G30E by bimolecular fluorescence complementation in *N. benthamiana* leaf cells. Candidate T-DNAs were co-transformed as fusions to the N- or C-terminal half of YFP (YFP^N or YFP^C) via *A. tumefaciens*. YFP fluorescence (shown in yellow) indicates interaction. Pictures represent overlay of brightfield images with micrographs recorded with a YFP filter. Bars: 25 μ m.

(A-C) Nuclear localized YFP fluorescence indicates homodimerization of (A) CYCLOPS, (B) CYCLOPS-AA and (C) CYCLOPS-DD.

(D-F) Nuclear localized YFP fluorescence demonstrates interaction of CCaMK-YFP^N with either YFP^C-CYCLOPS (D), YFP^C-CYCLOPS-AA (E), or YFP^C-CYCLOPS-DD (F).

(G-I) No YFP signal was detected in leaf cell nuclei co-expressing CCaMK-G30E-YFP^N and either YFP^C-CYCLOPS (G), YFP^C-CYCLOPS-AA (H), or YFP^C-CYCLOPS-DD (I), although in all cases the relevant proteins were detected by protein blot analysis. Inset CYC: Protein blot anti-HA-CYCLOPS. Inset CC: Protein blot probed with anti-CCaMK antibody. Squares in G, H and I indicate the position of the nucleus.

3.9 CYCLOPS-DD transactivates the *NIN* promoter via the *CYC-RE* in *L. japonicus* independently of NSP1, NSP2 and NIN

Our results so far are consistent with a model in which the phosphorylation of S50 and S154 leads to a structural change in CYCLOPS that alleviates autoinhibition of the transcriptional AD and promotes the DNA binding activity of CYCLOPS. The phospho-mimetic aspartate replacements of these two serine residues turn CYCLOPS into an autoactive transcription

factor. A prediction from this model is that this autoactive version (CYCLOPS-DD) should trigger symbiosis-related transcriptional activation and related phenotypic responses in roots of *L. japonicus*. Indeed, *UB_{pro}:3xHA-gCYCLOPS-DD* triggered strong and specific induction of the *2xCYC-RE:GUS* reporter only when containing the WT but not a mutant version of the palindrome (Figure 39A, B, Table 8) demonstrating that sequence specificity of the activation is retained in *L. japonicus*. Consistent with the observations in *N. benthamiana* (Figure 34A), only weak expression of *2xCYC-RE:GUS* was detected in roots co-transformed with *UB_{pro}:3xHA-gCYCLOPS-WT*, whereas no expression was visible in those co-transformed with *UB_{pro}:3xHA-gCYCLOPS-AA*, or the empty vector control (Figure 39C-E and Table 8). To test whether the endogenous *NIN* gene is indeed a target of CYCLOPS-DD in *L. japonicus* we employed quantitative real-time RT-PCR analysis on transgenic *ccamk-13* roots, constitutively expressing either *CYCLOPS-DD* or *CYCLOPS-AA* (Figure 40Q). Although both transgenes were expressed at similarly high levels, only in root systems transformed with *CYCLOPS-DD* transcription of *NIN* and the *NIN* target gene *NF-YAI* (Soyano et al., 2013) were activated (Figure 40Q). GUS expression matching this pattern was also observed in roots of a transgenic *L. japonicus* *NIN_{pro}:GUS* reporter line transformed with *UB_{pro}:3xHA-CYCLOPS-WT*, *-DD*, *-AA* or the empty vector control (data not shown). As transcription factors can act in a combinatorial manner as heteromeric complexes, we also asked whether transactivation of *2xCYC-RE:GUS* by CYCLOPS-DD in *L. japonicus* depended on putative transcriptional regulators required for nodulation, such as the GRAS domain proteins NSP1, NSP2 and the transcription factor *NIN*, all of which have previously been positioned downstream of CCaMK (Madsen et al., 2010; Marsh et al., 2007; Tirichine et al., 2006). Transformation of *nsp1*, *nsp2* and *nin* mutant roots with *UB_{pro}:3xHA-gCYCLOPS-DD* and *2xCYC-RE:GUS* in all cases resulted in strong reporter expression, indicating that these transcriptional activators were dispensable for CYCLOPS-DD mediated transactivation (Figure 39F-H and Table 8). We conclude that CYCLOPS-DD acts as a transcriptional activator which is sufficient to drive *2xCYC-RE:GUS* and *NIN_{pro}:GUS* reporter expression in *L. japonicus*.

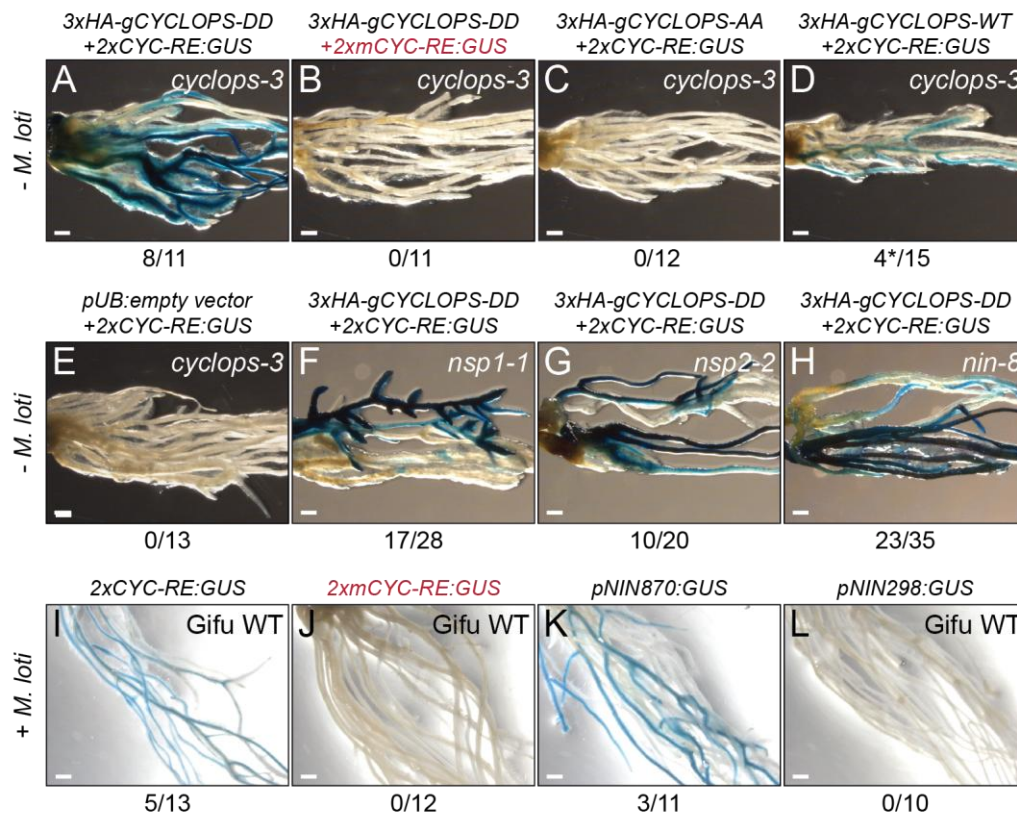


Figure 39. The 2xCYC-RE:GUS reporter is activated in *L. japonicus* roots transformed with *CYCLOPS-DD* independently of NSP1, NSP2 and NIN, and is also activated after treatment with *M. loti*.

(A-L) Analysis of GUS reporter (as indicated) induction in *L. japonicus* Gifu WT and mutant roots (*cyclops-3*, *nsp1-1*, *nsp2-2*, *nin8*, as indicated) four weeks post co-transformation with $UB_{pro}3xHA-gCYCLOPS-WT$, $-DD$, $-AA$, or the empty vector control (A-H), or one week after treatment with *M. loti*-DsRed (I-L). Reporter activation is visualised by blue GUS staining of transformed roots. Numbers below images indicate number of GUS positive root systems per total number of stained root systems. (A) Strong 2xCYC-RE:GUS activity was detected in roots co-transformed with 3xHA-gCYCLOPS-DD. (B) No GUS activity was detected in roots co-transformed with 3xHA-gCYCLOPS-DD and 2xmCYC-RE:GUS. (C, E) No GUS activity was detected in roots co-transformed with 2xCYC-RE:GUS and either 3xHA-gCYCLOPS-AA (C), or the empty vector control (E). (D) Faint GUS staining was occasionally observed in roots co-transformed with 2xCYC-RE:GUS and 3xHA-gCYCLOPS-WT. (F-H) Induction of 2xCYC-RE:GUS in *nsp1-1* (F), *nsp2-2* (G) and *nin-8* (H) mutant roots, co-transformed with 3xHA-gCYCLOPS-DD. (I) The reporters 2xCYC-RE:GUS and (K) *pNIN870:GUS* (containing the *CYC-RE*) were induced, while no GUS activity was observed in roots transformed with 2xmCYC-RE:GUS (J) and *pNIN298:GUS* (L, lacking the *CYC-RE*) 1 week after *M. loti*-DsRed treatment. *: Weak GUS staining. Bars: 1 mm.

Table 8. *CYC-RE:GUS* activation by *CYCLOPS-DD* in *Lotus* is independent of *NSP1*, *NSP2* and *NIN*.

Plant Genotype	Transgene1 ^a	Transgene2	GUS+/total ^b	%GUS+/total ^c
<i>cyclops-3</i>	<i>empty vector</i>	<i>2xCYC-RE:GUS</i>	0/13	0%
<i>cyclops-3</i>	<i>empty vector</i>	<i>2xmCYC-RE:GUS</i> ^d	0/12	0%
<i>cyclops-3</i>	<i>3xHA-gCYCLOPS-DD</i>	<i>2xCYC-RE:GUS</i>	8/11	73%
<i>cyclops-3</i>	<i>3xHA-gCYCLOPS-DD</i>	<i>2xmCYC-RE:GUS</i> ^d	0/11	0%
<i>cyclops-3</i>	<i>3xHA-gCYCLOPS-AA</i>	<i>2xCYC-RE:GUS</i>	0/12	0%
<i>cyclops-3</i>	<i>3xHA-gCYCLOPS</i>	<i>2xCYC-RE:GUS</i>	4 ^e /15	27%
<i>nsp1-1</i>	<i>empty vector</i>	<i>2xCYC-RE:GUS</i>	0/7	0%
<i>nsp1-1</i>	<i>3xHA-gCYCLOPS-DD</i>	<i>2xCYC-RE:GUS</i>	3/9	33%
<i>nsp1-2</i>	<i>empty vector</i>	<i>2xCYC-RE:GUS</i>	0/33	0%
<i>nsp1-2</i>	<i>3xHA-gCYCLOPS-DD</i>	<i>2xCYC-RE:GUS</i>	17/28	61%
<i>nsp2-2</i>	<i>empty vector</i>	<i>2xCYC-RE:GUS</i>	0/17	0%
<i>nsp2-2</i>	<i>3xHA-gCYCLOPS-DD</i>	<i>2xCYC-RE:GUS</i>	10/20	50%
<i>nin-2</i>	<i>empty vector</i>	<i>2xCYC-RE:GUS</i>	0/16	0%
<i>nin-2</i>	<i>3xHA-gCYCLOPS-DD</i>	<i>2xCYC-RE:GUS</i>	5/13	38%
<i>nin-8</i>	<i>empty vector</i>	<i>2xCYC-RE:GUS</i>	0/27	0%
<i>nin-8</i>	<i>3xHA-gCYCLOPS-DD</i>	<i>2xCYC-RE:GUS</i>	23/35	66%

^aConstructs were equipped with the ubiquitin promoter.

^bNumber of GUS positive root systems per total number of root systems analysed. Transformed roots were GUS stained 5 weeks post co-transformation.

^cPercentage of GUS positive root systems of total (100%) root systems analysed.

^dReporter construct in which the entire palindromic sequence within the *CYC-RE* is mutated.

^eWeak GUS staining.

3.10 The *2xCYC-RE:GUS* reporter is activated in *L. japonicus* roots after inoculation with *M. loti*

To determine whether the *2xCYC-RE:GUS* reporter is also activated during symbiosis establishment, we transformed *L. japonicus* Gifu WT roots with either *2xCYC-RE:GUS* or *2xmCYC-RE:GUS*, and analysed GUS expression in roots one week post inoculation with *M. loti*-DsRed. GUS expression was only detected with the WT- but not the mutant palindrome, indicating that the *CYC-RE* is targeted upon *M. loti* initiated signaling (Figure 39I, J, Table 9). This finding was also supported by the results obtained from the analysis of *pNIN870:GUS* (containing the *CYC-RE*) and *pNIN298:GUS* (lacking the *CYC-RE*), as reporter, which yielded a positive GUS staining only in roots transformed with *pNIN870:GUS*, (Figure 39K, L, Table 9).

Table 9. The *CYC-RE:GUS* and *pNIN870:GUS* reporters are activated after *M. loti*-DsRed treatment.

Plant Genotype	Transgene	Condition	GUS+/total ^a	%GUS+/total ^b
Gifu wild-type	<i>2xCYC-RE:GUS</i>	non-inoculated	0/7	0%
Gifu wild-type	<i>2xCYC-RE:GUS</i>	<i>M. loti</i> -DsRed, 1wpi	5/13	38%
Gifu wild-type	<i>2xmCYC-RE:GUS^c</i>	non-inoculated	0/10	0%
Gifu wild-type	<i>2xmCYC-RE:GUS^c</i>	<i>M. loti</i> -DsRed, 1wpi	0/12	0%
Gifu wild-type	<i>pNIN870:GUS</i>	non-inoculated	0/9	0%
Gifu wild-type	<i>pNIN870:GUS</i>	<i>M. loti</i> -DsRed, 1wpi	3/11	27%
Gifu wild-type	<i>pNIN298:GUS</i>	non-inoculated	0/7	0%
Gifu wild-type	<i>pNIN298:GUS</i>	<i>M. loti</i> -DsRed, 1wpi	0/10	0%

^aNumber of GUS positive root systems per total number of root systems analysed.

^bPercentage of GUS positive root systems of total (100%) root systems analysed.

^cReporter construct in which the entire palindromic sequence within the *CYC-RE* is mutated.

wpi: week post infection.

3.11 CYCLOPS-DD induced spontaneous nodules in *L. japonicus* roots independently of CCaMK

Deregulated versions of CCaMK lead to spontaneous initiation of nodule organogenesis in the absence of rhizobia (Gleason et al., 2006; Tirichine et al., 2006). If CYCLOPS phosphorylation was indeed a key event in symbiotic signaling downstream of CCaMK, one prediction would be that *CYCLOPS-DD* expression leads to a symbiotic gain-of-function phenotype *in planta* independent of the presence of CCaMK. We transformed *CYC_{pro}:3xHA-gCYCLOPS-DD* into two different *ccamk* mutant backgrounds: *ccamk-3* (encoding a kinase-dead CCaMK mutant) and *ccamk-13* (a CCaMK null mutant carrying a premature stop codon) (Perry et al., 2009) and cultivated the plants in the absence of rhizobia. Strikingly, CYCLOPS-DD triggered the spontaneous formation of root nodules (Figure 40, Table 10) with 30-40% of transformed plants forming an average of 2-5 nodules per nodulated plant (Table 10). This effect was specifically observed on roots transformed with *3xHA-gCYCLOPS-DD*, as spontaneous nodules were not formed on roots transformed with either the empty vector control, *3xHA-gCYCLOPS-WT* or other *CYCLOPS* mutant derivatives (Table 10). This observation indicated that CYCLOPS-DD was able to activate the nodule organogenesis program bypassing the requirement for CCaMK.

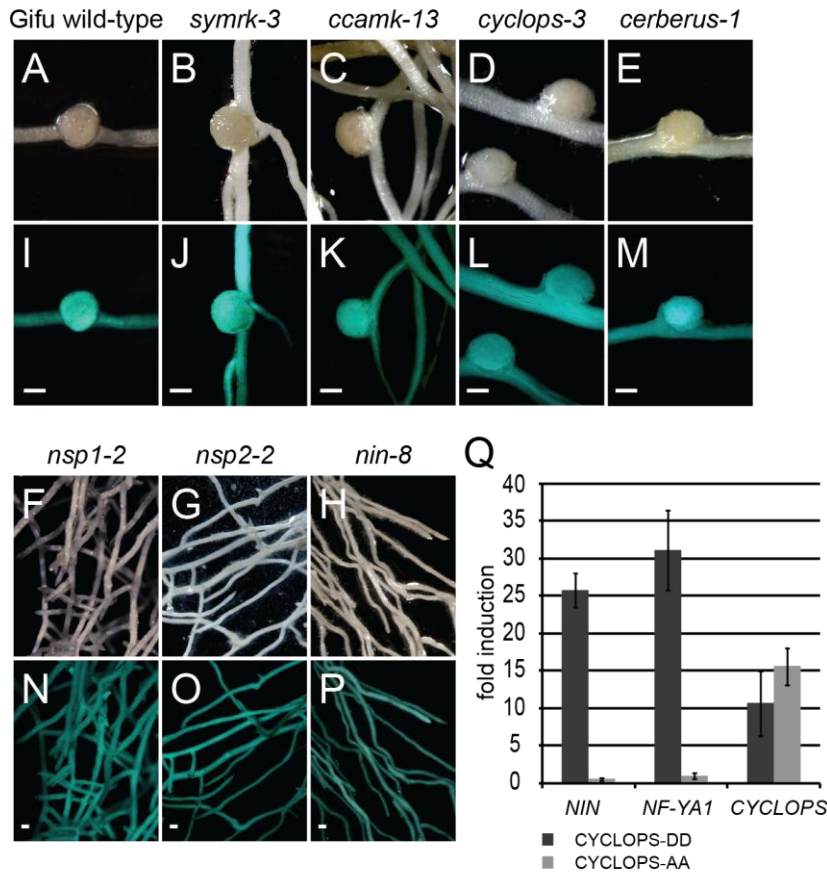


Figure 40. CYCLOPS-DD induces the formation of root nodules in the absence of rhizobia independently of CCaMK and upregulates *NIN* and *NF-YA1* transcript levels.

Spontaneous root nodule development induced in roots transformed with *CYC_{pro}3xHA-gCYCLOPS-DD* was observed on transgenic roots of the *L. japonicus* Gifu WT (A, I) and *symrk-3* (B, J), *ccamk-13* (C, K), *cyclops-3* (D, L), and *cerberus-1* (E, M) mutants, but not on transgenic roots of *nsp1-2* (F, N), *nsp2-2* (G, O) and *nin-8* (H, P) mutants. Spontaneous nodule formation was evaluated eight weeks post transformation and cultivation in the absence of rhizobia. (A-H) Brightfield images and (I-P) fluorescence images of transformed roots. Bars: 0.5 mm. (Q) Quantitative real-time RT-PCR analysis of *NIN*, *NF-YA1* and *CYCLOPS* expression in *ccamk-13* roots transformed with *UB_{pro}:3xHA-gCYCLOPS-DD*, -AA or the empty vector control. Expression analysis was performed four weeks post transformation. Relative expression was normalized to the reference genes *EF-1alpha* and *ubiquitin*. Fold induction levels were calculated relative to the expression obtained from hairy roots transformed with the empty vector control (expression level = 1). Graph represents mean values and standard deviations obtained from the analysis of three biological replicates.

Data related to figures 40E-H and 40M-P and the corresponding pictures were generated by Jayne Lambert.

Table 10. Analysis of spontaneous nodulation induced by CYCLOPS-DD.

Plant Genotype	Transgene ^a (Condition) ^b	SpN ⁺ ^c	#SpN/SpN+ Plant ^d
<i>cyclops-3</i>	empty vector	0/26	0
Gifu wild-type	<i>3xHA-gCYCLOPS-S50D-S154D</i> (non-inoculated)	6/27	5 ± 2
<i>symrk-3</i>	<i>3xHA-gCYCLOPS-S50D-S154D</i> (non-inoculated)	12/24	3 ± 1
<i>ccamk-3</i>	<i>3xHA-gCYCLOPS-S50D-S154D</i> (non-inoculated)	12/40	5 ± 3
<i>ccamk-3</i>	<i>3xHA-gCYCLOPS-S50D-S154D</i> (AM)	3/23	2 ± 2
<i>ccamk-13</i>	<i>3xHA-gCYCLOPS-S50D-S154D</i> (non-inoculated)	12/27	5 ± 3
<i>cyclops-3</i>	<i>3xHA-gCYCLOPS-S50D-S154D</i> (non-inoculated)	19/58	6 ± 4
<i>cyclops-3</i>	<i>3xHA-gCYCLOPS-S50D-S154D</i> (AM)	12/38	3 ± 2
<i>nsp1-2</i>	<i>3xHA-gCYCLOPS-S50D-S154D</i> (non-inoculated)	0/24	0
<i>nsp2-2</i>	<i>3xHA-gCYCLOPS-S50D-S154D</i> (non-inoculated)	0/30	0
<i>nin-2</i>	<i>3xHA-gCYCLOPS-S50D-S154D</i> (non-inoculated)	0/32	0
<i>nin-8</i>	<i>3xHA-gCYCLOPS-S50D-S154D</i> (non-inoculated)	0/57	0
<i>cerberus-1</i>	<i>3xHA-gCYCLOPS-S50D-S154D</i> (non-inoculated)	11/27	2 ± 1
<i>cyclops-3</i>	<i>3xHA-gCYCLOPS</i> (non-inoculated)	0/23	0
<i>ccamk-3</i>	<i>3xHA-gCYCLOPS</i> (non-inoculated)	0/17	0
<i>ccamk-13</i>	<i>3xHA-gCYCLOPS</i> (non-inoculated)	0/14	0
<i>cyclops-3</i>	<i>3xHA-gCYCLOPS-S14D</i> (non-inoculated)	0/11	0
<i>cyclops-3</i>	<i>3xHA-gCYCLOPS-S50D</i> (non-inoculated)	0/18	0
<i>cyclops-3</i>	<i>3xHA-gCYCLOPS-S154D</i> (non-inoculated)	0/30	0
<i>cyclops-3</i>	<i>3xHA-gCYCLOPS-S251D</i> (non-inoculated)	0/16	0
<i>cyclops-3</i>	<i>3xHA-gCYCLOPS-S412D</i> (non-inoculated)	0/12	0

^aConstructs were equipped with the endogenous promoter.

^bPlants were either cultivated in the absence of rhizobia and AM fungi (non-inoculated) or co-cultivated for 4 weeks with the AM fungus *R. irregularis* (AM).

^cSpN+: Number of root systems with spontaneous nodules per number of total root systems analysed. Spontaneous nodules were scored 8 weeks post transformation.

^dAverage number of spontaneous nodules per spontaneously nodulated root system ± standard deviation.

Further, sectioning of spontaneous nodules induced by *CYC_{pro}:3xHA-gCYCLOPS-DD* demonstrated that histologically these nodules exhibit a genuine nodule morphology which is characterized by the presence of two peripheral vascular bundles as typically formed in *M. loti* infected wild-type nodules (Figure 41).

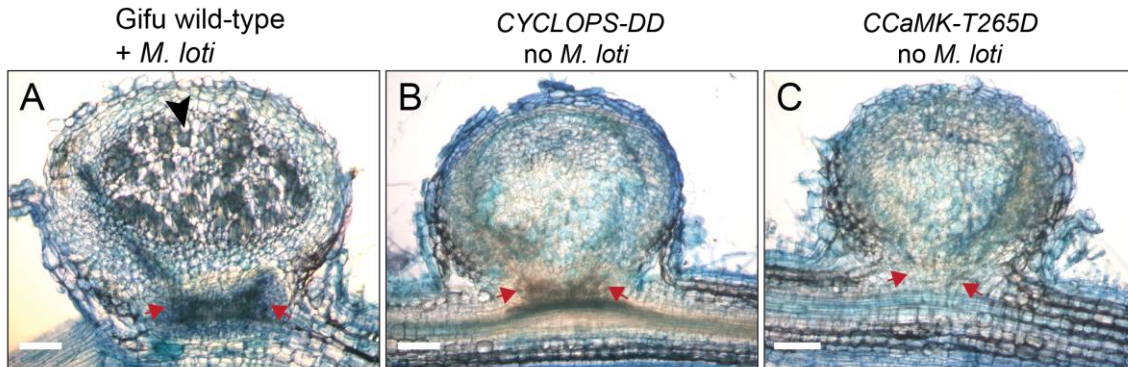


Figure 41. *CYCLOPS-DD* induced nodules show a genuine nodule morphology.

(A-C) Longitudinal 80 μ m thin nodule sections stained with toluidine blue. Red arrows indicate the position of the two peripheral vascular bundles, a typical histological criterion for genuine nodule morphology. Scale bars: 100 μ m.

(A) Section of a *L. japonicus* Gifu wild-type nodule formed 4 weeks post inoculation with *M. loti*-DsRed. Note the dark blue stained cells in the central nodule tissue (black arrowhead) indicating the presence of bacteroids. (B) Section of a spontaneous nodule formed on *L. japonicus ccamk-13* roots 8 weeks post transformation with *CYC_{pro}:3xHA-gCYCLOPS-DD* and incubated in the absence of rhizobia. (C) Section of a spontaneous nodule formed in *L. japonicus ccamk-13* roots 8 weeks post transformation with *UB_{pro}:CCaMK-T265D* and incubated in the absence of rhizobia.

To genetically position *CYCLOPS-DD* relative to other genes required for nodule organogenesis, we transformed *L. japonicus* Gifu WT, *symrk-3*, *cyclops-3*, *nsp1-2*, *nsp2-2*, *nin-8* and *cerberus-1* mutant roots with *CYC_{pro}:3xHA-gCYCLOPS-DD*. Spontaneous nodules were induced in the Gifu WT, *symrk-3*, *cyclops-3* and *cerberus-1* mutants, whereas no nodules were formed on *nsp1-2*, *nsp2-2* and *nin-8* mutants (Figure 40, Table 10). Spontaneous nodulation in the *symrk* mutant is consistent with the role of SYMRK in the activation of calcium spiking, which is upstream of CYCLOPS (Hayashi et al., 2010; Madsen et al., 2010). Furthermore, spontaneous nodules were formed in the *cerberus* mutant which is in agreement with the positioning of *CERBERUS* on the infection related pathway, due to its role in infection thread formation (Madsen et al., 2010; Yano et al., 2009). The requirement of *NSP1*, *NSP2* and *NIN* for *CYCLOPS-DD* mediated nodulation places these genes downstream of *CYCLOPS*.

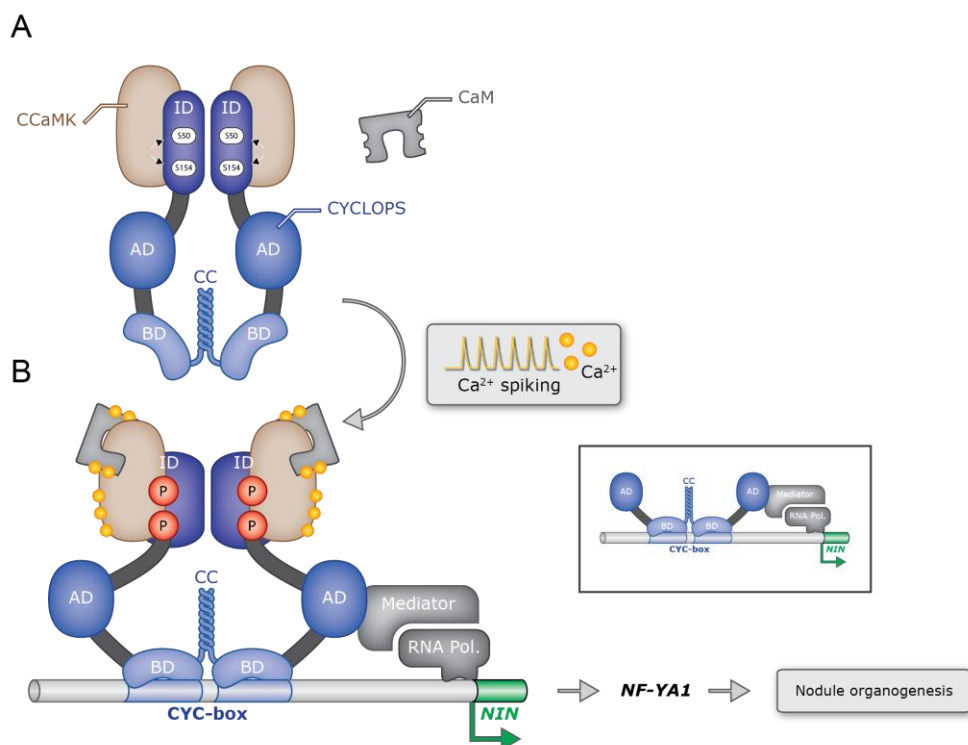


Figure 42. Proposed function of the CCaMK/CYCLOPS complex in the decoding of nuclear calcium signatures leading to root nodule development.

A) CCaMK and CYCLOPS form a preassembled, inactive and autoinhibited complex in root cell nuclei in which CYCLOPS dimerisation may occur via the carboxy-terminal coiled-coil domain. B) Upon initiation of symbiotic nuclear calcium spiking, CCaMK is activated by Ca^{2+} /Calmodulin (CaM) and phosphorylates CYCLOPS at S50 and S154. CYCLOPS phosphorylation induces a conformational change releasing the C-terminal transcriptional activation (AD) and DNA-binding (BD) domains from autoinhibition exerted by the N-terminal inhibitory domain (ID). Consequently, CYCLOPS binds the *CYC-box* in the *NIN* promoter and recruits the basal transcription machinery via its transcriptional AD, inducing *NIN* expression. Deregulated CYCLOPS is sufficient to reinitiate the cell cycle in differentiated cortical cells resulting in nodule organogenesis. This involves the cascade of transcriptional activation of *NIN* and *NF-YA1* in hierarchical succession. Inset: Experimental removal of the ID has an activating structural consequence. RNA-Pol. = RNA Polymerase II. This figure was prepared by Andreas Binder.

4 Discussion

4.1 CCaMK/CYCLOPS activates *NIN* transcription upon perception of calcium signals

The decoding of nuclear calcium signatures in multicellular organisms is involved in important cell fate decisions. In both animals and plants, the cell division program of specific cell types is triggered by nuclear calcium signatures in response to external stimuli (Clapham, 2007; Dodd et al., 2010). In plants, nuclear calcium spiking in root hair cells upon symbiotic stimulation was detected almost two decades ago (Ehrhardt et al., 1996) and CCaMK has emerged as the central regulator of symbiotic development (Singh and Parniske, 2012). However, the mechanism by and phosphorylation targets through which CCaMK mediates symbiotic development have been completely unclear. The *CYCLOPS* gene has been cloned

in 2003 through map-based cloning, and its product interacts and is phosphorylated by CCaMK *in vitro* (Figure 30A and 33). However, the role of CYCLOPS and its mechanism of action have been elusive, not least because CYCLOPS has no sequence homology to proteins of known function (Yano et al., 2008).

Here we show that CYCLOPS is a DNA binding transcriptional activator that connects phosphorylation by CCaMK directly to transcriptional gene regulation. Expression of autoactive CYCLOPS-DD in *ccamk* mutant roots induced the spontaneous development of root nodules in the absence of rhizobia, thus recapitulating the effect of deregulated CCaMK (Figure 40). This observation revealed that CYCLOPS phosphorylation is sufficient and additional CCaMK phosphorylation targets are dispensable for the initiation of nodule organogenesis by CCaMK. This together with its immediate early position within the calcium decoding complex pinpoints CYCLOPS as master regulator of root nodule organogenesis.

We propose a cascade of transcriptional regulation, which is initiated upon the activation of CCaMK by nuclear calcium signatures. Site-specific phosphorylation by CCaMK turns CYCLOPS into a transcriptional activator of the *NIN* gene. *NIN* induction alone can conceptually explain the spontaneous formation of lateral organs, because ectopic expression of *NIN*, which regulates *NF-YAI* and *NF-YBI* expression, induced the formation of abnormal lateral root organs partly resembling nodule primordia (Soyano et al., 2013). Based on accumulating evidence in legumes (Comber et al., 2006; Soyano et al., 2013) and in analogy to their mammalian homologs, a heterotrimeric NF-Y complex is believed to trigger entry into the cell division cycle (Laloum et al., 2013). Although ectopic *NIN* expression triggered lateral organ formation, full-sized round-shaped nodules as mediated by CYCLOPS-DD were not observed (Soyano et al., 2013). This may indicate that the precise spatiotemporal regulation of *NIN* is important for proper organogenesis, possibly achieved through a combination of local calcium signaling and *CYCLOPS* gene expression pattern. It is also possible that alternative CYCLOPS target genes beside *NIN* are required for nodule formation. Our data demonstrate that CYCLOPS-DD is sufficient to trigger nodule development (Figure 40). However, autoactive CCaMK was previously shown to also form nodules (albeit with reduced frequency) in the *cyclops* mutant and *ipd3* mutants of the *M. truncatula* *CYCLOPS* ortholog *IPD3* produced uninfected nodule primordia or nodules, respectively, upon rhizobia inoculation (Horvath et al., 2011; Ovchinnikova et al., 2011; Yano et al., 2008). Genetic redundancy at the hierarchical level of *CYCLOPS* could be one explanation for this discrepancy.

4.2 CYCLOPS carries a non-canonical DNA binding domain

We identified a modular domain structure in CYCLOPS comprising a functionally separable DNA binding and activation domain (Figure 36). This structure is typical for eukaryotic DNA binding transcriptional activators. We delimited the position of the CYCLOPS DNA binding domain to the C-terminal end (aa 364-518), which contains a highly conserved coiled-coil domain (aa 450-518). A sequence-based prediction of DNA or RNA-binding residues with BindN+ (Wang et al., 2010b) predicted three stretches of 13-15 amino acids, overrepresenting basic and polar amino acid residues which may act as DNA binding motifs inside the delimited BD. Two of these stretches are located outside of the coiled-coil domain (Figure 30B). However, by interrogating a range of specific databases (see methods) we were unsuccessful in detecting similarity to canonical DNA binding motifs. Therefore, we conclude that CYCLOPS represents a hitherto uncharacterized, novel type of DNA binding protein.

4.3 The CYCLOPS AD contains a peptide stretch with predicted intrinsic disorder

We narrowed down the CYCLOPS AD to aa 267-380. This region carries a conserved serine/threonine-rich stretch (aa 332-350; Figure 30B) which is located in an intrinsically disordered region as predicted by the DISPHOS (DISorder-enhanced PHOSphorylation) predictor (see methods). By being serine/threonine-rich and intrinsically unstructured (Liu et al., 2006), the CYCLOPS AD region shares two features with characterized transcriptional activation domains. In analogy, the CYCLOPS AD may become structured by a conformational change upon CYCLOPS phosphorylation at S50 and S154 and/or upon interaction with the basal transcriptional machinery (Figure 42). The delimited CYCLOPS AD was active in yeast and plant cells (Figure 36), indicating its ability of direct interaction with conserved parts of the transcriptional machinery such as the mediator (Conaway et al., 2005).

4.4 The N-terminal half of CYCLOPS functions as a negative regulatory domain

Our domain analysis confined the transcriptional AD and the DNA-BD of CYCLOPS to the C-terminal half (267-518) (Figure 36). A construct composed of the C-terminal AD and BD domains fully transactivated via the *CYC-RE*, displaying the same sequence specificity as CYCLOPS full length (Figure 36C). Since the N-terminus is not required and its removal leads to an active transcription factor, we conclude that it acts as a negative regulatory domain.

4.5 The consequences of CYCLOPS phosphorylation

CYCLOPS phosphorylation by CCaMK leads to transcriptional activation of the *NIN*

promoter (Figure 34A). This effect can be mimicked by phospho-mimetic versions of the two CCaMK substrate residues S50 and S154, and phospho-ablative versions are completely blocked in this activity (Figure 34A and 40Q). Since both regulatory serines are located in the N-terminal region, which is inhibiting CYCLOPS' activity (Figure 36C), we postulate that the 'DD' replacement (and by inference, phosphorylation) induces a conformational change that releases the DNA-binding and transcriptional AD from autoinhibition by the N-terminus (Figure 42).

This model is further supported by the strong effect of CYCLOPS phosphorylation on DNA binding activity (Figure 35). Only CYCLOPS-DD or CCaMK-phosphorylated CYCLOPS specifically bound to *CYC-RE* DNA *in vitro*, while CYCLOPS-AA, non- or de-phosphorylated CYCLOPS did not.

The fusions to the N-terminus utilized for the mapping of the CYCLOPS functional domains led to a release of CYCLOPS-WT from autoinhibition (Figure 36A and B). One explanation for this behavior is an influence of the added domain on the structure of the N-terminal domain thus releasing the C-terminus from autoinhibition. However, the CYCLOPS-AA version was not rescued by these fusions, suggesting that the hydroxyl groups of serine 50 and 154 play an important role in allowing the N-terminus to adopt a permissive conformation.

Our analysis of CYCLOPS and the phospho-site mutant versions did not reveal any effects on subcellular localization, or CCaMK interaction (Figure 32, 33 and 38), indicating that phosphorylation does not influence these traits and that the proteins were still appropriately folded. This behavior is contrasting that of transcription factors that are located in the cytoplasm and move to the nucleus upon phosphorylation. Gelfiltration of copurified CCaMK/CYCLOPS complexes revealed a soluble complex larger than 720 kDa with a one to one stoichiometry (Figure 45). This complex formed in the absence of calcium which is consistent with the FLIM-FRET data. The tight and preformed complex of CYCLOPS with the cognate kinase is an unusual feature and adds another layer of complexity to its regulation. It is likely that conformational changes induced by CYCLOPS phosphorylation may precipitate in higher order transitions between complex conformers. This may alter the spacing of DNA binding sites between CYCLOPS monomers, thus influencing affinity to palindromic targets.

4.6 Decoding of symbiotic calcium oscillations by the CCaMK/CYCLOPS complex provides a new paradigm in nuclear calcium-based signal transduction

The closest homolog of CCaMK in vertebrates is calcium/calmodulin-dependent kinase II (CaMKII) involved in the decoding of calcium spiking in neuronal and cardiac signaling

(Stratton et al., 2013). Although sequence related, there are some fundamental differences in their mode of action (Hudmon and Schulman, 2002a; Sathyanarayanan et al., 2001). In addition, CaMKII isoforms exist, that localize to both compartments the cytosol and the nucleus (Buchthal et al., 2012). However, the only known CaMKII pathway involved in direct transcriptional regulation is the CAMKII/MeCP2 (Methyl-CpG-binding protein) pathway (Buchthal et al., 2012; Wayman et al., 2008) in which nuclear calcium stimulated CaMKII activity phosphorylates MeCP2, a genome-wide transcriptional repressor or activator. However, the mechanism of action of MeCP2, which binds to methylated cytosines, is very different from the one discovered here. The only known exclusively nuclear localized CaMK is CaMKIV (Wayman et al., 2008), acting in the CAMKIV/CREB/CBP (cAMP-response element-binding/CREB-binding protein) ‘CCC’ pathway. Activated CaMKIV phosphorylates the transcription factor CREB and the coactivator CBP, which are both required for calcium induced CREB-dependent gene expression (Wayman et al., 2008). Mechanistically, the CCC pathway is the closest known system to CCaMK/CYCLOPS for the decoding of nuclear calcium signatures. Yet, in contrast to the CCC pathway there are no additional CCaMK-phosphorylated coactivators required for transactivation by CYCLOPS. Therefore we report a novel and hitherto most parsimonious mechanism of nuclear calcium signal transduction leading to stimulus specific gene expression. The CCaMK/CYCLOPS pair and the CCC system are phylogenetically restricted to plants (Wang et al., 2010a) and metazoans (Tombes et al., 2003) respectively. Apparently, plant and animal cells have convergently evolved independent nuclear kinase-substrate pairs for mediating calcium stimulated transcriptional regulation.

5 Materials and Methods

5.1 Plant lines and plant transformation

L. japonicus plant lines used in this study were: Gifu B-129 WT, *NINpro:GUS* (Radutoiu et al., 2003), *symrk-3*, *ccamk-3*, *ccamk-13*, *cyclops-3*, *nsp1-1*, *nsp1-2*, *nsp2-2*, *nin-2*, *nin-8*, (Perry et al., 2009), *cerberus-1* (Yano et al., 2009).

Transgenic hairy roots were induced by *A. rhizogenes* strain AR1193 (Offringa et al., 1986) as described (Diaz et al., 2005). Transformation of *N. benthamiana* leaves was performed with *A. tumefaciens* strains GV3101 pMP90 (Koncz and Schell, 1986) or AGL1 (Lazo et al., 1991) as described (Yano et al., 2008).

5.2 Plant growth and inoculation conditions

For analysis of spontaneous nodulation, gene expression and symbiosis complementation in hairy roots, *L. japonicus* plants with transformed hairy roots were transplanted two weeks post transformation into autoclaved pots containing a 1:1 mixture of sterilized sand/vermiculite (300 ml) supplemented with 100 ml sterile half-strength Hoagland solution (Hoagland and Arnon, 1950). Plants were watered regularly and supplied with 100 ml sterile half-strength Hoagland solution once per week. Plant growth conditions were 24 °C constant at 16-h-light/8-h-dark cycles in growth chambers.

For transactivation assays in *L. japonicus*, co-transformed plants were cultivated sterile on solid Fahraeus medium (supplemented with 0.1 µM AVG) (Fahraeus, 1957) for two weeks in a growth cabinet (24 °C constant at 16-h-light/8-h-dark) prior to histochemical GUS staining. Spontaneous nodule formation in the absence of rhizobia was evaluated eight weeks post hairy root transformation. To evaluate complementation of root nodule symbiosis, plants were inoculated with *M. loti* MAFF303099 carrying DsRed as marker (Maekawa et al., 2008) set to a final OD₆₀₀ of 0.05 and incubated for five weeks. AM establishment was tested with the AM fungus *Rhizophagus irregularis*, which was propagated in a chive (*Allium schoenoprasum*) nurse pot system (Demchenko et al., 2004). Co-cultivation of transformed plants was carried out for six weeks in nurse pots after removal of the chive shoot.

5.3 Symbiosis phenotyping

Formation of *M. loti*-DsRed infected root nodules was evaluated by microscopic observation of red fluorescent root nodules indicating the presence of DsRed expressing *M. loti*. RNS was scored as restored wild-type-like, if the abundant formation of red fluorescing nodules was observed. Microscopy was performed with a fluorescence stereomicroscope (Leica MZt6 FA). AM fungal colonization was visualized by ink vinegar staining of transformed inoculated roots (Vierheilig et al., 1998) using brightfield microscopy (inverted microscope Leica DMI6000). AM was scored as restored wild-type-like if the simultaneous formation of the AM fungal infection structures intracellular hyphae and arbuscules was observed and if a substantial proportion (in contrast to occasional small <2 mm patches) of the root length was colonized.

5.4 Nodule sectioning

Root material containing nodules was embedded in 6% low melt agarose (Roth, Germany) and sections (80 µm) were produced using the vibratome VT1000S (Leica). Sections were subsequently stained with toluidine blue (0.05%) and micrographs were recorded with a Leica

DMI6000 inverted light microscope using brightfield illumination.

5.5 Histochemical GUS staining

N. benthamiana leaf discs or *L. japonicus* hairy roots co-transformed with various transactivator and promoter:*GUS* reporter combinations were harvested 60 hours post transformation (hpt) (*N. benthamiana*) or five weeks post hairy root transformation (*L. japonicus*), vacuum infiltrated with GUS staining solution (0.1 M NaPO₄ pH 7.0, 5 mM EDTA, 1 mM K₃[Fe(CN)₆], 1 mM K₄[Fe(CN)₆], 0.1% Triton-X100; 1 mM X-Gluc) and incubated over night at 37 °C in the dark. The enzymatic reaction was stopped by removal of GUS staining solution. Leaf discs were cleared in 100% ethanol.

5.6 Fluorimetric GUS assay

Two infiltrated *N. benthamiana* leaf discs per sample were harvested 60 hpt and frozen in liquid nitrogen. Samples were homogenized in a tissue lyser, protein was extracted and GUS activity measured as described by (Römer et al., 2010). Mean values and standard deviations were determined from three biological replicates.

5.7 FLIM-FRET analysis

FLIM-FRET analysis was performed on transformed *N. benthamiana* leaf discs essentially as described by (Bayle et al., 2008). Analysis was performed with a Leica TCS SP5 confocal laser scanning microscope equipped with Ti:Sapphire multiphoton laser (Spectra Physics) and a FLIM PMT detector (Becker & Hickl GmbH, Berlin). For excitation of TSapphire fluorescence, the multiphoton laser (running at 80 MHz with 100 fs pulse length) was tuned to 800 nm. 20 scanning cycles (5s/cycle) were applied per FLIM measurement at a spatial resolution of 256x256 pixel. Signals were recorded with the TCSPC system using photon counting software TCSPC 2.80 (Becker & Hickl). For lifetime calculation, data were imported into SPCImage software. A region of interest was set around the nucleus and the double exponential model was applied. Scatter and shift were fixed to zero.

5.8 Bimolecular fluorescence complementation (BiFC) and subcellular localization analysis

BiFC and *in planta* localization analysis were performed as described previously (Yano et al., 2008).

5.9 CYCLOPS domain analysis in *N. benthamiana*

CYCLOPS DNA-binding domain and transcriptional activation domain analysis was carried out in *N. benthamiana* using a reporter system derived from the plant codon usage adapted

Gal4:VP16/UAS system (Haseloff, 1999). CYCLOPS DNA-binding domain and transcriptional activation domain analysis was carried out in *N. benthamiana* using a reporter system derived from the plant codon usage adapted Gal4:VP16/UAS system (Haseloff, 1999). To test CYCLOPS autoactivity, T-DNAs of *BD_{Gal4}-CYCLOPS* fusions were co-delivered with the reporter T-DNA *5xUAS_{Gal4}:eGFP-GUS_{intron}* encoded on vector pSDM7006 kind gift of R. Offringa, (Weijers et al., 2003) via *A. tumefaciens* transformation. To test CYCLOPS DNA-binding activity *AD_{VP16}:CYCLOPS* wild-type, mutant or truncated fusions were co-delivered together with the *pNIN870:GUS* reporter T-DNA. Transactivation of the reporter constructs was quantified using a fluorimetric GUS assay (Römer et al., 2010).

5.10 CYCLOPS domain analysis in yeast

CYCLOPS and mutant coding sequences were cloned into Gateway modified yeast vector pBDGAL4-GW (Stratagene). Transformation into the yeast reporter strain HF7c (Feilotter et al., 1994) was carried out according to standard procedures (Stratagene Product Manual). Three independent clones per construct were selected and transactivation activity was calculated in Miller units via determination of β -Galactosidase (*lacZ*) activity as described in the Clontech Manual PT1030-1.

5.11 Protein expression and purification

Expression of all proteins was induced in *E. coli* Rosetta pLacI (Novagen) for 4 h at 28 °C by addition of 0.5-1 mM IPTG. CCaMK was purified via CaM-Sepharose beads (GE-Healthcare) according to the manufacturer's protocol. Desalting was performed with PD10 desalting column (GE Healthcare) using buffer containing 25 mM Tris and 10 mM β -mercaptoethanol (pH 7.6). Expression and purification of 6xHis-CYCLOPS was performed as described by Yano et al., 2008. For EMSA analysis, GST-CYCLOPS, GST-CYCLOPS-AA, GST-CYCLOPS-DD, GST-CYCLOPS-BD and GST-CYCLOPS-DD Δ BD were purified with Glutathione HiCap Matrix (Qiagen) according to the manufacturer's protocol. StrepII-tagged CYCLOPS protein was co-expressed with CCaMK and purified via Strep-Tactin-Sepharose column (IBA) according to the manufacturer's instruction. Protein concentration was determined by the Bradford method (Bio-Rad), using BSA (Sigma) as a standard and protein purity was analysed by SDS-PAGE and Coomassie staining of the gel.

5.12 *In vitro* phosphorylation and dephosphorylation

CYCLOPS was phosphorylated *in vitro* by CCaMK as described (Liao et al., 2012). Strep-CYCLOPS-WT protein purified after co-expression with CCaMK was dephosphorylated with Lambda Protein Phosphatase (NEB) according to the manufacturer's instruction.

5.13 Mass spectrometric analysis

For mass spectrometric analysis of CCaMK-phosphorylated 6xHis-CYCLOPS, 3 µg of 6xHis-CYCLOPS protein were incubated with 2 µg of CCaMK and 1 µM bovine calmodulin (Sigma) in the presence of 0.1 mM CaCl₂ using the same buffer conditions as described by Liao et al., 2012, but replacing radioactive [γ -³²P] ATP with ATP (400 µM). In gel digestion of phosphorylated CYCLOPS, liquid chromatography (LC)-MS data acquisition and database search was performed as described by Liao et al., 2012.

5.14 Electrophoretic mobility shift assay

EMSAs were performed as described in the presence of 50 mM KCl (Strauß et al., 2012). To increase DNA-binding specificity, the EMSAs shown in Figure 35A were performed in the presence of 150 mM KCl and the EMSAs shown in Figure 37A (probing GST-CYCLOPS-BD and GST-CYCLOPS-DD-ΔBD) were performed in the presence of 250 mM KCl

The complementary pairs of labeled (5' DY682) and unlabeled oligonucleotide probes used for EMSAs are listed in 5.20.

5.15 Microscale thermophoresis

Specific binding between GST-CYCLOPS-BD or GST-CYCLOPS-ΔBD-DD protein and *CYC-RE* DNA probe was measured by the microscale thermophoresis (MST) method as described (Jerabek-Willemsen et al., 2011). Binding experiments were performed with 25 nM Cy5 labeled *CYC-RE* and 1.3 µM GST-CYCLOPS-BD or GST-CYCLOPS-DD-ΔBD protein. Increasing amounts (from 381 pM to 12.5 µM) of unlabeled competitor probe (*CYC-RE*, or mutated *mCYC-RE*) were added. Binding reactions were carried out in buffer containing 20 mM Tris pH 7.4, 150 mM NaCl, 10 mM MgCl₂ and 0.05% Tween. Samples were loaded into NT.115 standard capillaries (Nanotemper Technologies) and MST was carried out at 25 °C, 80% LED and 40% IR-laser power using the Monolith NT.115 (Nanotemper Technologies). Data analysis was performed with Nanotemper Analysis software, v.1.2.101. Average thermophoresis values and standard deviations were calculated from three independent measurements and curve fitting was calculated using SigmaPlot 11.0 software (Systat software).

5.16 Protein blot analysis

Two transformed hairy root systems were combined per sample and frozen in liquid nitrogen. Root material was ground to fine powder with a tissue lyser (Qiagen) and protein was extracted with extraction buffer (50 mM Tris-HCl, pH 7.5, 150 mM NaCl, 1 mM EDTA, 1.0% Triton X-100, 0.5% sodium deoxycholate, 0.05% SDS, 5 mM DTT, 1mM EGTA, 1%

plant protease inhibitor cocktail, Sigma). Extracts were clarified by centrifugation (10000 xg, 15 min, 4 °C), equal volumes of clarified extracts were separated on 10% SDS gels and proteins were transferred to PVDF membrane (GE-Healthcare). Immunodetection of 3xHA-tagged CYCLOPS proteins was performed using rat monoclonal antibody anti-HA-HRP (clone 3F10, Roche). Proteins expressed in *N. benthamiana* were extracted as described by (Waadt et al., 2008) and detected using anti-HA-HRP antibody (clone 3F10, Roche), or rabbit polyclonal anti-CCaMK antibody (<http://www.pineda-abservice.de>).

5.17 Gene expression analysis

Total RNA was extracted from *L. japonicus* hairy roots four weeks post transformation using the SpectrumTM Plant Total RNA Kit (Sigma-Aldrich). RNA samples were DNaseI (Invitrogen) treated and absence of DNA contamination was confirmed by PCR. First strand cDNA synthesis was performed from 300 ng total RNA in 20 µl reaction volume using SuperScriptIII Kit (Invitrogen). Real-time RT-PCR analysis was carried out in a CFX96 Real-Time PCR machine (BioRad) using 1 µl of diluted (1:2) cDNA in a total reaction volume of 20 µl containing Fast SYBR Green Master Mix (Applied Biosystems) and the respective primer pairs (Table S6). Thermal cycling conditions were: 95 °C 1 min, 45 cycles of 95 °C 10 sec, 60 °C 30 sec, followed by dissociation curve analysis. Expression values were calculated as described by (Gutjahr et al., 2008). Relative expression was normalized to the reference genes *EF-1alpha* and *ubiquitin* (Takeda et al., 2009). Mean and standard deviation values were calculated from three biological replicates.

5.18 CYCLOPS amino acid sequence alignment

CYCLOPS amino acid sequences were aligned with CLC Main Workbench version 6.6.2. The following accession numbers were used: *Lotus japonicus* CYCLOPS ABU63668; *Medicago truncatula* CYCLOPS, ABU63671; *Pisum sativum* (pea) CYCLOPS, ABU63669; *Oryza sativa* (rice) CYCLOPS, ABU63670. To obtain the protein sequences of *Populus trichocarpa* CYCLOPS and *Physcomitrella patens* CYCLOPS, the corresponding genomic sequences POPTRDRAFT_757268 (Tuskan et al., 2006) and PHYPADRAFT_171948 (Rensing et al., 2008) were aligned with the *L. japonicus* CYCLOPS sequence and intron/exon borders were predicted based on a combination of alignment of the predicted protein sequences with Lotus CYCLOPS and the consensus sequence of intron-exon borders. Adjusted coding sequences were then translated into the corresponding amino acid sequence and used for protein sequence alignment.

5.19 Computational analysis

The following online resources were used for DNA binding domain and activation domain analysis: InterPro, <http://www.ebi.ac.uk/interpr/> (Hunter et al., 2012); 2zip, <http://2zip.molgen.mpg.de> (Bornberg-Bauer et al., 1998); DBD Threader, <http://cssb.biology.gatech.edu/skolnick/webservice/DBD-Threader/index.html> (Gao and Skolnick, 2009); BindN+, <http://bioinfo.ggc.org/bindn+/> (Wang and Brown, 2006; Wang et al., 2010b). DISPHOS (DISorder-enhanced PHOSphorylation predictor), <http://www.ist.temple.edu/DISPHOS>), prediction was computed using default predictor setting (Iakoucheva et al., 2004).

5.20 Oligonucleotides used for primers and EMSA probes

f = forward

r = reverse

(A) Oligonucleotides for *CYCLOPS* constructs (5'-3')

CYCLOPS promoter

caccccaactatcaggtcaagtctgc_f (CEW7)

tcaaagtcgacggtttggctcaacagcacttcc_rSalI (CEW8)

CYCLOPS genomic

caccatggaagggagggggg_f

catttttcagtttctgatag_r

CYCLOPS-S14A genomic + coding sequence

tatagaaactcagctgaagaattgttctg_f (SY12)

caggaacaattctcagctgagtttctata_r (SY13)

CYCLOPS-S50A genomic + coding sequence

ggctttcgcgcatgcccaggagcttttc_f (SY14)

gaaaagctcctcgccatctgcccgaagcc_r (SY15)

CYCLOPS-S154A genomic

gacaagaagccggcctctgaattgcggtac_f (SY16)

gtaccgcaattcagagggcccggcttctgtc_r (SY17)

CYCLOPS-S154A coding sequence

caagaagccggcctctgaattgcggtc_f (SY51)

cgccgcaattcagagggcccggcttctgtc_r (SY52)

CYCLOPS-S251A genomic + coding sequence

caacgccgagactgccagtcaactgag_f (SY18)

ctcaagttgactggcgagtctccggcgttg_r (SY19)

CYCLOPS-S412A genomic + coding sequence

ctagaaagatatggagctataacatcagctg_f (SY20)

cagctgatgttatagctccatatcttctag_r (SY21)

CYCLOPS-S14D genomic + coding sequence
tatagaaactcagatgaagaattgttctg_f (SY34)
caggaacaattctcatctgagtttctata_r (SY35)

CYCLOPS-S50D genomic + coding sequence
ctttcgcgcagatgacgaggagctttc_f (SY36)
gaaaagctcctcgtcatctgcgcgaaag_r (SY37)

CYCLOPS-S154D genomic
gacaagaagccgggactctgaattgcggtac_f (SY42)
gtaccgcaattcagagtcccggcttctgtc_r (SY43)

CYCLOPS-S154D coding sequence
acaagaagccgggactctgaattgcgg_f (SY48)
ccgcaattcagagtcccggcttctgt_r (SY49)

CYCLOPS-S251D genomic + coding sequence
caacgccggagactcgacagtcaacttgag_f (SY38)
ctcaagttgactgtcaggtctccggcgtt_r (SY39)

CYCLOPS-S412D genomic + coding sequence
ctagaaagatatggagatataacatcagctg_f (SY40)
cagctgatgttatatctccatatttctag_r (SY41)

CYCLOPS-364-518 = *CYCLOPS-BD*
caccatgcaaactctctgcgaaagctc_f (KK54)
ttacatttttcagtttctgatag_r (KK92)

CYCLOPS-267-380 = *CYCLOPS-AD*
caccatgtttatcctcaagaacctc_f (KK53)
ttagaactttactcactcctactgtttc_r (KK51)

CYCLOPS-2x267-380 = *CYCLOPS-2xAD*
atgcggccgcattttatcctcaagaaccttttc_f NotI (KK77)
atgcggccgcctgaactttactcactcctactgtttc_r NotI (KK78)

(B) Oligonucleotides used for FLIM-FRET constructs (5'-3')

p35S:mOrange cloning:

mOrange_f
gcaagcttgatggtgagcaagggcgagga_f HindIII (JL41)
p35SΔGW_r
gcaagcttatcgataccgtcgacctc_r HindIII (JL42)

T-Sapphire Δstop
cacctcgaggcatggtgagcaagggcgagg_f XhoI (SY140)
cacaagcttctgtacagctcgtccatgc_r HindIII (SY141)

(C) Oligonucleotides used for *NIN* promoter rough mapping (5'-3')

pNIN870

cgctctagattgtactggaattatag_f XbaI (SY134)
cgcgatccctagctgatccaattaagtac_r BamHI (SY130)

pNIN298

cgcaagcttattctgtctcttctgaat_f HindIII (SY132)
cgcgatccctagctgatccaattaagtac_r BamHI (SY130)

pNIN98 (pNINmin)

cgctctagatgcttacactgtgggtcc_f XbaI (SY153)
cgcgatccctagctgatccaattaagtac_r BamHI (SY130)

pNIN7

cgcaagctttcattttcccaagcactgc_f HindIII (SY133)
cgcgatccctagctgatccaattaagtac_r BamHI (SY130)

(D) Oligonucleotides used for *NIN* promoter fine mapping (5'-3')

pNIN -834 to -299 (D1)

cgctctagagcaataatgtatgtaattgt_f XbaI (SY158)
cgctctagatctaaaacttaactactcatg_r XbaI (SY160)

pNIN -785 to -299 (D2)

cgctctagatttcgccgatatcgtagac_f XbaI (SY163)
cgctctagatctaaaacttaactactcatg_r XbaI (SY160)

pNIN -735 to -299 (D3)

cgctctagaaggtacacaaattttgtacg_f XbaI (SY162)
cgctctagatctaaaacttaactactcatg_r XbaI (SY160)

pNIN -685 to -299 (D4)

cgctctagacaagaggcgagaccctatttc_f XbaI (SY164)
cgctctagatctaaaacttaactactcatg_r XbaI (SY160)

pNIN -635 to -299 (D5)

cgctctagaagtcaagttcatcatgataatc_f XbaI (SY165)
cgctctagatctaaaacttaactactcatg_r XbaI (SY160)

pNIN -579 to -299 (D6)

cgctctagagggtagatatagatatgtt_f XbaI (SY156)
cgctctagatctaaaacttaactactcatg_r XbaI (SY160)

pNIN -735 to -615 (B1)

cgctctagatttcgccgatatcgtagac_f XbaI (SY163)
cgctctagacgtacaaaattgtgtacct_r XbaI (SY167)

pNIN -785 to -716 (B2)

cgctctagaaggtacacaaattttgtacg_f XbaI (SY162)
cgctctagagattatcatgatgaactgact_r XbaI (SY169)

pNIN -785 to -615 (B3)

cgctctagaaggtacacaaatTTgtacg_f XbaI (SY162)
cgctctagagaaatagggtctcgcctctg_r XbaI (SY168)

pNIN -735 to -666 (B4)

cgctctagatttcgccgatatcgtagac_f XbaI (SY163)
cgctctagagattatcatgatgaactgact_r XbaI (SY169)

pNIN -735 to -701 (F1)

ctagaggtacacaaatTTgtacgattgccatgtggcacg_f XbaI (SY170)
ctagcgtgccacatggcaatcgtacaaaatTTgttacct_r XbaI (SY171)

pNIN -717 to -683 (F2)

ctagcgattgccatgtggcacgcagagaggagcccacaag_f XbaI (SY174)
ctagcttgtgggctcctctctcgtgccacatggcaatcg_r XbaI (SY175)

pNIN -700 to -666 (F3)

ctaggcagagaggagcccacaagaggcgagaccctatttc_f XbaI (SY172)
ctaggaaatagggtctcgcctcttgggctcctctctgc_r XbaI (SY173)

(E) Oligonucleotides used for *CYC-RE* analysis (5'-3')

2xCYC-RE wild-type (SY184, SY185)

ctagcgattgccatgtggcacgcagagaggagcccattgccatgtggcacgcagagaggagcc_f XbaI
ctagggctcctctctcgtgccacatggcaatcgggctcctctctcgtgccacatggcaatcg_r XbaI

2xCYC-RE M1 (SY186, SY187)

ctagtagccaccatgtggcacgcagagaggagcctagccaccatgtggcacgcagagaggagcc_f XbaI
ctagggctcctctctcgtgccacatgggctaggtcctctctcgtgccacatggtgcta_r XbaI

2xCYC-RE M2 (SY188, SY189)

ctagcgattgttcacggcacgcagagaggagcccattgttcacggcacgcagagaggagcc_f XbaI
ctagggctcctctctcgtgccacatgggctcctctctcgtgccacatggcaatcg_r XbaI

2xCYC-RE M3 (SY190, SY191)

ctagcgattgccatgtaattgtacagagaggagcccattgccatgtaattgtacagagaggagcc_f XbaI
ctagggctcctctctgtacattacatggcaatcgggctcctctctgtacattacatggcaatcg_r XbaI

2xCYC-RE M4 (SY192, SY193)

ctagcgattgccatgtggcacgtgagagggagcccattgccatgtggcacgtgagagggagcc_f XbaI
ctagggctcctctcactgccacatggcaatcgggctcctctcactgccacatggcaatcg_r XbaI

2xCYC-RE M5 (SY194, SY195)

ctagcgattgccatgtggcacgcagagaaagattcgattgccatgtggcacgcagagaaagatt_f XbaI
ctagaatcttctctcgtgccacatggcaatcgaatcttctctcgtgccacatggcaatcg_r XbaI

2x mCYC-RE (SY196, SY197)

ctagcgatcattgtgcaatgcgagagaggagcccattgtgcaatgcgagagaggagcc_f XbaI
ctagggctcctctctcgtgccacatgggctcctctctcgtgccacatggcaatcg_r XbaI

(F) Oligonucleotides used for CYCLOPS domain analysis (5'-3')

Gal4:VP16 (SY59, SY60)

caccatgaagctcctgtcctc_f
ctaccaccgtactcgtcaattc_r

Gal4-BD domain (SY61, SY62)

cgcaagcttatgaagctcctgtcc_f HindIII
cgcaagcttcgtcgtcgtcgtc_r HindIII

VP16-AD domain (KK55, KK56)

ctaagctttcgacggccccccg_f HindIII
ccaagcttcccaccgtactcgtcaattc_r HindIII

(G) Oligonucleotides used for protein expression (5'-3')

StrepII-TEV-CYCLOPS (SY55)

accatatgatggctagctggagccacccgcagttcgaaaaagagaatctttatcttcaggcaatggaagggagggggtt_f
NdeI

CYCLOPS_r (SY56)

cacctcgtgagttacatttttcagtttc_r XhoI

TEV-CCaMK (SY53)

gtcgcagcagaatctttatcttcaggcattgggatgatgacaaac_f SallI

CCaMK_r (SY54)

ggggccgcctatgatggacgaagagaag_r NotI

(H) EMSA probes (5'-3')

CYC-RE wild-type (M4PAL14) (SY182, SY183)

cgattgccatgtggcacgcagagaggagcc_f
ggctcctctctgcgtgccacatggcaatcg_r

mCYC-RE (M4mPAL14) (SY200, SY201)

cgatcattgtgcaatgcgcagagaggagcc_f
ggctcctctctgcgattgcacaatgatcg_r

CYC-RE palindrome -/+1 bp (1PAL1) (SY212, SY213)

ttgcatgtggcac_f
gtgccacatggcaa_r

Mutated *CYC-RE* palindrome -/+1 bp (1mPAL1) (SY214, SY215)

tcattgtgcaatgc_f
gcattgcacaatga_r

(I) Oligonucleotides used for expression analysis (5'-3')

Ubiquitin

atgcagatcttcgtcaagaccttg_f
acctcccctcagacgaag_r

EF-1 alpha

gcaggtctttgtgtcaagtctt_f
cgatccagaaccagttct_r

NIN

aactcactggaacaggtgcttc_f
ctattgcggaatgtattagctaga_r

NF-YA1

gaagctgctcaacctaaagtc_f
cgagatgtagaactgaactgtcac_r

CYCLOPS (endogenous and transgenic)

gctcaaggaaaatggctgaa_f
gcgatcgaacttccttctca_r

5.21 Plasmid construction

(A) Entry clones

pENTR:CYCLOPS _{pro} (CYC _{pro})	Phusion PCR product of a 2439 bp CYCLOPS promoter fragment amplified from pIV10:genomic CYCLOPS with <i>CYCLOPS</i> promoter_fwd/rev cloned into pENTR/D-TOPO via TOPO reaction (Invitrogen)
pENTR:gCYCLOPS	Phusion PCR product of the 4059 bp genomic CYCLOPS nucleotide sequence amplified from pIV10:genomic CYCLOPS with <i>CYCLOPS</i> genomic_fwd/rev cloned into pENTR/D-TOPO via TOPO reaction (Invitrogen)
pENTR:3xHA _g CYCLOPS	<i>Nco</i> I fragment (containing 3xHA) from pAMPAT:p35S:3xHA-GW (Gateway-compatible pAMPAT-MCS derivative (GenBank accession AY436765) cloned into <i>Nco</i> I site of pENTR:gCYCLOPS
pENTR:3xHA _g CYCLOPS-S14A	Site directed mutagenesis Phusion PCR with <i>CYCLOPS-S14A</i> genomic + coding sequence_fwd/rev on pENTR:3xHA _g CYCLOPS
pENTR:3xHA _g CYCLOPS-S50A	Site directed mutagenesis Phusion PCR with <i>CYCLOPS-S50A</i> genomic + coding sequence_fwd/rev on pENTR:3xHA _g CYCLOPS
pENTR:3xHA _g CYCLOPS-S154A	Site directed mutagenesis Phusion PCR with <i>CYCLOPS-S154A</i> genomic_fwd/rev on pENTR:3xHA _g CYCLOPS
pENTR:3xHA _g CYCLOPS-S251A	Site directed mutagenesis Phusion PCR with <i>CYCLOPS-S251A</i> genomic + coding sequence_fwd/rev on pENTR:3xHA _g CYCLOPS
pENTR:3xHA _g CYCLOPS-S412A	Site directed mutagenesis Phusion PCR with <i>CYCLOPS-S412A</i> genomic + coding sequence_fwd/rev on pENTR:3xHA _g CYCLOPS
pENTR:3xHA _g CYCLOPS-S14A-S50A	Site directed mutagenesis Phusion PCR with <i>CYCLOPS-S50A</i> genomic + coding sequence_fwd/rev on pENTR:3xHA _g CYCLOPS-S14A
pENTR:3xHA _g CYCLOPS-S14A-S154A	Site directed mutagenesis Phusion PCR with <i>CYCLOPS-S154A</i> genomic_fwd/rev on pENTR:3xHA _g CYCLOPS-S14A
pENTR:3xHA _g CYCLOPS-S50A-S154A	Site directed mutagenesis Phusion PCR with <i>CYCLOPS-S154A</i> genomic_fwd/rev on pENTR:3xHA _g CYCLOPS-S50A
pENTR:3xHA _g CYCLOPS-	Site directed mutagenesis Phusion PCR with <i>CYCLOPS-S14A</i>

S14A-50A-S154A	genomic + coding sequence_fwd/rev on pENTR:3xHAgCYCLOPS-S50A-S154A
pENTR:3xHAgCYCLOPS-S14A-50A-S154A-S251A	Site directed mutagenesis Phusion PCR with <i>CYCLOPS-S251A</i> genomic + coding sequence_fwd/rev on pENTR:3xHAgCYCLOPS-S14A-S50A-S154A
pENTR:3xHAgCYCLOPS-S14A-50A-S154A-S251A-S412A	Site directed mutagenesis Phusion PCR with <i>CYCLOPS-S412A</i> genomic + coding sequence_fwd/rev on pENTR:3xHAgCYCLOPS-S14A-S50A-S154A-S251A
pENTR:3xHAgCYCLOPS-S14D	Site directed mutagenesis Phusion PCR with <i>CYCLOPS-S14D</i> genomic + coding sequence_fwd/rev on pENTR:3xHAgCYCLOPS
pENTR:3xHAgCYCLOPS-S50D	Site directed mutagenesis Phusion PCR with <i>CYCLOPS-S50D</i> genomic + coding sequence_fwd/rev on pENTR:3xHAgCYCLOPS
pENTR:3xHAgCYCLOPS-S154D	Site directed mutagenesis Phusion PCR with <i>CYCLOPS-S154D</i> genomic_fwd/rev on pENTR:3xHAgCYCLOPS
pENTR:3xHAgCYCLOPS-S251D	Site directed mutagenesis Phusion PCR with <i>CYCLOPS-S251D</i> genomic + coding sequence_fwd/rev on pENTR:3xHAgCYCLOPS
pENTR:3xHAgCYCLOPS-S412D	Site directed mutagenesis Phusion PCR with <i>CYCLOPS-S412D</i> genomic + coding sequence_fwd/rev on pENTR:3xHAgCYCLOPS
pENTR:3xHAgCYCLOPS-S50D-S154D	Site directed mutagenesis Phusion PCR with <i>CYCLOPS-S50D</i> genomic + coding sequence_fwd/rev on pENTR:3xHAgCYCLOPS-S154D
pENTR:3xHAgCYCLOPS-S14A-S50D-S154D-S251A-S412A	Sequential site directed mutagenesis Phusion PCRs with 1) <i>CYCLOPS-S14A</i> genomic + coding sequence_fwd/rev, 2) <i>CYCLOPS-S251A</i> genomic + coding sequence_fwd/rev and 3) <i>CYCLOPS-S412A</i> genomic + coding sequence_fwd/rev on 1)pENTR:3xHAgCYCLOPS-S50D-S154D, 2)pENTR:3xHAgCYCLOPSS14A-S50D-S154D, 3) pENTR:3xHAgCYCLOPSS14A-S50D-S154D-S251A
pENTR:cCYCLOPS	Entry clone with <i>CYCLOPS</i> coding sequence (c), (Yano et al., 2008)
pENTR:cCYCLOPS-S50A-S154A	Sequential site directed mutagenesis Phusion PCRs with 1) <i>CYCLOPS-S50A</i> genomic + coding sequence_fwd/rev, 2) <i>CYCLOPS-S154A</i> coding sequence_fwd/rev on 1) pENTR:cCYCLOPS and 2) pENTR:cCYCLOPS-S50A
pENTR:cCYCLOPS-S50D-S154D	Sequential site directed mutagenesis Phusion PCRs with 1) <i>CYCLOPS-S50D</i> genomic + coding sequence_fwd/rev, 2) <i>CYCLOPS-S154D</i> coding sequence_fwd/rev on 1) pENTR:cCYCLOPS and 2) pENTR:cCYCLOPS-S50D
pENTR:cCYCLOPS-1-265-DD	Sequential site directed mutagenesis Phusion PCRs with 1) <i>CYCLOPS-S50D</i> genomic + coding sequence_fwd/rev, 2) <i>CYCLOPS-S154D</i> coding sequence_fwd/rev on 1) pENTR:cCYCLOPS1-265 (Yano et al., 2008) and 2) pENTR:cCYCLOPS1-265-S50D
pENTR:cCYCLOPS-1-366-DD= (CYCLOPS-DD-ΔBD	Sequential site directed mutagenesis Phusion PCRs with 1) <i>CYCLOPS-S50D</i> genomic + coding sequence_fwd/rev, 2) <i>CYCLOPS-S154D</i> coding sequence_fwd/rev on 1) pENTR:cCYCLOPS1-366 (Yano et al., 2008) and 2) pENTR:cCYCLOPS1-366-S50D
pENTR:cCYCLOPS-255-518	Yano et al., 2008
pENTR:cCYCLOPS-364-518= (CYCLOPS-BD)	Phusion PCR product from pENTR:cCYCLOPS with <i>CYCLOPS-364-518</i> _fwd/rev cloned into pENTR/D-TOPO via TOPO reaction

	(Invitrogen)
pENTR:cCYCLOPS-267-380=(CYCLOPS-AD)	Phusion PCR product from pENTR:cCYCLOPS with <i>CYCLOPS</i> -267-380_fwd/rev cloned into pENTR/D-TOPO via TOPO reaction (Invitrogen)
pENTR:cCYCLOPS-2x(267-380)	Phusion PCR product from pENTR:cCYCLOPS with <i>CYCLOPS</i> -2x267-380_fwd/rev cloned into <i>NotI</i> site of pENTR:cCYCLOPS-267-380
pENTR:cCCaMK	Entry clone with <i>CCaMK</i> coding sequence (Yano et al., 2008)
pENTR:cCCaMK-T265D	Entry clone with <i>CCaMK-T265D</i> coding sequence (Yano et al., 2008)
pENTR:cCCaMK-G30E	Entry clone with <i>CCaMK-G30E</i> coding sequence (Yano et al., 2008)
pENTR:BD _{Gal4} -AD _{VP16}	Phusion PCR product from genomic DNA of <i>A. thaliana</i> Gal4-GFP enhancer trap line (Haseloff, 1999) with <i>Gal4:VP16</i> _fwd/rev cloned into pENTR/D-TOPO via TOPO reaction (Invitrogen)

(B) Plasmids for *L. japonicus* hairy root transformation

pK7WG2D:3xHA-gCYCLOPS	LR reaction (Invitrogen) of pENTR:3xHA-gCYCLOPS and pK7WG2D (Karimi et al., 2002)
pK7:CYC _{pro} :3xHA-gCYCLOPS	Removal of 35S promoter from pK7WG2D:3xHA-gCYCLOPS by <i>SalI</i> digest and replacement through CYCLOPS promoter fragment (2250 bp) obtained from <i>SalI</i> digest of pENTR:CYCLOPS _{pro}
pK7:CYC _{pro} :GW	BP reaction (Invitrogen) of pK7:CYC _{pro} :3xHA-gCYCLOPS and pDONR207 (Invitrogen)
pK7:CYC _{pro} :3xHA-gCYCLOPS phosphosite mutants	LR reaction (Invitrogen) of pENTR:3xHA-gCYCLOPS mutants (listed in 5.21A) and pK7:CYC _{pro} :GW
pUB:3xHA-gCYCLOPS or phosphosite mutants	LR reaction (Invitrogen) of pENTR:3xHA-gCYCLOPS or phosphosite mutants (listed in 5.21A) and pUB:GW-GFP (Maekawa et al., 2008)

(C) Plasmids for FLIM-FRET, subcellular localization and BiFC analysis

p35S:TSapphire-GW	Phusion PCR product of TSapphire Δ stop amplified from p35S:GW-TSapphire-nos (Bayle et al., 2008) with T-Sapphire Δ stop_fwd/rev and cloned into <i>XhoI/HindIII</i> sites of pAMPATp35S:GFP-GW (Yano et al., 2008), Gateway-compatible pAMPAT-MCS derivative (GenBank accession AY436765)
p35S:TSapphire-cCYCLOPS or phospho-site mutants	LR reaction (Invitrogen) of pENTR:cCYCLOPS or phosphosite mutants and p35S:TSapphire-GW-nos
p35S:mOrange	Phusion PCR product from p35S:GW-mOrange (Bayle et al., 2008) with mOrange_fwd, p35S Δ GW_rev, digested with <i>HindIII</i> and self-ligated
p35S:CCaMK-mOrange	LR reaction (Invitrogen) of pENTR:cCCaMK and p35S:GW-mOrange (Bayle et al., 2008)
p35S:CYCLOPS-Cerulean (or CYCLOPS phosphosite mutants)	LR reaction (Invitrogen) of pENTR:cCYCLOPS (or phosphosite mutants, listed in 5.21A) and p35S:GW-Cerulean (gift of R. Bhat)
pGW735/1:CYCLOPS (or phosphosite mutants)	Yano et al., 2008 and LR reaction (Invitrogen) of pENTR:cCYCLOPS-S50A-S154A or pENTR:cCYCLOPS-S50D-S154D with pGW735/1 (unpublished, gift from T. Lahaye)
pSPYNE35S:CYCLOPS (or phosphosite mutants)	LR reaction (Invitrogen) of pENTR:cCYCLOPS (or phosphosite mutants listed in 5.21A) with pSPYNE35S:GW

	(unpublished, gift from T. Lahaye)
pSPYNE35S:CCaMK	Yano et al., 2008
pSPYNE35S:CCaMK-G30E	Yano et al., 2008

(D) Plasmids for *NIN* promoter analysis

pAMPATp35S:3xHA-CYCLOPS (or phosphosite mutants)	LR reaction (Invitrogen) of pENTRcCYCLOPS (or phosphosite mutants, listed in 5.21A) with pAMPATp35S:3xHA-GW (Gateway-compatible pAMPAT-MCS derivative (GenBank accession AY436765))
pAMPATp35S:3xHA-CCaMK	LR reaction (Invitrogen) of pENTRcCCaMK with pAMPATp35S:3xHA-GW (Gateway-compatible pAMPAT-MCS derivative (GenBank accession AY436765))
pAMPATp35S:3xHA-CCaMK-T265D	LR reaction (Invitrogen) of pENTRcCCaMK-T265D with pAMPATp35S:3xHA-GW (Gateway-compatible pAMPAT-MCS derivative (GenBank accession AY436765))
pNIN870:GUS	Phusion PCR product from pNIN:GUS (gift of M. Hayashi) with <i>pNIN870_fwd/rev</i> cloned into <i>XbaI/BamHI</i> sites of pBI101 (Jefferson et al., 1987)
pNIN298:GUS	Phusion PCR product from pNIN:870 with <i>pNIN298_fwd/rev</i> cloned into <i>HindIII/BamHI</i> sites of pBI101 (Jefferson et al., 1987)
pNIN98:GUS = pNINmin	Phusion PCR product from pNIN:870 with <i>pNIN98_fwd/rev</i> cloned into <i>XbaI/BamHI</i> sites of pBI101 (Jefferson et al., 1987)
pNIN7:GUS	Phusion PCR product from pNIN:870 with <i>pNIN7_fwd/rev</i> cloned into <i>HindIII/BamHI</i> sites of pBI101 (Jefferson et al., 1987)
D1 = pNIN(-834 to -299):GUS	Phusion PCR product from pNIN:870 with <i>pNIN -834 to -299_fwd/rev</i> cloned into <i>XbaI</i> site of pNINmin
D2 = pNIN(-785 to -299):GUS	Phusion PCR product from pNIN:870 with <i>pNIN -785 to -299_fwd/rev</i> cloned into <i>XbaI</i> site of pNINmin
D3 = pNIN(-735 to -299):GUS	Phusion PCR product from pNIN:870 with <i>pNIN -735 to -299_fwd/rev</i> cloned into <i>XbaI</i> site of pNINmin
D4 = pNIN(-685 to -299):GUS	Phusion PCR product from pNIN:870 with <i>pNIN -685 to -299_fwd/rev</i> cloned into <i>XbaI</i> site of pNINmin
D5 = pNIN(-635 to -299):GUS	Phusion PCR product from pNIN:870 with <i>pNIN -635 to -299_fwd/rev</i> cloned into <i>XbaI</i> site of pNINmin
D6 = pNIN(-579 to -299):GUS	Phusion PCR product from pNIN:870 with <i>pNIN -579 to -299_fwd/rev</i> cloned into <i>XbaI</i> site of pNINmin
B1 = pNIN(-735 to -615):GUS	Phusion PCR product from pNIN:870 with <i>pNIN -735 to -615_fwd/rev</i> cloned into <i>XbaI</i> site of pNINmin
B2 = pNIN(-785 to -716):GUS	Phusion PCR product from pNIN:870 with <i>pNIN -785 to -716_fwd/rev</i> cloned into <i>XbaI</i> site of pNINmin
B3 = pNIN(-785 to -615):GUS	Phusion PCR product from pNIN:870 with <i>pNIN -785 to -615_fwd/rev</i> cloned into <i>XbaI</i> site of pNINmin
B4 = pNIN(-735 to -666):GUS	Phusion PCR product from pNIN:870 with <i>pNIN -735 to -666_fwd/rev</i> cloned into <i>XbaI</i> site of pNINmin
F1 = pNIN(-735 to -701):GUS	Annealed oligonucleotides <i>pNIN -735 to -701_fwd/rev</i> cloned into <i>XbaI</i> site of pNINmin
F2 = pNIN(-717 to -683):GUS	Annealed oligonucleotides <i>pNIN -717 to -683_fwd/rev</i> cloned into <i>XbaI</i> site of pNINmin
F3 = pNIN(-700 to -666):GUS	Annealed oligonucleotides <i>pNIN -700 to -666_fwd/rev</i> cloned into <i>XbaI</i> site of pNINmin
2xCYC-RE:GUS	Annealed oligonucleotides <i>2xCYC-RE wild-type_fwd/rev</i>

	cloned into <i>XbaI</i> site of pNINmin
2xM1:GUS	Annealed oligonucleotides <i>2xCYC-RE M1_fwd/rev</i> cloned into <i>XbaI</i> site of pNINmin
2xM2:GUS	Annealed oligonucleotides <i>2xCYC-RE M2_fwd/rev</i> cloned into <i>XbaI</i> site of pNINmin
2xM3:GUS	Annealed oligonucleotides <i>2xCYC-RE M3_fwd/rev</i> cloned into <i>XbaI</i> site of pNINmin
2xM4:GUS	Annealed oligonucleotides <i>2xCYC-RE M4_fwd/rev</i> cloned into <i>XbaI</i> site of pNINmin
2xM5:GUS	Annealed oligonucleotides <i>2xCYC-RE M5_fwd/rev</i> cloned into <i>XbaI</i> site of pNINmin
2xmCYC-RE:GUS	Annealed oligonucleotides <i>2xmCYC-RE_fwd/rev</i> cloned into <i>XbaI</i> site of pNINmin

(E) Plasmids for CYCLOPS domain analysis in *N. benthamiana* and yeast

p35S:BD _{Gal4} -3xHA-GW	Phusion PCR product amplified from pENTR:BD _{Gal4} -AD _{VP16} with <i>Gal4-BD domain_fwd/rev</i> cloned into <i>HindIII</i> site of pAMPAT-35S:3xHA-GW (Gateway-compatible pAMPAT-MCS derivative (GenBank accession AY436765))
p35S:AD _{VP16} -3xHA-GW	Phusion PCR product amplified from pENTR:BD _{Gal4} -AD _{VP16} with <i>VP16-AD domain_fwd/rev</i> cloned into <i>HindIII</i> site of pAMPAT-35S:3xHA-GW (Gateway-compatible pAMPAT-MCS derivative (GenBank accession AY436765))
p35S:3xHA-BD _{Gal4} -AD _{VP16}	LR reaction (Invitrogen) of pENTR:BD _{Gal4} -AD _{VP16} with pAMPAT-35S:3xHA-GW (Gateway-compatible pAMPAT-MCS derivative (GenBank accession AY436765))
p35S:BD _{Gal4} -3xHA-CYCLOPS, phosphosite mutants or truncated versions	LR reaction (Invitrogen) of pENTR:cCYCLOPS (or phosphosite mutants or truncated versions, listed in 5.21A) and p35S:BD _{Gal4} -3xHA-GW
p35S:AD _{VP16} -3xHA-CYCLOPS, phosphosite mutants or truncated versions	LR reaction (Invitrogen) of pENTR:cCYCLOPS (or phosphosite mutants or truncated versions, listed in 5.21A) and p35S:BD _{Gal4} -3xHA-GW
pBDGAL4:CYCLOPS, phosphosite mutants or truncated versions	LR reaction (Invitrogen) of pENTR:cCYCLOPS (or phosphosite mutants or truncated versions, listed in 5.21A) and Gateway modified pBDGAL4 Cam (Stratagene)

(F) Plasmids for protein expression

pDEST15:CYCLOPS, phosphosite and truncated versions (N-terminal GST tag)	LR reaction (Invitrogen) of pENTR:cCYCLOPS (phosphosite mutants or truncated versions, listed in 5.21A) and pDEST15 (Invitrogen)
pDEST17:CYCLOPS (N-terminal 6xHis tag)	LR reaction (Invitrogen) of pENTR:cCYCLOPS and pDEST17 (Invitrogen)
pDEST14:CCaMK (no tag)	LR reaction of (Invitrogen) pENTR:cCCaMK and pDEST14 (Invitrogen)

6 Acknowledgements

We thank Andreas Binder (University of Munich, Germany) for preparing Figure 42, Dr. Riyaz A. Bhat (Solazyme, Inc., San Francisco, USA) for the kind gift of the FLIM-FRET vectors, Prof. Makoto Hayashi (National Institute of Agrobiological Sciences, Tsukuba, Japan) for providing vector pNIN:GUS, Prof. Remko Offringa (Leiden University, Netherlands) for providing vector pSDM7006, Martina Ried for critically reading the manuscript, Prof. Jens Stougaard (Aarhus University, Denmark) for providing *L. japonicus ccamk-13* and *NINpro:GUS* seeds and Dr. Trevor Wang (John Innes Centre, United Kingdom) for providing *L. japonicus nsp1-1* seeds. This work was funded by a grant from the German Research Foundation (DFG) to M.P. within Research Unit FOR 964 ‘Calcium signaling via protein phosphorylation in plant model cell types during environmental stress adaptation’

7 Appendix: Biochemical characterisation of the CCaMK/CYCLOPS complex

7.1 Results and Discussion

7.1.1 Size-exclusion chromatography of purified CCaMK

In order to determine whether CCaMK exists as a monomer, or assumes an oligomeric state in solution, gel filtration analysis was performed with a 6xHis-CCaMK protein preparation obtained after purification using immobilized metal ion affinity chromatography (IMAC). This analysis revealed, that CCaMK (MW: 57.5 kDa) does not elute as a single peak or single monomeric fraction. In total six partly overlapping peak fractions, corresponding to the MW of monomeric, dimeric, nonameric, dodecameric, as well as a high MW (HMW) fraction of CCaMK were obtained. The MW of the latter fraction exceeded the resolution range (>720 kDa) of the utilized size-exclusion column. The resulting elution profile (Figure 43) suggests, that to some extent CCaMK is present in a monomeric and to a larger extent in a dimeric state in solution, which is in line with the finding that the autophosphorylation mechanism of CCaMK is intermolecular (Tirichine et al., 2006). A higher order oligomeric state, similar to the CaMKII holoenzyme, which forms a dodecamer composed of two stacked hexamers of dimers (Rosenberg et al., 2005), is also possible. However, a distinct peak at the expected MW was not observed due to the tendency of CCaMK to form aggregates, resulting in several overlapping and distorted HMW peaks.

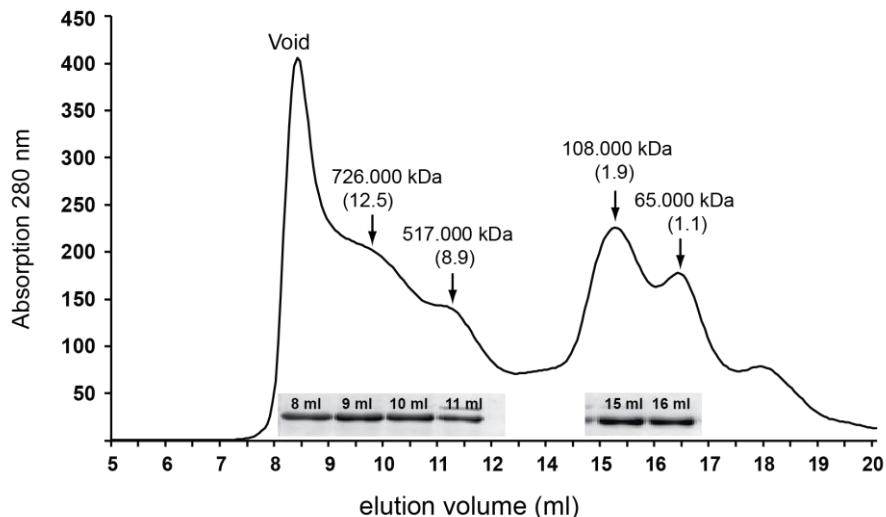


Figure 43. Size-exclusion chromatography of CCaMK.

Elution profile of purified 6xHis-CCaMK (MW: 57.5 kDa) after gel filtration on a Superdex 200 10/300 GL column. A large proportion is eluted in the void volume (>720 kDa) consisting of CCaMK aggregates. Four partly overlapping elution peaks were obtained (indicated by arrows). Numbers in brackets indicate deduced oligomeric or monomeric state of the CCaMK protein in the elution fraction ($MW_{\text{peak fraction}}/MW_{\text{CCaMK}}$). Insets show Coomassie stained CCaMK protein bands of the individual elution fractions resolved by SDS-PAGE (10%).

7.1.2 Biochemical characterization of the CCaMK/CYCLOPS complex

Biochemical characterization of CYCLOPS and the assembled CCaMK/CYCLOPS complex was initially impeded, because CYCLOPS was expressed insoluble in inclusion bodies in *E. coli*. The observation that CYCLOPS interacts with CCaMK and is phosphorylated by CCaMK *in vitro* suggested that CYCLOPS' solubility may improve if it is expressed together with its interaction partner and cognate kinase CCaMK. Therefore, coexpression of 6xHis-CYCLOPS (MW: 61.3 kDa) together with CCaMK (MW: 57.5 kDa) in *E. coli* was performed, and after IMAC, yielded soluble CYCLOPS protein in association with CCaMK, the identity of which was confirmed by subsequent kinase assays (Figure 44A and D). The kinase assay revealed that the copurified CCaMK was functional (Figure 44D). The phosphorylation pattern of the coexpressed CCaMK/CYCLOPS complex was the same as observed previously, with weak CYCLOPS phosphorylation -but stronger CCaMK autophosphorylation- in the presence of calcium and enhanced CYCLOPS phosphorylation if $\text{Ca}^{2+}/\text{CaM}$ was supplemented (Figure 44D) (Yano et al., 2008, Liao et al., 2012). When visualized on a Coomassie stained SDS-PAGE gel, the purified 6xHis-CYCLOPS protein seemed to be present in the form of several phosphorylated species, because the protein band occurred more diffuse in contrast to a sharp, single-species band (Figure 44A). Protein blot analysis using an antibody directed against the 6xHis-tag identified a band corresponding to the size of 6xHis-CYCLOPS, confirming that the purified protein was 6xHis-CYCLOPS

(Figure 44B). Previous mass spectrometric analysis of CCaMK-phosphorylated CYCLOPS identified the phosphorylation motif RXXpS as a preferred motif of CCaMK on CYCLOPS (Figure 30). In order to prove that CYCLOPS' solubility was mediated by CCaMK phosphorylation during coexpression, protein blot analysis on 6xHis-CYCLOPS protein obtained in the absence or presence of CCaMK was carried out using an anti-RXXpS/T antibody. This analysis demonstrated that in the absence of CCaMK 6xHis-CYCLOPS was not phosphorylated, while coexpression with CCaMK, resulted in clear 6xHis-CYCLOPS phosphorylation (Figure 44C).

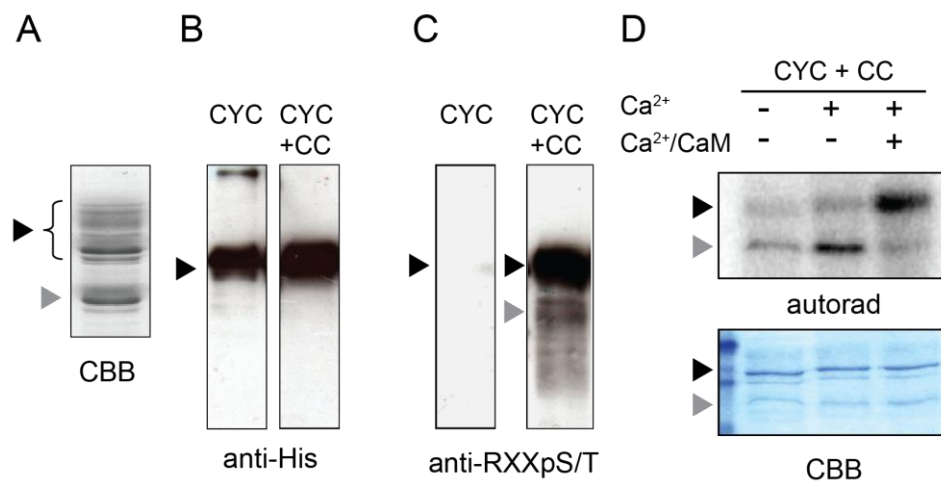


Figure 44. Coexpression of CYCLOPS with CCaMK in *E. coli* yields soluble, phosphorylated CYCLOPS protein.

6xHis-CYCLOPS (CYC) was coexpressed with CCaMK (CC) in *E. coli* and purified via immobilized metal ion affinity chromatography (IMAC). Black arrowheads indicate 6xHis-CYCLOPS, grey arrowheads indicate CCaMK. CBB: Coomassie brilliant blue stained gel; autorad: Autoradiograph of the radioactive (γ - ^{32}P) gel.

(A) 6xHis-CYCLOPS elution fraction separated by SDS-PAGE (10%) and CBB stained. Note the diffuse 6xHis-CYCLOPS protein band which presumably contains several CYCLOPS phospho-species (indicated by a bracket). (B) Protein blot analysis of 6xHis-CYCLOPS (0.3 μg) expressed in the absence and presence of CCaMK. In both cases a band of the expected size of 6xHis-CYCLOPS (61 kDa) is detected. (C) Protein blot analysis of 6xHis-CYCLOPS (0.6 μg) with an anti-RXXpS/T antibody (recognizing phosphorylated serines and threonines located within the amino acid motif RXXpS/T) demonstrating that 6xHis-CYCLOPS is only phosphorylated when coexpressed with CCaMK. (D) The copurified CCaMK/6xHis-CYCLOPS complex is functional *in vitro*. Kinase assay performed in the absence (-) or presence (+) of 0.1 mM CaCl_2 (Ca^{2+}) or 0.1 mM CaCl_2 and 1 μM calmodulin ($\text{Ca}^{2+}/\text{CaM}$) with 1 μg coexpressed 6xHis-CYCLOPS/CCaMK sample obtained after IMAC purification. The lower protein band present in the 6xHis-CYCLOPS elution (shown in A) is CCaMK, displaying the typical auto- and CYCLOPS phosphorylation pattern as has been described previously (Yano et al., 2008).

In order to obtain the assembled CCaMK/CYCLOPS complex, both proteins were coexpressed as tagged versions (6xHis-CCaMK/Strep-CYCLOPS) and tandem affinity purification was performed. This protocol led to a higher and purer Strep-CYCLOPS protein yield after the first purification step (Figure 45A compared to Figure 44A). The associated 6xHis-CCaMK protein amount was considerably less compared to the purified Strep-CYCLOPS protein amount, suggesting, that either only part of the purified CYCLOPS protein was associated with CCaMK, or the association ratio differed from a 1:1 ratio. Size-exclusion chromatography of the Strep-CYCLOPS elution (Figure 45A) yielded two distinct peaks: A HMW peak exceeding the resolution range (>720 kDa) of the gelfiltration column and a second peak with a MW of ~ 660 kDa (Figure 45B). SDS-PAGE of the HMW fraction showed that CCaMK and CYCLOPS were present in a 1:1 ratio, while CYCLOPS was the predominant protein species in the ~ 660 kDa peak (Figure 45B). This result suggests that the 1:1 CCaMK/CYCLOPS complex might be a HMW complex with a size >720 kDa. Surprisingly, no peak was detected at the MW of the CYCLOPS monomer or dimer, indicating, that CYCLOPS is presumably assembled as oligomer. In order to purify the assembled CCaMK/CYCLOPS complex, the elution fraction of Strep-CYCLOPS (associated with 6xHis-CCaMK) was subjected to a second purification step capturing 6xHis-CCaMK by IMAC. The obtained elution fraction contained both proteins in an approximate 1:1 ratio (Figure 45C). Furthermore, both proteins were present as a doublet band, presumably as different isoforms (e.g. phosphorylated vs. unphosphorylated isoform). Gelfiltration of the tandem purified fraction resulted in a single HMW (<720 kDa) peak suggesting that the 1:1 complex assembles as multimer (Figure 45C).

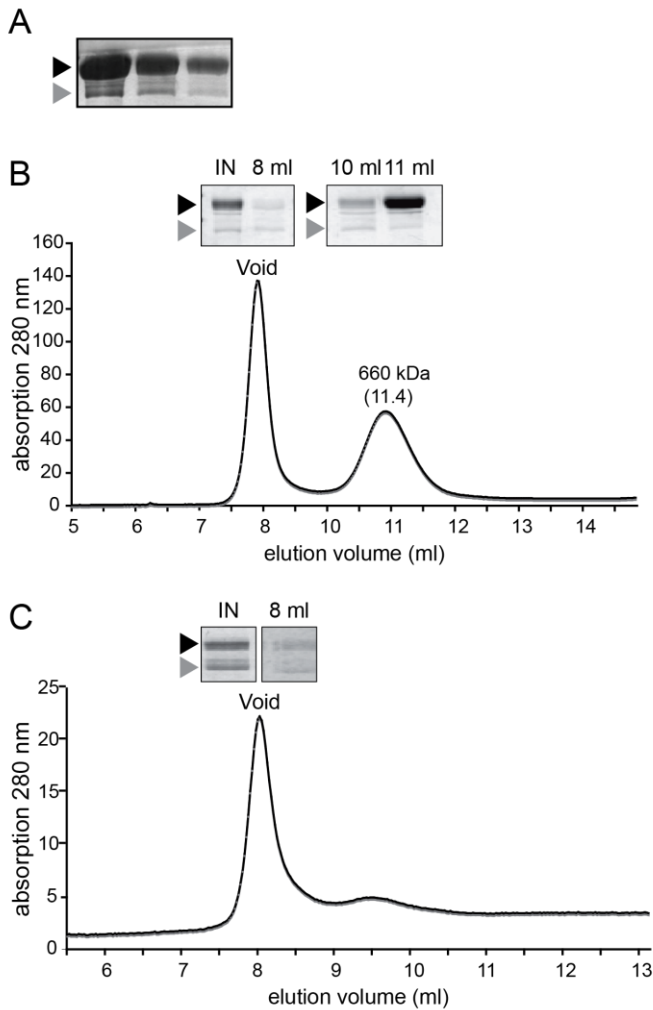


Figure 45. Analysis of the copurified CCaMK/CYCLOPS complex.

6xHis-CCaMK and Strep-CYCLOPS were coexpressed in *E. coli* and tandem affinity purification was performed. The obtained elution fraction of the 1st affinity purification step (capturing Strep-CYCLOPS associated with 6xHis-CCaMK), was subjected to a 2nd purification step (capturing 6xHis-CCaMK), to obtain the assembled complex. Black arrowheads: Strep-CYCLOPS; grey arrowheads: 6xHis-CCaMK. IN: Input fraction.

(A) Elution fractions of Strep-CYCLOPS obtained after the first purification step. Note that Strep-CYCLOPS is more abundantly present than 6xHis-CCaMK. (B) Gel filtration chromatogram of the Strep-CYCLOPS elution fraction obtained after the 1st purification step. Two peak fractions were obtained: A HMW (>720 kDa) fraction eluting in the void volume and containing the CCaMK/CYCLOPS complex in an approximate 1:1 ratio and a ~660 kDa fraction containing CYCLOPS as the predominant protein species. (C) Gel filtration chromatogram of the 6xHis-CCaMK elution fraction obtained after the 2nd purification step. A single HMW peak fraction (>720 kDa) was obtained, containing the copurified CCaMK/CYCLOPS protein complex in an approximate 1:1 ratio. Note, that both proteins are present as a doublet band, suggesting the presence of unphosphorylated and phosphorylated isoforms within the complex. (B and C) Insets show resolved (10% SDS-PAGE) Coomassie stained protein bands present in the input and peak elution fractions.

7.2 Materials and Methods

7.2.1 Protein expression and purification

Expression of 6xHis-CYCLOPS and coexpression of 6xHis-CYCLOPS together with CCaMK was induced in *E. coli* Rosetta pLaqI (Novagen) for 16 h (overnight) at 21 °C by addition of 0.25 mM isopropyl β -D-1-thiogalactopyranoside (IPTG). Cell pellets were lysed with a French Press (Aminco). Protein purification was carried out with Ni-NTA agarose resin (Qiagen) according to the manufacturer's instruction. The wash buffer contained 50 mM Tris, 150 mM NaCl, 10 mM β -mercaptoethanol, 0.010 mM imidazole, pH 7.8 and the same buffer containing 0.25 mM imidazole was used as elution buffer. Proteins were desalted by dialysis in buffer containing 20 mM Tris, 100 mM NaCl, 1 mM β -mercaptoethanol, 5% glycerol, pH 7.8.

Expression of 6xHis-CCaMK was induced in *E. coli* Rosetta pLaqI (Novagen) for 4 h at 28 °C by addition of 0.5 mM IPTG. 6xHis-CCaMK was purified using a Co^{2+} charged HiTrap column (GE Healthcare) with washbuffer containing 50 mM Tris, 300 mM NaCl, 0.020 mM imidazole, 10 mM β -mercaptoethanol, pH 7.8 and eluted with the same buffer containing 0.25 mM imidazole (ACS grade; Merck). The purified protein was then analysed by size-exclusion chromatography.

Coexpression of 6xHis-CCaMK/Strep-CYCLOPS was carried out in *E. coli* Rosetta pLaqI (Novagen) for 4 h at 28 °C by addition of 0.5 mM IPTG. A tandem affinity purification protocol was applied to purify the 6xHis-CCaMK/Strep-CYCLOPS complex. First, Strep-CYCLOPS (associated with 6xHis-CCaMK) was purified via Strep-tactin resin (IBA) with wash buffer containing 100 mM Tris, 150 mM NaCl, 1 mM EDTA, 10 mM β -mercaptoethanol, pH 7.8. Elution was performed in the same buffer supplemented with 2.5 mM desthiobiotin. The second purification step capturing 6xHis-CCaMK was carried out with TALON resin (Clontech) in washbuffer containing 50 mM Tris, 150 mM NaCl, 0.02 mM imidazole (ACS grade; Merck), 10 mM β -mercaptoethanol, pH 7.8. Elution was carried out with the same buffer containing 0.25 mM imidazole (ACS grade; Merck). Elutions of the 1st and 2nd purification step were analysed by size-exclusion chromatography.

7.2.2 Size-exclusion chromatography

Size-exclusion chromatography was performed according to the manufacturer's protocols using a Superdex 200 10/300 GL column (GE Healthcare) connected to an Äkta purifier 10 system (GE Healthcare). Prior to analysis, the column was calibrated with standard proteins (thyroglobulin, ferritin, aldolase, conalbumin and ovalbumin; GE Healthcare) according to the manufacturer's instruction. Prior to gelfiltration analysis purified protein elutions were

concentrated with Amicon Ultra-15 Centrifugal Filter Units (30k) (Millipore). Gelfiltration analysis of 6xHis-CCaMK was performed in buffer containing 20 mM Tris, 250 mM NaCl, 5 mM DTT, pH 7.8. Gelfiltration analysis of Strep-CYCLOPS/6xHis-CCaMK (elution of the 1st purification step) and the tandem affinity purified Strep-CYCLOPS/6xHis-CCaMK complex was performed in buffer containing 50 mM Tris, 150 mM NaCl, 5 mM DTT, pH 7.8. Peak fractions were collected and 15-20 µl of each fraction were separated by SDS-PAGE (10% gels) and Coomassie stained, to determine protein purity and protein sizes.

7.2.3 *In vitro* kinase assay

The *in vitro* kinase assay of the copurified 6xHis-CYCLOPS/CCaMK complex was performed as described (Yano et al., 2008) using 1 µg purified protein sample.

7.2.4 Protein blot analysis

Equal amounts of purified 6xHis-CYCLOPS or coexpressed 6xHis-CYCLOPS/CCaMK protein samples were separated by SDS-PAGE (10% gels) and blotted onto PVDF membrane (GE-Healthcare). Immunodetection of 6xHis-CYCLOPS proteins was performed according to the manufacturer's instruction using mouse anti-His₆(2) (Roche) as primary antibody and anti-mouse-HRP (Biomol) as secondary antibody. Immunodetection of phosphorylated CYCLOPS was carried out according to the manufacturer's instruction using rabbit Phospho-Akt Substrate (RXXS*/T*) antibody (Cell Signaling) as primary and anti-rabbit-HRP (Amersham) as secondary antibody.

7.2.5 Plasmids for protein expression

pETDuet-6xHis-CYCLOPS	Phusion PCR product of CYCLOPS coding sequence amplified from pENTR:cCYCLOPS (Yano et al., 2008) with primers CYCLOPS- <i>SalI</i> _f and CYCLOPS- <i>NotI</i> _r inserted into the expression vector pETDuet-1 (Novagen)
pETDuet-6xHis-CYCLOPS-CCaMK (for CCaMK/ CYCLOPS coexpression)	Phusion PCR product of CCaMK coding sequence amplified from pENTR:cCCaMK (Yano et al., 2008) with primers CCaMK- <i>NdeI</i> _f and CCaMK- <i>XhoI</i> _r inserted into the expression vector pETDuet-6xHis-CYCLOPS
pETDuet-6xHis-CCaMK	Phusion PCR product of CCaMK coding sequence amplified from pENTR:cCCaMK (Yano et al., 2008) with primers TEV-CCaMK_f and CCaMK_r inserted into the expression vector pETDuet-1 (Novagen) via <i>SalI/NotI</i> sites
pETDuet-6xHis-CCaMK-Strep-CYCLOPS (for CCaMK/CYCLOPS coexpression)	Phusion PCR product of CYCLOPS coding sequence amplified from pENTR:cCYCLOPS (Yano et al., 2008) StrepII-TEV-CYCLOPS_f and CYCLOPS_r and cloned into <i>NdeI/XhoI</i> site of pETDuet-6xHis-CCaMK.

7.2.6 Oligonucleotides

f = forward

r = reverse

CYCLOPS_SalI_f/NotI_r (SY31, SY45)

gcgtcgacatggaaggaggggg_f *SalI*
cacggccgcttacatttttcag_r *NotI*

CCaMK-NdeI_f/XhoI_r (SY46, SY47)

cacatgatgggatgatcaaac_f *NdeI*
cacctcgagctatgatggacgaagag_r *XhoI*

TEV-CCaMK_f/r (SY53, SY54)

gtcgacgagaatctttattttcagggcatgggatgatcaaac_f
SalI
ggggccgcctatgatggacgaagagaag_r *NotI*

StrepII-TEV-CYCLOPS_f/r (SY55, SY56)

accatgatggctagctggagccaccgcagttcgaaaaagagaatctttattttcaggcaatggaaggagggggtt_f
NdeI
cacctcgagttacatttttcagttc_r *XhoI*

VII General Discussion

This study was conducted to gain a clearer picture of the signaling process downstream of the calcium spiking response which initiates in root cell nuclei after perception of symbiotic signaling molecules. It is commonly assumed that the main target of the calcium spikes is CCaMK which is activated by calcium and calmodulin and propagates the signal via phosphorylation of its associated substrate CYCLOPS. A combination of domain and phosphorylation site analysis of both proteins *in vitro* and *in vivo* has been used as powerful tool in this study to provide novel insights into the function and regulation of both proteins, pinpointing the nuclear CCaMK/CYCLOPS complex as a central node in root endosymbiosis signaling.

1 CCaMK and the role of its calcium regulatory domains in symbiosis formation

The unusual presence of two distinct calcium regulatory domains in CCaMK suggests a different mechanism of action and symbiotic function for each. Biochemical analysis of both domains (CaM-BD linked to the VLD) derived from MtCCaMK established, that EF-hand 3 exhibits high affinity for calcium and binds basal calcium concentrations ($K_d \leq 20$ nM) as present in root hair cells under un-stimulated conditions (125-150 nM) (Swainsbury et al., 2012). In contrast, EF-hands 1 and 2 have lower affinity ($K_d = 200 \pm 50$ nM), enabling the interpretation of calcium spiking (Swainsbury et al., 2012). Further, the affinity for calcium of the VLD is only considerably affected if EF-hand 2 (but not if EF-hand 1 or 3) is disrupted, suggesting that this EF-hand is most essential for calcium sensing (Swainsbury et al., 2012). However, simultaneous point mutations in EF-hands 1 and 2 still supported symbiosis formation while point mutations in EF-hand 1, or 2 in combination with EF-hand 3 in all cases impaired symbiosis establishment (Shimoda et al., 2012). Further, single mutations in either of the three EF-hands did not affect symbiosis formation, but truncations lacking EF-hand 3 (CCaMK-1-471) or EF-hands 2 and 3 (CCaMK-1-429) were impaired (Shimoda et al., 2012). Concerning the CaM-BD, a truncation comprising the kinase and CaM-BD (CCaMK-1-340) did not complement rhizobial infection even if autoactivated (CCaMK-1-340-T265D), although the latter construct triggered spontaneous nodules (Shimoda et al., 2012).

These findings differ from the findings presented in this study, where the truncations CCaMK-1-453 (retaining only EF-hand 1) and CCaMK-1-351 (retaining the kinase and CaM-BD) both restored symbiosis (Figure 5 and 6). Several reasons for this discrepancy and simultaneous effects are possible. For instance, the tested constructs are not identical, which could result in differential behaviour. Promoter differences may also play a role. Possibly, the strong *L. japonicus* ubiquitin promoter used in this study leads to higher expression levels

compared to the 35S promoter used by Shimoda et al., ultimately resulting in higher nuclear-localized protein levels of the mutant proteins. This is an aspect to be considered as the subcellular localization analysis in *L. japonicus* protoplasts demonstrated that only the CCaMK wild-type protein exclusively localized to the nucleus, while all mutant proteins were also partly mislocalized in the cytosol (Figure 10). Another important aspect is the mutant background used for complementation analysis. Shimoda et al., used the *L. japonicus ccamk-3* mutant which carries a point mutation in a conserved glycine residue (G30E) in kinase subdomain I, leading to a kinase-dead version. It is unknown whether the mutant protein is expressed *in planta* and interferes with the function of the transgenically expressed CCaMK mutant versions. Interestingly, *snf1-1* is a recessive allele and presumably the wild-type CCaMK protein suppresses spontaneous nodulation (conferred by CCaMK-T265I) in heterozygous plants (Tirichine et al., 2006). This phenotype could be explained by the possibility that CCaMK is not acting as a monomer but as dimer or oligomer. Such a mode of action is also suggested by autophosphorylation kinetics (Tirichine et al., 2006) and CCaMK size-exclusion chromatographic results presented in this study (Figure 43). Therefore, the complementation results might depend on the *ccamk* mutant background used for symbiosis phenotyping. In this study the presumed *ccamk-13* null mutant was used where the encoded CCaMK-1-154 + PPRGSQG protein was not detected in root extracts by immunoblot analysis using three different polyclonal CCaMK antibodies (Figure 4). This result largely excludes an impact of the endogenous CCaMK protein on the complementation results.

According to results obtained in this study, the EF-hand containing VLD *per se* is dispensable for downstream signaling towards rhizobial infection, as obviously its loss can be compensated by a certain level of protein concentration in combination with the CaM-BD (Figure 5, Table 1). In contrast, the presence of the CaM-BD was essential for rhizobial infection and during calcium signaling may confer substrate specificity by inducing a conformation required for the correct positioning and/or adequate phosphorylation of a downstream target. In addition, Ca²⁺/CaM binding increased the efficiency of substrate phosphorylation which might be important for providing enough phosphorylated molecules to overcome a certain threshold required for downstream signaling. Such a view is also supported by *in vitro* kinase assays of CCaMK and its presumed native substrate CYCLOPS, where a change in substrate specificity (from auto- to substrate phosphorylation) and enhanced substrate phosphorylation in the presence of Ca²⁺/CaM has been observed (Figures 27 and 30A). Thus Ca²⁺/CaM binding and release may represent a regulatory switch which turns CCaMK on and off. CaM binds calcium (and thus CCaMK) only when concentrations are

high (in the μM range) as is the case during spiking (Swainsbury et al., 2012). High calcium concentrations promote $\text{Ca}^{2+}/\text{CaM}$ -binding resulting in increased substrate phosphorylation required for downstream signaling towards rhizobial infection. Low calcium concentrations lead to the dissociation of $\text{Ca}^{2+}/\text{CaM}$, converting CCaMK into the autophosphorylation mode, which switches off the kinase (as has been discussed in more detail in chapter 2).

In contrast to RNS, AM formation is possible with autoactivated constructs lacking the VLD and the CaM-BD and which did not perform less efficient compared to the truncated versions containing the CaM-BD and restoring rhizobial infection (Figure 7). This result provides evidence that signaling via CCaMK towards AM and rhizobial infection is different and suggests that signaling specificity at the level of CCaMK exists. Equally, the kinase domain (CCaMK-1-314) and the autoactivated CCaMK-FNDD mutant (with an abrogated CaM-BD) are sufficient for the formation of spontaneous nodules which, like AM formation, is also a process with less stringent requirements for the calcium regulatory domains. Nodule organogenesis and arbuscule formation during AM infection have in common that both processes involve the inner cortical root cells, while rhizobial entry initiates via infection of epidermis derived root hair cells. It was recently suggested that two distinct symbiotic signaling programs exist in root epidermal and cortical cells (Kosuta et al., 2011; Liao et al., 2012; Madsen et al., 2010). This implies that CCaMK-1-314 and CCaMK-FNDD are not functional in epidermal but their function is sufficient for cortical processes like nodule organogenesis and arbuscule formation.

Due to the observation that CCaMK-FNED (analogous to CCaMK-FNDD) exhibited no kinase activity Shimoda et al. concluded that biological activity of CCaMK is not solely defined by its kinase activity, which somehow contradicts the result obtained in the same study, where the kinase-inactive double mutant CCaMK-G30E-FNED lost the ability to form spontaneous nodules (Shimoda et al., 2012). This together with the observation in this study of weak phosphorylation activity of CCaMK-FNDD towards CYCLOPS-81-366 suggests that the lower efficiency of spontaneous nodulation and AM formation may result from weaker autoactivity (compared to the autoactive full-length versions) (Figure 5, 7, 8 and 9B; Table 1, 2 and 4). Therefore, the proposed kinase activity-independent signaling hypothesis proposed by Shimoda et al., seems rather unlikely.

Substitution of the autophosphorylation site T265 by phospho-mimetic and phospho-ablative amino acids and expression of the kinase domain alone is sufficient to activate the nodule organogenesis program in the absence of calcium spiking indicating that the CaM-BD and the VLD are dispensable for this process (Figure 8; Table 4).

Taken together, in the indigenous context and with endogenous expression levels, wild-type CCaMK with both calcium regulatory domains is required to support AM, root nodule development and rhizobial infection, indicating that CCaMK must be activated by calcium and Ca²⁺/CaM to gain a certain level of kinase activity. CCaMK overexpression on the other hand demonstrated that the VLD is dispensable for the establishment of both symbioses and required for the activation of CCaMK, while the CaM-BD was specifically required for rhizobial infection processes, but its precise function apart from CCaMK activation remains to be determined.

2 Positive and negative regulation of CCaMK by autophosphorylation

CCaMK is capable of regulating its own activity by autophosphorylation. Currently three autophosphorylation sites have been identified which are: LjT265/MtT271, LjS337/MtS343 and LjS338/Mt344 (Gleason et al., 2006; Liao et al., 2012; Routray et al., 2013; Tirichine et al., 2006). T265 was initially identified in *L. longiflorum* CCaMK (LIT267) as calcium-induced *in vitro* autophosphorylation site (Sathyanarayanan et al., 2001). The finding that the spontaneously nodulating *L. japonicus snf1-1* mutant carried a mutation in the orthologous site implied that T265 is an important regulatory site in legume CCaMKs and analogous to the activating mechanism of LICCaMK suggested that elevated calcium concentrations lead to its phosphorylation with subsequent activation of CCaMK (Sathyanarayanan et al., 2000; Tirichine et al., 2006). However, experimental proof *in vitro* and *in vivo* that this site is indeed autophosphorylated upon calcium stimulation in legume CCaMKs is lacking. The finding that phospho-mimetic and phospho-ablative substitutions of this site equally lead to spontaneous nodule formation with no significant difference in spontaneous nodule number was unexpected and indicated that both replacements lead to the deregulation of the kinase as suggested by homology modeling (Shimoda et al., 2012). Nevertheless, as revealed in this study, both versions showed differences. Compared to wild-type CCaMK, CCaMK-T265D displayed much higher *in vitro* kinase activity (Figure 9A), and a large proportion of the nodules remained uninfected after treatment with rhizobia (Figure 5C and Table 1), suggesting that CCaMK-T265D is hyperactive. In contrast, CCaMK-T265A apart from forming spontaneous nodules in the absence of rhizobia behaved more wild-type-like in terms of *in vitro* kinase activity and restoration of symbiosis. In summary, from the observation that phospho-mimetic and phospho-ablative mutations equally lead to a gain-of-function phenotype of CCaMK, no conclusions can be drawn whether autophosphorylation at T265 is induced upon calcium stimulation (symbiosis signaling) or is the default state under asymbiotic conditions and conversely, dephosphorylation is the activating mechanism. The

latter hypothesis is supported by the recent finding that various spontaneous nodulation inducing MtCCaMK mutant versions lack autophosphorylation of MtT271 *in vitro*, while the wild-type protein and other CCaMK versions, which do not trigger spontaneous nodules, are autophosphorylated at this site (B. Miller and G. Oldroyd, personal communication). This model is equally possible, but calls for the existence of an yet unidentified, probably calcium inducible phosphatase regulating CCaMK activity. Thus, the current working model of CCaMK activation, which was built from the analysis of LICCaMK and also applied to legume CCaMK activation might be incorrect and is likely to be substantially refined in the near future.

Mass spectrometric analysis of calcium-induced CCaMK autophosphorylation and the identification of the *ccamk-14* mutant pinpointed LjS337 as autophosphorylation site required to negatively regulate CCaMK activity. The phospho-mimetic form is impaired in CaM binding and the single amino acid substitution was sufficient to completely abolish symbiosis establishment. A similar finding was recently obtained with *M. truncatula* CCaMK, where a phospho-mimetic substitution of MtS344 (orthologous site to LjS338) led to the same impairment (Routray et al., 2013). In addition, the analysis of the MtCCaMK-T271A-S344D double mutant revealed that S344D was epistatic to T271A and suppressed spontaneous nodulation (Routray et al., 2013). Autophosphorylation of the CaM-BD was therefore proposed as a negative regulatory switch shutting off the kinase when calcium concentrations decline and CaM dissociates (Routray et al., 2013).

Whether LjT265/MtT271 is a negative or positive regulatory autophosphorylation site remains unclear, but due to the fact that LjS337 and MtS344 phosphorylation have a negative effect, autophosphorylation may in general lead to CCaMK deactivation. This would represent the most parsimonious model implicating a single CCaMK activation step by a regulating phosphatase. In this view the proposed model of CCaMK activation might be refined in the following way: Under basal calcium concentrations CCaMK is autophosphorylated at S337 and S338 which prevents Ca²⁺/CaM binding. Simultaneously, CCaMK is autophosphorylated at T265 which only in the phosphorylated state partakes in a hydrogen-bond network, stabilizing the autoinhibitory helix. Calcium spiking leads to the activation of a putative phosphatase, dephosphorylating CCaMK. The association of T265 with the hydrogen-bond network is then only disrupted after dephosphorylation of S337/S338. This causes the release of autoinhibition and exposes the CaM-binding domain which subsequently binds Ca²⁺/CaM and ultimately stimulates substrate phosphorylation activity.

How nodule organogenesis is prevented during AM establishment is still unclear but this

study provides evidence that AM formation negatively impacts on (spontaneous) nodulation, and possible mechanisms have been proposed (see discussion in chapter 1). With regard to the alternative CCaMK activation model and considering the hypothesis that CCaMK is differentially activated by AM signals, the possibility exists, that CCaMK is not dephosphorylated at T265 during AM signaling. Thus it still remains to be solved whether lack of nodule formation in AM involves differential activation of CCaMK, another mechanism, or both.

3 The role of CCaMK and CYCLOPS in nodule organogenesis

Auto-activated CCaMK is able to trigger the nodule organogenesis program (Gleason et al., 2006; Tirichine et al., 2006). Nodule organogenesis depends on the induction of cytokinin production in the root cortex which in *L. japonicus* is perceived by the cytokinin receptor Lotus Histidine Kinase I (LHKI) (Tirichine et al., 2007). A gain-of-function mutation in the extracellular domain of this receptor LHKI^{L266F} leads to auto-activity triggering the formation of spontaneous nodules, while the loss-of-function mutant *hit1-1* (*HYPERINFECTED 1*) is characterized by the extensive formation of ITs but lack of nodule formation (Gonzalez-Rizzo et al., 2006; Murray et al., 2007; Tirichine et al., 2007). CCaMK acts upstream of LHKI, as no spontaneous nodules are formed in *snf1 hit1-1* double mutants (Madsen et al., 2010). In addition, genetic analysis has demonstrated that the GRAS proteins NSP1 and NSP2 and the transcriptional activator NIN are required for nodule organogenesis downstream of LHKI (Madsen et al., 2010; Tirichine et al., 2007). It is currently unknown how cytokinin production is induced during RNS to promote nodule organogenesis. The observation that CYCLOPS acts downstream of CCaMK and nodule organogenesis by autoactive CCaMK in *cyclops* mutants is severely (albeit not entirely) impaired (Madsen et al., 2010; Ovchinnikova et al., 2011; Yano et al., 2008), while autoactive CYCLOPS-DD induces nodules independently of CCaMK, suggests that cytokinin production is triggered downstream of CYCLOPS and might be mediated by CYCLOPS itself. *cyclops snf2* double mutants are not impaired in spontaneous nodule organogenesis, which indicates that CYCLOPS acts upstream of LHKI (Madsen et al., 2010).

In this study CYCLOPS was identified as transcription factor which directly targets the promoter of the *NIN* gene, which is required for nodule organogenesis and rhizobial infection. Further, a palindromic CYCLOPS binding site 'CYC-box' was identified which is proposed to be specifically bound by phosphorylated CYCLOPS. Due to the symbiosis-deficient phenotype of *cyclops* mutants it is likely that *NIN* is not the only CYCLOPS target and several targets with the same or a CYC-box similar binding site might exist. It is also possible

that cytokinin induction is mediated by NIN, or further downstream via NIN target genes. Three NIN target genes with a role in initiation of cortical cell divisions and rhizobial infection have been identified (Soyano et al., 2013; Xie et al., 2012). The promoters of the genes encoding the nuclear factors NF-YA1 and NF-YB1 are directly bound and activated by NIN and the ectopic expression of *NF-YA1* and *NF-YB1* as well as *NIN* overexpression induced cortical cell divisions leading to the formation of nodule primordia-like structures (Soyano et al., 2013). However, full-sized nodules were not formed, suggesting that either *NIN* expression alone is not sufficient, or that ectopic expression impaired further nodule development. Considering the possibility that NIN does not trigger the cytokinin biosynthesis machinery, the lack of cytokinin synthesis during *NIN* overexpression may account for the arrest in nodule development. *NIN* expression is partly regulated by cytokinin depending on the cell type (Heckmann et al., 2011). In the cortex, where nodules are formed, *NIN* induction depends on cytokinin (Heckmann et al., 2011) and requires *de novo* protein synthesis, indicating that *NIN* is not a primary response gene (Plet et al., 2011; Tirichine et al., 2007). In the epidermis where infection is initiated, *NIN* induction is cytokinin independent (Plet et al., 2011). *NIN* was also shown to bind to the promoter of the *NPL* gene, encoding a putative cell wall degrading enzyme involved in the initial steps of rhizobial root hair infection (Xie et al., 2012). This finding suggests that one epidermal function of NIN is the induction of *NPL* in root hairs to permit rhizobial infection. The finding that *NPL* expression is impaired in *cyclops* mutants, and the almost identical phenotype of *cyclops* and *npl* mutants suggests, that *NIN* might also be activated by CYCLOPS in the epidermis (Hogslund et al., 2009; Xie et al., 2012; Yano et al., 2008). Yet, as *CYCLOPS-DD* expression in *ccamk* mutants was not sufficient to restore rhizobial (and AM fungal) infection, the mode of action of CYCLOPS may be different (e.g. exerted by another CYCLOPS phospho-isoform) or may require the presence of CCaMK and/or additional interaction partners of the complex. Such a view is also supported by the finding that autoactive CCaMK is not sufficient to restore rhizobial infection in Nod factor receptor mutants, which points to the existence of a parallel calcium spiking independent signaling pathway required for infection, which also converges at CCaMK and may involve the initial calcium influx (Miwa et al., 2006b) which is induced upon rhizobial infection (Madsen et al., 2010; Shimoda et al., 2012).

4 Conclusions and outlook

CCaMK and CYCLOPS act together in the nucleus and emerge as a central hub in symbiosis signaling. With the identification of CYCLOPS as transcriptional regulator of symbiosis gene expression it is now possible to mechanistically explain how symbiosis-induced calcium

spiking is decoded and converted into a specific transcriptional response leading to the symbiosis specific gene expression pattern required for nodule development.

The results provided in this study describe a novel and direct nuclear calcium signaling mechanism (Figure 42) whereby Ca^{2+} /CaM stimulated CCaMK specifically phosphorylates CYCLOPS. The activating phosphorylation releases CYCLOPS from autoinhibition alleviating the DNA binding domain and promoting sequence specific DNA binding affinity to the *CYC-box* in the *NIN* promoter. *NIN* expression and the subsequent upregulation of two subunits of the heterotrimeric NF-Y complex, NF-YA1 and NF-YB1, are conceptually sufficient to explain the induction of nodule organogenesis. Considering the severity of the *cyclops* mutant phenotype, the induction of only one target gene by activated CYCLOPS is unlikely. Therefore, the identification of novel CYCLOPS target genes will add to our knowledge about the targets of the CCaMK/CYCLOPS complex. Furthermore, it is obvious that further associated proteins, e.g. CaM, phosphatases and components of the transcriptional machinery are associated with the complex, whose identification will shed light on the mechanism of activation, action and regulation of this central signaling complex.

Initial biochemical characterization in this study suggests that CCaMK and CYCLOPS are each assembled as oligomer, which implies that both form a large multimeric complex. Therefore, a detailed biochemical characterization and ultimately, the analysis of the crystal structure of the single components and of the assembled complex will be key steps towards a comprehensive understanding of this central node in symbiosis signaling.

VIII References

- Abdel-Lateif, K., Bogusz, D., and Hocher, V. (2012).** The role of flavonoids in the establishment of plant roots endosymbioses with arbuscular mycorrhiza fungi, rhizobia and *Frankia* bacteria. *Plant Signal Behav* 7, 636-641.
- Akashi, R., Kawano, T., Hashiguchi, M., Kutsuna, Y., Hoffmann-Tsay, S.-S., and Hoffmann, F. (2003).** Super roots in *Lotus corniculatus*: A unique tissue culture and regeneration system in a legume species. In *Roots: The Dynamic Interface between Plants and the Earth*, J. Abe, ed. (Springer Netherlands), pp. 27-33.
- Akiyama, K., Matsuzaki, K., and Hayashi, H. (2005).** Plant sesquiterpenes induce hyphal branching in arbuscular mycorrhizal fungi. *Nature* 435, 824-827.
- Amor BB, Shaw SL, Oldroyd GE, Maillet F, Penmetsa RV, Cook D, Long SR, Denarie J, Gough C (2003).** The *NFP* locus of *Medicago truncatula* controls an early step of Nod factor signal transduction upstream of a rapid calcium flux and root hair deformation. *Plant J* 34, 495-506.
- Andriankaja, A., Boisson-Dernier, A., Frances, L., Sauviac, L., Jauneau, A., Barker, D.G., and de Carvalho-Niebel, F. (2007).** AP2-ERF transcription factors mediate Nod factor dependent *Mt ENOD11* activation in root hairs via a novel *cis*-regulatory motif. *Plant Cell* 19, 2866-2885.
- Ané, J.-M., Kiss, G.B., Riely, B.K., Penmetsa, R.V., Oldroyd, G.E.D., Ajax, C., Lévy, J., Debelle, F., Baek, J.-M., Kalo, P., et al. (2004).** *Medicago truncatula DMII* required for bacterial and fungal symbioses in legumes. *Science* 303, 1364-1367.
- Antolin-Llovera, M., Ried, M.K., Binder, A., and Parniske, M. (2012).** Receptor kinase signaling pathways in plant-microbe interactions. *Annu Rev Phytopathol* 50, 451-473.
- Arrighi, J.F., Barre, A., Ben Amor, B., Bersoult, A., Soriano, L.C., Mirabella, R., de Carvalho-Niebel, F., Journet, E.P., Gherardi, M., Huguet, T., et al. (2006).** The *Medicago truncatula* lysin motif-receptor-like kinase gene family includes NFP and new nodule-expressed genes. *Plant Physiol* 142, 265-279.
- Banba, M., Gutjahr, C., Miyao, A., Hirochika, H., Paszkowski, U., Kouchi, H., and Imaizumi-Anraku, H. (2008).** Divergence of evolutionary ways among common sym genes: *CASTOR* and *CCaMK* show functional conservation between two symbiosis systems and constitute the root of a common signaling pathway. *Plant Cell Physiol* 49, 1659-1671.
- Bapaume, L., and Reinhardt, D. (2012).** How membranes shape plant symbioses: signaling and transport in nodulation and arbuscular mycorrhiza. *Front Plant Sci* 3, 223.
- Bayle, V., Nussaume, L., and Bhat, R.A. (2008).** Combination of novel green fluorescent protein mutant TSapphire and DsRed variant mOrange to set up a versatile *in planta* FRET-FLIM assay. *Plant Physiol* 148, 51-60.
- Bek, A.S., Sauer, J., Thygesen, M.B., Duus, J.O., Petersen, B.O., Thirup, S., James, E., Jensen, K.J., Stougaard, J., and Radutoiu, S. (2010).** Improved characterization of nod factors and genetically based variation in LysM receptor domains identify amino acids expendable for nod factor recognition in *Lotus spp.* *Mol Plant Microbe Interact* 23, 58-66.
- Bensmihen, S., de Billy, F., and Gough, C. (2011).** Contribution of NFP LysM domains to the recognition of Nod factors during the *Medicago truncatula/Sinorhizobium meliloti* symbiosis. *Plos One* 6, e26114.
- Berridge, M.J., Lipp, P., and Bootman, M.D. (2000).** The versatility and universality of calcium signalling. *Nat Rev Mol Cell Biol* 1, 11-21.
- Besserer, A., Puech-Pages, V., Kiefer, P., Gomez-Roldan, V., Jauneau, A., Roy, S., Portais, J.C., Roux, C., Becard, G., and Sejalón-Delmas, N. (2006).** Strigolactones stimulate arbuscular mycorrhizal fungi by activating mitochondria. *PLoS Biol* 4, e226.
- Binder, A., and Parniske, M. (2013).** The nuclear pore complex in symbiosis and pathogen defence. In *Annual Plant Reviews* (John Wiley & Sons Ltd), pp. 229-254.

- Bonfante, P., and Genre, A. (2010).** Mechanisms underlying beneficial plant-fungus interactions in mycorrhizal symbiosis. *Nat Commun* 1, 48.
- Bootman, M.D., Fearnley, C., Smyrniak, I., MacDonald, F., and Roderick, H.L. (2009).** An update on nuclear calcium signalling. *J Cell Sci* 122, 2337-2350.
- Bornberg-Bauer, E., Rivals, E., and Vingron, M. (1998).** Computational approaches to identify leucine zippers. *Nucleic Acids Res* 26, 2740-2746.
- Brewin, N.J. (2004).** Plant cell wall remodelling in the *Rhizobium*-legume symbiosis. *Crit Rev Plant Sci* 23, 293-316.
- Broghammer, A., Krusell, L., Blaise, M., Sauer, J., Sullivan, J.T., Maolanon, N., Vinther, M., Lorentzen, A., Madsen, E.B., Jensen, K.J., et al. (2012).** Legume receptors perceive the rhizobial lipochitin oligosaccharide signal molecules by direct binding. *Proc Natl Acad Sci USA* 109, 13859-13864.
- Buchthal, B., Lau, D., Weiss, U., Weislogel, J.M., and Bading, H. (2012).** Nuclear calcium signaling controls methyl-CpG-binding protein 2 (MeCP2) phosphorylation on serine 421 following synaptic activity. *J Biol Chem* 287, 30967-30974.
- Buee, M., Rossignol, M., Jauneau, A., Ranjeva, R., and Becard, G. (2000).** The pre-symbiotic growth of arbuscular mycorrhizal fungi is induced by a branching factor partially purified from plant root exudates. *Mol Plant Microbe Interact* 13, 693-698.
- Capoen, W., Sun, J., Wysham, D., Otegui, M.S., Venkateshwaran, M., Hirsch, S., Miwa, H., Downie, J.A., Morris, R.J., Ane, J.M., et al. (2011).** Nuclear membranes control symbiotic calcium signaling of legumes. *Proc Natl Acad Sci USA* 108, 14348-14353.
- Catford, J.G., Staehelin, C., Lerat, S., Piche, Y., and Vierheilig, H. (2003).** Suppression of arbuscular mycorrhizal colonization and nodulation in split-root systems of alfalfa after pre-inoculation and treatment with Nod factors. *J Exp Bot* 54, 1481-1487.
- Catoira, R., Galera, C., de Billy, F., Penmetsa, R.V., Journet, E.P., Maillet, F., Rosenberg, C., Cook, D., Gough, C., and Denarie, J. (2000).** Four genes of *Medicago truncatula* controlling components of a nod factor transduction pathway. *Plant Cell* 12, 1647-1666.
- Cerri, M.R., Frances, L., Laloum, T., Auriac, M.C., Niebel, A., Oldroyd, G.E., Barker, D.G., Fournier, J., and de Carvalho-Niebel, F. (2012).** *Medicago truncatula* ERN transcription factors: regulatory interplay with NSP1/NSP2 GRAS factors and expression dynamics throughout rhizobial infection. *Plant Physiol* 160, 2155-2172.
- Chabaud, M., Genre, A., Sieberer, B.J., Faccio, A., Fournier, J., Novero, M., Barker, D.G., and Bonfante, P. (2011).** Arbuscular mycorrhizal hyphopodia and germinated spore exudates trigger Ca²⁺ spiking in the legume and nonlegume root epidermis. *New Phytol* 189, 347-355.
- Charpentier, M., Bredemeier, R., Wanner, G., Takeda, N., Schleiff, E., and Parniske, M. (2008).** *Lotus japonicus* CASTOR and POLLUX are ion channels essential for perinuclear calcium spiking in legume root endosymbiosis. *Plant Cell* 20, 3467-3479.
- Chen, C., Ane, J.M., and Zhu, H. (2008).** OsIPD3, an ortholog of the *Medicago truncatula* DMI3 interacting protein IPD3, is required for mycorrhizal symbiosis in rice. *New Phytol* 180, 311-315.
- Clapham, D.E. (2007).** Calcium signaling. *Cell* 131, 1047-1058.
- Combiér, J.P., Frugier, F., de Billy, F., Boualem, A., El-Yahyaoui, F., Moreau, S., Vernie, T., Ott, T., Gamas, P., Crespi, M., et al. (2006).** MtHAP2-1 is a key transcriptional regulator of symbiotic nodule development regulated by microRNA169 in *Medicago truncatula*. *Genes Dev* 20, 3084-3088.
- Conaway, R.C., Sato, S., Tomomori-Sato, C., Yao, T., and Conaway, J.W. (2005).** The mammalian mediator complex and its role in transcriptional regulation. *Trends Biochem Sci* 30, 250-255.

- De Koninck, P., and Schulman, H. (1998).** Sensitivity of CaM Kinase II to the frequency of Ca²⁺ oscillations. *Science* 279, 227-230.
- Delaux, P.-M., Bécard, G., and Combier, J.-P. (2013).** NSP1 is a component of the Myc signaling pathway. *New Phytol* 199, 59-65.
- Demchenko, K., Winzer, T., Stougaard, J., Parniske, M., and Pawlowski, K. (2004).** Distinct roles of *Lotus japonicus* SYMRK and SYM15 in root colonization and arbuscule formation. *New Phytol* 163, 381-392.
- Den Herder, G., Yoshida, S., Antolin-Llovera, M., Ried, M.K., and Parniske, M. (2012).** *Lotus japonicus* E3 ligase SEVEN IN ABSENTIA4 destabilizes the symbiosis receptor-like kinase SYMRK and negatively regulates rhizobial infection. *Plant Cell* 24, 1691-1707.
- Diaz, C.L., Grønlund, M., Schlaman, H.R.M., and Spaik, H.P. (2005).** Induction of hairy roots for symbiotic gene expression studies. *Lotus japonicus* Handbook, AJ Marquez, ed (Dordrecht, The Netherlands:Springer), pp 261-277
- Dodd, A.N., Kudla, J., and Sanders, D. (2010).** The language of calcium signaling. *Annu Rev Plant Biol* 61, 593-620.
- Doyle, J.J. (2011).** Phylogenetic perspectives on the origins of nodulation. *Mol Plant Microbe Interact* 24, 1289-1295.
- Duc, G., Trouvelot, A., Gianinazzi-Pearson, V., and Gianinazzi, S. (1998).** First report of non-mycorrhizal plant mutants (Myc) obtained in pea (*Pisum sativum* L.) and fababean (*Vicia faba* L.). *Plant Sci* 60, 215-222.
- Ehrhardt, D.W., Wais, R., and Long, S.R. (1996).** Calcium spiking in plant root hairs responding to *Rhizobium* nodulation signals. *Cell* 85, 673-681.
- Endre, G., Kereszt, A., Kevei, Z., Mihacea, S., Kalo, P., and Kiss, G.B. (2002).** A receptor kinase gene regulating symbiotic nodule development. *Nature* 417, 962-966.
- Fahraeus, G. (1957).** The infection of clover root hairs by nodule bacteria studied by a simple glass slide technique. *J Gen Microbiol* 16, 374-381.
- Feddermann, N., Duvvuru Muni, R.R., Zeier, T., Stuurman, J., Ercolin, F., Schorderet, M., and Reinhardt, D. (2010).** The *PAMI* gene of petunia, required for intracellular accommodation and morphogenesis of arbuscular mycorrhizal fungi, encodes a homologue of *VAPYRIN*. *Plant J* 64, 470-481.
- Feilotter, H.E., Hannon, G.J., Ruddell, C.J., and Beach, D. (1994).** Construction of an improved host strain for two hybrid screening. *Nucleic Acids Res* 22, 1502-1503.
- Ferguson, B.J., Indrasumunar, A., Hayashi, S., Lin, M.H., Lin, Y.H., Reid, D.E., and Gresshoff, P.M. (2010).** Molecular analysis of legume nodule development and autoregulation. *J Integr Plant Biol* 52, 61-76.
- Floss, D.S., Levy, J.G., Levesque-Tremblay, V. and Harrison M.J. (2013).** DELLA proteins regulate arbuscule formation in arbuscular mycorrhizal symbiosis. *Proc Natl Acad Sci USA* 110, E5025-E5034.
- Foo, E., and Davies, N.W. (2011).** Strigolactones promote nodulation in pea. *Planta* 234, 1073-1081.
- Foo, E., Ross, J.J., Jones, W.T., and Reid, J.B. (2013).** Plant hormones in arbuscular mycorrhizal symbioses: an emerging role for gibberellins. *Ann Bot* 111, 769-779.
- Fournier, J., Timmers, A.C., Sieberer, B.J., Jauneau, A., Chabaud, M., and Barker, D.G. (2008).** Mechanism of infection thread elongation in root hairs of *Medicago truncatula* and dynamic interplay with associated rhizobial colonization. *Plant Physiol* 148, 1985-1995.
- Fox, J.D., Routzahn, K.M., Bucher, M.H., and Waugh, D.S. (2003).** Maltodextrin-binding proteins from diverse bacteria and archaea are potent solubility enhancers. *FEBS Lett* 537, 53-57.

- Gao, M., and Skolnick, J. (2009).** A threading-based method for the prediction of DNA-binding proteins with application to the human genome. *PLoS Comput Biol* 5, e1000567.
- Genre, A., Chabaud, M., Balzergue, C., Puech-Pagès, V., Novero, M., Rey, T., Fournier, J., Rochange, S., Bécard, G., Bonfante, P., et al. (2013).** Short-chain chitin oligomers from arbuscular mycorrhizal fungi trigger nuclear Ca²⁺ spiking in *Medicago truncatula* roots and their production is enhanced by strigolactone. *New Phytol* 198, 190-202.
- Genre, A., Chabaud, M., Timmers, T., Bonfante, P., and Barker, D.G. (2005).** Arbuscular mycorrhizal fungi elicit a novel intracellular apparatus in *Medicago truncatula* root epidermal cells before infection. *Plant Cell* 17, 3489-3499.
- Gianinazzi, S., Golotte, A., Binet, M.N., van Tuinen, D., Redecker, D., and Wipf, D. (2010).** Agroecology: the key role of arbuscular mycorrhizas in ecosystem services. *Mycorrhiza* 20, 519-530.
- Gietz, R.D., and Woods, R.A. (2002).** Transformation of yeast by lithium acetate/single-stranded carrier DNA/polyethylene glycol method. *Methods Enzymol* 350, 87-96.
- Gleason, C., Chaudhuri, S., Yang, T., Munoz, A., Poovaiah, B.W., and Oldroyd, G.E. (2006).** Nodulation independent of rhizobia induced by a calcium-activated kinase lacking autoinhibition. *Nature* 441, 1149-1152.
- Gobbato, E., Marsh, J.F., Vernie, T., Wang, E., Maillet, F., Kim, J., Miller, J.B., Sun, J., Bano, S.A., Ratet, P., et al. (2012).** A GRAS-type transcription factor with a specific function in mycorrhizal signaling. *Curr Biol* 22, 2236-2241.
- Gonzalez-Rizzo, S., Crespi, M., and Frugier, F. (2006).** The *Medicago truncatula* CRE1 cytokinin receptor regulates lateral root development and early symbiotic interaction with *Sinorhizobium meliloti*. *Plant Cell* 18, 2680-2693.
- Gough, C., and Cullimore, J. (2011).** Lipo-chitoooligosaccharide signaling in endosymbiotic plant-microbe interactions. *Mol Plant Microbe Interact* 24, 867-878.
- Groth, M., Takeda, N., Perry, J., Uchida, H., Draxl, S., Brachmann, A., Sato, S., Tabata, S., Kawaguchi, M., Wang, T.L., et al. (2010).** *NENA*, a *Lotus japonicus* homolog of *Sec13*, is required for rhizodermal infection by arbuscular mycorrhiza fungi and rhizobia but dispensable for cortical endosymbiotic development. *Plant Cell* 22, 2509-2526.
- Gust, A.A., Willmann, R., Desaki, Y., Grabherr, H.M., and Nürnberger, T. (2012).** Plant LysM proteins: modules mediating symbiosis and immunity. *Trends Plant Sci* 17, 495-502.
- Gutjahr, C., Banba, M., Croset, V., An, K., Miyao, A., An, G., Hirochika, H., Imaizumi-Anraku, H., and Paszkowski, U. (2008).** Arbuscular mycorrhiza-specific signaling in rice transcends the common symbiosis signaling pathway. *Plant Cell* 20, 2989-3005.
- Gutjahr, C., Novero, M., Guether, M., Montanari, O., Udvardi, M., and Bonfante, P. (2009).** Presymbiotic factors released by the arbuscular mycorrhizal fungus *Gigaspora margarita* induce starch accumulation in *Lotus japonicus* roots. *New Phytol* 183, 53-61.
- Gutjahr, C., Radovanovic, D., Geoffroy, J., Zhang, Q., Siegler, H., Chiapello, M., Casieri, L., An, K., An, G., Guiderdoni, E., et al. (2012).** The half-size ABC transporters STR1 and STR2 are indispensable for mycorrhizal arbuscule formation in rice. *Plant J* 69, 906-920.
- Haney, C.H., and Long, S.R. (2010).** Plant flotillins are required for infection by nitrogen-fixing bacteria. *Proc Natl Acad Sci USA* 107, 478-483.
- Haney, C.H., Riely, B.K., Tricoli, D.M., Cook, D.R., Ehrhardt, D.W., and Long, S.R. (2011).** Symbiotic rhizobia bacteria trigger a change in localization and dynamics of the *Medicago truncatula* receptor kinase LYK3. *Plant Cell* 23, 2774-2787.
- Harrison, M.J. (2012).** Cellular programs for arbuscular mycorrhizal symbiosis. *Curr Opin Plant Biol* 15, 691-698.

- Harrison, M.J., Dewbre, G.R., and Liu, J. (2002).** A phosphate transporter from *Medicago truncatula* involved in the acquisition of phosphate released by arbuscular mycorrhizal fungi. *Plant Cell* 14, 2413-2429.
- Haseloff, J. (1999).** GFP variants for multispectral imaging of living cells. *Meth Cell Biol* 58, 139-151.
- Hayashi, T., Banba, M., Shimoda, Y., Kouchi, H., Hayashi, M., and Imaizumi-Anraku, H. (2010).** A dominant function of CCaMK in intracellular accommodation of bacterial and fungal endosymbionts. *Plant J* 63, 141-154.
- Heckmann, A.B., Sandal, N., Bek, A.S., Madsen, L.H., Jurkiewicz, A., Nielsen, M.W., Tirichine, L., and Stougaard, J. (2011).** Cytokinin induction of root nodule primordia in *Lotus japonicus* is regulated by a mechanism operating in the root cortex. *Mol Plant Microbe Interact* 24, 1385-1395.
- Helber, N., Wippel, K., Sauer, N., Schaarschmidt, S., Hause, B., and Requena, N. (2011).** A versatile monosaccharide transporter that operates in the arbuscular mycorrhizal fungus *Glomus sp* is crucial for the symbiotic relationship with plants. *Plant Cell* 23, 3812-3823.
- Held, M., Hossain, M.S., Yokota, K., Bonfante, P., Stougaard, J., and Szczyglowski, K. (2010).** Common and not so common symbiotic entry. *Trends Plant Sci* 15, 540-545.
- Hirsch, S., Kim, J., Muñoz, A., Heckmann, A.B., Downie, J.A., and Oldroyd, G.E.D. (2009).** GRAS proteins form a DNA binding complex to induce gene expression during nodulation signaling in *Medicago truncatula*. *Plant Cell* 21, 545-557.
- Hoagland, D.R., and Arnon, D.I. (1950).** The water culture method for growing plants without soil. *Calif Agric Exp Stn Circ* 347, 1-32.
- Hogekamp, C., Arndt, D., Pereira, P.A., Becker, J.D., Hohnjec, N., and Kuster, H. (2011).** Laser microdissection unravels cell-type-specific transcription in arbuscular mycorrhizal roots, including CAAT-box transcription factor gene expression correlating with fungal contact and spread. *Plant Physiol* 157, 2023-2043.
- Hogslund, N., Radutoiu, S., Krusell, L., Voroshilova, V., Hannah, M.A., Goffard, N., Sanchez, D.H., Lippold, F., Ott, T., Sato, S., et al. (2009).** Dissection of symbiosis and organ development by integrated transcriptome analysis of *Lotus japonicus* mutant and wild-type plants. *Plos One* 4, e6556.
- Horvath, B., Yeun, L.H., Domonkos, A., Halasz, G., Gobbato, E., Ayaydin, F., Miro, K., Hirsch, S., Sun, J., Tadege, M., et al. (2011).** *Medicago truncatula* *IPD3* is a member of the common symbiotic signaling pathway required for rhizobial and mycorrhizal symbioses. *Mol Plant Microbe Interact* 24, 1345-1358.
- Hrabak, E.M., Chan, C.W.M., Gribskov, M., Harper, J.F., Choi, J.H., Halford, N., Kudla, J., Luan, S., Nimmo, H.G., Sussman, M.R., et al. (2003).** The *Arabidopsis* CDPK-SnRK superfamily of protein kinases. *Plant Physiol* 132, 666-680.
- Hudmon, A., and Schulman, H. (2002a).** Neuronal Ca²⁺/calmodulin-dependent protein kinase II: the role of structure and autoregulation in cellular function. *Annu Rev Biochem* 71, 473-510.
- Hudmon, A., and Schulman, H. (2002b).** Structure-function of the multifunctional Ca²⁺/calmodulin-dependent protein kinase II. *Biochem J* 364, 593-611.
- Hunter, S., Jones, P., Mitchell, A., Apweiler, R., Attwood, T.K., Bateman, A., Bernard, T., Binns, D., Bork, P., Burge, S., et al. (2012).** InterPro in 2011: new developments in the family and domain prediction database. *Nucleic Acids Res* 40, D306-312.
- Iakoucheva, L.M., Radivojac, P., Brown, C.J., O'Connor, T.R., Sikes, J.G., Obradovic, Z., and Dunker, A.K. (2004).** The importance of intrinsic disorder for protein phosphorylation. *Nucleic Acids Res* 32, 1037-1049.
- Imaizumi-Anraku, H., Takeda, N., Charpentier, M., Perry, J., Miwa, H., Umehara, Y., Kouchi, H., Murakami, Y., Mulder, L., Vickers, K., et al. (2005).** Plastid proteins crucial for symbiotic fungal and bacterial entry into plant roots. *Nature* 433, 527-531.

- Ivashuta, S., Liu, J., Lohar, D.P., Haridas, S., Bucciarelli, B., VandenBosch, K.A., Vance, C.P., Harrison, M.J., and Gantt, J.S. (2005).** RNA interference identifies a calcium-dependent protein kinase involved in *Medicago truncatula* root development. *Plant Cell* 17, 2911-2921.
- Jarsch, I.K., and Ott, T. (2011).** Perspectives on remorin proteins, membrane rafts, and their role during plant-microbe interactions. *Mol Plant Microbe Interact* 24, 7-12.
- Jefferson, R.A., Kavanagh, T.A., and Bevan, M.W. (1987).** GUS fusions: beta-glucuronidase as a sensitive and versatile gene fusion marker in higher plants. *EMBO J* 6, 3901-3907.
- Jerabek-Willemsen, M., Wienken, C.J., Braun, D., Baaske, P., and Duhr, S. (2011).** Molecular interaction studies using microscale thermophoresis. *Assay Drug Dev Technol* 9, 342-353.
- Jeworutzki, E., Roelfsema, M.R., Anschutz, U., Krol, E., Elzenga, J.T., Felix, G., Boller, T., Hedrich, R., and Becker, D. (2010).** Early signaling through the *Arabidopsis* pattern recognition receptors FLS2 and EFR involves Ca²⁺-associated opening of plasma membrane anion channels. *Plant J* 62, 367-378.
- Jones, K.M., Kobayashi, H., Davies, B.W., Taga, M.E., and Walker, G.C. (2007).** How rhizobial symbionts invade plants: the *Sinorhizobium-Medicago* model. *Nat Rev Microbiol* 5, 619-633.
- Kalo, P., Gleason, C., Edwards, A., Marsh, J., Mitra, R.M., Hirsch, S., Jakab, J., Sims, S., Long, S.R., Rogers, J., et al. (2005).** Nodulation signaling in legumes requires NSP2, a member of the GRAS family of transcriptional regulators. *Science* 308, 1786-1789.
- Kanamori, N., Madsen, L.H., Radutoiu, S., Frantescu, M., Quistgaard, E.M., Miwa, H., Downie, J.A., James, E.K., Felle, H.H., Haaning, L.L., et al. (2006).** A nucleoporin is required for induction of Ca²⁺ spiking in legume nodule development and essential for rhizobial and fungal symbiosis. *Proc Natl Acad Sci USA* 103, 359-364.
- Kang, H., Zhu, H., Chu, X., Yang, Z., Yuan, S., Yu, D., Wang, C., Hong, Z., and Zhang, Z. (2011).** A novel interaction between CCaMK and a protein containing the Scythe_N ubiquitin-like domain in *Lotus japonicus*. *Plant Physiol* 155, 1312-1324.
- Karas, B., Murray, J., Gorzelak, M., Smith, A., Sato, S., Tabata, S., and Szczyglowski, K. (2005).** Invasion of *Lotus japonicus* root *hairless 1* by *Mesorhizobium loti* involves the nodulation factor-dependent induction of root hairs. *Plant Physiol* 137, 1331-1344.
- Karimi, M., Inze, D., and Depicker, A. (2002).** GATEWAY vectors for *Agrobacterium*-mediated plant transformation. *Trends Plant Sci* 7, 193-195.
- Kereszt, A., Mergaert, P., and Kondorosi, E. (2011).** Bacteroid development in legume nodules: evolution of mutual benefit or of sacrificial victims? *Mol Plant Microbe Interact* 24, 1300-1309.
- Kevei, Z., Loughon, G., Mergaert, P., Horvath, G.V., Kereszt, A., Jayaraman, D., Zaman, N., Marcel, F., Regulski, K., Kiss, G.B., et al. (2007).** 3-hydroxy-3-methylglutaryl coenzyme a reductase 1 interacts with NORK and is crucial for nodulation in *Medicago truncatula*. *Plant Cell* 19, 3974-3989.
- Kistner, C., and Parniske, M. (2002).** Evolution of signal transduction in intracellular symbiosis. *Trends Plant Sci* 7, 511-518.
- Kistner, C., Winzer, T., Pitzschke, A., Mulder, L., Sato, S., Kaneko, T., Tabata, S., Sandal, N., Stougaard, J., Webb, K.J., et al. (2005).** Seven *Lotus japonicus* genes required for transcriptional reprogramming of the root during fungal and bacterial symbiosis. *Plant Cell* 17, 2217-2229.
- Koncz, C., and Schell, J. (1986).** The promoter of TL DNA gene 5 controls the tissue-specific expression of chimaeric genes carried by a novel type of *Agrobacterium* binary vector. *Mol Gen Genetics* 204, 383-396.
- Kosuta, S., Hazledine, S., Sun, J., Miwa, H., Morris, R.J., Downie, J.A., and Oldroyd, G.E.D. (2008).** Differential and chaotic calcium signatures in the symbiosis signaling pathway of legumes. *Proc Natl Acad Sci USA* 105, 9823-9828.

- Kosuta, S., Held, M., Hossain, M.S., Morieri, G., Macgillivray, A., Johansen, C., Antolin-Llovera, M., Parniske, M., Oldroyd, G.E., Downie, A.J., et al. (2011). *Lotus japonicus symRK-14* uncouples the cortical and epidermal symbiotic program. *Plant J* 67, 929-940.
- Kosuta, S., Winzer, T., and Parniske, M. (2005). Arbuscular mycorrhiza. *Lotus japonicus Handbook*, (AJ Marquez, ed) Dordrecht, The Netherlands: Springer, 87-95.
- Kretschmar, T., Kohlen, W., Sasse, J., Borghi, L., Schlegel, M., Bachelier, J.B., Reinhardt, D., Bours, R., Bouwmeester, H.J., and Martinoia, E. (2012). A petunia ABC protein controls strigolactone-dependent symbiotic signalling and branching. *Nature* 483, 341-344.
- Krüger, M., Krüger, C., Walker, C., Stockinger, H., and Schüßler, A. (2012). Phylogenetic reference data for systematics and phylotaxonomy of arbuscular mycorrhizal fungi from phylum to species level. *New Phytol* 193, 970-984.
- Kuhn, H., Kuster, H., and Requena, N. (2010). *Membrane steroid-binding protein 1* induced by a diffusible fungal signal is critical for mycorrhization in *Medicago truncatula*. *New Phytol* 185, 716-733.
- Laloum, T., De Mita, S., Gamas, P., Baudin, M., and Niebel, A. (2013). CCAAT-box binding transcription factors in plants: Y so many? *Trends Plant Sci* 18, 157-166.
- Langmead, B., Trapnell, C., Pop, M., and Salzberg, S.L. (2009). Ultrafast and memory-efficient alignment of short DNA sequences to the human genome. *Genome Biol* 10, R25.
- Larkan, N.J., Ruzicka, D.R., Edmonds-Tibbett, T., Durkin, J.M., Jackson, L.E., Smith, F.A., Schachtman, D.P., Smith, S.E., and Barker, S.J. (2013). The reduced mycorrhizal colonisation (*rnc*) mutation of tomato disrupts five gene sequences including the *CYCLOPS/IPD3* homologue. *Mycorrhiza*. Springer Verlag, 1-12.
- Lauressergues, D., Delaux, P.M., Formey, D., Lelandais-Briere, C., Fort, S., Cottaz, S., Becard, G., Niebel, A., Roux, C., and Combier, J.P. (2012). The microRNA miR171h modulates arbuscular mycorrhizal colonization of *Medicago truncatula* by targeting *NSP2*. *Plant J* 72, 512-522.
- Lazo, G.R., Stein, P.A., and Ludwig, R.A. (1991). A DNA transformation-competent *Arabidopsis* genomic library in *Agrobacterium*. *Biotechnology (N Y)* 9, 963-967.
- Lecourieux, D., Ranjeva, R., and Pugin, A. (2006). Calcium in plant defence-signalling pathways. *New Phytol* 171, 249-269.
- Lefebvre, B., Klaus-Heisen, D., Pietraszewska-Bogiel, A., Hervé, C., Camut, S., Auriac, M.-C., Gascioli, V., Nurisso, A., Gadella, T.W.J., and Cullimore, J. (2012). Role of N-glycosylation sites and CXC motifs in trafficking of *Medicago truncatula* Nod Factor Perception protein to the plasma membrane. *J Biol Chem* 287, 10812-10823.
- Lefebvre, B., Timmers, T., Mbengue, M., Moreau, S., Hervé, C., Tóth, K., Bittencourt-Silvestre, J., Klaus, D., Deslandes, L., Godiard, L., et al. (2010). A remorin protein interacts with symbiotic receptors and regulates bacterial infection. *Proc Natl Acad of Sci USA* 107, 2343-2348.
- Lerouge, P., Roche, P., Faucher, C., Maillet, F., Truchet, G., Prome, J.C., and Denarie, J. (1990). Symbiotic host-specificity of *Rhizobium meliloti* is determined by a sulphated and acylated glucosamine oligosaccharide signal. *Nature* 344, 781-784.
- Lévy, J., Bres, C., Geurts, R., Chalhoub, B., Kulikova, O., Duc, G., Journet, E.-P., Ané, J.-M., Lauber, E., Bisseling, T., et al. (2004). A putative Ca²⁺ and calmodulin-dependent protein kinase required for bacterial and fungal symbioses. *Science* 303, 1361-1364.
- Liao, J., Singh, S., Hossain, M.S., Andersen, S.U., Ross, L., Bonetta, D., Zhou, Y., Sato, S., Tabata, S., Stougaard, J., et al. (2012). Negative regulation of CCaMK is essential for symbiotic infection. *Plant J* 72, 572-584.
- Limpens, E., Franken, C., Smit, P., Willemse, J., Bisseling, T., and Geurts, R. (2003). LysM domain receptor kinases regulating rhizobial Nod Factor-induced infection. *Science* 302, 630-633.

- Liu, J., Perumal, N.B., Oldfield, C.J., Su, E.W., Uversky, V.N., and Dunker, A.K. (2006).** Intrinsic disorder in transcription factors. *Biochemistry* 45, 6873-6888.
- Liu, W., Kohlen, W., Lillo, A., Op den Camp, R., Ivanov, S., Hartog, M., Limpens, E., Jamil, M., Smaczniak, C., Kaufmann, K., et al. (2011).** Strigolactone biosynthesis in *Medicago truncatula* and rice requires the symbiotic GRAS-type transcription factors NSP1 and NSP2. *Plant Cell* 23, 3853-3865.
- Lohmann, G.V., Shimoda, Y., Nielsen, M.W., Jorgensen, F.G., Grossmann, C., Sandal, N., Sorensen, K., Thirup, S., Madsen, L.H., Tabata, S., et al. (2010).** Evolution and regulation of the *Lotus japonicus* LysM receptor gene family. *Mol Plant Microbe Interact* 23, 510-521.
- Lopez-Lara, I.M., van der Drift, K.M., van Brussel, A.A., Haverkamp, J., Lugtenberg, B.J., Thomas-Oates, J.E., and Spalink, H.P. (1995).** Induction of nodule primordia on *Phaseolus* and *Acacia* by lipo-chitin oligosaccharide nodulation signals from broad-host-range *Rhizobium* strain GRH2. *Plant Mol Biol* 29, 465-477.
- Lopez-Raez, J.A., Charnikhova, T., Fernandez, I., Bouwmeester, H., and Pozo, M.J. (2011).** Arbuscular mycorrhizal symbiosis decreases strigolactone production in tomato. *J Plant Physiol* 168, 294-297.
- Lupas, A., Van Dyke, M., and Stock, J. (1991).** Predicting coiled coils from protein sequences. *Science* 252, 1162-1164.
- Madsen, E.B., Antolín-Llovera, M., Grossmann, C., Ye, J., Vieweg, S., Broghammer, A., Krusell, L., Radutoiu, S., Jensen, O.N., Stougaard, J., et al. (2011).** Autophosphorylation is essential for the *in vivo* function of the *Lotus japonicus* Nod factor receptor 1 and receptor-mediated signalling in cooperation with Nod factor receptor 5. *Plant J* 65, 404-417.
- Madsen, E.B., Madsen, L.H., Radutoiu, S., Olbryt, M., Rakwalska, M., Szczyglowski, K., Sato, S., Kaneko, T., Tabata, S., Sandal, N., et al. (2003).** A receptor kinase gene of the LysM type is involved in legume perception of rhizobial signals. *Nature* 425, 637-640.
- Madsen, L.H., Tirichine, L., Jurkiewicz, A., Sullivan, J.T., Heckmann, A.B., Bek, A.S., Ronson, C.W., James, E.K., and Stougaard, J. (2010).** The molecular network governing nodule organogenesis and infection in the model legume *Lotus japonicus*. *Nature Comm* 1.
- Maekawa, T., Kusakabe, M., Shimoda, Y., Sato, S., Tabata, S., Murooka, Y., and Hayashi, M. (2008).** Polyubiquitin promoter-based binary vectors for overexpression and gene silencing in *Lotus japonicus*. *Mol Plant Microbe Interact* 21, 375-382.
- Maekawa, T., Maekawa-Yoshikawa, M., Takeda, N., Imaizumi-Anraku, H., Murooka, Y., and Hayashi, M. (2009).** Gibberellin controls the nodulation signaling pathway in *Lotus japonicus*. *Plant J* 58, 183-194.
- Maillet, F., Poinot, V., Andre, O., Puech-Pages, V., Haouy, A., Gueunier, M., Cromer, L., Giraudet, D., Formey, D., Niebel, A., et al. (2011).** Fungal lipochitoooligosaccharide symbiotic signals in arbuscular mycorrhiza. *Nature* 469, 58-63.
- Markmann, K., Giczey, G., and Parniske, M. (2008).** Functional adaptation of a plant receptor-kinase paved the way for the evolution of intracellular root symbioses with bacteria. *PLoS Biol* 6, e68.
- Markmann, K., and Parniske, M. (2009).** Evolution of root endosymbiosis with bacteria: How novel are nodules? *Trends Plant Sci* 14, 77-86.
- Marsh, J.F., Rakocevic, A., Mitra, R.M., Brocard, L., Sun, J., Eschstruth, A., Long, S.R., Schultze, M., Ratet, P., and Oldroyd, G.E. (2007).** *Medicago truncatula* NIN is essential for rhizobial-independent nodule organogenesis induced by autoactive calcium/calmodulin-dependent protein kinase. *Plant Physiol* 144, 324-335.
- Mbengue, M., Camut, S., de Carvalho-Niebel, F., Deslandes, L., Froidure, S., Klaus-Heisen, D., Moreau, S., Rivas, S., Timmers, T., Herve, C., et al. (2010).** The *Medicago truncatula* E3 ubiquitin ligase PUB1 interacts with the LYK3 symbiotic receptor and negatively regulates infection and nodulation. *Plant Cell* 22, 3474-3488.

- McGonigle, T.P., Miller, M.H., Evans, D.G., Fairchild, G.L., and Swan, J.A. (1990).** A new method which gives an objective measure of colonization of roots by vesicular arbuscular mycorrhizal fungi. *New Phytol* *115*, 495-501.
- Messinese, E., Mun, J.-H., Yeun, L.H., Jayaraman, D., Rougé, P., Barre, A., Loughon, G., Schornack, S., Bono, J.-J., Cook, D.R., et al. (2007).** A novel nuclear protein interacts with the symbiotic DMI3 calcium- and calmodulin-dependent protein kinase of *Medicago truncatula*. *Mol Plant Microbe Interact* *20*, 912-921.
- Middleton, P.H., Jakab, J., Penmetsa, R.V., Starker, C.G., Doll, J., Kalo, P., Prabhu, R., Marsh, J.F., Mitra, R.M., Kereszt, A., et al. (2007).** An ERF transcription factor in *Medicago truncatula* that is essential for Nod factor signal transduction. *Plant Cell* *19*, 1221-1234.
- Mitra, R.M., Gleason, C.A., Edwards, A., Hadfield, J., Downie, J.A., Oldroyd, G.E.D., and Long, S.R. (2004).** A Ca²⁺/calmodulin-dependent protein kinase required for symbiotic nodule development: Gene identification by transcript-based cloning. *Proc Natl Acad Sci USA* *101*, 4701-4705.
- Miwa, H., Sun, J., Oldroyd, G.E.D., and Allan Downie, J. (2006a).** Analysis of calcium spiking using aameleon calcium sensor reveals that nodulation gene expression is regulated by calcium spike number and the developmental status of the cell. *Plant J* *48*, 883-894.
- Miwa, H., Sun, J., Oldroyd, G.E.D., and Downie, J.A. (2006b).** Analysis of Nod-Factor-induced calcium signaling in root hairs of symbiotically defective mutants of *Lotus japonicus*. *Mol Plant Microbe Interact* *19*, 914-923.
- Mortier, V., Holsters, M., and Goormachtig, S. (2012).** Never too many? How legumes control nodule numbers. *Plant Cell Environ* *35*, 245-258.
- Motchoulski, A., and Liscum, E. (1999).** *Arabidopsis* NPH3: A NPH1 photoreceptor-interacting protein essential for phototropism. *Science* *286*, 961-964.
- Murray, J., Karas, B., Ross, L., Brachmann, A., Wagg, C., Geil, R., Perry, J., Nowakowski, K., MacGillivray, M., Held, M., et al. (2006).** Genetic suppressors of the *Lotus japonicus har1-1* hypernodulation phenotype. *Mol Plant Microbe Interact* *19*, 1082-1091.
- Murray, J.D. (2011).** Invasion by invitation: rhizobial infection in legumes. *Mol Plant Microbe Interact* *24*, 631-639.
- Murray, J.D., Karas, B.J., Sato, S., Tabata, S., Amyot, L., and Szczyglowski, K. (2007).** A cytokinin perception mutant colonized by rhizobium in the absence of nodule organogenesis. *Science* *315*, 101-104.
- Murray, J.D., Muni, R.R.D., Torres-Jerez, I., Tang, Y., Allen, S., Andriankaja, M., Li, G., Laxmi, A., Cheng, X., Wen, J., et al. (2011).** *Vapyrin*, a gene essential for intracellular progression of arbuscular mycorrhizal symbiosis, is also essential for infection by rhizobia in the nodule symbiosis of *Medicago truncatula*. *Plant J* *65*, 244-252.
- Offringa, I.A., Melchers, L.S., Regensburg-Tuinik, A.J., Costantino, P., Schilperoort, R.A., and Hooykaas, P.J. (1986).** Complementation of *Agrobacterium tumefaciens* tumor-inducing *aux* mutants by genes from the T(R)-region of the Ri plasmid of *Agrobacterium rhizogenes*. *Proc Natl Acad Sci USA* *83*, 6935-6939.
- Oláh, B., Brière, C., Bécard, G., Dénarié, J., and Gough, C. (2005).** Nod factors and a diffusible factor from arbuscular mycorrhizal fungi stimulate lateral root formation in *Medicago truncatula* via the DMI1/DMI2 signalling pathway. *Plant J* *44*, 195-207.
- Oldroyd, G.E., and Downie, J.A. (2006).** Nuclear calcium changes at the core of symbiosis signalling. *Curr Opin Plant Biol* *9*, 351-357.
- Oldroyd, G.E., and Downie, J.A. (2008).** Coordinating nodule morphogenesis with rhizobial infection in legumes. *Annu Rev Plant Biol* *59*, 519-546.
- Oldroyd, G.E., Harrison, M.J., and Paszkowski, U. (2009).** Reprogramming plant cells for endosymbiosis. *Science* *324*, 753-754.

- Oldroyd, G.E., Mitra, R.M., Wais, R.J., and Long, S.R. (2001).** Evidence for structurally specific negative feedback in the Nod factor signal transduction pathway. *Plant J* 28, 191-199.
- Oldroyd, G.E.D. (2013).** Speak, friend, and enter: signalling systems that promote beneficial symbiotic associations in plants. *Nat Rev Micro* 11, 252-263.
- Op den Camp, R., Streng, A., De Mita, S., Cao, Q., Polone, E., Liu, W., Ammiraju, J.S.S., Kudrna, D., Wing, R., Untergasser, A., et al. (2011).** LysM-Type mycorrhizal receptor recruited for *rhizobium* symbiosis in nonlegume *Parasponia*. *Science* 331, 909-912.
- Op den Camp, R.H.M., Polone, E., Fedorova, E., Roelofsen, W., Squartini, A., Op den Camp, H.J.M., Bisseling, T., and Geurts, R. (2012).** Nonlegume *Parasponia andersonii* deploys a broad *rhizobium* host range strategy resulting in largely variable symbiotic effectiveness. *Mol Plant Microbe Interact* 25, 954-963.
- Ortu, G., Balestrini, R., Pereira, P.A., Becker, J.D., Kuster, H., and Bonfante, P. (2012).** Plant genes related to gibberellin biosynthesis and signaling are differentially regulated during the early stages of AM fungal interactions. *Mol Plant* 5, 951-954.
- Ovchinnikova, E., Journet, E.P., Chabaud, M., Cosson, V., Ratet, P., Duc, G., Fedorova, E., Liu, W., den Camp, R.O., Zhukov, V., et al. (2011).** *IPD3* controls the formation of nitrogen-fixing symbiosomes in pea and *Medicago Spp.* *Mol Plant Microbe Interact* 24, 1333-1344.
- Parniske, M. (2008).** Arbuscular mycorrhiza: the mother of plant root endosymbioses. *Nat Rev Micro* 6, 763-775.
- Patil, S., Takezawa, D., and Poovaiah, B.W. (1995).** Chimeric plant calcium/calmodulin-dependent protein kinase gene with a neural visinin-like calcium-binding domain. *Proc Natl Acad Sci USA*, 92, 4897-4901.
- Penmetsa, R.V., and Cook, D.R. (1997).** A legume ethylene-insensitive mutant hyperinfected by its rhizobial symbiont. *Science* 275, 527-530.
- Perry, J., Brachmann, A., Welham, T., Binder, A., Charpentier, M., Groth, M., Haage, K., Markmann, K., Wang, T.L., and Parniske, M. (2009).** TILLING in *Lotus japonicus* identified large allelic series for symbiosis genes and revealed a bias in functionally defective ethyl methanesulfonate alleles toward glycine replacements. *Plant Physiol* 151, 1281-1291.
- Plet, J., Wasson, A., Ariel, F., Le Signor, C., Baker, D., Mathesius, U., Crespi, M., and Frugier, F. (2011).** MtCRE1-dependent cytokinin signaling integrates bacterial and plant cues to coordinate symbiotic nodule organogenesis in *Medicago truncatula*. *Plant J* 65, 622-633.
- Pumplin, N., and Harrison, M.J. (2009).** Live-cell imaging reveals periarbuscular membrane domains and organelle location in *Medicago truncatula* roots during arbuscular mycorrhizal symbiosis. *Plant Physiol* 151, 809-819.
- Pumplin, N., Mondo, S.J., Topp, S., Starker, C.G., Gantt, J.S., and Harrison, M.J. (2010).** *Medicago truncatula* Vapyrin is a novel protein required for arbuscular mycorrhizal symbiosis. *Plant J* 61, 482-494.
- Pumplin, N., Zhang, X., Noar, R.D., and Harrison, M.J. (2012).** Polar localization of a symbiosis-specific phosphate transporter is mediated by a transient reorientation of secretion. *Proc Natl Acad Sci USA* 109, E665-672.
- Radutoiu, S., Madsen, L.H., Madsen, E.B., Felle, H.H., Umehara, Y., Gronlund, M., Sato, S., Nakamura, Y., Tabata, S., Sandal, N., et al. (2003).** Plant recognition of symbiotic bacteria requires two LysM receptor-like kinases. *Nature* 425, 585-592.
- Radutoiu, S., Madsen, L.H., Madsen, E.B., Jurkiewicz, A., Fukai, E., Quistgaard, E.M., Albrechtsen, A.S., James, E.K., Thirup, S., and Stougaard, J. (2007).** LysM domains mediate lipochitin-oligosaccharide recognition and *Nfr* genes extend the symbiotic host range. *EMBO J* 26, 3923-3935.

- Radutoiu, S., Madsen, L.H., Madsen, E.B., and Stougaard, J. (2005).** *Agrobacterium rhizogenes* pRi TL-DNA integration system: a gene vector for *Lotus japonicus* transformation. *Lotus japonicus* Handbook, (AJ Marquez, ed) Dordrecht, The Netherlands: Springer, 285-287.
- Reid, D.E., Ferguson, B.J., Hayashi, S., Lin, Y.H., and Gresshoff, P.M. (2011).** Molecular mechanisms controlling legume autoregulation of nodulation. *Ann Bot* 108, 789-795.
- Rellos, P., Pike, A.C.W., Niesen, F.H., Salah, E., Lee, W.H., von Delft, F., and Knapp, S. (2010).** Structure of the CaMKII δ /Calmodulin complex reveals the molecular mechanism of CaMKII kinase activation. *PLoS Biol* 8, e1000426.
- Remy, W., Taylor, T.N., Hass, H., and Kerp, H. (1994).** Four hundred-million-year-old vesicular arbuscular mycorrhizae. *Proc Natl Acad Sci USA* 91, 11841-11843.
- Rensing, S.A., Lang, D., Zimmer, A.D., Terry, A., Salamov, A., Shapiro, H., Nishiyama, T., Perroud, P.F., Lindquist, E.A., Kamisugi, Y., et al. (2008).** The *Physcomitrella* genome reveals evolutionary insights into the conquest of land by plants. *Science* 319, 64-69.
- Roberts, N.J., Morieri, G., Kalsi, G., Rose, A., Stiller, J., Edwards, A., Xie, F., Gresshoff, P.M., Oldroyd, G.E., Downie, J.A., et al. (2013).** Rhizobial and mycorrhizal symbioses in *Lotus japonicus* require lectin nucleotide phosphohydrolase, which acts upstream of calcium signaling. *Plant Physiol* 161, 556-567.
- Römer, P., Recht, S., Strauß, T., Elsässer, J., Schornack, S., Boch, J., Wang, S., and Lahaye, T. (2010).** Promoter elements of rice susceptibility genes are bound and activated by specific TAL effectors from the bacterial blight pathogen, *Xanthomonas oryzae* pv. *oryzae*. *New Phytol* 187, 1048-1057.
- Rosenberg, O.S., Deindl, S., Sung, R.J., Nairn, A.C., and Kuriyan, J. (2005).** Structure of the autoinhibited kinase domain of CaMKII and SAXS analysis of the holoenzyme. *Cell* 123, 849-860.
- Routray, P., Miller, J.B., Du, L., Oldroyd, G., and Poovaiah, B.W. (2013).** Phosphorylation of S344 in the calmodulin-binding domain negatively affects CCaMK function during bacterial and fungal symbioses. *Plant J* 76, 287-296.
- Rowland, O., Ludwig, A.A., Merrick, C.J., Baillieul, F., Tracy, F.E., Durrant, W.E., Fritz-Laylin, L., Nekrasov, V., Sjolander, K., Yoshioka, H., et al. (2005).** Functional analysis of *Avr9/Cf-9* rapidly elicited genes identifies a protein kinase, ACIK1, that is essential for full Cf-9-dependent disease resistance in tomato. *Plant Cell* 17, 295-310.
- Rudd, J.J., and Franklin-Tong, V.E. (2001).** Unravelling response-specificity in Ca²⁺ signalling pathways in plant cells. *New Phytol* 151, 7-33.
- Saito, K., Yoshikawa, M., Yano, K., Miwa, H., Uchida, H., Asamizu, E., Sato, S., Tabata, S., Imaizumi-Anraku, H., Umehara, Y., et al. (2007).** NUCLEOPORIN85 is required for calcium spiking, fungal and bacterial symbioses, and seed production in *Lotus japonicus*. *Plant Cell* 19, 610-624.
- Sathyanarayanan, P.V., Cremo, C.R., and Poovaiah, B.W. (2000).** Plant chimeric Ca²⁺/calmodulin-dependent protein kinase. Role of the neural visinin-like domain in regulating autophosphorylation and calmodulin affinity. *J Biol Chem* 275, 30417-30422.
- Sathyanarayanan, P.V., and Poovaiah, B.W. (2002).** Autophosphorylation-dependent inactivation of plant chimeric calcium/calmodulin-dependent protein kinase. *Eur J Biochem* 269, 2457-2463.
- Sathyanarayanan, P.V., Siems, W.F., Jones, J.P., and Poovaiah, B.W. (2001).** Calcium-stimulated autophosphorylation site of plant chimeric calcium/calmodulin-dependent protein kinase. *J Biol Chem* 276, 32940-32947.
- Schaarschmidt, S., Gresshoff, P.M., and Hause, B. (2013).** Analyzing the soybean transcriptome during autoregulation of mycorrhization identifies the transcription factors GmNF-YA1a/b as positive regulators of arbuscular mycorrhization. *Genome Biol* 14, R62.

- Schauser, L., Roussis, A., Stiller, J., and Stougaard, J. (1999).** A plant regulator controlling development of symbiotic root nodules. *Nature* *402*, 191-195.
- Schneeberger, K., Ossowski, S., Lanz, C., Juul, T., Petersen, A.H., Nielsen, K.L., Jorgensen, J.E., Weigel, D., and Andersen, S.U. (2009).** SHOREmap: simultaneous mapping and mutation identification by deep sequencing. *Nat Methods* *6*, 550-551.
- Schüßler, A., Schwarzott, D., and Walker, C. (2001).** A new fungal phylum, the *Glomeromycota*: phylogeny and evolution. *Mycol Res* *105*, 1413-1421.
- Shaul-Keinan, O., Gadkar, V., Ginzberg, I., Grünzweig, J.M., Chet, I., Elad, Y., Wininger, S., Belausov, E., Eshed, Y., Atzmon, N., et al. (2002).** Hormone concentrations in tobacco roots change during arbuscular mycorrhizal colonization with *Glomus intraradices*. *New Phytol* *154*, 501-507.
- Shaw, S.L., and Long, S.R. (2003).** Nod factor elicits two separable calcium responses in *Medicago truncatula* root hair cells. *Plant Physiol* *131*, 976-984.
- Shimoda, Y., Han, L., Yamazaki, T., Suzuki, R., Hayashi, M., and Imaizumi-Anraku, H. (2012).** Rhizobial and fungal symbioses show different requirements for calmodulin binding to calcium calmodulin-dependent protein kinase in *Lotus japonicus*. *Plant Cell* *24*, 304-321.
- Siciliano, V., Genre, A., Balestrini, R., Cappellazzo, G., deWit, P.J., and Bonfante, P. (2007).** Transcriptome analysis of arbuscular mycorrhizal roots during development of the prepenetration apparatus. *Plant Physiol* *144*, 1455-1466.
- Sieberer, B.J., Chabaud, M., Fournier, J., Timmers, A.C.J., and Barker, D.G. (2012).** A switch in Ca²⁺ spiking signature is concomitant with endosymbiotic microbe entry into cortical root cells of *Medicago truncatula*. *Plant J* *69*, 822-830.
- Sieberer, B.J., Chabaud, M., Timmers, A.C., Monin, A., Fournier, J., and Barker, D.G. (2009).** A nuclear-targetedameleon demonstrates intranuclear Ca²⁺ spiking in *Medicago truncatula* root hairs in response to rhizobial nodulation factors. *Plant Physiol* *151*, 1197-1206.
- Singh, S., and Parniske, M. (2012).** Activation of calcium- and calmodulin-dependent protein kinase (CCaMK), the central regulator of plant root endosymbiosis. *Curr Opin Plant Biol* *15*, 444-453.
- Singh, S., Katzer, K., Lambert, J., Cerri, M. and Parniske, M. (2014).** CYCLOPS, a DNA-binding transcriptional activator, orchestrates symbiotic root nodule development. *Cell Host Microbe* *15*, 139-152
- Smit, P., Limpens, E., Geurts, R., Fedorova, E., Dolgikh, E., Gough, C., and Bisseling, T. (2007).** *Medicago* LYK3, an entry receptor in rhizobial nodulation factor signaling. *Plant Physiol* *145*, 183-191.
- Smit, P., Raedts, J., Portyanko, V., Debellé, F., Gough, C., Bisseling, T., and Geurts, R. (2005).** NSP1 of the GRAS protein family is essential for rhizobial nod factor-induced transcription. *Science* *308*, 1789-1791.
- Smith, S.E., and Read, D.J. (2008).** Mycorrhizal Symbiosis. Academic Press, London.
- Soltis, D.E., Soltis, P.S., Morgan, D.R., Swensen, S.M., Mullin, B.C., Dowd, J.M., and Martin, P.G. (1995).** Chloroplast gene sequence data suggest a single origin of the predisposition for symbiotic nitrogen fixation in angiosperms. *Proc Natl Acad Sci USA* *92*, 2647-2651.
- Soyano, T., Kouchi, H., Hirota, A., and Hayashi, M. (2013).** Nodule inception directly targets *NF-Y* subunit genes to regulate essential processes of root nodule development in *Lotus japonicus*. *PLoS Genet* *9*, e1003352.
- Sprenger-Haussels, M., and Weisshaar, B. (2000).** Transactivation properties of parsley proline-rich bZIP transcription factors. *Plant J* *22*, 1-8.
- Sprent, J.I. (2007).** Evolving ideas of legume evolution and diversity: a taxonomic perspective on the occurrence of nodulation. *New Phytol* *174*, 11-25.

- Sprent, J.I., and James, E.K. (2007).** Legume evolution: where do nodules and mycorrhizas fit in? *Plant Physiol* 144, 575-581.
- Stracke, S., Kistner, C., Yoshida, S., Mulder, L., Sato, S., Kaneko, T., Tabata, S., Sandal, N., Stougaard, J., Szczyglowski, K., et al. (2002).** A plant receptor-like kinase required for both bacterial and fungal symbiosis. *Nature* 417, 959-962.
- Stratton, M.M., Chao, L.H., Schulman, H., and Kuriyan, J. (2013).** Structural studies on the regulation of Ca²⁺/calmodulin dependent protein kinase II. *Curr Opin Struct Biol* 23, 292-301.
- Strauß, T., van Poecke, R.M., Strauß, A., Römer, P., Minsavage, G.V., Singh, S., Wolf, C., Kim, S., Lee, H.A., Yeom, S.I., et al. (2012).** RNA-seq pinpoints a *Xanthomonas* TAL-effector activated resistance gene in a large-crop genome. *Proc Natl Acad Sci USA* 109, 19480-19485.
- Svistoonoff, S., Benabdoun, F.M., Nambiar-Veetil, M., Imanishi, L., Vaissayre, V., Cesari, S., Diagne, N., Hocher, V., de Billy, F., Bonneau, J., et al. (2013).** The independent acquisition of plant root nitrogen-fixing symbiosis in fabids recruited the same genetic pathway for nodule organogenesis. *Plos One* 8, e64515.
- Swainsbury, D.J., Zhou, L., Oldroyd, G.E., and Bornemann, S. (2012).** Calcium ion binding properties of *Medicago truncatula* calcium/calmodulin-dependent protein kinase. *Biochemistry* 51, 6895-6907.
- Takeda, N., Maekawa, T., and Hayashi, M. (2012).** Nuclear-localized and deregulated calcium- and calmodulin-dependent protein kinase activates rhizobial and mycorrhizal responses in *Lotus japonicus*. *Plant Cell* 24, 810-822.
- Takeda, N., Sato, S., Asamizu, E., Tabata, S., and Parniske, M. (2009).** Apoplastic plant subtilases support arbuscular mycorrhiza development in *Lotus japonicus*. *Plant J* 58, 766-777.
- Takezawa, D., Ramachandiran, S., Paranjape, V., and Poovaiah, B.W. (1996).** Dual regulation of a chimeric plant serine/threonine kinase by calcium and calcium/calmodulin. *J Biol Chem* 271, 8126-8132.
- Tirichine, L., Imaizumi-Anraku, H., Yoshida, S., Murakami, Y., Madsen, L.H., Miwa, H., Nakagawa, T., Sandal, N., Albrektsen, A.S., Kawaguchi, M., et al. (2006).** Deregulation of a Ca²⁺/calmodulin-dependent kinase leads to spontaneous nodule development. *Nature* 441, 1153-1156.
- Tirichine, L., Sandal, N., Madsen, L.H., Radutoiu, S., Albrektsen, A.S., Sato, S., Asamizu, E., Tabata, S., and Stougaard, J. (2007).** A gain-of-function mutation in a cytokinin receptor triggers spontaneous root nodule organogenesis. *Science* 315, 104-107.
- Tombes, R.M., Faison, M.O., and Turbeville, J.M. (2003).** Organization and evolution of multifunctional Ca²⁺/CaM-dependent protein kinase genes. *Gene* 322, 17-31.
- Tóth, K., Stratil, T.F., Madsen, E.B., Ye, J., Popp, C., Antolín-Llovera, M., Grossmann, C., Jensen, O.N., Schüßler, A., Parniske, M., et al. (2012).** Functional domain analysis of the remorin protein LjSYMREM1 in *Lotus japonicus*. *Plos One* 7, e30817.
- Trinick, M.J. (1973).** Symbiosis between *rhizobium* and the non-legume, *Trema aspera*. *Nature* 244, 459-460.
- Tuskan, G.A., Difazio, S., Jansson, S., Bohlmann, J., Grigoriev, I., Hellsten, U., Putnam, N., Ralph, S., Rombauts, S., Salamov, A., et al. (2006).** The genome of black cottonwood, *Populus trichocarpa* (Torr. & Gray). *Science* 313, 1596-1604.
- Umehara, M., Hanada, A., Yoshida, S., Akiyama, K., Arite, T., Takeda-Kamiya, N., Magome, H., Kamiya, Y., Shirasu, K., Yoneyama, K., et al. (2008).** Inhibition of shoot branching by new terpenoid plant hormones. *Nature* 455, 195-200.
- van Brussel, A.A.N., Bakhuizen, R., van Spronsen, P.C., Spaink, H.P., Tak, T., Lugtenberg, B.J.J., and Kijne, J.W. (1992).** Induction of pre-infection thread structures in the leguminous host plant by mitogenic lipo-oligosaccharides of *rhizobium*. *Science* 257, 70-72.

- Venkateshwaran, M., Cosme, A., Han, L., Banba, M., Satyshur, K.A., Schleiff, E., Parniske, M., Imaizumi-Anraku, H., and Ane, J.M. (2012). The recent evolution of a symbiotic ion channel in the legume family altered ion conductance and improved functionality in calcium signaling. *Plant Cell* 24, 2528-2545.
- Vernié, T., Moreau, S., de Billy, F., Plet, J., Combiér, J.-P., Rogers, C., Oldroyd, G., Frugier, F., Niebel, A., and Gamas, P. (2008). EFD Is an ERF transcription factor involved in the control of nodule number and differentiation in *Medicago truncatula*. *Plant Cell* 20, 2696-2713.
- Vierheilig, H., Coughlan, A.P., Wyss, U., and Piche, Y. (1998). Ink and vinegar, a simple staining technique for arbuscular-mycorrhizal fungi. *Appl Environ Microbiol* 64, 5004-5007.
- Waadt, R., Schmidt, L.K., Lohse, M., Hashimoto, K., Bock, R., and Kudla, J. (2008). Multicolor bimolecular fluorescence complementation reveals simultaneous formation of alternative CBL/CIPK complexes *in planta*. *Plant J* 56, 505-516.
- Wais, R.J., Galera, C., Oldroyd, G., Catoira, R., Penmetza, R.V., Cook, D., Gough, C., Denarie, J., and Long, S.R. (2000). Genetic analysis of calcium spiking responses in nodulation mutants of *Medicago truncatula*. *Proc Natl Acad Sci USA* 97, 13407-13412.
- Walker, S.A., and Downie, J.A. (2000). Entry of *Rhizobium leguminosarum* *bv. viciae* into root hairs requires minimal Nod factor specificity, but subsequent infection thread growth requires *nodO* or *nodE*. *Mol Plant Microbe Interact* 13, 754-762.
- Wang, B., Yeun, L.H., Xue, J.Y., Liu, Y., Ane, J.M., and Qiu, Y.L. (2010a). Presence of three mycorrhizal genes in the common ancestor of land plants suggests a key role of mycorrhizas in the colonization of land by plants. *New Phytol* 186, 514-525.
- Wang, E., Schornack, S., Marsh, J.F., Gobbato, E., Schwessinger, B., Eastmond, P., Schultze, M., Kamoun, S., and Oldroyd, G.E. (2012). A common signaling process that promotes mycorrhizal and oomycete colonization of plants. *Curr Biol* 22, 2242-2246.
- Wang, L., and Brown, S.J. (2006). BindN: a web-based tool for efficient prediction of DNA and RNA binding sites in amino acid sequences. *Nucleic Acids Res* 34, W243-248.
- Wang, L., Huang, C., Yang, M.Q., and Yang, J.Y. (2010b). BindN+ for accurate prediction of DNA and RNA-binding residues from protein sequence features. *BMC Syst Biol* 4 *Suppl 1*, S3.
- Wayman, G.A., Lee, Y.S., Tokumitsu, H., Silva, A.J., and Soderling, T.R. (2008). Calmodulin-kinases: modulators of neuronal development and plasticity. *Neuron* 59, 914-931.
- Weijers, D., Van Hamburg, J.P., Van Rijn, E., Hooykaas, P.J., and Offringa, R. (2003). Diphtheria toxin-mediated cell ablation reveals interregional communication during *Arabidopsis* seed development. *Plant Physiol* 133, 1882-1892.
- Xie, F., Murray, J.D., Kim, J., Heckmann, A.B., Edwards, A., Oldroyd, G.E.D., and Downie, J.A. (2012). Legume pectate lyase required for root infection by rhizobia. *Proc Natl Acad Sci USA* 109, 633-638.
- Yang, E., and Schulman, H. (1999). Structural examination of autoregulation of multifunctional calcium/calmodulin-dependent protein kinase II. *J Biol Chem* 274, 26199-26208.
- Yano, K., Shibata, S., Chen, W.L., Sato, S., Kaneko, T., Jurkiewicz, A., Sandal, N., Banba, M., Imaizumi-Anraku, H., Kojima, T., et al. (2009). CERBERUS, a novel U-box protein containing WD-40 repeats, is required for formation of the infection thread and nodule development in the legume-*Rhizobium* symbiosis. *Plant J* 60, 168-180.
- Yano, K., Yoshida, S., Müller, J., Singh, S., Banba, M., Vickers, K., Markmann, K., White, C., Schuller, B., Sato, S., et al. (2008). CYCLOPS, a mediator of symbiotic intracellular accommodation. *Proc Natl Acad Sci USA* 105, 20540-20545.
- Yokota, K., Fukai, E., Madsen, L.H., Jurkiewicz, A., Rueda, P., Radutoiu, S., Held, M., Hossain, M.S., Szczyglowski, K., Morieri, G., et al. (2009). Rearrangement of actin cytoskeleton mediates invasion of *Lotus japonicus* roots by *Mesorhizobium loti*. *Plant Cell* 21, 267-284.

- Yoshida, S., and Parniske, M. (2005).** Regulation of plant symbiosis receptor kinase through serine and threonine phosphorylation. *J Biol Chem* 280, 9203-9209.
- Young, N.D., Debelle, F., Oldroyd, G.E., Geurts, R., Cannon, S.B., Udvardi, M.K., Bedito, V.A., Mayer, K.F., Gouzy, J., Schoof, H., et al. (2011).** The *Medicago* genome provides insight into the evolution of rhizobial symbioses. *Nature* 480, 520-524.
- Zhang, Q., Blaylock, L.A., and Harrison, M.J. (2010).** Two *Medicago truncatula* half-ABC transporters are essential for arbuscule development in arbuscular mycorrhizal symbiosis. *Plant Cell* 22, 1483-1497.
- Zhu, H., Riely, B.K., Burns, N.J., and Ane, J.M. (2006).** Tracing nonlegume orthologs of legume genes required for nodulation and arbuscular mycorrhizal symbioses. *Genetics* 172, 2491-2499.

IX List of Figures

Figure 1. Symbiotic signal transduction in plant root cells.	25
Figure 2. CCaMK regulation.....	29
Figure 3. Overview of <i>L. japonicus</i> CCaMK domain structure and mutant derivatives.	39
Figure 4. Immunodetection of CCaMK in root extract of the <i>ccamk-13</i> mutant.....	40
Figure 5. Restoration of RNS in the <i>L. japonicus ccamk-13</i> mutant by various CCaMK versions.....	41
Figure 6. Restoration of AM in the <i>L. japonicus ccamk-13</i> mutant by various CCaMK versions.	43
Figure 7. Quantitative analysis of AM restoration in <i>L. japonicus ccamk-13</i> mutant roots expressing various CCaMK versions.....	46
Figure 8. Induction of spontaneous nodules in the <i>L. japonicus ccamk-13</i> mutant by CCaMK mutant versions.	49
Figure 9. <i>In vitro</i> kinase activity of recombinant CCaMK mutant proteins.	52
Figure 10. Subcellular localization of CCaMK and CCaMK mutant proteins in <i>L. japonicus</i> protoplasts.....	53
Figure 11. Plant phenotypes.	70
Figure 12. Kinetics of nodule development in <i>har1-1</i> parental line and <i>sup11</i>	71
Figure 13. <i>sup11</i> aborts normal root colonization by <i>M. loti</i> and AM fungus.	71
Figure 14. Map-based cloning and next generation sequencing identify two linked mutations.....	73
Figure 15. The genotypes.	74
Figure 16. <i>nph3-1</i> single mutant phenotypes.	75
Figure 17. The <i>L. japonicus CCaMK</i> gene restores AM development in <i>sup11</i>	75
Figure 18. The <i>L. japonicus CCaMK</i> gene restores wild-type nodulation and AM development in <i>ccamk-14</i>	76
Figure 19. <i>ccamk-14</i> forms a mixture of un-colonized, partially colonized and wild-type-like nodules.	78
Figure 20. Kinetics of nodule formation in wild-type Gifu and <i>ccamk-14</i>	78
Figure 21. The <i>ccamk-14</i> mutation impairs cortical infections.	79
Figure 22. <i>ccamk-14</i> is defective in AM symbiosis.	80
Figure 23. MS/MS spectrum of CCaMK phosphopeptide 329-AAAIASVWpSSTIFLR-343 containing pS337.....	81
Figure 24. Calmodulin binding capability of CCaMK and calmodulin binding site mutants CCaMK ^{S337N} and CCaMK ^{S337D}	82
Figure 25. Expression of CCaMK ^{S337D} does not rescue the <i>ccamk-13</i> null symbiotic phenotype.....	83
Figure 26. Quantitative yeast two-hybrid interaction analysis of CCaMK, kinase dead CCaMK ^{G30E} , CCaMK ^{S337N} and CCaMK ^{S337D} with CYCLOPS.	84
Figure 27. <i>In vitro</i> kinase activity of CCaMK, CCaMK ^{S337N} and CCaMK ^{S337D} in the presence of CYCLOPS.....	86
Figure 28. <i>In vitro</i> kinase activity of CCaMK, CCaMK ^{S337N} and CCaMK ^{S337D} in the presence of MBP.	87
Figure 29. <i>In vitro</i> autophosphorylation activity of CCaMK, CCaMK ^{S337N} and CCaMK ^{S337D} in the absence of substrate.	88
Figure 30. CYCLOPS is phosphorylated by CCaMK <i>in vitro</i> and the identified phosphorylation sites S50 and S154 are conserved in symbiotic plants and the moss <i>Physcomitrella</i>	102
Figure 31. Serines 50 and 154 are redundantly required for root symbiosis.....	104
Figure 32. CYCLOPS and CYCLOPS phospho-site mutant proteins are expressed and localize to the nucleus in <i>N. benthamiana</i> leaf cells.....	107
Figure 33. FLIM-FRET interaction analysis between CCaMK and CYCLOPS phospho-site variants.....	108

Figure 34. CYCLOPS-DD transactivates the <i>NIN</i> promoter via a minimal responsive palindromic <i>cis</i> element.....	110
Figure 35. CYCLOPS binds the <i>NIN</i> promoter in a sequence-specific and phosphorylation dependent manner.	111
Figure 36. CYCLOPS is a modular DNA-binding transcriptional activator.....	113
Figure 37. The delimited CYCLOPS DNA binding domain specifically binds the <i>CYC-box in vitro</i>	115
Figure 38. CYCLOPS and CYCLOPS phospho-site mutants form homodimers and interact with CCaMK.	116
Figure 39. The <i>2xCYC-RE:GUS</i> reporter is activated in <i>L. japonicus</i> roots transformed with <i>CYCLOPS-DD</i> independently of NSP1, NSP2 and NIN, and is also activated after treatment with <i>M. loti</i>	118
Figure 40. CYCLOPS-DD induces the formation of root nodules in the absence of rhizobia independently of CCaMK and upregulates <i>NIN</i> and <i>NF-YA1</i> transcript levels.	121
Figure 41. <i>CYCLOPS-DD</i> induced nodules show a genuine nodule morphology.	123
Figure 42. Proposed function of the CCaMK/CYCLOPS complex in the decoding of nuclear calcium signatures leading to root nodule development.	124
Figure 43. Size-exclusion chromatography of CCaMK.....	145
Figure 44. Coexpression of CYCLOPS with CCaMK in <i>E. coli</i> yields soluble, phosphorylated CYCLOPS protein.	146
Figure 45. Analysis of the copurified CCaMK/CYCLOPS complex.....	148

X List of Tables

Table 1. Restoration of RNS in the <i>L. japonicus ccamk-13</i> mutant by various <i>CCaMK</i> versions.....	42
Table 2. AM fungal root length colonization of <i>L. japonicus ccamk-13</i> roots expressing various <i>CCaMK</i> versions.	45
Table 3. Quantification of arbusculated cell files in <i>L. japonicus ccamk-13</i> roots expressing various <i>CCaMK</i> versions.	47
Table 4. Spontaneous nodule formation under asymbiotic conditions.....	50
Table 5. Spontaneous nodule formation in the presence of the AM fungus <i>R. irregularis</i>	50
Table 6. Restoration of root symbiosis in <i>cyclops-3</i> by <i>CYCLOPS</i> phospho-ablative mutant versions. ..	105
Table 7. Restoration of root symbiosis in <i>cyclops-3</i> by <i>CYCLOPS</i> phospho-mimetic mutant versions. ..	106
Table 8. <i>CYC-RE:GUS</i> activation by <i>CYCLOPS-DD</i> in <i>Lotus</i> is independent of NSP1, NSP2 and NIN.....	119
Table 9. The <i>CYC-RE:GUS</i> and <i>pNIN870:GUS</i> reporters are activated after <i>M. loti</i> -DsRed treatment...	120
Table 10. Analysis of spontaneous nodulation induced by <i>CYCLOPS-DD</i>	122

XI Acknowledgements

First of all I am most grateful to my PhD supervisor Martin Parniske for giving me the opportunity to graduate in his lab and to work on the fascinating CCaMK/CYCLOPS project. I am thankful for his continuous support, valuable advice and motivation, openness for discussion at any time, and for giving me the freedom to also pursue my own ideas.

I also would like to thank the reviewers of my thesis for taking the time and effort to evaluate this work.

Big thanks go to all past and present members of the Genetics Department and especially to the members of the Parniske group for the continuous support and helpfulness.

Very special thanks go to my first excellent instructor and supervisor Satoko Yoshida who introduced me into the research topic and taught me how to clone and many other basic experimental procedures and skills. Sincere thanks go also to my diploma thesis supervisor Cathy White who competently taught me with great enthusiasm how to express and purify proteins and who paved the way to the successful purification of the recalcitrant CYCLOPS protein. I would also like to specially acknowledge 'my' two diploma thesis students and pleasant office colleagues, Jayne Lambert and Katja Katzer who both did a great job and with big effort and commitment supported the CYCLOPS project.

I also would like to personally acknowledge the following people: Andi Binder for his valuable support with Illustrator and 'model figure' issues, his permanent and spontaneous helpfulness and especially for the cheerful and relaxing atmosphere in the office; Tina Wolf, for help with EMSA and other techniques and the stimulating scientific discussions; Andreas Brachmann for the perfect organization and coordination of the Genetics II practical course and his helpfulness and openness; Ana Cosme for organizing lab events and for her pleasant company in the lab, during lunch and on the way to and back home from the institute; George Githure for his kind help and support in various protein purification techniques; Caro Gutjahr for teaching me the qRT-PCR technique and for exciting scientific exchange; Verena Klingl for her helpfulness, funny car drives and cheerful conversations at the bench; Macarena Marin for valuable advice and exchange on protein purification issues; Martina Ried for sharing plates, reagents, cooking ingredients and a good lunch time on wednesdays; Petra Winterholler for excellent technical support with the CCaMK project; Meritxell Antolin-Llovera, Aline Banhara, Ute Bergmann, Joana Bittencourt-Silvestre, Karl-Heinz Braun, Gisela Brinkmann, Samy Carbonnel, Marion Cerri, David Chiasson, Barbara Dollrieß, Matthias Ellerbeck, Jasmin Gossman, Martin Groth, Kristina Haage, Simone Hardel, Regina Kühner and Priya Pimprikar which were always open for any help and who also contributed

to the nice atmosphere in the lab.

I would also like to highly appreciate Thomas Lahaye, Thomas Ott and Arthur Schüßler and all members of their group for their valuable and often immediate help and expertise in all kinds of issues.

Finally a big and sincere 'thank you' goes to my family and friends, especially to my daughter Upsi, my sister, my parents and my great grandma who all made my studies possible and whom I could count on at any time.